Molecular Mechanisms Regulating Chronological Aging and Cell Death in the Toxic Dinoflagellate, Karenia brevis

Jillian Grace Johnson
Medical University of South Carolina

MOLECULAR MECHANISMS REGULATING CHRONOLGICAL AGING AND CELL DEATH IN THE TOXIC DINOFLAGELLATE, *KARENIA BREVIS*

by

Jillian Grace Johnson
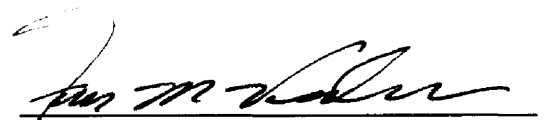
A dissertation submitted to the faculty of the Medical University of South Carolina in partial fulfillment of the requirements for the degree of Doctor of Philosophy in the College of Graduate Studies.

Department of Molecular and Cellular Biology and Pathobiology,

Marine Biomedicine and Environmental Science

2012

Approved by:

_____
Chairman, Advisory Committee
Dr. Frances Van Dolah

_____
Dr. Kay Bidle

_____
Dr. Michael Janech

_____
Dr. Edward Krug

_____
Dr. Christina Voelkel-Johnson

LIST OF TABLES

LIST OF FIGURES

CHAPTER 2

CHAPTER 3

CHAPTER 4

ACKNOWLEDGMENTS

ABSTRACT

The toxic dinoflagellate, *Karenia brevis*, forms nearly annual blooms in the Gulf of Mexico that persist for many months in coastal wate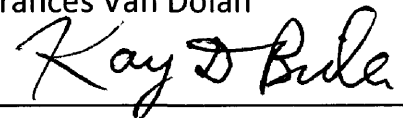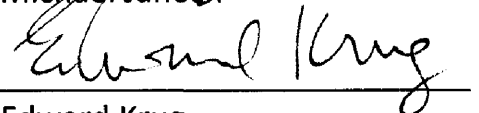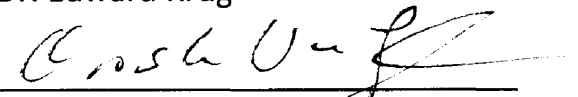rs, causing extensive marine animal mortalities and human health impacts. The molecular mechanisms that contribute to cell survival in high density, low growth blooms, and the mechanisms leading to often rapid bloom demise are not well understood. The studies presented in this dissertation investigate the existence and involvement of a programmed cell death-like (PCD-like) pathway in the demise of *K. brevis* cultures following oxidative stress and chronological aging. Firstly, to gain an understanding of the molecular processes that underlie chronological aging in this dinoflagellate, a microarray study was carried out and identified extensive transcriptomic remodeling during the transition into stationary phase indicative of a shift in the metabolic and signaling requirements for survival in a quiescent non-dividing phase. To better understand the connection between the transcriptomic context identified in the microarray study and the presence of a PCD-like pathway in *K. brevis*, hallmark morphological and biochemical changes (DNA fragmentation, caspase-like activity, and caspase 3-like protein expression) were used to define PCD-like morphological changes following chronological aging and oxidative stress. Targeted *in silico* bioinformatic mining was used to identify enzymes potentially responsible for the activities observed, as well as the substrates. Finally, *K. brevis* S-adenosylmethionine synthetase (KbAdoMetS), a putative caspase substrate predicted from the bioinformatics screen, was examined using MALDI-TOF MS to confirm the validity of the bioinformatics approach. Taken together, this work identified that *K. brevis* contains morphological changes indicative of a caspase-dependent PCD-like pathway and that KbAdoMetS is a caspase 3-like substrate. Finally, we sought to characterize the presence of metacaspases in *Karenia brevis*, and specifically evaluated the role of metacaspase 1 (KbMC1) during chronological aging and

death in culture. Immunocytochemistry, subcellular fractionation, and western blotting results using a custom KbMC1 peptide antibody indicate that KbMC1 may be involved in PCD-like execution through its chloroplastic localization with proposed interactions with the photosynthetic machinery. This study provides the first comprehensive investigation of the molecular processes regulating chronological aging and execution of PCD-like death in a toxic dinoflagellate.

CHAPTER 1

INTRODUCTION

***Karenia brevis* and Florida Red Tide Bloom Dynamics**

Karenia brevis (Davis) G. Hansen & Moestrup (formerly *Gymnodiunium breve* (Davis)) is

the unarmored, fucoxanthin-containing dinoflagellate responsible for the near annual harmful

algal bloom (HAB) events in the Gulf of Mexico. *K. brevis* is classified as a harmful algal species

due to its production of a suite of potent neurotoxins known as the brevetoxins. Brevetoxins are

lipophilic, cyclic polyether compounds that exhibit their toxic effects by binding and persistently

activating voltage-gated sodium channels in nerve, skeletal, and cardiac cells (Baden 1989).

Brevetoxin accumulates and is concentrated at higher trophic levels during bloom events

resulting in massive fish kills, marine mammal mortalities, and contaminated shellfisheries

(Flewelling et al. 2005; Heil and Steidinger 2009). Human consumption of contaminated

shellfish results in neurotoxic shellfish poisoning (NSP) and is characterized by parethesia,

myalgia, vertigo, ataxia, abdominal pain, nausea, diarrhea, headache, bradycardia, and dilated

pupils (Van Dolah 2000). Inhalation of brevetoxin is associated with respiratory irritation and

poses an additive threat to individuals with asthma (Abraham et al. 2005; Fleming et al. 2005).

Coastal HAB events have been conservatively estimated to cause an economic loss to the US of

at least $82 million per year, with the majority of these impacts seen within the public health,

commercial fishery, and tourism divisions (Hoagland and Scatasta 2006; Larkin and Adams

2007). Although red tides have been observed since the 1840s, the occurrence of these HABs

appears to have increased in frequency and duration over the past half century (Hallegraeff

1993; Van Dolah 2000; Brand and Compton 2007).

K. brevis is found in the Gulf of Mexico at background concentrations ranging from 1 to 1,000 cells L^{-1} (Geesey, 1993, Kusek, 1999). Bloom initiation factors are not completely understood; however, it is thought that a change in the nutritional status of the water column through physical and chemical processes such as upwelling events, circulation patterns, and nutrient inputs from Saharan dust storms may contribute to the initial stage of *K. brevis* bloom formation (Walsh and Steidinger 2001; Vargo 2009). Once initiated, the population steadily increases by asexual division (< 1 division day^{-1}) and oceanographic concentration by advection which can cause blooms to reach concentrations of 1 x 10^8 cells L^{-1} (Van Dolah et al. 2008). Blooms are concentrated and transported inshore by prevailing winds and currents (Walsh et al. 2006; Stumpf et al. 2008), where they may persist for months. Once inshore, *K. brevis* encounters variability in temperature, salinity, pH, light, and turbulence in the water column leading to either adaptation and persistence or bloom demise (Van Dolah et al. 2009). *K. brevis* possesses a number of distinguishing qualities which allow this species to outcompete other phytoplankton and persist as the dominant species for months. The majority of the advantages *K. brevis* possesses originates from the species' ability to efficiently take up nutrients from oligotrophic waters (Steidinger et al. 1998; Vargo et al. 2008), use both organic and inorganic forms of nitrogen and phosphorous (Baden and Mende 1979; Mulholland et al. 2006; Sinclair et al. 2009), and vertically migrate to take advantage of increased stratification, reduced turbulence, and assist in nutrient acquisition at depth (Schaeffer et al. 2007; Schaeffer et al. 2009). Other important advantages include photoadaptive abilities to prevent UV damage (Evans, 2001) and the ability to produce allelopathic substances which work to reduce the growth rate of competing phytoplankton species (Prince et al. 2008). While the physiological properties of *K. brevis* and environmental factors related to the initiation and maintenance

phase of blooms have been studied extensively, mechanisms of regulated bloom termination remain largely uninvestigated.

General mechanisms hypothesized to regulate bloom termination include cell lysis due to lytic bacteria and viruses, nutrient limitation, grazing by zooplankton and benthic filter feeders, dilution, or oceanographic processes disrupting the concentration mechanisms. However, each of these mechanisms alone appears insufficient to cause termination (Vargo 2009). It appears that neither normal cell death rates, nutrient availability, nor grazing plays a significant role in termination, given the fact that blooms often persist for months (Vargo 2009). There are also insufficient data supporting a major role of bacterial or viral lysis in initiating bloom termination (Paul et al. 2002). Recent reviews on this topic have concluded that it does not appear as if "normal" mechanisms for bloom termination outlined above exist; therefore, they emphasize a role for the physical breakdown of oceanographic processes promoting the concentration of blooms as major drivers in termination (Vargo 2009). This most recent compilation of bloom termination hypotheses overlooks a potential role for PCD in triggering massive dissolution of a population. Although PCD has been identified in a range of phytoplankton (detailed below), there have not been any studies to date designed to identify the molecular machinery for programmed cell death processes in *K. brevis*, and as such, its contribution to bloom termination remains a viable possibility.

K. brevis Molecular Biology and Genomic Tools

Due to the devastating impacts of *K. brevis*, significant research investment has been made in developing genomic tools to study the genetic structure and gene regulation in this dinoflagellate. *K. brevis* possesses an extremely large haploid genome (1×10^{11} bp) which is permanently condensed in a liquid cholesteric DNA crystal state containing peripheral loops of

DNA where active transcription can occur (Rizzo 1981; Rizzo and Burghardt 1982; Rizzo et al. 1982; Sigee 1983). Dinoflagellates lack nucleosomes that typically aid in chromatin packaging; however, their DNA is fully eukaryotic in sequence organization with large amounts of repetitive DNA (Minguez et al., 1994), but is unusual in that many genes occur in large tandem repeat copies (Bachvaroff and Place 2008). The high copy number of genes and expansion of the genome is thought to be due to gene or whole genome duplication events and possible retroposition of cDNA back into the genome (Lin et al. 2010). A combined library of *K. brevis* ESTs obtained from cells grown in replete logarithmic and stationary conditions, nitrogen and phosphorus limitation, and cells exposed to heat, oxidative, and metal stresses was sequenced to yield a total of 11,937 unigenes of which 10,263 were developed as probes on a custom 11K oligonucleotide microarray (Lidie et al. 2005; Monroe and Van Dolah 2008). Studies in our lab have previously used this genomic tool to investigate the global gene expression patterns under photoperiod control to determine underlying molecular processes regulating bloom growth (Van Dolah et al. 2007) as well as during acute stress conditions aimed to understand the physiological basis for bloom adaptation (Lidie et al. 2005; Lidie 2007). These studies yielded unexpected results that implied a lack of transcriptional control of the cell cycle genes and acute stress response, which were supported with the discovery that *K. brevis* possesses a spliced leader gene, suggesting the potential role of spliced-leader t*rans*-splicing post-transcriptional control to modulate gene expression (Lidie and Van Dolah 2007). Spliced leader *trans*-splicing is a mechanism by which monocystronic mRNA transcripts are matured from polycistronic messages by the addition of a 22bp spliced leader sequence that caps the 5' end simultaneously with the addition ofa 3'-polyA tail (Zhang et al. 2007; Zhang et al. 2009). This discovery suggests that the observed lack of transcriptional control may be attributed to post-transcriptional control mediated by this mechanism. An observed increase in transcript levels in acute time

points may be due to increased splicing of polycistronic messages into multiple polyA transcripts (Morey et al. 2011). Conversely, spliced-leader silencing has been proposed as a regulatory mechanism to decrease available pools of mature transcripts in trypanosomes under stress (Lustig et al. 2007). It remains unclear whether *K. brevis* relies on this exact mechanism for decreasing transcript pools available for translation under stress. It should also be noted that recent mRNA stability estimates suggest long transcript half-lives, upwards of 10 hours suggesting that the analysis of differential expression may be a reflection of differential message stability. Recent global transcriptomic analyses in chronically stressed *K. brevis* cultures have identified a substantial number of differentially expressed transcripts when compared to control culture conditions, suggesting *K. brevis* is capable of adapting to chronic stress conditions, which is reflected in an extensive transcriptomic shift (Morey et al. 2011). Using these studies as a basis for understanding the transcriptomic changes during bloom initiation and adaptation, this genomic tool continues to be a successful tool for identifying molecular processes critical to bloom dynamics, and has been applied in the current study to better understand mechanisms involved in bloom termination.

Programmed Cell Death (PCD) in Unicellular Eukaryotes

Programmed cell death (PCD) is an active, genetically controlled process leading to the elimination of damaged cells in eukaryotes, and has been established as a critical process for growth and development of multicellular organisms. In mammalian systems, programmed cell death (or apoptosis) can be initiated by a diverse group of external and internal signals such as toxins, hormones, growth factors, nitric oxide, reactive oxygen species, Ca_{2+} levels, and DNA damage. These death inducing signals are potentiated by caspase (cysteine-dependent aspartic acid proteases) enzymes (Chowdhury et al. 2008) ultimately leading to the orderly destruction of

the cell, as opposed to necrotic death which can be characterized by nonspecific and disorderly lysis. External signals, such as Fas ligand (FasL) and tumor necrosis factor alpha (TNFα) activate death receptors, causing recruitment of receptor adapter proteins such as Fas-associated death domain protein (FADD). FADD recruits initiator caspases, such as caspase 8, causing autoprocessing and activation that can directly cleave and activate executioner caspases (3, 6, and 7) which cleave death substrates such as enzymes involved in DNA repair, structural nuclear proteins, and fragmentation of DNA resulting in apoptotic death morphologies. Caspase 8 can potentiate the death signal through the internal caspase pathway where it cleaves BH3-interacting domain death agonist (BID) to its activated form, tBID, which initiates the mitochondrial outer membrane permeabilization (MOMP) process leading to the release of cytochrome c and other apoptogenic factors. Cytochrome c release triggers the formation of the apoptosome, which includes a seven-homodimer complex of caspase 9 and apoptotic protease-activating factor 1 (APAF1). The apoptosome functions to activate executioner caspases which cleave a diverse set of downstream targets. Cleavage of the downstream targets such as the major constituents of the cytoskeletal system gives the cell its rounded morphology and causes membrane blebbing, while degradation of nuclear lamins and actin cause the disintegration of the nuclear envelope and nuclear fragmentation. Cleavage of proteins found in focal adhesion sites and desmosomes disrupts the cell's interaction with the extracellular matrix. In addition to weakening the cell's structural integrity, caspases cleave many proteins involved with general maintenance functions such as transcription and translation, mediate DNA condensation and degradation, as well as orchestrate fragmentation of the ER, Golgi, and mitochondria. Removal of the cell with its plasma membrane still intact is considered the most important part of this process and is aided by the formation of apoptotic bodies and externalization of phosphaditylserine in the plasma membrane which serves as a

7

recognition ligand for phagocytes. This summary of the common scheme of the mammalian apoptotic pathway exemplifies the classical coordinated events necessary for the programmed destruction of a cell in the context of a multicellular environment (Boyce et al. 2004; Degterev and Yuan 2008; Taylor et al. 2008).

Extensive research across all major unicellular eukaryotic taxa has now demonstrated the presence of a PCD pathway (Shemarova, 2010); however, the homologs of many of the above pathway constituents have not been identified or do not exist, suggesting more ancient organisms contain a simpler PCD-like pathway. The majority of unicellular PCD research to date has been performed in the common baker's yeast, *Saccharomyces cerevisiae* (Madeo et al. 2002; Herker et al. 2004; Madeo et al. 2004; Buttner et al. 2006; Carmona-Gutierrez et al. 2010). Similarly, extensive effort has been made in understanding the constituents of parasitic protozoan PCD, such as *Leishmania* and trypanosomes, as it appears that death via a PCD-like pathway may represent an alternative method for clonal selection, immune response evasion, and population size regulation, and as such is an important pathway for directing therapeutics (Bruchhaus et al. 2007). PCD-like pathway constituents and morphological characteristics have been demonstrated in a wide range of phytoplankton groups including dinoflagellates (Vardi et al. 1999; Franklin et al. 2006; Vardi et al. 2007; Bouchard and Purdie 2011), chlorophytes (Segovia et al. 2003; Segovia and Berges 2005; Segovia and Berges 2009), diatoms (Allen et al. 2006; Bidle and Bender 2008; Vardi et al. 2008; Thamatrakoln et al. 2012), coccolithophores (Bidle et al. 2007), cyanobacteria (Ning et al. 2002; Berman-Frank et al. 2004; Berman-Frank et al. 2007), and Archaea (Bidle et al. 2010). The induction of PCD in various types of phytoplankton has been described for a wide range of death-inducing conditions such as cell age, CO_2 and nutrient limitation, light intensity, osmotic shock, UV damage, viral infection, and heat stress resulting in a wide variety of death morphologies (reviewed in Bidle et al. 2004;

reviewed in Table 1, Dingman and Lawrence 2012). This was particularly exemplified in the unicellular chlorophyte, *Dunaliella virdis*, which demonstrated a wide range of morphotypes dependent on the type of death insult (Jiménez et al. 2009). Due to the extensive research in this phytoplankton species, it currently serves as the best model for demonstrating the diversity of morphological phenotypes that can occur during cell death in an algal species. Phenotypic changes in *D. virdis* most characteristic of mammalian apoptosis were described for senescence, defined as natural cell aging, with hallmarks being classic chromatin condensation, DNA fragmentation, intact organelles, and membrane blebbing. Acute heat stress appeared to induce a necrotic-like death, while UV irradiance demonstrated an intermediate phenotype indicative of aponecrosis-like death. Hyperosmotic stress induced a parapoptotic phenotype, which included chromatin spotting and extensive cytoplasmic swelling, while nitrogen starved cells underwent a death reminiscent of autophagy with extensive vacuolization. In all cases, *D. virdis* (as well as in *D. tertiolecta* placed in darkness (Segovia et al. 2003; Segovia and Berges 2009)) demonstrated an increase in caspase-like activities and expression levels of a caspase-like protein (determined from western blotting with human caspase 3 anti-sera) suggesting biochemical events similar to the classical mammalian pathway also exists in this chlorophyte. Research in this organism has elegantly demonstrated that the type of death, pathways induced, and subsequent morphologies can differ greatly based on the initial death signal. However, this is also the case when comparing death morphologies across taxa, as the same death signal may not induce the same phenotypic changes (Segovia et al. 2003; Jiménez et al. 2009; Segovia and Berges 2009).

Metacaspases

Metacaspases are caspase orthologs first discovered *in silico* in plants, fungi, and protists (Uren et al. 2000). Caspases (cysteine-dependent aspartic acid proteases) in metazoan PCD are involved in initiating the signal transduction death pathway, while also serving as downstream executioners. These proteases are highly specific and only cleave after an aspartate residue in the P1 position once a specific tetrapeptide sequence is recognized immediately upstream of the P1 cleavage site. Such specificity allows for this pathway to be turned on under strict circumstances, and PCD as a whole can be defined by these coordinated cleavage events (Chowdhury et al. 2008). Metacaspases contain a well-conserved cysteine-histidine catalytic diad and a p20 caspase domain, both distinguishing structural features of all clan CD Cys proteases; however, their cleavage specificity appears to have a preference for arginine and lysine residues in the P1 position (Uren et al. 2000; Vercammen et al. 2007). Plant metacaspases have been shown to be activated by cleavage of a C-terminal p10 domain, rather than the prodomain like mammalian caspases, with the catalytic cysteine critical for autoprocessing (Vercammen et al. 2004). Further analyses of metacaspase activation identified that the catalytic cysteine is regulated at the post-translational level by S-nitrosylation in plant systems (Belenghi et al. 2007). Initial evidence of metacaspase involvement in PCD came from studies in the baker's yeast, *Saccharomyces cereviciae* (Madeo et al. 2002), whereby the disruption of the metacaspase 1 (*yca1*) gene rescued the cells from death induced by hydrogen peroxide (Khan et al. 2005). Further studies in other fungi, protists, and plants including *Aspergillus fumigatus, Trypanosoma brucei, Leishmania major*, and *Arabidopsis thaliana* have also indicated a central role for metacaspases in mediating PCD (Szallies et al. 2002; Vercammen et al. 2004; González et al. 2007; Lee et al. 2007; Richie et al. 2007). Similarly, metacaspase sequences are widespread throughout all phytoplankton lineages spanning an extensive

evolutionary history (Bidle and Falkowski 2004). Interest in phytoplankton PCD fueled

particularly by its potential role in coupling primary productivity to the microbial food web led to

convincing morphological, biochemical, and molecular evidence of metacaspase-mediated PCD

in response to nutrient limitation and cell age in the marine diatom, *Thalassiosira pseudonana*

(Bidle and Bender 2008) and during viral lysis in the dominant coccilithophore, *Emiliania huxleyi*

(Bidle et al. 2007). Although the cellular processes and molecular machinery regulating cell

death in phytoplankton are starting to receive more attention, it remains unknown whether *K.*

brevis possesses this machinery and utilizes this process.

The Role of Chloroplasts and ROS Accumulation in Regulating PCD

Common to the PCD-triggering insults studied in phytoplankton appears to be the

generation of reactive oxygen species (ROS). Reactive forms of oxygen including superoxide

radicals ($O_2\cdot-$), hydroxyl radical ($\cdot OH$), and hydrogen peroxide (H_2O_2) are inevitably formed by

leakage of electrons onto molecular oxygen from the electron transport activities in the

chloroplasts and mitochondria (Van Breusegem and Dat 2006). In photosynthetic organisms, it

has been established that the major source of ROS stems from photosynthesis in the chloroplast

as opposed to the respiratory chain in the mitochondria (Gechev et al. 2006). ROS have been

identified as key modulators of growth, development, stress adaptation, and PCD in plants

(Gechev et al. 2006). Plants possess an active defense system against invading pathogens

through rapid and localized PCD, termed the hypersensitive response (HR). Plant HR- cell death

has been characterized as a form of PCD, in which the production of ROS, altered ion flux,

protein kinase/phospatase activity, and gene activation have been shown to be crucial (Gechev

et al. 2006; Williams and Dickman 2008). An increasing number of reports have now identified a

role for mitogen-activated protein kinases (MAPK) in the perception of ROS for the execution of

PCD (Cvetkovska et al. 2005). More specifically, following MAPK activation, carbon fixation was inhibited causing excess excitation energy and the formation of ROS in the chloroplast which led to PCD. Consistent with previous findings that light is necessary for chloroplastic ROS formation and death, *Arabidopsis thaliana* plants kept in the dark did not accumulate ROS and did not undergo PCD. Furthermore, *A. thaliana* metacaspase 1 (AtMC1) is localized to the chloroplast during HR (Castillo-Olamendi et al. 2007). Other studies in this field have also established the requirement for light in rapid HR-PCD and activation of the same MAPK pathway, further implicating these factors in the execution of HR-PCD (Chandra-Shekara et al. 2006). Together, these data suggest a connection of chloroplast-localized death machinery with photosynthetically driven MAPK-dependent ROS accumulation.

The accumulation of ROS as a trigger of bloom termination in response to environmental CO_2 limitation has been established in the freshwater bloom-forming dinoflagellate, *Peridiunium gatunense*. Consistent with the proposed role for ROS in plants, the observed programmed cell death in *P. gatunense* was suppressed by the addition of catalase and E64, a ROS scavenger and cysteine protease inhibitor respectively (Vardi et al. 1999). The identification of a quorum sensing-like thiol protease excreted from compromised *P. gatunense* possessing high ROS levels further established the central role of ROS in the execution of PCD; however it also identified an intriguing role for population structuring (Vardi et al. 2007). The availability of light is considered one of the most important factors for phytoplankton growth; therefore dark treatment has been extensively studied in the aforementioned unicellular chlorophyte, *D. tertiolecta*. Numerous reports have been published using this culture model establishing that dark treatment is a crucial factor for inducing PCD in this organism (Segovia et al. 2003; Segovia and Berges 2005; Segovia and Berges 2009). Central to dark induced PCD appears to be the accumulation of ROS, the induction of caspase-like protein expression and

activity, and subsequent death with phosphatidylserine externalization, chromatin margination, nuclear degradation, and DNA fragmentation, all of which were reversed with a broad-spectrum caspase inhibitor, Boc-D-FMK. Several pieces of evidence including the existence of a *T. pseudonana* metacaspases that contains a chloroplast transit peptide (Bidle and Bender 2008) and the identification of Ca2+-dependent death specific proteins putatively localized to the chloroplast during iron and oxidative stress (Thamatrakoln et al. 2012) support the need to further define the role of chloroplast localized death machinery in the execution of PCD-like death in phytoplankton.

Evolutionary Drivers of PCD in Phytoplankton and Potential Roles in Controlling Bloom Dynamics

Historically, phytoplankton cell death has been ignored with research efforts more focused on understanding the environmental factors and underlying molecular pathways regulating cell growth and division. This has, however, shifted over the last decade, providing intriguing evidence that PCD in phytoplankton plays a previously unrecognized, but potentially crucial role in population structuring, species succession, biodiversity/selection, and biogeochemical cycling (Bidle and Falkowski 2004; Franklin et al. 2006). The identification of PCD in basal, unicellular organisms has established that the origin of apoptosis had erroneously been placed with the evolution of multicellular life. In fact, it has now been proposed to have evolved during an endosymbiotic event from the resolution of the conflicting heterogeneous genomes (Ameisen 1996). Several hypotheses for retaining this machinery have suggested that PCD in unicellular organisms is an altruistic adaptation used to preserve the overall fitness of a population. The elimination of genetically damaged cells from the population ensures long term species succession, while immediate utilization of the dead cells' extruded organic matter

13

provides nutrients for the uncompromised individuals of the population. The identification of PCD in phytoplankton has now revealed a previously unidentified term in calculating energy flux through the ocean environment. It has been hypothesized that PCD induced by environmental stress and viral lysis may "short circuit" up to 50% of the primary production to the microbial loop instead of supporting carbon flux up the food chain through larger grazers (Bidle and Falkowski 2004). Overall, PCD in phytoplankton represents an important biogeochemical cycling mechanism for shunting photosynthetically fixed carbon away from secondary producers, creating a more regenerative system.

Aging and Death in *K. brevis*

The role of PCD in *K. brevis* is currently unknown, as is the molecular machinery involved in its execution. As outlined in the National Oceanographic and Atmospheric Administration's 2005 – 2015 Harmful Algal Research and Response National Environmental Science Strategy (HARRNESS 2005), management and control strategies are needed to reduce impacts on coastal resources, local economies, and threats to public health. The capability to forecast or influence the demise of blooms would be of immediate value to coastal managers. However, the development of such strategies requires fundamental understanding of the biological processes involved. The studies presented in this dissertation were carried out to further our understanding of the molecular mechanisms involved in aging and cell death in the Florida red tide dinoflagellate, *Karenia brevis,* by addressing the following specific aims.

1. Characterize the molecular processes involved in the chronological aging process by evaluating the global transcriptomic signatures during the entry and maintenance of stationary phase growth.

2. Evaluate the existence of a PCD-like pathway in *K. brevis*

3. Evaluate the involvement of *K. brevis* metacaspases in the execution of PCD-like death.

To better understand the chronological aging process in *K. brevis,* Chapter 2 investigates the transcriptomic response to aging using microarray analysis over a full 18-day growth curve, with an emphasis on the transition from exponential growth to maintenance or stationary phase. Chapter 3 addresses the proteins responsible for caspase-like activity in *K. brevis* during chronological aging as well as during ROS-induced cell death. Morphological changes associated with PCD are assessed to determine the connection between caspase activity and the induction of a PCD-like pathway. A bioinformatic approach was taken to identify the downstream target sequences of caspase-like enzyme activity. Validation of a novel caspase substrate, S-adenosylmethionine synthetase (KbAdoMetS), was analyzed by MALDI-TOF and demonstrated it is capable of being cleaved at the predicted motif by caspase 3. Chapter 4 characterizes the *K. brevis* metacaspase 1 (KbMC1) protein in the context of the chronologically aging process and ROS driven PCD-like death, with an analysis of KbMC1's protein processing biochemistry, localization, and abundance. A bioinformatics approach is then employed to define the likely downstream substrates of KbMC1 in the *K. brevis* transcriptome. Finally, Chapter 5 provides a synthesis of the molecular processes regulating aging and death in *K. brevis,* as well as a perspective on the contributions of this study to the improvement of diagnostics for defining the physiological status in field populations and improved forecasting methods to reduce the impacts of HABs.

REFERENCES

Abraham WM, Bourdelais AJ, Ahmed A, Serebriakov I, Baden DG (2005) Effects of Inhaled Brevetoxins in Allergic Airways: Toxin–Allergen Interactions and Pharmacologic Intervention. Environ Health Perspect 113: 632 - 637

Allen A, Vardi A, Bowler C (2006) An ecological and evolutionary context for integrated nitrogen metabolism and related signaling pathways in marine diatoms. Curr Opin Plant Biol 9: 264 - 273

Ameisen JC (1996) The origin of programmed cell death. Science 272: 1278-1279

Bachvaroff TR, Place AR (2008) From stop to start: tandem gene arrangement, copy number and *trans*-splicing sites in the dinoflagellate *Amphidinium carterae*. PLoS One 3: e2929

Baden D (1989) Brevetoxins: unique polyether dinoflagellate toxins. The FASEB Journal 3: 1807-1817

Baden DG, Mende TJ (1979) Amino acid utilization by *Gymnodinium breve*. Phytochemistry 18: 247-251

Belenghi B, Romero-Puertas MC, Vercammen D, Brackenier A, Inzé D, Delledonne M, Van Breusegem F (2007) Metacaspase Activity of *Arabidopsis thaliana* Is Regulated by S-Nitrosylation of a Critical Cysteine Residue. J Biol Chem 282: 1352-1358

Berman-Frank I, Bidle K, Haramaty L, Falkowski P (2004) The demise of the marine cyanobacterium, *Trichodesmium* spp., via an autocatalyzed cell death pathway. ASLO 49: 9

Berman-Frank I, Rosenberg G, Levitan O, Haramaty L, Mari X (2007) Coupling between autocatalytic cell death and transparent exopolymeric particle production in the marine cyanobacterium *Trichodesmium*. Environ Microbiol 9: 1415 - 1422

Bidle KA, Haramaty L, Baggett N, Nannen J, Bidle KD (2010) Tantalizing evidence for caspase-like protein expression and activity in the cellular stress response of Archaea. Environ Microbiol 12: 1161-1172

Bidle KD, Bender SJ (2008) Iron starvation and culture age activate metacaspases and programmed cell death in the marine diatom *Thalassiosira pseudonana*. Eukaryot Cell 7: 223-236

Bidle KD, Falkowski PG (2004) Cell death in planktonic, photosynthetic microorganisms. Nat Rev Microbiol 2: 643-655

Bidle KD, Haramaty L, Barcelos ERJ, Falkowski P (2007) Viral activation and recruitment of metacaspases in the unicellular coccolithophore, *Emiliania huxleyi*. PNAS 104: 6049-6054

Bouchard JN, Purdie DA (2011) Temporal variation of caspase 3-like protein activity in cultures of the harmful dinoflagellates *Karenia brevis* and *Karenia mikimotoi*. Journal of Plankton Research 33: 961-972

Boyce M, Degterev A, Yuan J (2004) Caspases: an ancient cellular sword of Damocles. Cell Death Differ 11: 29 - 37

Brand LE, Compton A (2007) Long-term increase in *Karenia brevis* abundance along the Southwest Florida Coast. Harmful Algae 6: 232-252

Bruchhaus I, Roeder T, Rennenberg A, Heussler VT (2007) Protozoan parasites: programmed cell death as a mechanism of parasitism. Trends in Parasitology 23: 376-383

Buttner S, Eisenberg T, Herker E, Carmona-Gutierrez D, Kroemer G, Madeo F (2006) Why yeast cells can undergo apoptosis: death in times of peace, love, and war. J Cell Biol 175: 521-525

Carmona-Gutierrez D, Eisenberg T, Buttner S, Meisinger C, Kroemer G, Madeo F (2010) Apoptosis in yeast: triggers, pathways, subroutines. Cell Death Differ 17: 763-773

Castillo-Olamendi L, Bravo-Garcìa A, Morán J, Rocha-Sosa M, Porta H (2007) AtMCP1b, a chloroplast-localised metacaspase, is induced in vascular tissue after wounding or pathogen infection. Functional Plant Biology 34: 1061-1071

Chandra-Shekara AC, Gupte M, Navarre D, Raina S, Raina R, Klessig D, Kachroo P (2006) Light-dependent hypersensitive response and resistance signaling against Turnip Crinkle Virus in *Arabidopsis*. Plant J 45: 320-334

Chowdhury I, Tharakan B, Bhat GK (2008) Caspases — An update. Comp. Biochem. Physiol. Part B Biochem. Mol. Biol. 151: 10-27

Cvetkovska M, Rampitsch C, Bykova N, Xing T (2005) Genomic analysis of MAP kinase cascades in *Arabidopsis* defense responses. Plant Molecular Biology Reporter 23: 331-343

Degterev A, Yuan J (2008) Expansion and evolution of cell death programmes. Nat Rev Mol Cell Biol 9: 378-390

Fleming LE, Backer LC, Baden DG (2005) Overview of Aerosolized Florida Red Tide Toxins: Exposures and Effects. Environ Health Perspect 113

Flewelling LJ, Naar JP, Abbott JP, Baden DG, Barros NB, Bossart GD, Bottein MY, Hammond DG, Haubold EM, Heil CA, Henry MS, Jacocks HM, Leighfield TA, Pierce RH, Pitchford TD, Rommel SA, Scott PS, Steidinger KA, Truby EW, Van Dolah FM, Landsberg JH (2005) Brevetoxicosis: red tides and marine mammal mortalities. Nature 435: 755-756

Franklin D, Brussaard C, Berges J (2006) What is the role and nature of programmed cell death in phytoplankton ecology? Eur J Phycol 41: 1-14

Gechev TS, Van Breusegem F, Stone JM, Denev I, Laloi C (2006) Reactive oxygen species as signals that modulate plant stress responses and programmed cell death. BioEssays 28: 1091-1101

González IJ, Desponds C, Schaff C, Mottram JC, Fasel N (2007) Leishmania major metacaspase can replace yeast metacaspase in programmed cell death and has arginine-specific cysteine peptidase activity. International Journal for Parasitology 37: 161-172

Hallegraeff GM (1993) A review of harmful algal blooms and their apparent global increase. Phycologia 32: 79-99

HARRNESS (2005) Harmful Algal Research and Response: A National Environmental Science Strategy: 2005-2015. Ramsdell, J.S., D.M. Anderson and P.M. Glibert, eds. Washington, DC: Ecological Society of America.

Heil CA, Steidinger KA (2009) Monitoring, management, and mitigation of *Karenia* blooms in the eastern Gulf of Mexico. Harmful Algae 8: 611-617

Herker E, Jungwirth H, Lehmann KA, Maldener C, Frohlich KU, Wissing S, Buttner S, Fehr M, Sigrist S, Madeo F (2004) Chronological aging leads to apoptosis in yeast. J Cell Biol 164: 501-507

Hoagland P, Scatasta S (2006). Ecological Studies 189: Ecology of Harmful Algae. E. Graneli and J. T. Turner. Springer-Verlag, Berlin: 391-402.

Jiménez C, Capasso JM, Edelstein CL, Rivard CJ, Lucia S, Breusegem S, Berl T, Segovia M (2009) Different ways to die: cell death modes of the unicellular chlorophyte *Dunaliella viridis* exposed to various environmental stresses are mediated by the caspase-like activity DEVDase. J Exp Bot 60: 815-828

Khan M, Chock P, Stadtman E (2005) Knockout of caspase-like gene, YCA1, abrogates apoptosis and elevates oxidized proteins in Saccharomyces cerevisiae. PNAS 102: 17326 - 17331

Larkin SL, Adams CM (2007) Harmful algal blooms and coastal business: Economic consequences in Florida. Society & Natural Resources 20: 849-859

Lee N, Gannavaram S, Selvapandiyan A, Debrabant A (2007) Characterization of metacaspases with trypsin-like activity and their putative role in programmed cell death in the protozoan parasite *Leishmania*. Eukaryot Cell 6: 1745-1757

Lidie KB (2007). Characterization and regulation of gene expression networks in response to acute environmental stress in the Florida red tide dinoflagellate, *Karenia brevis*. Charleston, SC, Medical University of South Carolina.

Lidie KB, Ryan JC, Barbier M, Van Dolah FM (2005) Gene expression in Florida red tide dinoflagellate *Karenia brevis*: Analysis of an expressed sequence tag library and development of DNA microarray. Mar Biotechnol 7: 481-493

Lidie KB, Van Dolah FM (2007) Spliced leader RNA-mediated trans-splicing in a dinoflagellate, *Karenia brevis*. J Eukaryot Microbiol 54: 427-435

Lin SJ, Zhang HA, Zhuang YY, Tran B, Gill J (2010) Spliced leader-based metatranscriptomic analyses lead to recognition of hidden genomic features in dinoflagellates. PNAS 107: 20033-20038

Lustig Y, Sheiner L, Vagima Y, Goldshmidt H, Das A, Bellofatto V, Michaeli S (2007) Spliced-leader RNA silencing: a novel stress-induced mechanism in *Trypanosoma brucei*. EMBO Rep 8: 408-413

Madeo F, Herker E, Maldener C, Wissing S, Lachelt S, Herlan M, Fehr M, Lauber K, Sigrist SJ, Wesselborg S, Frohlich KU (2002) A caspase-related protease regulates apoptosis in yeast. Mol Cell 9: 911-917

Madeo F, Herker E, Wissing S, Jungwirth H, Eisenberg T, Frohlich KU (2004) Apoptosis in yeast. Curr Opin Microbiol 7: 655-660

Monroe EA, Van Dolah FM (2008) The toxic dinoflagellate *Karenia brevis* encodes novel type I-like polyketide synthases containing discrete catalytic domains. Protist 159: 471-482

Morey J, Monroe E, Kinney A, Beal M, Johnson J, Hitchcock G, Van Dolah F (2011) Transcriptomic response of the red tide dinoflagellate, *Karenia brevis*, to nitrogen and phosphorus depletion and addition. BMC Genomics 12: 346

Mulholland MR, Bernhardt PW, Heil CA, Bronk DA, O'Neil JM (2006) Nitrogen fixation and release of fixed nitrogen by *Trichodesmium* spp. in the Gulf of Mexico. Limnol Oceanogr 51: 20-20

Ning S, Guo H, Wang L, Song Y (2002) Salt stress induces programmed cell death in prokaryotic organism Anabaena. J Appl Microbiol 93: 15 - 28

Paul JH, Houchin L, Griffin D, Slifko T, Guo M, Richardson B, Steidinger K (2002) A filterable lytic agent obtained from a red tide bloom that caused lysis of Karenia brevis (*Gymnodinum breve*) cultures. Aquat Microb Ecol 27: 21-27

Prince EK, Myers TL, Naar J, Kubanek J (2008) Competing phytoplankton undermines allelopathy of a bloom-forming dinoflagellate. P Roy Soc Lond B Bio 275: 2733-2741

Richie DL, Miley MD, Bhabhra R, Robson GD, Rhodes JC, Askew DS (2007) The Aspergillus fumigatus metacaspases CasA and CasB facilitate growth under conditions of endoplasmic reticulum stress. Molecular Microbiology 63: 591-604

Rizzo PJ (1981) Comparative aspects of basic chromatin proteins in dinoflagellates. Biosystems 14: 433-443

Rizzo PJ, Burghardt RC (1982) Histone-like protein and chromatin structure in the wall-less dinoflagellate *Gymnodinium nelsoni*. Biosystems 15: 27-34

Rizzo PJ, Jones M, Ray SM (1982) Isolation and properties of isolated nuclei from the Florida red tide dinoflagellate *Gymnodinium breve* (Davis). J Protozool 29: 217-222

Schaeffer BA, Kamykowski D, McKay L, Sinclair G, Milligan EJ (2007) A comparison of photoresponse among ten different *Karenia brevis* (Dinophyceae) isolates. J Phycol 43: 702-714

Schaeffer BA, Kamykowski D, Sinclair G, Mckay L, Milligan EJ (2009) Diel vertical migration thresholds of *Karenia brevis* (*Dinophyceae*). Harmful Algae 8: 692-698

Segovia M, Berges JA (2005) Effect of inhibitors of protein synthesis and DNA replication on the induction of proteolytic activities, caspase-like activities and cell death in the unicellular chlorophyte *Dunaliella tertiolecta*. Eur J Phycol 40: 21-30

Segovia M, Berges JA (2009) Inhibition of caspase-like activities prevents the appearance of reactive oxygen species and dark-induced apoptosis in the unicellular chlorophyte *Dunaliella tertiolecta*. J Phycol 45: 1116-1126

Segovia M, Haramaty L, Berges JA, Falkowski PG (2003) Cell death in the unicellular chlorophyte *Dunaliella tertiolecta*. A hypothesis on the evolution of apoptosis in higher plants and metazoans. Plant Physiol. 132: 99-105

Sigee DC (1983) Structural DNA and genetically active DNA in dinoflagellate chromosomes. Biosystems 16: 203-210

Sinclair G, Kamykowski D, Glibert PM (2009) Growth, uptake, and assimilation of ammonium, nitrate, and urea, by three strains of *Karenia brevis* grown under low light. Harmful Algae 8: 770-780

Steidinger KA, Landsberg JH, Truby EW, Roberts BS (1998) First report of *Gymnodinium pulchellum* (*Dinophyceae*) in North America and associated fish kills in the Indian River, Florida. J Phycol 34: 431-437

Stumpf RP, Litaker RW, Lanerolle L, Tester PA (2008) Hydrodynamic accumulation of *Karenia* off the west coast of Florida. Cont Shelf Res 28: 189-213

Szallies A, Kubata B, Duszenko M (2002) A metacaspase of *Trypanosoma brucei* causes loss of respiration competence and clonal death in the yeast *Saccharomyces cerevisiae*. FEBS Lett 517: 144 - 150

Taylor RC, Cullen SP, Martin SJ (2008) Apoptosis: controlled demolition at the cellular level. Nat Rev Mol Cell Biol 9: 231-241

Uren AG, O'Rourke K, Aravind L, Pisabarro MT, Seshagiri S, Koonin EV, Dixit VM (2000) Identification of paracaspases and metacaspases: Two ancient families of caspase-like proteins, one of which plays a key role in MALT lymphoma. Molecular Cell 6: 961-967

Van Breusegem F, Dat JF (2006) Reactive Oxygen Species in Plant Cell Death. Plant Physiol 141: 384-390

Van Dolah F, Leighfield T, Kamykowski D, Kirkpatrick G (2008) Cell cycle behavior of laboratory and field populations of the Florida red tide dinoflagellate, *Karenia brevis*. Cont Shelf Res 28: 11 - 23

Van Dolah FM (2000) Marine algal toxins: Origins, health effects, and their increased occurrence. Environ Health Persp Supp 108: 133

Van Dolah FM, Lidie KB, Monroe EA, Bhattacharya D, Campbell L, Doucette GJ, Kamykowski D (2009) The Florida red tide dinoflagellate *Karenia brevis*: New insights into cellular and molecular processes underlying bloom dynamics. Harmful Algae 8: 562-572

Van Dolah FM, Lidie KB, Morey JS, Brunelle SA, Ryan JC, Monroe EA, Haynes BL (2007) Microarray analysis of diurnal- and circadian-regulated genes in the Florida red-tide dinoflagellate *Karenia brevis* (Dinophyceae). J Phycol 43: 741-752

Vardi A, Berman-Frank I, Rozenberg T, Hadas O, Kaplan A, Levine A (1999) Programmed cell death of the dinoflagellate *Peridinium gatunense* is mediated by CO_2 limitation and oxidative stress. Curr Biol 9: 1061-1064

Vardi A, Bidle KD, Kwityn C, Hirsh DJ, Thompson SM, Callow JA, Falkowski P, Bowler C (2008) A diatom gene regulating nitric-oxide signaling and susceptibility to diatom-derived aldehydes. Curr Biol 18: 895-899

Vardi A, Eisenstadt D, Murik O, Berman-Frank I, Zohary T, Levine A, Kaplan A (2007) Synchronization of cell death in a dinoflagellate population is mediated by an excreted thiol protease. Environ Microbiol 9: 360-369

Vargo GA (2009) A brief summary of the physiology and ecology of *Karenia brevis* Davis (G. Hansen and Moestrup comb. nov.) red tides on the West Florida Shelf and of hypotheses posed for their initiation, growth, maintenance, and termination. Harmful Algae 8: 573-584

Vargo GA, Heil CA, Fanning KA, Dixon LK, Neely MB, Lester K, Ault D, Murasko S, Havens J, Walsh J, Bell S (2008) Nutrient availability in support of *Karenia brevis* blooms on the central West Florida Shelf: What keeps *Karenia* blooming. Cont Shelf Res 28: 73-98

Vercammen D, Declercq W, Vandenabeele P, Van Breusegem F (2007) Are metacaspases caspases? J Cell Biol 179: 375 - 380

Vercammen D, van de Cotte B, De Jaeger G, Eeckhout D, Casteels P, Vandepoele K, Vandenberghe I, Van Beeumen J, Inzé D, Van Breusegem F (2004) Type II metacaspases Atmc4 and Atmc9 of *Arabidopsis thaliana* cleave substrates after arginine and lysine. J Biol Chem 279: 45329-45336

Walsh JJ, Jolliff JK, Darrow BP, Lenes JM, Milroy SP, Remsen A, Dieterle DA, Carder KL, Chen FR, Vargo GA, Weisberg RH, Fanning KA, Muller-Karger FE, Shinn E, Steidinger KA, Heil CA, Tomas CR, Prospero JS, Lee TN, Kirkpatrick GJ, Whitledge TE, Stockwell DA, Villareal TA, Jochens AE, Bontempi PS (2006) Red tides in the Gulf of Mexico: Where, when, and why? J Geophys Res-Oceans 111: -

Walsh JJ, Steidinger KA (2001) Saharan dust and Florida red tides: The cyanophyte connection. J. Geophys. Res. 106: 11597-11612

Williams B, Dickman M (2008) Plant programmed cell death: can't live with it; can't live without it. Mol Plant Pathol 9: 531-544

Zhang H, Campbell DA, Sturm NR, Lin S (2009) Dinoflagellate spliced leader RNA genes display a variety of sequences and genomic arrangements. Mol Biol Evol 26: 1757-1771

Zhang H, Hou Y, Miranda L, Campbell DA, Sturm NR, Gaasterland T, Lin S (2007) Spliced leader RNA trans-splicing in dinoflagellates. PNAS 104: 4618-4623

CHAPTER 2

TRANSCRIPTOME REMODELING ASSOCIATED WITH THE CHRONOLOGICAL AGING IN THE

DINOFLAGELLATE, *KARENIA BREVIS*

INTRODUCTION

The budding yeast *Saccharomyces cerevisiae* has provided a robust model for understanding the cellular processes of chronological aging, defined as the processes a cell undergoes to survive in a sub-optimal, non-dividing state, i.e. stationary phase (Fabrizio and Longo 2003). In this aging model, genomic tools have greatly augmented mutant-based screening studies to provide better resolution of the processes of chronological aging (Gasch et al. 2000; Martinez et al. 2004; Fabrizio et al. 2005; Matecic et al. 2010). In particular, analyses of the yeast transcriptome during the entry and maintenance of stationary phase identified genes essential for survival, including genes important to mitochondrial function, post-translational modification, and the induction of stress resistance (Gasch et al. 2000; Martinez et al. 2004). Understanding the signaling and metabolic requirements of surviving quiescent yeast cells has not only led to a better understanding of the mechanisms underlying the chronological aging process, but has also allowed for greater insight into areas such as pathogen control (Roux et al. 2010) and the impact of the quiescent state on carbon fixation and other environmental processes (Martinez et al. 2004). By comparison, it remains largely unknown what molecular processes regulate chronological aging in unicellular eukaryotes in the marine environment. Until recently, it has been assumed that phytoplankton are immortal, with cells growing indefinitely, primarily by vegetative cell division, and controls imposed entirely by predation or sinking (Bidle and Falkowski 2004). However, a range of terminal phenotypic changes indicative of programmed cell death (PCD) has recently been described in several phytoplankton species from diatom, dinoflagellate, and chlorophyte lineages for a wide range of death inducing stimuli

(Vardi et al. 1999; Segovia et al. 2003; Bidle and Falkowski 2004; Franklin et al. 2006; Bidle and Bender 2008, Thamatrakoln et al. 2012). Yet, the molecular mechanisms involved in the aging processes that may precede the induction of PCD during natural cell demise in these organisms remain unexplored. For this reason, the current study carries out a broad survey of the transcriptome over the growth curve of a dinoflagellate, *Karenia brevis*, to gain insight into chronological aging, defined here as processes that underlie entry into and maintenance of stationary phase.

Karenia brevis is the dinoflagellate responsible for the nearly annual harmful algal bloom (HAB) events in the Gulf of Mexico. *K. brevis* is classified as a harmful algal species due to its production of a suite of potent neurotoxins known as the brevetoxins. Brevetoxins are lipophilic, cyclic polyether compounds that exhibit their toxic effects by binding and persistently activating voltage-gated sodium channels in nerve, skeletal, and cardiac cells (Baden 1989). Brevetoxin accumulates and is concentrated at higher trophic levels during bloom events resulting in massive fish kills, marine mammal mortalities, and contaminated shellfisheries (Flewelling et al. 2005; Heil and Steidinger 2009), while human consumption of contaminated shellfish results in neurotoxic shellfish poisoning (NSP) (Van Dolah 2000). Inhalation of brevetoxin is associated with respiratory irritation and poses an additive threat to individuals with asthma (Abraham et al. 2005; Fleming et al. 2005). Coastal HAB events have been conservatively estimated to cause an economic loss to the US of at least $82 million year^{-1}, with the majority of these impacts seen within the public health, commercial fishery, and tourism divisions (Hoagland and Scatasta 2006; Larkin and Adams 2007). Although red tides have been observed since the 1840s, the occurrence of these HABs appears to have increased in frequency and duration over the past half century (Hallegraeff 1993; Van Dolah 2000; Brand and Compton 2007). For these reasons, understanding the molecular processes regulating chronological aging

in relation to the ability of dense *K. brevis* blooms to persist in the coastal environment is of great interest.

Blooms of *K. brevis* are initiated offshore in oligotrophic waters in response to physical and chemical processes resulting in nutrient inputs from upwelling events, changing circulation patterns, and possibly Saharan aolean dust (Walsh and Steidinger 2001; Vargo et al. 2008; Vargo 2009). Once initiated, the population increases slowly by asexual division ($\sim$0.3 division day^{-1}) which, with oceanographic concentration by advection, can produce blooms at concentrations of 1 x 10^8 cells L^{-1} (Van Dolah et al. 2008). Blooms transported inshore by prevailing winds and currents (Walsh et al. 2006; Stumpf et al. 2008) encounter increased variability in temperature, salinity, pH, light, and turbulence, leading to either adaptation and persistence (maintenance phase) or bloom demise (termination phase) (Van Dolah et al. 2009). *K. brevis* possesses a number of distinguishing physiological attributes that may allow this species to outcompete other phytoplankton, including the ability to efficiently take up nutrients from oligotrophic waters (Vargo et al. 2008; Vargo 2009), the use of both organic and inorganic forms of nitrogen and phosphorous (Baden and Mende 1979; Mulholland et al. 2006; Sinclair et al. 2009), and vertical migration to assist in nutrient acquisition (Schaeffer et al. 2007; Schaeffer et al. 2009). Other adaptive characteristics include photoadaptive abilities to prevent UV damage (Evens et al. 2001) and the production of allelopathic substances which work to reduce the growth rate of competing phytoplankton species (Prince et al. 2008). While *K. brevis* does possess a number of physiological properties aiding in its ability to persist and outcompete, very little is known about the underlying molecular processes that allow for *K. brevis* to be maintained in such dense, often unialgal populations that characterize maintenance phase (Van Dolah et al. 2008).

To gain an understanding of the molecular processes involved in chronological aging in *K. brevis*, here we determined the global transcriptomic signatures during entry and maintenance of stationary phase using a custom 11K microarray (Lidie et al. 2005). This genomic tool has previously been used to investigate the global gene expression patterns under photoperiod control to determine underlying molecular processes regulating growth in relation to bloom initiation (Van Dolah et al. 2007) as well as during acute stress conditions aimed to understand the physiological basis for cellular stress adaptation and toxin biosynthesis (Van Dolah et al. 2007; Monroe et al. 2010)). These studies yielded unexpected results that implied a lack of transcriptional control of diverse processes, including the cell cycle and acute stress response genes, which were later supported with the discovery that *K. brevis* possesses a spliced leader gene (Lidie and Van Dolah 2007; Zhang et al. 2007). Spliced leader *trans*-splicing is a mechanism by which mRNA transcripts are matured from polycistronic messages by the addition of a 22bp spliced leader sequence to the 5′ end and while simultaneously a 3′ polyA tail is added (Zhang et al. 2007; Zhang and Lin 2009). This discovery suggests that the observed lack of transcriptional control may be attributed to post-transcriptional regulation of gene expression, as observed in trypanosomes.

Despite the uncertainty regarding whether dinoflagellate genomes are regulated solely at the post-transcriptional level, transcriptomic studies in this dinoflagellate have identified key molecular processes important to the ecology of *K. brevis* (Lidie 2007; Van Dolah et al. 2007; Monroe et al. 2010; Morey et al. 2011). The current study further identifies a significant reorganization of the *K. brevis* transcriptome between logarithmic and stationary phase growth, demonstrated by approximately 29% of the array features being differentially expressed. Gene ontology enrichment analysis indicates that this dramatic transition represents a global rearrangement of metabolic and signaling requirements for survival in stationary phase.

MATERIALS AND METHODS

Culture Conditions

Karenia brevis (Wilson isolate) was maintained in batch cultures in 1-L glass bottles with autoclaved, 20 μm filtered seawater at 36 psu obtained from the Vero Beach Field Station seawater system at the Florida Institute of Technology. Seawater was enriched with modified *f/2* medium with 0.01 mM selenous acid (final concentration) and ferric sequestrene used in place of $EDTA \cdot Na_2$ and $FeCl_3 \cdot 6H_2O$. Cultures were maintained on a 16:8 light-dark cycle, with illumination from cool white lights at a photon flux density of 50 − 65 $\mu E \cdot m^{-2} \cdot ^{-1}$ measured with a LiCor 2π meter.

Growth Curve Study Design

Twenty seven 900ml batch cultures were inoculated at a starting concentration of approximately 1000 cells/ml from mid-logarithmic stage starter cultures on day 0. Triplicate cultures were harvested every other day from day 2 to 18. Growth and cell abundance was determined for each sampling day using a Beckman Coulter Multisizer 3 (Fullerton, CA), and the specific growth rate and divisions per day were calculated over the growth curve (Levasseur et al. 1993).

RNA Processing

At each time point triplicate 900ml cultures were harvested by centrifugation (600g for 10 minutes at room temperature) and total RNA was extracted using Tri-Reagent according to the manufacturer's protocol (Molecular Research Center, Inc., Cincinnati, OH). Following RNA isolation, suspended RNA was cleaned using an RNeasy mini column (Qiagen, Valencia, CA)

according to the manufacturer's protocol, and quantified and qualified using a NanoDrop ND-1000 (Wilmington, DE) and Agilent 2100 Bioanalyzer (Santa Clara, CA) respectively.

One Color Microarray Analysis

A *K. brevis* 60-mer oligonucleotide microarray containing 10,263 probes designed from cDNA libraries made under nutrient replete and a combination of stress conditions (Lidie et al. 2005) was used in a one-color format to compare gene expression over the growth curve. Total RNA (700ng) from the biological triplicates from days 4, 6, 10, 14, and 18 was amplified and labeled with Cy3 dye using the Low Input Linear Amplification Kit (Agilent, Santa Clara, CA). Amplified and labeled RNA (cRNA) was measured for dye incorporation and total quantity using a Nanodrop ND-1000 (Wilmington, DE). cRNA (480ng total) from each biological replicate was hybridized to a single array for 17 hours at 60°C then washed according to manufacturer's protocol (Agilent). Microarrays were imaged using an Agilent microarray scanner. The images were extracted with Agilent Feature Extraction version 9.5.3.1 and data was analyzed with Rosetta Resolver version 7.2 gene expression analysis system (Rosetta Biosoftware, Cambridge, MA). Using a rank consistency filter, features were subjected to a combination linear and LOWESS normalization algorithm. The probes that displayed significant change in abundance over the growth curve were selected by applying a one way ANOVA ($p < 0.01$) on the normalized signal intensity values across time (n = 3/timepoint) with the Bonferonni multiple test correction adjustment ($p < 0.01$) and were found to be significantly different than day 6 using the Tukey-Kramer post-hoc test ($p < 0.10$) (Figure 1 – workflow summary). Based on the Rosetta error model for the Agilent platform, an average intensity was generated from the three biological replicates for each feature on the array to produce a composite array at each timepoint (Weng et al. 2006). Composite arrays generated for each timepoint were used to build ratios relative

to the day 6 mid-logarithmic phase timepoint. Only features that exhibited at least a 0.23 log ratio change (1.7 – fold change) relative to day 6, with a composite array p-value in at least one timepoint, and a BLAST e-value ≤ 0.0001, were included in the trend set. Due to the fact that low intensity features are unreliable (Shi et al. 2005), features with signal intensity less than 70 counts at all time-points were excluded from the trend set. The final trend set of significantly changing features was clustered using a Euclidean distance metric by an Agglomerative clustering algorithm. Identified clusters were further analyzed for GO term enrichment using the modified Fisher's Exact test in Blast2GO version 2.3.6 using both the standard and GO SLIM analyses (Conesa et al. 2005). All raw gene expression data have been deposited in NCBI's Gene Expression Omnibus (GEO, http://www.ncbi.nlm.nih.gov/geo/, GEO series accession number GSE30913).

Quantitative Real-Time PCR

Differentially expressed genes of interest identified from GO enrichment analysis were selected for validation of the microarray results by quantitative RT- PCR (qPCR). Reverse transcription reactions (n = 6) were carried out using 200 ng total RNA with an oligo(dT) primer using Ambion's RETROscript Kit (Austin, TX) and pooled for each sample. Gene specific primers (Supplemental Table 1) were used for qPCR on an ABI 7500 using the ABI Power SYBR Green master mix (Applied Biosystems, Foster City, CA). The efficiency of each primer set was determined using a standard curve of cDNA from *K. brevis*, and only reactions within 90 – 110% were analyzed. Melt curve analysis was performed following each PCR to confirm single product amplification. Each qPCR assay was run in triplicate on each pooled biological replicate cDNA sample at each time point. The average difference in the C_t values for day 10, 14, and 18 samples from day 6 was used to determine the relative expression of each gene compared to

mid-logarithmic phase. Contig_4846, a hypothetical protein, was assayed to verify that no change was observed over time as its expression did not change significantly in the microarray experiment (ANOVA, p > 0.05). Correlation to the microarray data set was determined using Spearman's Rho Correlation, due to the variables' non-normal distribution, using JMP version 5.1.2 (SAS Institute, Cary, NC).

Two Color Microarray Analysis

One microgram of each triplicate RNA sample from each day was pooled to perform two-color microarray analysis on the custom Agilent oligonucleotide microarray. Total RNA (600 ng) from each pooled timepoint sample was labeled with Cy3 or Cy5 dye using a low input linear RNA amplification kit according to manufacturer's recommendations (Agilent, Palo Alto, CA). Following cleanup, labeled cRNA was quantified by UV spectroscopy and 480 ng each of Cy3 and Cy5 labeled targets were hybridized to the array for 17 hours at 60°C, with Day 6 samples serving as the control for each array. After hybridization, arrays were washed consecutively in solutions of 6X SSPE and 0.005% N-laurylsarcosine and 0.06X SSPE and 0.005% N-laurylsarcosine for 1 min. each at room temperature, followed by a 30 second wash in a stabilization and drying solution (Agilent, Palo Alto, CA). Microarrays were imaged using an Agilent microarray scanner. Images were extracted with Agilent Feature Extraction version A7.5.1 and using a rank consistency filter, features were subjected to a combination linear/LOWESS normalization algorithm. The normalized array data was analyzed using Rosetta Resolver 5.1 gene expression analysis system. A composite array was generated from the two dye-swapped replicate arrays, in which a weighted average was calculated for each feature based on the Rosetta error model designed for the Agilent platform, in which feature quality (p-value) is taken into consideration. As in the one-color analysis, the probes that displayed significant change in abundance over the

growth curve were selected by applying a one way ANOVA (p < 0.01) on the normalized signal intensity values across time with the Bonferoni multiple test correction adjustment (p < 0.01) and were found to be significantly different than day 6 using the Tukey-Kramer post-hoc test (p < 0.10). Only features that exhibited at least a 0.23 log ratio change (1.7 – fold change) relative to day 6, with a composite array p-value in at least one timepoint, and a BLAST e-value ≤ 0.0001, were included in the trend set. Features with signal intensity less than 70 counts at all time-points were excluded from the trend set. The final trend set of significantly changing features was clustered using a Euclidean distance metric by an Agglomerative clustering algorithm. Identified clusters were further analyzed for GO term enrichment using the modified Fisher's Exact test in Blast2GO version 2.3.6 using both the standard and GO SLIM analyses (Conesa et al. 2005).

RESULTS

Overview of Differential Gene Expression Over the Growth Curve

To define growth stages, the cell concentration and growth rates were measured every other day from day 2 to day 18 for each replicate prior to harvest (Figure 2). Growth reached a maximum rate on day 6 (mid-logarithmic phase) at 0.6 ± 0.13 divisions per day with the logarithmic growth stage lasting approximately six days (day 2 – 8). The transition from logarithmic to stationary phase growth was defined by a 32% decrease of the growth rate on day 10, with stationary phase lasting until the end of the experimental sampling, day 18, when the mean divisions per day reached zero and cell concentrations decreased in two of three replicate cultures. In this study, we limited our focus to the transcriptional changes that occurred near growth stage transitions. Mid-logarithmic phase (day 6) was used as the point of

comparison to early-logarithmic phase (day 4), the transition to stationary phase (day 10), mid-stationary phase (day 14), and late-stationary phase (day 18) (Figure 2).

Microarray analysis of transcript abundance changes over the growth curve (Fig. 1 – workflow summary) resulted in a total of 2958 features differentially expressed with 35, 280, 2857, and 351 features differentially expressed on day 4, 10, 14, and 18, respectively. Of the 2958 significant features, 38.67% encoded proteins of known function or possessed a BLASTx e-value ≤ 1e^{-4}. Hierarchical clustering was applied to the final set of significantly changing features to determine the temporal dynamics of the transcriptome over the growth phases (Figure 3A). Two main groups were identified from this clustering method, representing transcripts that increased in abundance (red) and those that decreased in abundance (green) throughout stationary phase. Since only 0.34% of the features on the array were changing between the early (day 4) and mid-logarithmic time point (day 6), we further limited our focus to the differences in stationary phase (days 10, 14, 18) compared to mid-logarithmic. Trending analysis over time further demonstrated that the day 14 timepoint not only contained the majority of the significantly changing features, it also was the time point at which peak expression changes in both directions were observed (Figure 3B).

Overview of Enrichment Analysis

Enrichment analysis for coordinately expressed gene ontology (GO) categories in the increased and decreased transcript clusters was performed in Blast2GO (modified Fisher's Exact test, FDR < 0.05; Table 2). GO enrichment analysis was performed using the GO SLIM and standard functions in Blast2GO to obtain both broad and specific classification of gene product functions. Many of the shared GO terms were part of the same parent term, contained genes that were assigned to multiple GO terms, and were included in more than one enrichment

category. For these reasons, a select list of enriched ontology terms for features differentially expressed in stationary phase are reported (Figure 3C).

Generation of Precursor Metabolites and Energy

The changes in transcript level for genes encoding energy production machinery in stationary phase were profound and included multiple pathways and components. Enrichment analyses identified transcripts that were specific to the generation of precursor metabolites and energy (GO:0006091, FDR = 3.3E-02; Figure 4A). This functional category included a total of 42 genes representing photosynthesis (PS), respiration (ETC), glycolysis (GLY), and the tricarboxylic acid cycle (TCA). Transcripts encoding proteins associated with electron transport chains, including cytochrome b6-f complex, cytochrome c oxidase subunits, inorganic pyrophosphatase, and ATP synthase F_0 subunits, increased in expression in stationary phase. Among the photosynthesis related features present on the array, chloroplast light harvesting proteins, fucoxanthin chlorophyll a/c proteins, flavodoxin, ferrodoxin, plastocyanin, and the oxygen evolving complex of PSII increased in expression at the beginning of stationary and lasting until the end of the experiment. A notable exception to this trend was the two photosystem I core p700 apoprotein a1 and a2 transcripts which were decreased throughout stationary approximately 3-5-fold. In contrast to photosystem I, photosystem II core transcripts did not change in abundance. Components of carbon fixation, glycolysis and the TCA cycles that showed increased transcript abundance included GAPDH (Contig_1755), phosphoglycerate kinase (Contig_2474) and mutase (Contig_4786), malate dehydrogenase (Contig_777), and succinate ligase (5584), while several other components of these pathways including citrate synthase (Contig_9133), aldo keto reductase (Contig_7859), isocitrate dehydrogenase (Contig_6427 and

358), and fructose-bisphosphatases (Contig_9984 and 7125) were decreased throughout stationary phase.

Ribosome Biogenesis

Transcripts encoding structural constituents of the ribosome were found to be enriched with increased transcript abundance throughout stationary phase (GO:0042254, FDR = 1.8E-02). Differentially expressed genes encoding constituents of the ribosome included 30s and 60s ribosomal proteins as well as a small number of other ribosome biogenesis factors including translation initiation and elongation factors (Figure 4B). Ribosome biogenesis is a complex and tightly regulated process with major control points at the level of transcription of rDNA, regulation of the pre – rRNA processing and pre – ribosomal particle assembly steps, and during intracellular trafficking (Leary and Huang 2001). Although transcripts encoding structural components of the ribosome were induced during stationary phase, regulatory constituents of the biogenesis pathway were repressed. Six of eight features present on the array annotated as Sir2 transcriptional regulators (Contig_528, 5155, 9197, 11108, 475, and 8663), known to be involved in maintaining nucleolar structure and enhancing rDNA transcription, were significantly repressed. In addition, DEAD box helicases and other RNA helicases known to regulate not only ribosome processing and assembly, but also pre mRNA splicing, mRNA export, translation initiation, and organellar gene expression were also repressed during stationary phase with the only exception to this finding being Contig_9168, an RNA helicase which was induced by approximately 2-fold on day 14. Other regulatory factors of ribosome biogenesis including fibrillarin (Contig_10099) as well as downstream members of the protein kinase c signaling cascade, and mitogen activated protein kinases (Contig_4994 and 9926), were significantly induced during stationary phase.

Regulation of Gene Expression

Transcripts encoding proteins involved in the regulation of gene expression significantly decreased in abundance (GO:0011468, FDR = 3.3E-04) (Figure 5C). In contrast to the small number of genes required for translation initiation and elongation identified in the ribosome biogenesis category, over 73% of the genes identified in the data set as translation initiation and elongation factors decreased in abundance 1.9 – 3.1-fold throughout stationary phase. This was accompanied by the six silent information regulator proteins (sir2) previously mentioned, four high-mobility group box containing proteins, as well as numerous transcripts encoding regulators of nonsense transcripts, pumillo 1, response regulators, and an immediate early 2 gene with more than a 7-fold decrease in abundance. The remaining 47% of gene expression transcripts that decreased in abundance in stationary phase were identified as pentatricopeptide repeat proteins (PPR) known to be involved in post-transcriptional processes such as mRNA editing, splicing, translation, and stability in mitochondria and chloroplasts (Small and Peeters 2000; Schmitz-Linneweber and Small 2008). Of the 94 identified PPR probes present on the array, 58% were significantly changing, of which 75% demonstrated decreased transcript abundance (Figure 6). Most notable within this class of transcripts was the early onset and continued repression throughout stationary phase with an overwhelming 71, 81, and 90% significantly repressed on day 10, 14, and 18 respectively. This expression pattern was discernibly different from all other enriched categories (Figure 3C).

Response to Stress

Genes identified to be responsive to stress (GO:0006950, FDR = 8.4E-04) demonstrated significant downregulation in stationary phase (Figure 5A). Of the 56 genes included in this category, 30% were identified as coding for heat shock proteins (HSP), chaperones, dnaJ protein

homologs, and other proteins described as binding unfolded proteins (GO:0051082, FDR = 1.8E-02, Supplemental Table 3). In addition to the large number of HSPs and chaperones, this category included some of the largest changing features in terms of magnitude. Poly (adp-ribose) polymerase 1 (Contig_2963), a protein mainly involved in DNA repair and programmed cell death, had a striking 4-fold decrease in abundance at the start of stationary phase, with a minimum at day 14 with 14-fold decreased expression. Numerous ATP and GTP-dependent protein kinases were also found to have reduced expression throughout stationary phase, as well as other general enzymes involved in DNA repair such as DNA helicases and ligases. Several other interesting members of this category included dash family and PBS lyases, general cysteine proteases, as well as an endopeptidase clp-atp binding family protein that demonstrated greater than 6-fold repression in stationary phase. Messages for members of the classic ROS detoxification pathway, such as glutathione s – transferase (Contig_6393) and glutathione peroxidase (Contig_7929) were repressed 2.69 and 1.86-fold respectively, although superoxide dismutase (Contig_1876) was induced more than 2-fold in stationary phase. Other members of the oxidative and reductive reactions such as thioredoxins (Contig_5264, 8405) and glutaredoxin (Contig_7706) were also induced 1.7 to 3.2 fold.

Calcium Ion Binding

Results from the GO Slim enrichment analysis identified enrichment in the decreased expression of transcripts for proteins involved with the biological process of binding (GO:0005488, FDR = 7.9E-05; Supplemental Table 3). Further analyses using the full GO annotation analysis identified a major component of this category to be specifically involved with proteins that bind calcium ions (GO:0005509, FDR = 1.8E-02) (Figure 5B). A total of 46 features were significantly changing with many members of the same family represented within

this category multiple times, suggesting coordinate regulation of calcium throughout stationary phase. Selected constituents of this category included six calcium-dependent protein kinases, five calmodulins, three calreticulin precursors, two EF-hand family proteins, as well as two voltage-dependent p q type calcium channels. Other interesting members included calcineurin, an endoplasmic reticulum resident calcium binding protein that demonstrated 6-fold decreased expression, a calpain-like cysteine peptidase, and a calcium sensor.

Toxin Biosynthesis

Although not identified as enriched in the GO enrichment analyses, it is interesting to note that out of 24 probes on the array for genes annotated as polyketide synthase (PKS) genes, putative enzymes involved in brevetoxin biosynthesis, 12 were included in the trend set and all decreased in abundance during stationary phase (Figure 6B).

Quantitative Real-Time PCR Validation

Differentially expressed genes of interest were selected for validation of the microarray results by quantitative RT-PCR (qPCR) (Figure 7). Changes in gene expression measured by qPCR for the eleven genes, including Contig_4846 which exhibited no change in expression by microarray analysis, strongly supported the microarray results with a correlation of 0.9278 across the time series ($p < 0.0001$, $n = 33$). The strongest correlation of 0.9364 ($p < 0.0001$, $n = 11$) was observed at the day 18 time point. The correlations at day 10 and 14 were 0.9364 ($p < 0.0001$, $n = 11$) and 0.7818 ($p = 0.0045$, $n = 11$) respectively.

One versus Two- Color Microarray Analysis

Prior to this study, all gene expression studies utilizing the custom *K. brevis* oligonucleotide microarray were carried out in the two-color format, whereby biological replicates were pooled, labeled, and hybridized with technical dye swap controls (Lidie, 2007; Monroe, 2008; Van Dolah et al, 2007). In these studies, this experimental design focused on comparing a control sample to treatment samples, therefore implementing a competitive hybridization experimental design. At the inception of this study, Agilent recommendations shifted from running time-course experiments in two-color formats to one-color formats. Therefore, in the current study, given that the foundational question relies on a time series design, where samples are not compared to true control sample, the one-color format was performed. In order to compare previous findings in the lab to this study, it was imperative to define whether the one-color and two-color formats would perform well on measures of reproducibility, sensitivity, and accuracy when compared. To define the changes associated with the transition into the subsequent dynamics in stationary phase, samples were compared to day 6 in both formats. In the two color experiment, biological replicates were pooled and technical replicates (n = 2) in a dye swap design were hybridized to the array. Following the same statistical analysis scheme outlined in Fig. 1 for the one-color format, the two color experiment reported a total of 2236 differentially expressed genes, with 924 up regulated and 1312 down regulated (Table 3). To examine reproducibility between the two formats, a Pearson correlation on the log ratio data was performed for day 14 (Figure 8, Pearson r = 0.9252, p < 0.0001), as this was the timepoint in which the majority of differentially expressed genes were found, and thus the basis for the subsequent biological rationales presented, although it is important to note that days 4, 10, and 18 demonstrated greater than r = 0.85 (p <0.05) between the one-color and two-color formats (data not shown). Since identical thresholds for

significance was used between the formats, it appears that the one-color platform is more

sensitive in identifying differentially expressed genes or that the fold change values are less

compressed than in the two-color data, since the two-color format reported fewer differentially

expressed genes, and may reflect the consequence initial sample pooling (Figure 9A, and Table

3). When the numbers of significant changers were categorized by day and direction of change,

the two methods reported the same proportion of features, except on days 10 and 18 where

the two-color format reported a higher proportion of total changers in both the up and down

direction, therefore suggesting there may be a small discrepancy in sensitivity, as these days

overall reported small magnitude of change when compared to day 14 in both cases (Table 3).

Specificity for the two-color format was determined by assessing the false positive rate from the

self-self hybridization, and resulted in only 20 out of 10, 263 probes significantly changing (P =

0.0019). The two formats were assessed for sensitivity by comparing the resulting gene lists and

demonstrated that there was only a 54% overlap of genes identified by both approaches, with

the two-color approach identifying 11% unique genes and one-color format identifying 34%.

Only 10 genes were found to be anti-correlated (2.97% of total number of changers between

the two formats) (Figure 9A). However, enrichment analysis of the two color format results

indicated, that both formats reported similar biological processes, molecular functions, and

cellular compartments categories (Table 4, Figure 9B). Accuracy was assessed in both the one

and two-color formats by comparison with the well-accepted orthogonal quantitative

technology, SYBR-based qPCR. This assessment demonstrated that there is a strong correlation

between the qPCR data and both the one-color and two-color microarray data (Table 5).

Overall, measures of reproducibility, sensitivity, and accuracy strongly reflect that the custom *K.*

brevis microarray can be utilized in both formats with strong confidence, and thus direct

comparisons between the formats can be made when deciphering the potential molecular mechanisms across studies.

Programmed Cell Death Related Genes in *K. brevis*

Although no cell death or apoptosis related enrichment categories were significantly changing during the aging process, the EST library was therefore data mined to define whether *K. brevis* has the constituents of a typical eukaryotic programmed cell death pathway. A total of 59 contigs containing the gene ontology category cell death (GO:0008219) of which 8 were found to have increased message abundance and 2 with decreased abundance in stationary phase (Table 6). Two WD repeat domain containing proteins were identified, both of which were upregulated, while multiple features annotated as metacaspases were downregulated. Three death associated kinases were identified, with one demonstrating significant repression in stationary phase. Typical apoptosis domains/proteins not identified in the *K. brevis* transcriptome include BCL-2, Bid, Bax, Fas cytosolic domain, Ded domain, Card domain, Dap3, SKP, BCL-G, Bak, Bik, Ced4, Daxx, Apaf-1, Grim, Smac, Diablo, and BH3-only (Taylor et al. 2008). Overall, besides the group of contigs described as metacaspases, *K. brevis* does not appear to contain the suite of proteins known to be necessary for the induction of typical programmed cell death.

DISCUSSION

The *K. brevis* Transcriptome is Drastically Reorganized During Chronological Aging

This study identified changes in the abundance of approximately 29% of the transcriptome of *K. brevis* during its progression from log phase growth to stationary phase through the beginnings of culture decline. To our knowledge, this is the first genome wide

expression analysis of a dinoflagellate over a complete growth curve and provides some insight into processes mediating chronological aging in this organism. Previous studies in *K. brevis* reported little significant change in the abundance of transcripts in response to a diverse set of acute stresses over short time courses of 1-7 h (Lidie 2007) known to induce stress proteins (Miller-Morey and Van Dolah 2004). This observation, along with the identification of spliced leader mediated *trans*-splicing in *K. brevis* (Lidie and Van Dolah 2007), led to the hypothesis that the lack of transcriptional changes in response to acute stress is attributed to post-transcriptional control of gene expression, mediated by the spliced leader *trans*-splicing mechanism. Over a somewhat longer time course of a 24 h diel cycle, approximately 10% of array features (8.4K array) were found to change in *K. brevis* (Van Dolah et al. 2007), yet many processes expected to show transcriptional regulation, such as the cell cycle, did not. The extensive remodeling of the transcriptome observed in the current study, over a time course of 12 days, makes clear that the transcriptome is responsive to changes in environmental conditions, and the coordinate changes in expression of key metabolic processes and signaling pathways suggests their roles in the chronological aging process of *K. brevis.* Since microarrays simply report transcript abundance, the current results do not explain how these changes are achieved in the dinoflagellate. The spliced leader sequence is present on all nuclear encoded mRNAs in all dinoflagellates examined to date (Lidie and Van Dolah 2007; Zhang et al. 2007; Bachvaroff and Place 2008; Zhang and Lin 2009) and, although not rigorously tested, it is widely assumed that all nuclear encoded mRNAs are *trans*-spliced. In the absence of transcriptional control, changes in transcript abundance can be achieved through several mechanisms. These include selective changes in mRNA stability mediated by RNA binding proteins (Goldshmidt et al. 2010) and differential rates of processing from polycistronic precursors to mature messages (Vanhamme and Pays 1995). Thus, even in the absence of classical transcriptional regulation,

the current study demonstrates that the dinoflagellate transcriptome reflects the changing physiological needs within the cell and can reveal unexpected insights into their biology. This study also demonstrated that the microarray results are robust in that the final biological conclusions are supported by strong reproducibility, sensitivity, and accuracy scores between the one-color and two-color format (Patterson et al. 2006), suggesting direct comparisons can be made between separate experiments. This is in accordance with the conclusions drawn from the multi-platform microarray study that concluded that differences between the one-color and two-color approaches are minimal, and experimental design should drive format preference (Patterson et al. 2006). Comparability of data using this microarray between independent experiments was further demonstrated in a subsequent *K. brevis* microarray study that mined the logarithmic phase data from this study to inform interpretations of transcriptome responses to nutrient limitation (Morey et al. 2011).

Coordinately Regulated Changes in Transcript Expression Reveal Insight into Aging in Dinoflagellates

The transcript abundance of numerous genes encoding components of the photosynthetic machinery significantly increased at the transition from logarithmic to stationary phase and remained at elevated levels throughout stationary phase. The exception to this pattern was two PSI genes, which exhibited a marked decrease in abundance at the onset of stationary phase. Although the trigger for stationary phase entry in *K. brevis* cultures grown under nutrient replete conditions remains undefined, these opposing transcript pool abundances emphasize a shift in the bioenergetic needs upon transition to a non-dividing state. The photosynthetic redox state is now a well established signal to coordinate the expression of nuclear-encoded chloroplast genes in order to modulate the photosystem under changing

conditions (Fey et al. 2005). For example, in the chlorophyte *Dunaliella tertiolecta* the induction of the light harvesting complex of PSII and decrease in PSI transcripts in response from a shift from high to low light (Escoubas et al. 1995) is accompanied by a shift in redox state, as measured by the oxidized plastoquininone pool. Similar measures would be informative during stationary phase onset in *K. brevis,* as expression patterns suggest a crucial role in reorganizing the photosynthetic machinery. The redox state in cyanobacteria has also been linked to compensatory mechanisms for an increase in cell density, and thus a decrease in light intensity absorbed per cell, by inducing the expression of more light antennae (Tandeau De Marsac and Houmard 1993). Photosystem genes were also identified to be redox regulated in the dinoflagellate *Pyrocystis lunula* in response to reactive oxygen and nitrogen species forming conditions (Okamoto and Hastings 2003), both of which have been implicated in regulating senescence and programmed cell death in a variety of unicellular eukaryotes (Vardi et al. 1999; Carmona-Gutierrez et al. 2010). Redox control and subsequent retrograde nuclear transcription regulation have not been studied in dinoflagellates, and may provide physiological biomarkers for the onset of maintenance (stationary) phase in bloom conditions. Interestingly, studies in the chlorophyte *Chlamydomonas reinhardtii,* higher plant *Spinacia oleracea*, and eubacteria *Escherichia coli* have provided strong evidence that polyadenylation of chloroplast mRNAs are a signal for degradation (Kudla et al. 1996; Lisitsky et al. 1996; Lozatavera et al. 1996; Lisitsky et al. 1997; Hayes et al. 1999; Komine et al. 2000; Komine et al. 2002), suggesting that the measureable decrease in the (polyadenylated) photosystem I gene transcripts in the current study may actually represent a stabilization of PSI concurrent with acclimation of the photosystem to stationary phase conditions. This interpretation is supported by a decrease in photosynthetic efficiency observed in *K. brevis* at the onset of stationary phase as measured by Fv/Fm (Johnson et al., unpublished observation). Restructuring of the photosynthetic apparatus

to favor PSI could enhance cyclic ATP production around PSI, and has been previously seen in other phytoplankton species as a mechanism to "vent" the photosystem of excess electrons during stress. In addition to this, an increase in glycolysis and TCA cycle transcripts was observed, as well as transporters including an ammonium transporter (Contig_11443), nitrate transporters (Contig_780 and 1567), a sugar/H+ symporter (Contig_4765), a UDP-n-acetyl glucosamine (Contig_4483), inorganic pyrophosphatase (Contig_4809), and a phosphate phosphoenolpyruvate transporter (Contig_9723). Extensive research aimed at understanding how *K. brevis* outcompetes and persists both in the oligotrophic mid waters and the eutrophic coastal waters has suggested that *K. brevis'* mixotrophic abilities may enable it to maintain high cell concentrations under conditions where photoautotrophy alone cannot support it (Vargo et al. 2008). In culture, *K. brevis* has an apparent requirement for a natural bacterial assemblage, as axenic cultures have not been successfully established, which may be necessary to support heterotrophic metabolism. Further investigation is needed to connect physiological data with the transcriptomic signature during stationary phase; however, this work provides a foundation to direct such studies. Together, the transcriptomic data suggests that optimizing the production of energy appears to be an important factor to the survival of quiescent *K. brevis* cells in stationary phase, and fine-tuning of the energetic machinery may represent an important control point in maintaining cellular homeostasis during chronological aging in dinoflagellates.

In this study, transcripts involved in the regulation of gene expression were significantly over-represented in the pool of genes displaying decreased expression during stationary phase. Similar to previous microarray studies of *K. brevis* following acute stress (Lidie 2007), a marked decrease in abundance of transcripts involved in the regulation of transcription and translation was identified, suggesting a similar global decrease in gene expression upon entry of stationary

phase.   Most striking to the enriched category of the regulation of gene expression was the

coordinated downregulation of the PPR proteins. The PPR family of proteins, characterized by a

35 amino acid motif repeated up to 30 times, are nuclear encoded RNA binding proteins that

play essential roles in post-transcriptional processes regulating chloroplast and mitochondrial

gene expression, such as editing, splicing, translation, and RNA stability (Lurin et al. 2004;

Schmitz-Linneweber and Small 2008). Their importance to chloroplast physiology is highlighted

by the large number of PPR genes in plants (400-500) whereas non-photosynthetic eukaryotes

typically possess fewer than five (Pusnik et al. 2007). The *K. brevis* EST library includes over 100

PPR annotations. Although the exact role of PPR proteins in *K. brevis* is unknown, it is clear that

they are dramatically responsive to the transition between growth and stationary phase. Thirty-

four PPR protein transcripts were down – regulated at the entry into stationary phase (48.39%

of the 93 PPR features on the microarray). The PPR protein transcripts also demonstrated a

different expression pattern compared with the overall experimental trend as well as that of all

other enriched categories. These transcripts demonstrated significant repression (average 1.9-

fold) starting on day 10 that became increasingly pronounced as cells proceeded through

stationary phase and into early decline. This phenomenon has also been observed during

nitrogen and phosphorus limitation, whereby N- or P-starved stationary phase cultures

demonstrated marked reduction in PPR transcript abundance. Following addition of the limiting

nutrient (N or P) PPR proteins responded rapidly, with significant induction within 1 h, which

preceded the response of all other transcripts and the resumption in growth (Morey et al. 2011).

Together, these studies demonstrate that PPR protein transcript abundance is responsive to

physiological state and may represent a family of proteins indicative of bloom growth status.

Studies on acute stress response in *K. brevis* previously identified a lack of the classic

stress response at the transcriptional level (Lidie 2007), and counter-intuitively found a general

marked decrease in heat shock protein transcripts, along with a global decrease in transcripts for ribosomal processes, translation, photosynthesis and energy generation that are indicative of stress. The current study similarly identified a global decrease of heat shock protein (HSP) transcripts that corresponded to the pattern of expression of an extensive list of other genes identified to respond to stimuli/stress. HSPs, most notably known for their role in responding to environmental cues also contain housekeeping function by acting as chaperones during protein folding. Along with the marked decrease seen in transcripts involved in the regulation of gene expression, the response of HSPs may indicate a decreased need for chaperone functions during stationary phase of growth.

Calcium ion binding proteins have been identified in many systems to interpret abundance and spatial shifts in calcium and to coordinate subsequently needed metabolic and gene expression changes (Bush 1995). In particular, a calcium based stress surveillance system has been identified in diatoms in response to nitric oxide (NO) (Vardi et al. 2006). However, little is known regarding how calcium is perceived and utilized in the execution decisions in dinoflagellates. In this study, a coordinated decrease in transcripts encoding calcium binding proteins was observed in stationary phase, including calcium dependent protein kinases and calmodulin domain containing proteins capable of activating protein kinase cascades, which have previously been shown to be induced in response to elevated calcium during the plant defense responses and are involved in downstream ROS formation and activation of PCD (Blumwald et al. 1998). The downregulation of these proteins was paralleled by other similarly expressed calcium binding proteins known to function in endoplasmic reticulum homeostasis. Along with calmodulins, calreticulin proteins bind calcium; however, they function in the ER to prevent misfolded proteins from being transported to the cytoplasm. With the downregulation of a resident ER calcium binding protein as well as the coordinated reduction in the expression

of chaperones it appears that calcium homeostasis in the ER is important to the biology of stationary phase. Several other transcripts such as an EF hand protein, a calpain, and voltage dependent p q calcium channels demonstrated reduced expression levels, while calcium transporters are the only class of calcium related proteins with increased expression. The global decrease in calcium related genes, along with the decrease in stress response and gene expression categories is not consistent with several other phytoplankton stress studies (Thamatrakoln et al. 2012; Allen et al., 2008); however, it remains uncertain whether this is a reflection of the differences in dinoflagellate gene expression outputs given the complexity regarding gene expression control mechanisms compared to diatoms. Together, the decreased abundance of calcium binding protein transcripts in conjunction with an increase in calcium transport transcripts is suggestive that the modulation of intracellular calcium levels is an important direction to further investigate in the context of chronological aging in dinoflagellates.

Understanding the regulation of toxin biosynthesis in toxic dinoflagellates is an area of key interest. Brevetoxins are ladder-like polyketide compounds, a structural class unique to dinoflagellates, putatively synthesized by megasynthases called polyketide synthases (PKSs). *K. brevis* produces at least three unique polyketide precursors that generate at least nine unique brevetoxin congers due to the post-cyclization modification of functional groups, as well as a brevetoxin antagonist, brevenal that originates from a shorter chain precursor (Baden et al. 2005). The role brevetoxins play in the biology of *K. brevis* is unknown, although they appear to be constitutively produced with the intracellular concentrations of toxins unchanging over a growth curve (although the ratios of parent and derivative forms do change) (Lekan and Tomas 2010), as well as under a variety of stress conditions (nitrate limitation: 883μM control, 50μM, 10μM, and 1μM; phosphate limitation: 36μM control, 5μM, 1μM, 0.1μM; high light: 150μE control, 300 and 450μE; salinity: 36 ppt control, 22, 30, and 40 ppt) (Monroe 2008). This makes

the investigation of their biosynthetic pathways all the more challenging. A number of full length PKS gene transcripts have been identified in *K. brevis* with sequence homology to Type I PKS's, but gene structure unique to the dinoflagellate, all of which contain the spliced leader sequence (Monroe and Van Dolah 2008). However, the roles of these proteins in brevetoxin biosynthesis remain to be confirmed, including whether they are in fact producing polyketides or fatty acids, as they are chloroplast localized (Monroe et al. 2010), but the mature brevetoxin molecule is absent from the chloroplast (Zippay et al, unpubl.). In the current study, 12 of 24 PKS gene probes present on the array were downregulated in stationary phase cells. Together, these data suggest that brevetoxins are not classical "secondary metabolites", which are by definition produced when cells are stressed or aging.

CONCLUSION

The present study identified a significant reorganization of the transcriptome over the growth curve of *K. brevis*, an organism thought to use extensive post-transcriptional regulation of gene expression mediated by SL *trans*-splicing. The transcriptome demonstrated differential expression of transcripts for key processes involved in energy production, including photosynthesis, electron transport chain, and carbon metabolism that suggests a metabolic restructuring needed for coping with conditions encountered during stationary phase, and may provide important clues for their survival strategies during chronological aging. The overall decrease in transcripts for genes involved in the regulation of transcription and translation during stationary phase is similar to that seen in *K. brevis* in response to abiotic stress, and likely reflects the reduced metabolic state of aging cells. An unexpected finding of this study was the differential expression of gene transcripts involved in calcium binding, transport, and signaling during aging that highlights the importance of defining the role of calcium homeostasis in

dinoflagellates aging. Lastly, the transcriptome of aging *K. brevis* cells revealed that PKS gene transcripts, putatively involved in brevetoxin biosynthesis, also decreased during stationary phase. This expression pattern is not consistent with a classical secondary metabolite, which raises the question as to the role of brevetoxins in the cell or the role of the known PKS genes in brevetoxin biosynthesis. While further research is needed to discern the functions of many of the *K. brevis* transcripts responsive to the transition between growth and maintenance phases, this transcriptomic fingerprint of quiescent *K. brevis* provides a basis from which to understand the chronological aging process in a dinoflagellate.

REFERENCES

Abraham WM, Bourdelais AJ, Ahmed A, Serebriakov I, Baden DG (2005) Effects of Inhaled Brevetoxins in Allergic Airways: Toxin–Allergen Interactions and Pharmacologic Intervention. Environ Health Perspect 113: 632 - 637

Allen, Andrew E. and LaRoche, Julie and Maheswari, Uma and Lommer, Markus and Schauer, Nicolas and Lopez, Pascal J. and Finazzi, Giovanni and Fernie, Alisdair R. and Bowler, Chris (2008) Whole-cell response of the pennate diatom *Phaeodactylum tricornutum* to iron starvation. PNAS 105: 10438-10443

Bachvaroff TR, Place AR (2008) From stop to start: tandem gene arrangement, copy number and *trans*-splicing sites in the dinoflagellate *Amphidinium carterae*. PLoS One 3: e2929

Baden D (1989) Brevetoxins: unique polyether dinoflagellate toxins. The FASEB Journal 3: 1807-1817

Baden DG, Bourdelais AJ, Jacocks H, Michelliza S, Naar J (2005) Natural and derivative brevetoxins: historical background, multiplicity, and effects. Environ Health Perspect 113: 621 - 625

Baden DG, Mende TJ (1979) Amino acid utilization by *Gymnodinium breve*. Phytochemistry 18: 247-251

Bidle KD, Bender SJ (2008) Iron starvation and culture age activate metacaspases and programmed cell death in the marine diatom *Thalassiosira pseudonana*. Eukaryot Cell 7: 223-236

Bidle KD, Falkowski PG (2004) Cell death in planktonic, photosynthetic microorganisms. Nat Rev Microbiol 2: 643-655

Blumwald E, Aharon GS, C-H. Lam B (1998) Early signal transduction pathways in plant pathogen interactions. Trends Plant Sci 3: 342-346

Brand LE, Compton A (2007) Long-term increase in *Karenia brevis* abundance along the Southwest Florida Coast. Harmful Algae 6: 232-252

Bush DS (1995) Calcium Regulation in Plant Cells and its Role in Signaling. Ann Rev Plant Physio 46: 95-122

Carmona-Gutierrez D, Eisenberg T, Buttner S, Meisinger C, Kroemer G, Madeo F (2010) Apoptosis in yeast: triggers, pathways, subroutines. Cell Death Differ 17: 763-773

Conesa A, Götz S, García-Gómez JM, Terol J, Talón M, Robles M (2005) Blast2GO: a universal tool for annotation, visualization and analysis in functional genomics research. Bioinformatics 21: 3674-3676

Escoubas JM, Lomas M, LaRoche J (1995) Light intensity regulation of cab gene transcription is signaled by the redox state of the plastoquinone pool. P Natl Acad Sci USA 92: 10237-10241

Evens TJ, Kirkpatrick GJ, Millie DF, Chapman DJ, Schofield OME (2001) Photophysiological responses of the toxic red-tide dinoflagellate *Gymnodinium breve* (Dinophyceae) under natural sunlight. Journal of Plankton Research 23: 1177-1194

Fabrizio P, Li L, Longo VD (2005) Analysis of gene expression profile in yeast aging chronologically. Mech Ageing Dev 126: 11-16

Fabrizio P, Longo VD (2003) The chronological life span of *Saccharomyces cerevisiae*. Aging Cell 2: 73-81

Fey V, Wagner R, Bräutigam K, Pfannschmidt T (2005) Photosynthetic redox control of nuclear gene expression. J Exp Bot 56: 1491-1498

Fleming LE, Backer LC, Baden DG (2005) Overview of Aerosolized Florida Red Tide Toxins: Exposures and Effects. Environ Health Perspect 113

Flewelling LJ, Naar JP, Abbott JP, Baden DG, Barros NB, Bossart GD, Bottein MY, Hammond DG, Haubold EM, Heil CA, Henry MS, Jacocks HM, Leighfield TA, Pierce RH, Pitchford TD, Rommel SA, Scott PS, Steidinger KA, Truby EW, Van Dolah FM, Landsberg JH (2005) Brevetoxicosis: red tides and marine mammal mortalities. Nature 435: 755-756

Franklin D, Brussaard C, Berges J (2006) What is the role and nature of programmed cell death in phytoplankton ecology? Eur J Phycol 41: 1-14

Gasch AP, Spellman PT, Kao CM, Carmel-Harel O, Eisen MB, Storz G, Botstein D, Brown PO (2000) Genomic expression programs in the response of yeast cells to environmental changes. Mol Biol Cell 11: 4241-4257

Goldshmidt H, Matas D, Kabi A, Carmi S, Hope R, Michaeli S (2010) Persistent ER stress induces the spliced leader RNA silencing pathway (SLS), leading to programmed cell death in *Trypanosoma brucei*. PLoS Pathog 6: e1000731

Hallegraeff GM (1993) A review of harmful algal blooms and their apparent global increase. Phycologia 32: 79-99

Hayes R, Kudla J, Gruissem W (1999) Degrading chloroplast mRNA: the role of polyadenylation. Trends Biochem Sci 24: 199-202

Heil CA, Steidinger KA (2009) Monitoring, management, and mitigation of *Karenia* blooms in the eastern Gulf of Mexico. Harmful Algae 8: 611-617

Hoagland P, Scatasta S (2006). Ecological Studies 189: Ecology of Harmful Algae. E. Graneli and J. T. Turner. Springer-Verlag, Berlin: 391-402.

Komine Y, Kikis E, Schuster G, Stern D (2002) Evidence for in vivo modulation of chloroplast RNA stability by 3'-UTR homopolymeric tails in *Chlamydomonas reinhardtii*. P Natl Acad Sci USA 99: 4085-4090

Komine Y, Kwong L, Anguera MC, Schuster G, Stern DB (2000) Polyadenylation of three classes of chloroplast RNA in *Chlamydomonas reinhardtii*. RNA 6: 598-607

Kudla J, Hayes R, Gruissem W (1996) Polyadenylation accelerates degradation of chloroplast mRNA. Embo J 15: 7137-7146

Larkin SL, Adams CM (2007) Harmful algal blooms and coastal business: Economic consequences in Florida. Society & Natural Resources 20: 849-859

Leary DJ, Huang S (2001) Regulation of ribosome biogenesis within the nucleolus. FEBS Lett 509: 145-150

Lekan DK, Tomas CR (2010) The brevetoxin and brevenal composition of three *Karenia brevis* clones at different salinities and nutrient conditions. Harmful Algae 9: 39-47

Levasseur M, Thompson PA, Harrison PJ (1993) Physiological acclimation of marine phytoplankton to different nitrogen sources. J Phycol 29: 587-595

Lidie KB (2007). Characterization and regulation of gene expression networks in response to acute environmental stress in the Florida red tide dinoflagellate, *Karenia brevis*. Charleston, SC, Medical University of South Carolina.

Lidie KB, Ryan JC, Barbier M, Van Dolah FM (2005) Gene expression in Florida red tide dinoflagellate *Karenia brevis*: analysis of an expressed sequence tag library and development of DNA microarray. Mar Biotechnol 7: 481-493

Lidie KB, Van Dolah FM (2007) Spliced leader RNA-mediated trans-splicing in a dinoflagellate, *Karenia brevis*. J Eukaryot Microbiol 54: 427-435

Lisitsky I, Klaff P, Schuster G (1996) Addition of destabilizing poly(A)-rich sequences to endonuclease cleavage sites during the degradation of chloroplast mRNA. P Natl Acad Sci USA 93: 13398-13403

Lisitsky I, Kotler A, Schuster G (1997) The mechanism of preferential degradation of polyadenylated RNA in the chloroplast - the exoribonuclease 100RNP/polynucleotide phosphorylase displays high binding affinity for poly(A) sequence. J Biol Chem 272: 17648-17653

LozaTavera T, Hayes R, Kudla J, Schuster G, Gruissem W (1996) Regulation of chloroplast mRNA processing and stability. Plant Physiol 111: 50002-50002

Lurin C, Andres C, Aubourg S, Bellaoui M, Bitton F, Bruyere C, Caboche M, Debast C, Gualberto J, Hoffmann B, Lecharny A, Le Ret M, Martin-Magniette M-L, Mireau H, Peeters N, Renou J-P, Szurek B, Taconnat L, Small I (2004) Genome-wide analysis of *Arabidopsis*

pentatricopeptide repeat proteins reveals their essential role in organelle biogenesis. Plant Cell 16: 2089-2103

Martinez MJ, Roy S, Archuletta AB, Wentzell PD, Anna-Arriola SS, Rodriguez AL, Aragon AD, Quinones GA, Allen C, Werner-Washburne M (2004) Genomic analysis of stationary-phase and exit in *Saccharomyces cerevisiae*: gene expression and identification of novel essential genes. Mol Biol Cell 15: 5295-5305

Matecic M, Smith DL, Pan X, Maqani N, Bekiranov S, Boeke JD, Smith JS (2010) A microarray-based genetic screen for yeast chronological aging factors. PLoS Genet 6: e1000921

Miller-Morey JS, Van Dolah FM (2004) Differential responses of stress proteins, antioxidant enzymes, and photosynthetic efficiency to physiological stresses in the Florida red tide dinoflagellate, *Karenia brevis*. Comp Biochem Phys C 138: 493-505

Monroe EA (2008). Characterization of polyketide synthases in the Florida red tide dinoflagellate *Karenia brevis*. Molecular Cellular Biology and Pathobiology. Charleston, Medical University of South Carolina. PhD: 193.

Monroe EA, Johnson JG, Wang ZH, Pierce RK, Van Dolah FM (2010) Characterization and expression of nuclear-encoded polyketide synthases in the brevetoxin-producing dinoflagellate *Karenia brevis*. J Phycol 46: 541-552

Monroe EA, Van Dolah FM (2008) The toxic dinoflagellate *Karenia brevis* encodes novel type I-like polyketide synthases containing discrete catalytic domains. Protist 159: 471-482

Morey J, Monroe E, Kinney A, Beal M, Johnson J, Hitchcock G, Van Dolah F (2011) Transcriptomic response of the red tide dinoflagellate, *Karenia brevis*, to nitrogen and phosphorus depletion and addition. BMC Genomics 12: 346

Mulholland MR, Bernhardt PW, Heil CA, Bronk DA, O'Neil JM (2006) Nitrogen fixation and release of fixed nitrogen by *Trichodesmium* spp. in the Gulf of Mexico. Limnol Oceanogr 51: 20-20

Okamoto OK, Hastings JW (2003) Genome-wide analysis of redox-regulated genes in a dinoflagellate. Gene 321: 73-81

Patterson TA, Lobenhofer EK, Fulmer-Smentek SB, Collins PJ, Chu T-M, Bao W, Fang H, Kawasaki ES, Hager J, Tikhonova IR, Walker SJ, Zhang L, Hurban P, de Longueville F, Fuscoe JC, Tong W, Shi L, Wolfinger RD (2006) Performance comparison of one-color and two-color platforms within the Microarray Quality Control (MAQC) project. Nat Biotech 24: 1140-1150

Prince EK, Myers TL, Naar J, Kubanek J (2008) Competing phytoplankton undermines allelopathy of a bloom-forming dinoflagellate. P Roy Soc Lond B Bio 275: 2733-2741

Pusnik M, Small I, Read LK, Fabbro T, Schneider A (2007) Pentatricopeptide repeat proteins in *Trypanosoma brucei* function in mitochondrial ribosomes. Mol Cell Biol 27: 6876-6888

Roux AE, Chartrand P, Ferbeyre G, Rokeach LA (2010) Fission yeast and other yeasts as emergent models to unravel cellular aging in eukaryotes. J Gerontol A Biol Sci Med Sci 65: 1-8

Schaeffer BA, Kamykowski D, McKay L, Sinclair G, Milligan EJ (2007) A comparison of photoresponse among ten different *Karenia brevis* (Dinophyceae) isolates. J Phycol 43: 702-714

Schaeffer BA, Kamykowski D, Sinclair G, McKay L, Milligan EJ (2009) Diel vertical migration thresholds of *Karenia brevis* (Dinophyceae). Harmful Algae 8: 692-698

Schmitz-Linneweber C, Small I (2008) Pentatricopeptide repeat proteins: a socket set for organelle gene expression. Trends Plant Sci 13: 663-670

Segovia M, Haramaty L, Berges JA, Falkowski PG (2003) Cell death in the unicellular chlorophyte *Dunaliella tertiolecta*. A hypothesis on the evolution of apoptosis in higher plants and metazoans. Plant Physiol. 132: 99-105

Shi L, Tong W, Su Z, Han T, Han J, Puri RK, Fang H, Frueh FW, Goodsaid FM, Guo L, Branham WS, Chen JJ, Xu ZA, Harris SC, Hong H, Xie Q, Perkins RG, Fuscoe JC (2005) Microarray scanner calibration curves: characteristics and implications. BMC Bioinformatics 6 Suppl 2: S11

Sinclair G, Kamykowski D, Glibert PM (2009) Growth, uptake, and assimilation of ammonium, nitrate, and urea, by three strains of *Karenia brevis* grown under low light. Harmful Algae 8: 770-780

Small ID, Peeters N (2000) The PPR motif - a TPR-related motif prevalent in plant organellar proteins. Trends Biochem Sci 25: 45-47

Stumpf RP, Litaker RW, Lanerolle L, Tester PA (2008) Hydrodynamic accumulation of *Karenia* off the west coast of Florida. Cont Shelf Res 28: 189-213

Tandeau de Marsac N, Houmard J (1993) Adaptation of cyanobacteria to environmental stimuli: new steps towards molecular mechanisms. FEMS Microbiology Letters 104: 119-189

Taylor RC, Cullen SP, Martin SJ (2008) Apoptosis: controlled demolition at the cellular level. Nat Rev Mol Cell Biol 9: 231-241

Thamatrakoln K., Korenovska O., Niheu A. K., Bidle K. D. (2011). Whole-genome expression analysis reveals a role for death-related genes in stress acclimation of the diatom *Thalassiosira pseudonana*. Environ. Microbiol. 14, 67–81.

Van Dolah FM (2000) Marine algal toxins: Origins, health effects, and their increased occurrence. Environ Health Persp Supp 108: 133

Van Dolah FM, Leighfield TA, Kamykowski D, Kirkpatrick GJ (2008) Cell cycle behavior of laboratory and field populations of the Florida red tide dinoflagellate, *Karenia brevis*. Cont Shelf Res 28: 11-23

Van Dolah FM, Lidie KB, Monroe EA, Bhattacharya D, Campbell L, Doucette GJ, Kamykowski D (2009) The Florida red tide dinoflagellate *Karenia brevis*: New insights into cellular and molecular processes underlying bloom dynamics. Harmful Algae 8: 562-572

Van Dolah FM, Lidie KB, Morey JS, Brunelle SA, Ryan JC, Monroe EA, Haynes BL (2007) Microarray analysis of diurnal- and circadian-regulated genes in the Florida red-tide dinoflagellate *Karenia brevis* (Dinophyceae). J Phycol 43: 741-752

Vanhamme L, Pays E (1995) Control of gene expression in trypanosomes. Microbiol. Rev. 59: 223-240

Vardi A, Berman-Frank I, Rozenberg T, Hadas O, Kaplan A, Levine A (1999) Programmed cell death of the dinoflagellate *Peridinium gatunense* is mediated by CO_2 limitation and oxidative stress. Curr Biol 9: 1061-1064

Vardi A, Formiggini F, Casotti R, De Martino A, Ribalet F, et al. (2006) A Stress Surveillance System Based on Calcium and Nitric Oxide in Marine Diatoms. PLoS Biol 4(3): e60.

Vargo GA (2009) A brief summary of the physiology and ecology of *Karenia brevis* Davis (G. Hansen and Moestrup comb. nov.) red tides on the West Florida Shelf and of hypotheses posed for their initiation, growth, maintenance, and termination. Harmful Algae 8: 573-584

Vargo GA, Heil CA, Fanning KA, Dixon LK, Neely MB, Lester K, Ault D, Murasko S, Havens J, Walsh J, Bell S (2008) Nutrient availability in support of *Karenia brevis* blooms on the central West Florida Shelf: What keeps *Karenia* blooming. Cont Shelf Res 28: 73-98

Walsh JJ, Jolliff JK, Darrow BP, Lenes JM, Milroy SP, Remsen A, Dieterle DA, Carder KL, Chen FR, Vargo GA, Weisberg RH, Fanning KA, Muller-Karger FE, Shinn E, Steidinger KA, Heil CA, Tomas CR, Prospero JS, Lee TN, Kirkpatrick GJ, Whitledge TE, Stockwell DA, Villareal TA, Jochens AE, Bontempi PS (2006) Red tides in the Gulf of Mexico: Where, when, and why? J. Geophys. Res. 111: C11003

Walsh JJ, Steidinger KA (2001) Saharan dust and Florida red tides: The cyanophyte connection. J. Geophys. Res. 106: 11597-11612

Weng L, Dai H, Zhan Y, He Y, Stepaniants SB, Bassett DE (2006) Rosetta error model for gene expression analysis. Bioinformatics 22: 1111-1121

Zhang H, Hou Y, Miranda L, Campbell DA, Sturm NR, Gaasterland T, Lin S (2007) Spliced leader RNA trans-splicing in dinoflagellates. Proc Natl Acad Sci U S A 104: 4618-4623

Zhang H, Lin S (2009) Retrieval of missing spliced leader in dinoflagellates. PLoS One 4: e4129

Table 1. Primers used in qPCR validation analysis.

Contig	Sequence Description	Forward Primer Sequence	Reverse Primer Sequence	Annealing Temp.
2963	Poly (ADP - ribose) polymerase member 1	AGTGCAAGTGGTAGCAGTGA	TTCATTCCAAAGTTGTGTGG	55°C
5714	Peptidase caspase catalytic subunit p20	GACACTTCTCTCGGAAGCAT	CAAGACGTGTCTTCACTTCG	57°C
3257	Pentatricopeptide repeat protein	GGCTTGTCGCCTGACATATT	TGAGCACCTCACTGAGCAAC	60°C
9479	Photosystem II 44 kDa protein	GGTGGTCTGGAAATGCTCGATT	GGTCAACACCCCAGCCTAATGT	58°C
6216	Endoplasmic reticulum resident calcium binding protein	AGACAAGGATGGCTTTCTCA	CGTTCTTGTCAGCATCAAAG	60°C
6057	Antagonist of mitotic exit network 1 homolog	CACTGATCGGAGCCTGCAAA	GACTTGGCGCCCAGAGAGAT	62°C
4846	Hypothetical protein	CCCGTGAGGCATGATGGAA	CGGTGGTTTGCAGCAGGTT	55°C
9926	Mitogen activated protein kinase ser/thr kinase	ATGCACCAGATGTTCAAGTG	TTCTCATCATATGCCACAGG	54°C
8400	Peptidylproyl isomerase	TGCAAATTGAAGACAGAGGA	AAGCGACCGAAAATTCTCTA	54°C
117	Ubiquitin - ribosomal protein fusion s27a	GGAGCTTTCCGCAGAAATGAG	AGACACACTTACTTGGCAA	54°C
4994	Mitogen activated protein kinase	AGTTGTTTACGAGGCAAAGG	ACGTCGTAGATCCGCAGTAT	57°C

Table 2: GO enrichment analysis (Standard and GO SLIM) for up - regulated and down - regulated clusters in the one-color format.

A. Enriched GO terms with <u>increased</u> abundance in stationary phase (FDR < 0.05)

GO Term	Name	FDR	single test p-Value	# in test group	# in reference group	# non annot test	# non annot reference group	Over/ Under
GO:0044429†	mitochondrial part	2.20E-04	4.90E-07	26	44	398	2650	over
GO:0009055†	electron carrier activity	7.70E-04	4.90E-06	22	38	402	2656	over
GO:0045263†	factor F(o)	7.70E-04	5.80E-06	7	1	417	2693	over
GO:0033177†	transporting domain	7.70E-04	5.80E-06	7	1	417	2693	over
GO:0005743†	mitochondrial inner membrane	1.80E-03	1.90E-05	15	20	409	2674	over
GO:0019866†	organelle inner membrane	1.80E-03	1.90E-05	15	20	409	2674	over
GO:0031966†	mitochondrial membrane	3.80E-03	4.10E-05	16	25	408	2669	over
GO:0009152†	purine ribonucleotide biosynthetic process	5.50E-03	6.20E-05	14	20	410	2674	over
GO:0009206†	purine ribonucleoside triphosphate biosynthetic process	6.00E-03	9.10E-05	13	18	411	2676	over
GO:0009145†	purine nucleoside triphosphate biosynthetic process	6.00E-03	9.10E-05	13	18	411	2676	over
GO:0046933†	rotational mechanism	6.00E-03	1.00E-04	10	10	414	2684	over
GO:0009260†	ribonucleotide biosynthetic process	6.40E-03	1.30E-04	14	22	410	2672	over
GO:0009142†	nucleoside triphosphate biosynthetic process	6.40E-03	1.30E-04	13	19	411	2675	over
GO:0009201†	ribonucleoside triphosphate biosynthetic process	6.40E-03	1.30E-04	13	19	411	2675	over
GO:0006754†	ATP biosynthetic process	6.90E-03	1.90E-04	11	14	413	2680	over
GO:0015986†	ATP synthesis coupled proton transport	6.90E-03	1.90E-04	11	14	413	2680	over
GO:0015985†	gradient	6.90E-03	1.90E-04	11	14	413	2680	over
GO:0034220†	ion transmembrane transport	6.90E-03	1.90E-04	11	14	413	2680	over
GO:0046961†	mechanism	1.00E-02	2.70E-04	10	12	414	2682	over
GO:0016021†	integral to membrane	1.70E-02	3.60E-04	59	227	365	2467	over
GO:0006164†	purine nucleotide biosynthetic process	1.80E-02	4.10E-04	15	29	409	2665	over
GO:0042254†	**ribosome biogenesis**	**1.80E-02**	**4.70E-04**	**16**	**33**	**408**	**2661**	**over**
GO:0022613†	ribonucleoprotein complex biogenesis	1.80E-02	4.70E-04	16	33	408	2661	over
GO:0005739*	mitochondrion	1.90E-02	2.10E-04	44	150	375	2540	over
GO:0044444*	cytoplasmic part	1.90E-02	7.10E-04	119	569	300	2121	over
GO:0016020*	membrane	1.90E-02	8.10E-04	107	502	312	2188	over
GO:0031224†	intrinsic to membrane	2.00E-02	6.40E-04	59	233	365	2461	over
GO:0019829†	cation-transporting ATPase activity	2.00E-02	6.40E-04	10	14	414	2680	over
GO:0009150†	purine ribonucleotide metabolic process	2.60E-02	8.30E-04	14	28	410	2666	over
GO:0046034†	ATP metabolic process	2.60E-02	8.90E-04	11	18	413	2676	over
GO:0015078†	hydrogen ion transmembrane transporter activity	2.80E-02	1.10E-03	12	22	412	2672	over
GO:0006163†	purine nucleotide metabolic process	2.80E-02	1.20E-03	15	33	409	2661	over
GO:0009144†	purine nucleoside triphosphate metabolic process	2.90E-02	1.30E-03	13	26	411	2668	over
GO:0009205†	purine ribonucleoside triphosphate metabolic process	2.90E-02	1.30E-03	13	26	411	2668	over
GO:0008289‡	lipid binding	2.90E-02	1.40E-03	8	10	416	2684	over
GO:0009259†	ribonucleotide metabolic process	2.90E-02	1.40E-03	14	30	410	2664	over
GO:0055085†	transmembrane transport	2.90E-02	1.40E-03	14	30	410	2664	over
GO:0031090†	organelle membrane	2.90E-02	1.50E-03	28	89	396	2605	over
GO:0015077†	transporter activity	2.90E-02	1.50E-03	12	23	412	2671	over
GO:0006091*	**generation of precursor metabolites and energy**	**3.30E-02**	**2.10E-03**	**30**	**102**	**389**	**2588**	**over**
GO:0043227*	membrane-bounded organelle	3.30E-02	2.40E-03	138	703	281	1987	over
GO:0043231*	intracellular membrane-bounded organelle	3.30E-02	2.40E-03	138	703	281	1987	over
GO:0043226*	organelle	3.30E-02	2.80E-03	167	882	252	1808	over
GO:0043229*	intracellular organelle	3.30E-02	2.80E-03	167	882	252	1808	over
GO:0009199†	ribonucleoside triphosphate metabolic process	3.70E-02	1.70E-03	13	27	411	2667	over
GO:0009141†	nucleoside triphosphate metabolic process	3.70E-02	1.70E-03	13	27	411	2667	over
GO:0044085†	cellular component biogenesis	4.10E-02	1.90E-03	16	39	408	2655	over
GO:0033279†	ribosomal subunit	4.30E-02	2.00E-03	7	8	417	2686	over
GO:0008168†	methyltransferase activity	4.50E-02	2.30E-03	24	74	400	2620	over
GO:0044422†	organelle part	4.50E-02	2.30E-03	93	434	331	2260	over

Table 2 (cont.): GO enrichment analysis (Standard and GO SLIM) for up - regulated and down - regulated clusters in the one-color format.

B. Enriched GO terms with decreased abundance in stationary phase (FDR < 0.05)

GO Term	Name	FDR	single test p-Value	# in test group	# in reference group	# non annot test	# non annot reference group	Over/ Under
GO:0005488‡	binding	7.90E-05	1.80E-07	365	1725	109	919	over
GO:0006950‡	**response to stress**	**8.20E-04**	**6.90E-05**	**52**	**154**	**422**	**2490**	**over**
GO:0050896*	response to stimulus	1.20E-03	5.10E-05	63	198	410	2438	over
GO:0003676‡	nucleic acid binding	6.00E-03	2.00E-05	101	360	373	2284	over
GO:0032559†	adenyl ribonucleotide binding	1.60E-02	9.00E-05	105	395	369	2249	over
GO:0005524†	ATP binding	1.60E-02	1.00E-04	104	392	370	2252	over
GO:0005509†	**calcium ion binding**	**1.80E-02**	**2.40E-04**	**46**	**138**	**428**	**2506**	**over**
GO:0051082†	unfolded protein binding	1.80E-02	2.60E-04	22	46	452	2598	over
GO:0001883†	purine nucleoside binding	1.80E-02	2.80E-04	108	423	366	2221	over
GO:0001882†	nucleoside binding	1.80E-02	2.80E-04	108	423	366	2221	over
GO:0030554†	adenyl nucleotide binding	1.80E-02	2.80E-04	108	423	366	2221	over
GO:0030246*	carbohydrate binding	2.40E-02	1.20E-03	13	22	460	2614	over
GO:0065007*	biological regulation	2.70E-02	1.70E-03	72	273	401	2363	over
GO:0050789*	regulation of biological process	2.70E-02	2.10E-03	61	224	412	2412	over
GO:0044249*	cellular biosynthetic process	2.70E-02	2.80E-03	64	241	409	2395	over
GO:0034645*	cellular macromolecule biosynthetic process	2.70E-02	2.80E-03	64	241	409	2395	over
GO:0009059*	macromolecule biosynthetic process	2.70E-02	2.80E-03	64	241	409	2395	over
GO:0010468†	**regulation of gene expression**	**3.30E-02**	**4.80E-04**	**57**	**191**	**417**	**2453**	**over**
GO:0031974†	membrane-enclosed lumen	4.60E-02	6.10E-04	14	23	460	2621	over

Terms indicated in **bold** are respresented in Figures 3 - 5

† Term identified from Standard GO analysis only

* Term identified from GO SLIM analysis only

‡ Term identified from both Standard and GO SLIM analysis

Table 3. 1 vs. 2 Color Comparison - Numbers of significantly changing features

		# of 1-Color features	# of 2-Color features	% of total 1-Color # Changers	% of total 2-Color # Changers
Day 4	Up	1	3	0.03%	0.13%
Day 10	Up	114	128	3.85%	5.72%
Day 14	Up	1368	722	46.25%	32.29%
Day 18	Up	237	455	8.01%	20.35%
Day 4	Down	33	0	1.12%	0.00%
Day 10	Down	166	219	5.61%	9.79%
Day 14	Down	1489	1257	50.34%	56.22%
Day 18	Down	114	320	3.85%	14.31%
Day 4	Total	34	3	1.15%	0.13%
Day 10	Total	280	347	9.47%	15.52%
Day 14	Total	2857	1979	96.59%	88.51%
Day 18	Total	351	775	11.87%	34.66%
Up Cluster		1413	924	47.77%	41.32%
Down Cluster		1545	1312	52.23%	58.68%
Total # Changers		2958	2236		

Table 4. 1 vs. 2 Color Comparison - Shared enrichment categories and number of features shared.

	# of 1-Color features	# of 2-Color features	% of 1-Color
Polyketide Synthases	12	10	83.33%
Gen of Prec Met and Energy	31	22	70.97%
Ribosome Biogenesis	16	9	56.25%
Gene Expression	57	48	84.21%
Pentatricopeptide Repeat Proteins	43	30	69.77%
Response to Stress	56	49	87.50%
Calcium Binding	46	41	89.13%

Red	Enrichment Category - up
Green	Enrichment Category - down
Blue	Interest Category
Bold	Enrichment Categories found in both 1 and 2 Color sets

Table 5. Comparison of qPCR validation results.

	1 Color				2 Color	
	Spear. Rho	p value			Spear. Rho	p value
Overall	**0.9278**	**< 0.0001**		**Overall**	**0.9301**	**< 0.0001**
Day 4	0.1818	0.5926		Day 4	0.4636	0.1509
Day 10	0.9273	< 0.0001		Day 10	0.9273	< 0.0001
Day 14	0.7818	0.0045		Day 14	0.8091	0.0026
Day 18	0.9364	< 0.0001		Day 18	0.9364	< 0.0001

Table 6. Contigs from *K. brevis* EST library with associated GO Term: Cell Death (GO:0008219)

Contig	Description	E-value	D4	D10	D14	D18
11181	ankyrin repeat and kinase domain containing 1	2.73E-09	0.00	-0.06	0.08	0.05
912	ankyrin unc44	8.74E-12	-0.04	-0.13	0.00	-0.10
5649	aspartic protease	1.01E-43	0.06	-0.04	-0.04	-0.04
3779	ataxia telangiectasia mutated	2.46E-62	-0.03	-0.11	**-0.27**	-0.13
5943	atp gtp binding protein	1.26E-30	0.08	0.00	0.09	-0.01
3897	bifunctional apoptosis regulator	6.83E-09	0.01	0.08	**0.23**	0.09
6341	budding uninhibited by benzimidazoles 1beta	1.08E-16	0.01	0.03	-0.04	-0.07
1034	calreticulin	2.44E-95	-0.03	-0.07	**-0.70**	-0.12
804	caspase recruitment domainmemberisoform cra_b	5.82E-08	0.01	0.07	**0.26**	0.05
7922	cathepsin b	7.38E-29	-0.02	-0.04	0.05	-0.03
10047	cathepsin e	1.86E-15	0.02	-0.06	-0.14	-0.06
5430	death-associated protein kinase 1	2.17E-07	0.01	0.04	0.11	-0.06
2746	death-associated protein kinase 3	4.85E-18	-0.03	-0.18	**-0.32**	-0.18
3891	death-associated protein kinase 3	9.74E-17	0.02	-0.07	-0.06	-0.06
9795	dna ligase iv	1.93E-23	0.01	-0.15	**-0.38**	-0.16
7401	dna repair helicase rad25 family protein	1.15E-83	0.01	-0.22	**-0.51**	-0.15
3605	domain containing protein	2.02E-16	0.04	-0.02	-0.03	-0.12
7733	dual specificity phosphatase 22	1.04E-16	-0.06	-0.07	0.07	0.10
2842	dynamin 1-like	3.39E-46	-0.06	-0.02	-0.08	-0.11
8430	ef-hand domain (c-terminal) containing 1	1.83E-36	0.04	-0.03	0.02	-0.06
3624	elegans proteinconfirmed by transcript evidence	5.27E-33	0.00	0.00	0.16	0.12
4061	enhanced disease resistance 1	2.88E-04	0.08	-0.15	**-0.30**	-0.17
4509	fk506 binding proteinisoform cra_b	1.11E-06	-0.06	-0.08	-0.22	-0.16
9720	glutaredoxin 2	8.08E-06	0.02	0.01	0.16	0.07
3805	jumonji domain containing 6	7.77E-16	0.06	0.03	0.12	-0.02
3832	kinesin light chain 3	1.22E-29	0.03	-0.09	-0.09	-0.15
3698	l-asparaginase i	7.66E-07	0.05	-0.14	**-0.24**	-0.21
5647	metacaspase	2.29E-04	-0.01	-0.09	**-0.30**	-0.09
1663	metacaspase	7.06E-25	0.00	0.09	0.12	0.07
1664	metacaspase	2.30E-21	0.01	0.00	-0.09	-0.03
10244	metacaspase 5	1.58E-36	0.04	0.00	0.05	-0.03
5512	metacaspase type ii	3.16E-08	0.00	-0.04	-0.09	0.00
11202	metacaspase-like protein	5.17E-09	0.07	-0.15	**-0.27**	-0.15
11415	n terminus of rad21 rec8 like protein	5.41E-10	-0.03	-0.12	**-0.56**	-0.17
383	novel protein	2.35E-18	0.00	0.06	**-0.39**	-0.04
4844	novel protein	4.14E-15	-0.09	-0.03	-0.18	-0.07
6183	novel protein	2.32E-26	0.03	0.01	-0.17	-0.10
8289	nuclear serine protease2	2.07E-48	0.04	-0.01	-0.04	-0.03
7707	peptidasecaspase catalytic subunit p20	4.56E-12	0.01	0.00	0.16	0.04
8400	peptidylprolyl isomerase d	7.31E-39	-0.02	0.12	**0.28**	0.10
10450	phosphatidylinositol 3-kinase	1.66E-11	0.03	0.00	0.02	0.01
11852	protein	1.58E-12	0.03	-0.04	0.05	-0.03
9799	protein arginine n-methyltransferase	7.74E-14	0.03	0.06	0.19	-0.02
2480	protein phosphatase 2a	5.03E-138	0.02	0.09	0.13	**0.25**
6904	rraga protein	1.00E-63	0.04	0.12	0.09	0.14
538	sac3 ganp domain protein	6.73E-14	-0.05	0.00	**0.24**	-0.10
7633	slingshot-related protein	2.40E-18	-0.03	0.06	0.06	0.08
11407	thioredoxin domain containing 5	6.33E-08	0.03	0.06	-0.05	0.09
6692	tnf receptor-associated factor 6	1.87E-09	0.01	-0.09	-0.05	-0.01
4515	tpr domain protein	7.78E-35	-0.01	-0.10	**-0.23**	-0.07
6313	tpr repeat-containing protein	6.57E-12	-0.01	-0.01	-0.12	-0.06
9084	tpr repeat-containing protein	4.14E-05	0.07	0.02	0.07	0.01
11276	tumor necrosis factormember 5-induced protein 1	4.60E-08	0.03	-0.04	0.14	0.06
8327	wd repeat domainlike	4.39E-13	-0.42	-0.31	**0.37**	-0.51
10749	wd-40 repeat protein	2.03E-15	-0.09	0.16	**0.26**	0.08
5363	werner syndrome protein	1.19E-12	-0.09	-0.01	-0.12	-0.04
6805	white	8.57E-07	0.00	0.01	0.17	0.02
6980	ww domain-containing oxidoreductase	2.77E-19	0.01	0.15	**0.34**	0.15

Bold indicates log ratio values associated with a p-value < 0.0001

63

Figure 1. One color microarray workflow.

| RNA extracted from 1L cultures (n= 3/time point) | → | 480ng Cy3 labeled cRNA/sample hybridized to single array (n= 15) | → | One – way ANOVA (intensity values, n = 3/timepoint) (p < 0.01), Bonferroni Multiple Test Correction (p < 0.01) (5006 features) | → | Tukey Kramer post-hoc test (n = Day 4 (131), 10 (1492), 14 (4521), and 18 (2583) versus Day 6, p < 0.10) | → | Weighted average composite arrays generated for each time point (n = 4) |

| Total number of features significantly changing over the *K. brevis* growth curve (n = 2958)

Day 4 (35)
Day 10 (280)
Day 14 (2857)
Day 18 (351) | ← | Signal intensity > 70 counts at all time points (n = 2958) | ← | 0.23 log ratio difference (1.7 fold change) from day 6 and composite array p value < 0.0001 (n = 3034) | ← | Log ratio expression change calculated for each feature versus day 6 for all time points (n = 10263 features/array) |

Figure 2. *K. brevis* **abundance and growth rate over the growth curve.**

Independent biological triplicate cultures were sampled for cell abundance (■) and average

division•day^{-1} ± standard deviation were calculated for each time point (□). Time points

denoted by (★) were used for microarray analysis.
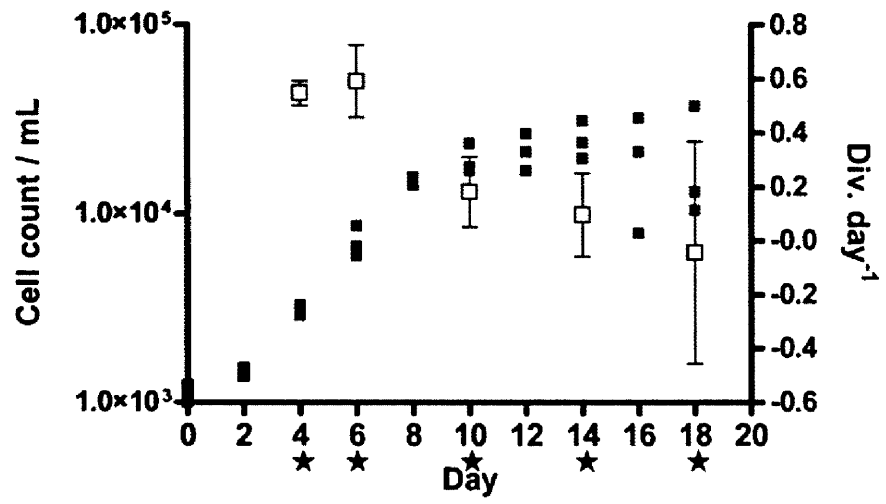
Figure 3. Global and enriched expression profiles of genes differentially expressed over the growth curve.

Transcripts that met all statistical requirements outlined in Figure 1 were clustered using a Euclidean distance metric by an Agglomerative clustering algorithm (2958 features total) **(A)**. Each horizontal line represents one gene and the intensity of color is proportional to the log ratio difference versus day 6. The two major clusters identified (increased expression (red), n = 1413 and decreased expression (green), n = 1545) were plotted over time in a trend plot (2958 features total) **(B)**. Gene ontology enrichment was determined relative to all sequences on the array using a modified Fisher's Exact Test in Blast2GO (FDR < 0.05). The plotted values are the average log ratio change for all probes in the category. GO Enrichment analysis resulted in five major functional categories. Red indicates significantly enriched categories with increased expression, green indicates significantly enriched categories with decreased expression, and blue indicates specific functional categories determined by manual data mining (Pentatricopeptide Repeat Proteins and Polyketide Synthases). Increased expression cluster: GO:0042254 Ribosome Biogenesis, FDR = 1.8E-02; GO:0006091 Generation of Precursor Metabolites and Energy, FDR = 3.3E-02; Decreased expression cluster: GO:0005509 Calcium Binding, FDR = 1.8E-02; GO:0006950 Response to Stress, FRD = 8.2E-04; GO:0010468 Regulation of Gene Expression, FDR = 3.3E-04) **(C)**.

A.

| Day | 4 | 10 | 14 | 18 |

-2.0   0   2.0

Log Ratio
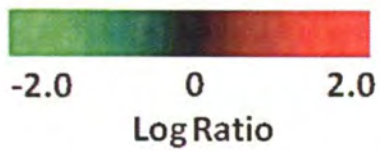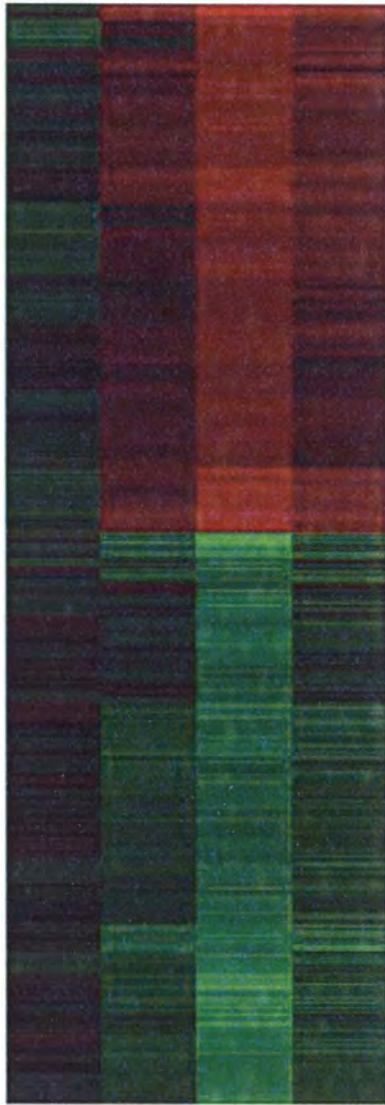
B.
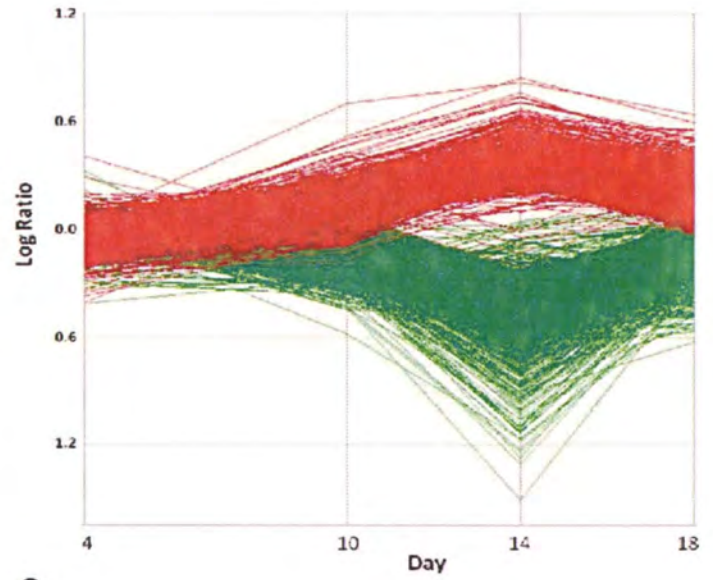
C.
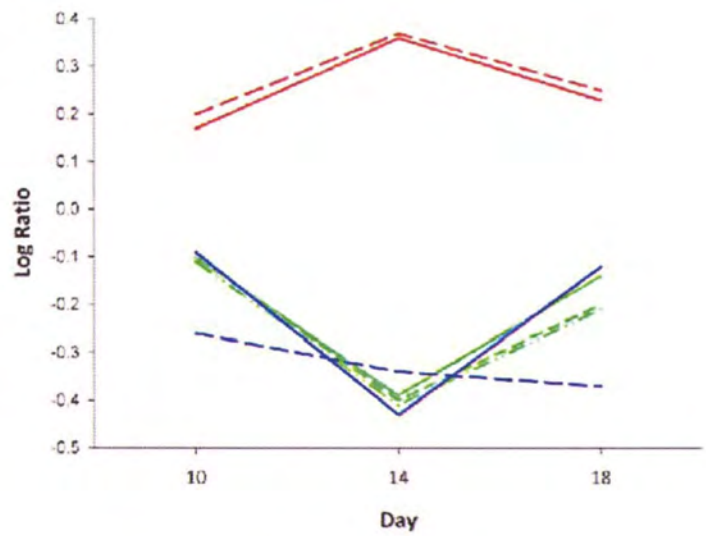
- - - Ribosome Biogenesis
——— Generation of Precursor Metabolites and Energy
——— Calcium Binding
- - - Response to Stress
-··-··- Regulation of Gene Expression
——— Polyketide Synthases
- - - Pentatricopeptide Repeat Proteins

Figure 4. Heat map of transcript abundance for GO terms significantly enriched in the increased expression cluster.

Log ratio profiles for transcripts for the Generation of Precursor Metabolites and Energy **(A)** and Ribosome Biogenesis **(B)** GO terms, identified to be enriched are represented for day 10, 14, and 18 timepoints. Transcripts not identified by enrichment analysis, but by manual data mining (not included in enrichment statistic) are represented by (*). Abbreviations: PS, photosystem; ATP, adenosine triphosphate generation; ETC, electron transport chain; GLY, glycolysis; TCA, citric acid cycle; TNP, transporter activity.

A. GO:0006091 Gen. of Prec. Metabolites. and Energy, FDR = 3.3E-02

	Contig	Day 10 14 18	Contig Description
PS	10994		photosystem i p700 apoprotein a2
	11850		photosystem i p700 chlorophyll a1
	239		chloroplast ferredoxin
	3516		chloroplast ferredoxin
	3213		chloroplast light harvesting protein
	1743		chloroplast light harvesting protein
	1654		chloroplast light harvesting protein
	1430		cytochrome b6-f complex iron-sulfur
	1939		flavodoxin
	356		flavodoxin
	1259		fucoxanthin chlorophyll a c protein
	1252		fucoxanthin chlorophyll a c protein
	1279		fucoxanthin chlorophyll a c protein
	3652		photosystem ii oxygen evolving complex
	1414		plastocyanin
	4535		plastocyanin
ATP	1500		atp synthase f0 subunit 9
	865		atp synthase f0 subunit 9
	114		atp synthase f0 subunit 9
	222		atp synthase f0 subunit 9
	1879		atp synthase f0 subunit 9
	787		atp synthase f0 subunit 9
	3084		atp synthase f0 subunit c
	9902		atp synthase subunit h family protein
	260		atph+mitochondrial f1 alpha subunit
	8266		atph+mitochondrial f1 beta subunit
	4809		inorganic pyrophosphatase
ETC	9925		cytochrome c oxidase subunit 2
	4705		cytochrome c oxidase subunit 2a
	685		cytochrome c oxidase subunit 2a
	7414		electron-transfer-beta polypeptide
GLY + TCA	1755*		glyceraldehyde-3-phosphate dehydrogenase
	2474*		phosphoglycerate kinase 2
	777*		malate dehydrogenase
	4786*		phosphoglycerate mutase
	5584*		succinate-ligase (adp-forming)
	9133*		atp citratesubunit
	7859*		aldo keto reductase family
	9984*		chloroplast fructose--bisphosphatase
	7125*		fructose-bisphosphateclass ii
	6427*		isocitratenadp-dependent
	358*		isocitrate dehydrogenase

B. GO:0042254 Ribosome Biogenesis, FDR = 1.8E-02

Contig	Day 10 14 18	Contig Description
10838		30s ribosomal protein s14
7526		30s ribosomal protein s4
10146		60s ribosomal protein l21
11420		60s ribosomal protein l34
1866		brix domain containing 2
5758		chromosome 14 open reading frame 169
11072		elongation factor ef-2
1867		elongation factor ts
551		euk. translation init. subunit e interacting prot.
11890		hypothetical protein
5220		loc564078 protein
8322		ribosomal protein
9596		ribosomal protein
9851		ribosomal protein l16
4126		ribosomal protein l19-like protein
3653		ribosomal protein s2
719		ribosomal protein s27a
10220		ribosome biogenesis protein
10607		translation initiation factor
6625		translation initiation factor if-2
117		ubiquitin-ribosomal protein fusion s27a
1332*		atp-dependent dead h rna helicase
9114*		atp-dependent rna helicase p62
1950*		chromodomain helicase dna binding protein
9048*		chromodomain helicase-dna-binding protein 3
11417*		dead (asp-glu-ala-asp) box polypeptide 51
9010*		deah (asp-glu-ala-asp his) box polypeptide 57
4971*		drh1 (dead box rna helicase 1)
8780*		drh1 (dead box rna helicase 1)
2978*		rna helicase-like
10099*		fibrillarin
4994*		mitogen-activated protein kinase
9926*		mitogen-activated ser/thr protein kinase
9168*		rna helicase

Log Ratio

> -0.4   0   0.4 <

Figure 5. Heat map of transcript abundance for GO terms significantly enriched in the decreased expression cluster.

Log ratio profiles for transcripts for the Regulation of Gene Expression **(A)**, Response to Stress **(B)**, and Calcium Binding **(C)** GO term categories identified to be enriched are represented for day 10, 14, and 18 timepoints. Transcripts not identified by enrichment analysis, but by manual data mining (not included in enrichment statistic) are represented by (*).

A: GO:0006950 Response to Stress, FDR = 8.2E-04

Day

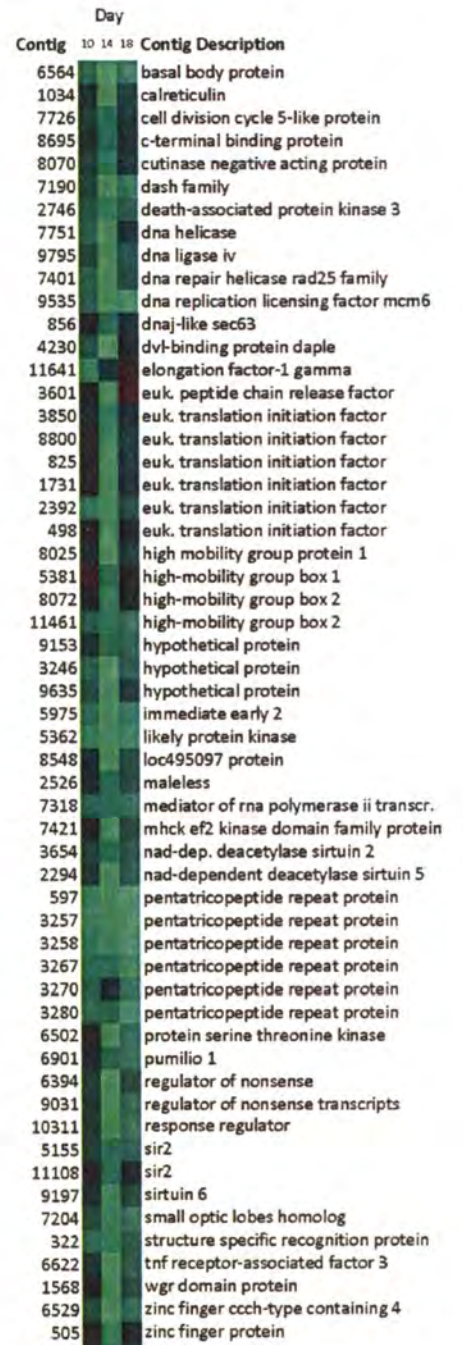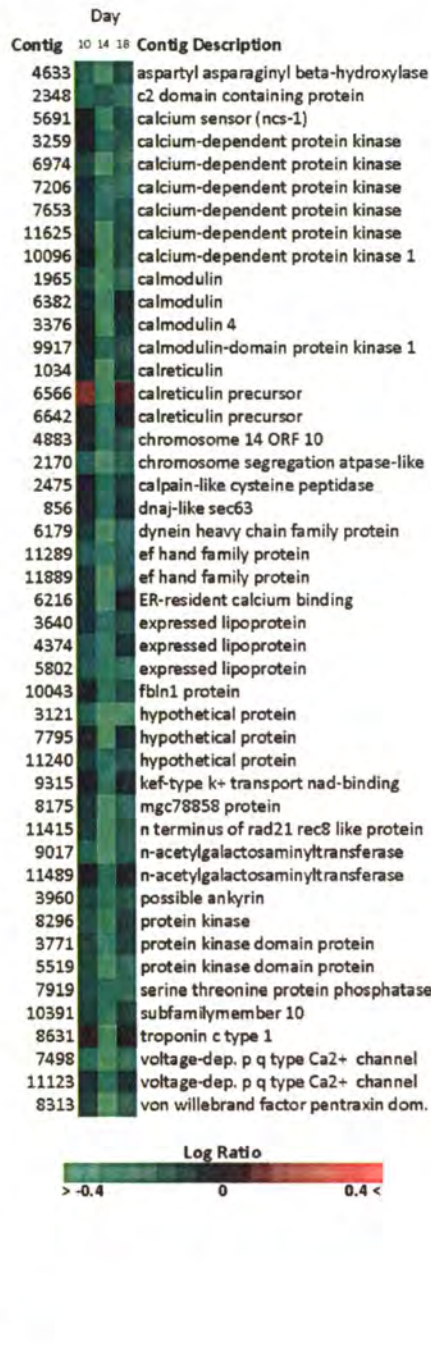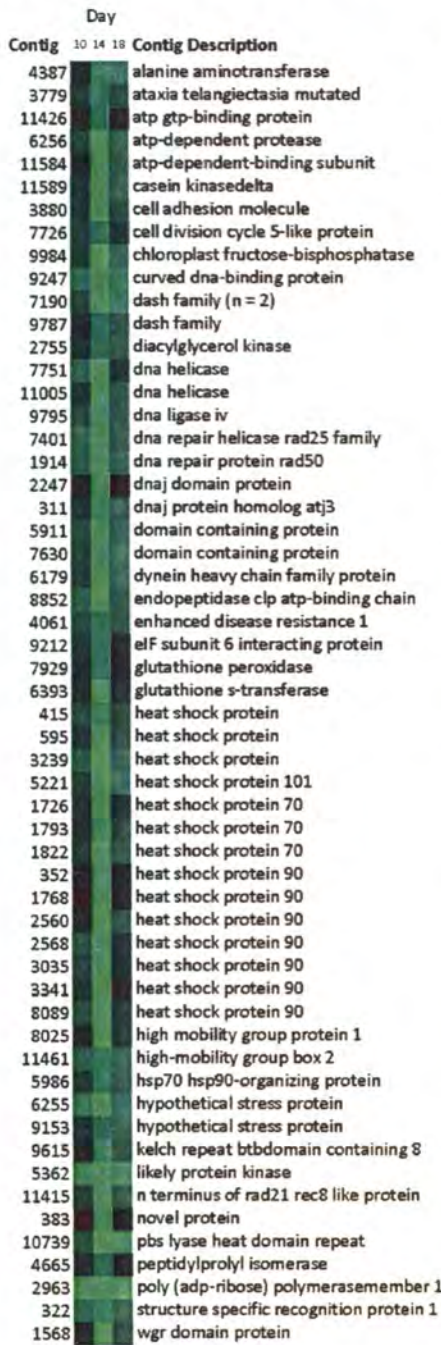| Contig	10	14	18	Contig Description
4387				alanine aminotransferase
3779				ataxia telangiectasia mutated
11426				atp gtp-binding protein
6256				atp-dependent protease
11584				atp-dependent-binding subunit
11589				casein kinasedelta
3880				cell adhesion molecule
7726				cell division cycle 5-like protein
9984				chloroplast fructose-bisphosphatase
9247				curved dna-binding protein
7190				dash family (n = 2)
9787				dash family
2755				diacylglycerol kinase
7751				dna helicase
11005				dna helicase
9795				dna ligase iv
7401				dna repair helicase rad25 family
1914				dna repair protein rad50
2247				dnaj domain protein
311				dnaj protein homolog atj3
5911				domain containing protein
7630				domain containing protein
6179				dynein heavy chain family protein
8852				endopeptidase clp atp-binding chain
4061				enhanced disease resistance 1
9212				eIF subunit 6 interacting protein
7929				glutathione peroxidase
6393				glutathione s-transferase
415				heat shock protein
595				heat shock protein
3239				heat shock protein
5221				heat shock protein 101
1726				heat shock protein 70
1793				heat shock protein 70
1822				heat shock protein 70
352				heat shock protein 90
1768				heat shock protein 90
2560				heat shock protein 90
2568				heat shock protein 90
3035				heat shock protein 90
3341				heat shock protein 90
8089				heat shock protein 90
8025				high mobility group protein 1
11461				high-mobility group box 2
5986				hsp70 hsp90-organizing protein
6255				hypothetical stress protein
9153				hypothetical stress protein
9615				kelch repeat btbdomain containing 8
5362				likely protein kinase
11415				n terminus of rad21 rec8 like protein
383				novel protein
10739				pbs lyase heat domain repeat
4665				peptidylprolyl isomerase
2963				poly (adp-ribose) polymerasemember 1
322				structure specific recognition protein 1
1568				wgr domain protein

B: GO: 0005509 Calcium Binding, FDR = 1.8E-02

Day

Contig	10	14	18	Contig Description
4633				aspartyl asparaginyl beta-hydroxylase
2348				c2 domain containing protein
5691				calcium sensor (ncs-1)
3259				calcium-dependent protein kinase
6974				calcium-dependent protein kinase
7206				calcium-dependent protein kinase
7653				calcium-dependent protein kinase
11625				calcium-dependent protein kinase
10096				calcium-dependent protein kinase 1
1965				calmodulin
6382				calmodulin
3376				calmodulin 4
9917				calmodulin-domain protein kinase 1
1034				calreticulin
6566				calreticulin precursor
6642				calreticulin precursor
4883				chromosome 14 ORF 10
2170				chromosome segregation atpase-like
2475				calpain-like cysteine peptidase
856				dnaj-like sec63
6179				dynein heavy chain family protein
11289				ef hand family protein
11889				ef hand family protein
6216				ER-resident calcium binding
3640				expressed lipoprotein
4374				expressed lipoprotein
5802				expressed lipoprotein
10043				fbln1 protein
3121				hypothetical protein
7795				hypothetical protein
11240				hypothetical protein
9315				kef-type k+ transport nad-binding
8175				mgc78858 protein
11415				n terminus of rad21 rec8 like protein
9017				n-acetylgalactosaminyltransferase
11489				n-acetylgalactosaminyltransferase
3960				possible ankyrin
8296				protein kinase
3771				protein kinase domain protein
5519				protein kinase domain protein
7919				serine threonine protein phosphatase
10391				subfamilymember 10
8631				troponin c type 1
7498				voltage-dep. p q type Ca2+ channel
11123				voltage-dep. p q type Ca2+ channel
8313				von willebrand factor pentraxin dom.

Log Ratio

> -0.4   0   0.4 <

C: GO:0010468 Reg. of Gene Expression, FDR = 3.3E-04)

Day

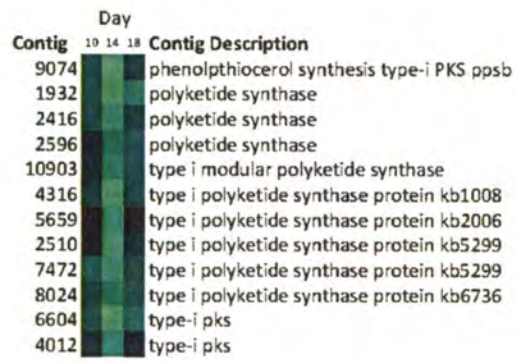| Contig	10	14	18	Contig Description
6564				basal body protein
1034				calreticulin
7726				cell division cycle 5-like protein
8695				c-terminal binding protein
8070				cutinase negative acting protein
7190				dash family
2746				death-associated protein kinase 3
7751				dna helicase
9795				dna ligase iv
7401				dna repair helicase rad25 family
9535				dna replication licensing factor mcm6
856				dnaj-like sec63
4230				dvl-binding protein daple
11641				elongation factor-1 gamma
3601				euk. peptide chain release factor
3850				euk. translation initiation factor
8800				euk. translation initiation factor
825				euk. translation initiation factor
1731				euk. translation initiation factor
2392				euk. translation initiation factor
498				euk. translation initiation factor
8025				high mobility group protein 1
5381				high-mobility group box 1
8072				high-mobility group box 2
11461				high-mobility group box 2
9153				hypothetical protein
3246				hypothetical protein
9635				hypothetical protein
5975				immediate early 2
5362				likely protein kinase
8548				loc495097 protein
2526				maleless
7318				mediator of rna polymerase ii transcr.
7421				mhck ef2 kinase domain family protein
3654				nad-dep. deacetylase sirtuin 2
2294				nad-dependent deacetylase sirtuin 5
597				pentatricopeptide repeat protein
3257				pentatricopeptide repeat protein
3258				pentatricopeptide repeat protein
3267				pentatricopeptide repeat protein
3270				pentatricopeptide repeat protein
3280				pentatricopeptide repeat protein
6502				protein serine threonine kinase
6901				pumilio 1
6394				regulator of nonsense
9031				regulator of nonsense transcripts
10311				response regulator
5155				sir2
11108				sir2
9197				sirtuin 6
7204				small optic lobes homolog
322				structure specific recognition protein
6622				tnf receptor-associated factor 3
1568				wgr domain protein
6529				zinc finger ccch-type containing 4
505				zinc finger protein
3195				zinc finger protein

Figure 6. Heat map of transcript abundance for Pentatricopeptide Repeat Proteins (A) and

Polyketide Synthases (B).

Log ratio profiles for transcripts for the PPR **(A)** and PKS **(B)**

for day 10, 14, and 18 timepoints.

A. Pentatricopeptide Repeat Proteins

B. Polyketide Synthases

	Day			
Contig	10	14	18	**BLAST E-value**
2853				7.08E-30
3292				1.42E-30
3255				1.24E-28
3254				2.25E-15
3266				3.25E-06
3278				1.09E-31
3307				8.15E-30
3287				6.37E-21
3258				2.26E-38
3279				3.15E-33
3288				0.00E+00
3271				7.19E-13
3261				3.14E-19
3291				8.68E-36
3973				4.57E-33
3308				2.12E-05
3257				9.51E-26
3280				1.93E-23
3293				2.36E-21
4443				6.58E-15
597				1.24E-12
3267				6.51E-09
3556				2.61E-33
3262				3.40E-04
4928				8.41E-21
3295				3.62E-07
3548				5.50E-38
3558				2.71E-27
5241				7.81E-14
3234				6.45E-10
5847				4.57E-14
4823				2.02E-21
3270				3.03E-13
3256				7.49E-13
8747				4.25E-09
3310				1.43E-07
6768				2.50E-14
5635				5.20E-19
5733				2.30E-22
11089				0.00E+00
5752				1.02E-10
3276				5.26E-21
3272				4.63E-23
4824				2.36E-20
3263				5.23E-18

	Day			
Contig	10	14	18	**Contig Description**
9074				phenolpthiocerol synthesis type-i PKS ppsb
1932				polyketide synthase
2416				polyketide synthase
2596				polyketide synthase
10903				type i modular polyketide synthase
4316				type i polyketide synthase protein kb1008
5659				type i polyketide synthase protein kb2006
2510				type i polyketide synthase protein kb5299
7472				type i polyketide synthase protein kb5299
8024				type i polyketide synthase protein kb6736
6604				type-i pks
4012				type-i pks

Log Ratio

> -0.4   0   0.4 <

Figure 7. Validation of microarray results by quantitative PCR (qPCR).

Eleven genes were selected for validation of the microarray results by qPCR. Overall, there was a correlation of 0.9278 across the time series (Spearman's Rho, $p < 0.0001$, n = 33). The correlations at the day 10, 14, and 18 time points were 0.9364 ($p < 0.0001$, n = 11), 0.7818 ($p = 0.0045$, n = 11), and 0.9364 ($p < 0.0001$, n = 11), respectively.

Contig		10	14	18	Contig Description
2963	qPCR	-0.89	-0.35	-0.33	Poly (ADP - ribose) polymerase member 1
	MA	-0.59	-1.17	-0.40	
5714	qPCR	-0.15	-0.43	-0.17	Peptidase caspase catalytic subunit p20
	MA		-0.32		
3257	qPCR	-0.32	-0.47	0.23	Pentatricopeptide repeat protein
	MA	-0.37	-0.46	-0.55	
9479	qPCR	-0.28	-0.67		Photosystem II 44kDa protein
	MA	-0.27	-0.31		
6216	qPCR	-0.24	-1.10	-0.17	Endoplasmic reticulum resident calcium binding protein
	MA		-0.77		
6057	qPCR	-0.51	-1.23	-0.66	Antagonist of mitotic exit network 1 homolog
	MA	-0.26	-0.54	-0.35	
4846	qPCR				Hypothetical protein
	MA		0.15		
9926	qPCR	0.17	0.20	0.13	Mitogen activated protein kinase ser/thr kinase
	MA	0.27	0.45	0.23	
8400	qPCR		0.27	0.10	Peptidylproyl isomerase
	MA	0.11	0.28	0.10	
117	qPCR	0.18	0.27	0.37	Ubiquitin - ribosomal protein fusion s27a
	MA	0.28	0.49	0.44	
4994	qPCR	0.11	0.35	0.13	Mitogen activated protein kinase
	MA		0.34	0.21	

Log Ratio

> -0.4   0   0.4 <

Figure 8. Comparison of log ratio estimate results from 1-color and 2-color format.

Each point represents a feature on the microarray (n = 10263). Blue line represents the linear regression (y = 0.8257x − 0.0189, r2 = 0.8560, p < 0.0001). The one-color and two-color log ratio values are significantly correlated (r = 0.9252, p < 0.0001).

$$y = 0.8257x - 0.0189$$
$$r^2 = 0.8560, p < 0.0001$$
$$\text{Pearson } r = 0.9252, p < 0.0001$$

Two-Color Log Ratio Values

One-Color Log Ratio Values
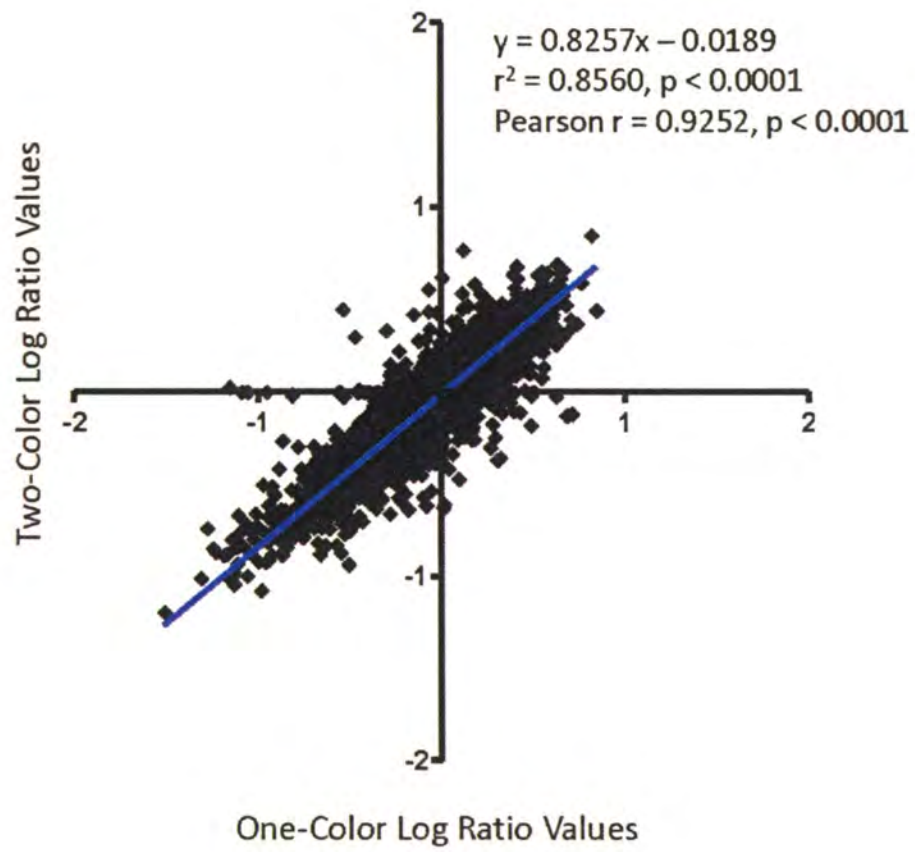
Figure 9. Common gene list results for one versus two-color microarray data based on

differentially expressed genes

Contig number **(A)** and Enrichment Categories **(B)** shared between the two microarray formats.

A.

Contig Comparison: 1 vs. 2 Color Format

1 Color
Down (1545)

9   417

1119

2 Color
Down (1312)

1   192

703   709   206

1 Color
Up (1413)
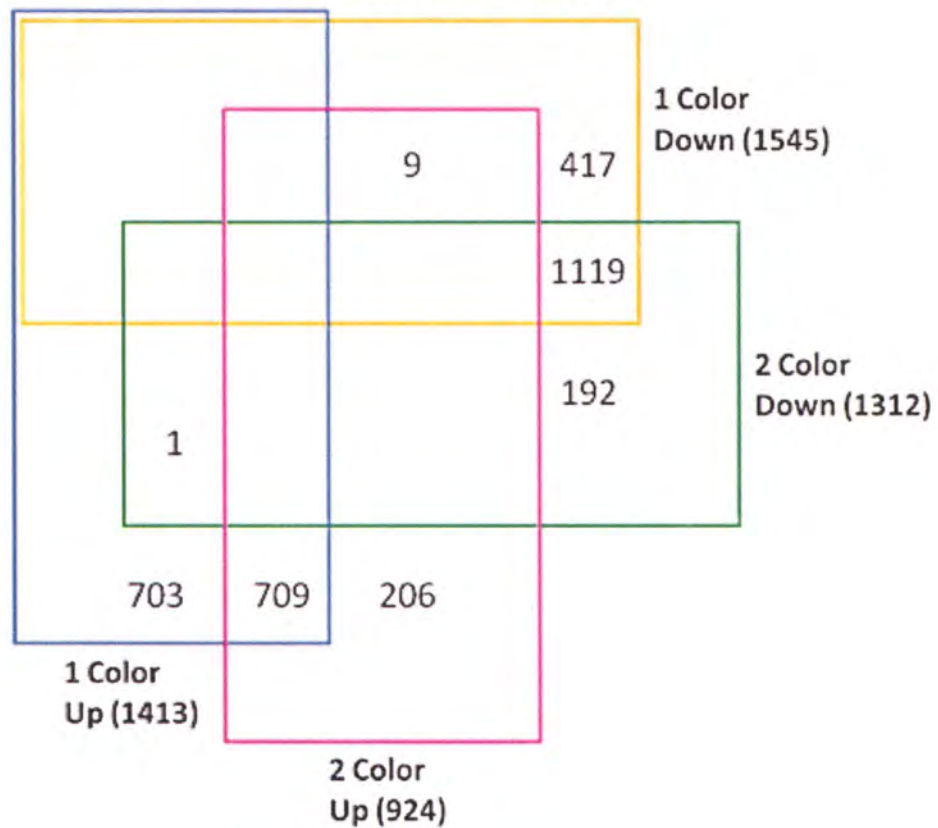
2 Color
Up (924)

B.

GO Enrichment Comparison: 1 vs. 2 Color Format

1 Color
Down (19)

15

4

2 Color
Down (7)

3

11   39   11

1 Color
Up (50)

2 Color
Up (50)
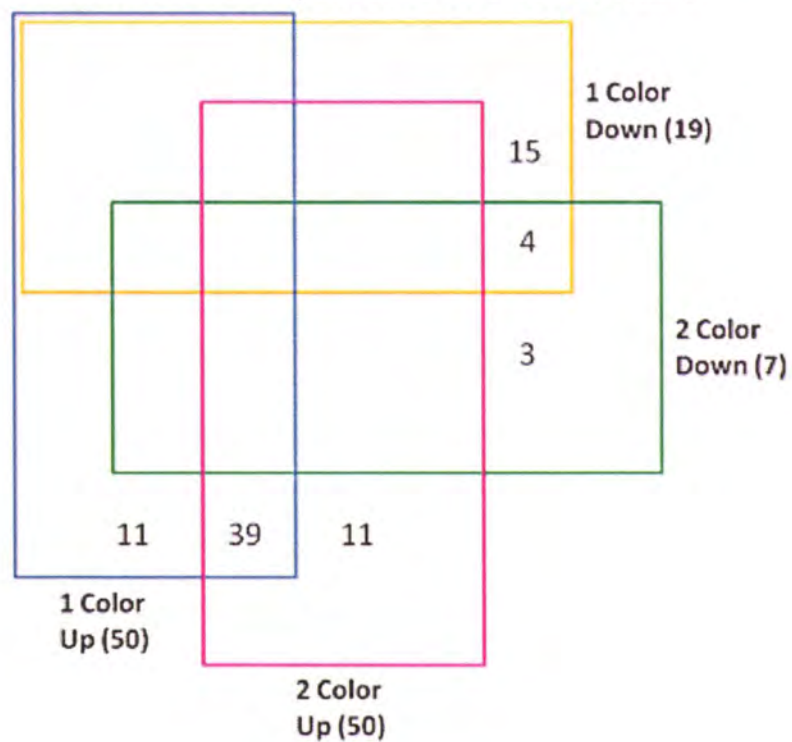
CHAPTER 3

PROGRAMMED CELL DEATH IN *K. BREVIS*

INTRODUCTION

Caspases, cysteine aspartic acid proteases, are key metazoan enzymes involved in potentiating signals through the programmed cell death (PCD) pathway. PCD, an active, genetically controlled process leading to the orderly destruction of damaged cells, has been identified as a key regulator of cell growth, development, and death. Caspase enzymes, divided into two functional categories, function in a cascade whereby the initiator enzymes (casp. 2, 8, 9, 10) work to regulate and activate the executioner caspases (casp. 3, 6, 7). The downstream executioner caspase enzymes cleave a diverse set of targets, such as proteins supporting the structural integrity of the cell (i.e. lamins and actin), proteins that integrate extracellular matrix interaction (i.e. focal adhesion and desmosome proteins), as well as general maintenance functions such as transcription, translation, DNA repair, and other metabolic processes (reviewed in Degterev and Yuan 2008; Taylor et al. 2008). Until recently, the PCD process was deemed unique to metazoans; however, molecularly regulated cell death has now been observed for plants, fungi, protozoa, bacteria, and archaea species.

Caspase homologs, termed metacaspases, were identified more than a decade ago in plants, fungi, and protists, including phytoplankton, and defined as clan CD cys proteases with the presence of a structurally homologous caspase/hemoglobinase fold (Uren et al. 2000). In addition to containing the well-conserved catalytic domain (p20), metacaspases contain a C-terminal domain reminiscent of a p10 caspase domain. Metacaspases have been delineated into Type I or Type II depending on whether the enzyme contains a prodomain (Type I) or an extended linker region between the p20 and p10 domains (Type II) (Tsiatsiani et al. 2011). The presence of a conserved histidine/cysteine catalytic dyad at the predicted active site within the

p20 domain, with the cysteine residue capable of acting as a nucleophile for substrate peptide bond hydrolysis, initially suggested that observed caspase activities measured by canonical caspase fluorogenic probes in these organisms could be attributed to metacaspases. Further *in silico* and biochemical analyses for metacaspase enzymes have since distinguished metacaspases as coordinating strict cleavage after basic residues, namely arginine and lysine, rather than aspartic acid as do metazoan caspases. This distinct biochemical difference has led to contradictory reports on the connection between caspase-like activities and the functional role of metacaspases in non-metazoans (reviewed in Tsiatsiani et al. 2011).

To date, no bona fide caspase enzymes with aspartic acid specificity have been identified in any phytoplankton species. However, caspase-like activity is present. Studies on caspase-like activity in microalgae have provided key information for understanding the evolutionary lineage for the PCD pathway and have shifted the paradigm for understanding population regulation, fitness, and selection, and as such the ecological contexts and consequences in the environment for these types of organisms (Franklin et al. 2006). Caspase-like activity is observed in death processes induced by various stressors such as nutrient starvation (Bidle and Bender 2008), dark treatment (Segovia et al. 2003; Segovia and Berges 2009), high light (Berman-Frank et al. 2004), CO_2 limitation (Vardi et al. 1999), viral infection (Bidle et al. 2007), and protein synthesis inhibition (Segovia and Berges 2005). Caspase activities associated with cellular aging have been also been documented during iron limitation in the diatom, *Thalassiosira pseudonana* (Bidle and Bender 2008), while more recent studies have further defined a larger context for caspase activity in regulating stress acclimation (Bidle et al. 2010; Thamatrakoln et al. 2011). Together, these findings have directed our interest in investigating the role of caspases or their homologs in chronological aging and cell death processes in *K. brevis*.

Caspase 3-like activity has been previously documented in *Karenia brevis* over a long term sampling regime; however, in that study DEVDase activity only spiked during a technical temperature failure, therefore, the involvement of caspase-like activity during the aging process of *K. brevis* remains unclear (Bouchard and Purdie 2011). In addition, the enzymes responsible for caspase-like activities observed in phytoplankton remain unresolved. The acidic cleavage pocket of metacaspases studied to date in plants, fungi, protists, and other phytoplankton species, results in Arg/Lys specificity in the P1 position of their substrate targets (Vercammen et al. 2004; Watanabe and Lam 2005), and not the Asp specificity of caspases; thus, it is evident that other candidate proteins need to be considered to gain insight into the mechanisms controlling caspase-like activity in phytoplankton. Biochemical analyses demonstrate a number of enzymes in plants posess caspase-like activity, including vacuolar processing enzyme (Hatsugai et al. 2004), proteasome subunit B1 (Hatsugai et al. 2009), and subtilisins (Chichkova et al. 2010). These provide clues for additional candidate caspase-like enzymes in phytoplankton. Similarly, while the activation of caspase-like activity has been documented in phytoplankton, no studies to date have defined the target proteins with caspase cleavage motifs. Identifying both the caspase-like enzymes and substrates for the caspase activities in phytoplankton will provide a basis for understanding the connections between signaling pathways, metabolic processes, and death programs in an evolutionary and ecological context.

In the current study, a combination of biochemical analyses and *in silico* EST sequence data mining was employed to identify the role caspase activity may play in the chronological aging and death processes in *K. brevis* and to identify the upstream and downstream pathway constituents of caspase-like activities. Quantification of caspase 1, 3/7, 6, 8, and 9-like activities was carried out to gain an understanding of their presence, timing, and magnitude during chronological aging. Next, a short-term ROS challenge was employed to assess a role for

caspase-like enzyme activity in death processes. DNA fragmentation, caspase-like activity, and

caspase 3-like protein expression were used to define PCD-like morphological changes present

in *K. brevis*. Targeted *in silico* bioinformatic mining was then used to identify enzymes

potentially responsible for the activities observed, as well as the substrates, by taking into

account both substrate sequence context and functional annotation information. Finally, *K.

brevis* S-adenosylmethionine synthetase (KbAdoMetS), a putative caspase substrate predicted

from the bioinformatics screen, was examined using matrix-associated laser desorption

ionization time of flight (MALDI-TOF) mass spectrometry (MS) to confirm if it is capable of being

cleaved at the proposed caspase DEVD motif by recombinant human caspase 3. Taken together,

this project identifies for the first time that *K. brevis* contains morphological changes indicative

of a PCD-like pathway. ROS-driven PCD in this organism appears to be coordinated by caspase-

like enzymes that are distinctive from the metacaspase family.

METHODS

Culture Maintenance and Sampling Regime

Karenia brevis (Wilson isolate) was maintained in batch cultures in 1-L glass bottles with

autoclaved, 20 μm filtered seawater at 36 psu obtained from the Vero Beach Field Station

seawater system at the Florida Institute of Technology. Seawater was enriched with modified

f/2 medium with 0.01 mM selenous acid (final concentration) and ferric sequestrene used in

place of EDTA $\cdot Na_2$ and $FeCl_3 \cdot 6H_2O$. Cultures were maintained on a 16:8 light-dark cycle, with

illumination from cool white lights at a photon flux density of 50 – 65 $\mu E \cdot m^{-2} \cdot sec^{-1}$ measured

with a LiCor 2pi meter at 25°C. Twenty - one 900 mL batch cultures were inoculated at a starting

concentration of approximately 1000 cells/mL, from a mid-logarithmic stage starter culture on

day 0. Independent triplicate cultures were sampled every other day from day 6 to 18. Cell

abundance and growth rates were determined for each sample using a Beckman Coulter

Multisizer 3. The specific growth rate and divisions per day were calculated as: Specific growth

rate; $K' = Ln (N2 / N1) / (t2 - t1)$, where N1 and N2 = biomass at time1 (t1) and time2 (t2),

respectively, and divisions per day as; $Div.day^{-1} = K' / Ln2$ (Levasseur et al. 1993).

Photosynthetic Efficiency (F_V/F_M)

To obtain an indication of photosynthetic health, the maximum photochemical quantum

yield of photosystem II (F_V/F_M) was determined using the method of (Vincent et al. 1984) with

modifications. Briefly, 3 mL of *K. brevis* culture from each experimental sample were dark

adapted for 30 minutes. The initial fluorescence emitted when all reaction centers are open (F_O)

was read on a Turner Designs Model 10-AU Fluorometer (Sunnyvale, CA). Cultures were then

exposed to 0.03 μM DCMU (3-3,4-Dichlorophenyl)-1,1-dimethylurea) (Sigma) to reduce Q_A, the

first electron acceptor of photosystem II, and maximal fluorescence (F_M) was read. PSII quantum

efficiency, F_V/F_M, defined as $(F_O - F_M)/F_M$ was determined for each sample.

Cell viability

Cell death was quantified using the mortal stain, SYTOX green (Invitrogen). 5 mL of

culture sample was incubated in the dark with SYTOX green at a final concentration of 5 nM for

15 minutes. Cells were fixed (final conc. 2% glutaraldehyde) for 5 minutes prior to

centrifugation at 600 x *g* for 5 minutes at room temperature. Sytox-positive (dead) cells were

counted on an Olympus BX51 epifluorescence microscope with an excitation wavelength of 450

– 490 nm and emission of 523 nm. The percentage of dead cells was calculated from a

minimum of 200 cells counted per slide. SYTOX – positive and negative cells were

photographed.

Measurement of Caspase Activity

K. brevis cells were pelleted by centrifugation at 600 x *g* for 10 minutes at room temperature. Cell pellets were lysed in 1X lysis buffer (Anaspec, Fremont, CA) for 30 minutes at 4°C with rotation. Cell extracts were centrifuged at 10,000 x *g* for 10 minutes at 4°C. The protein concentration of the supernatant was determined by the Bradford Assay (Pierce). Protein lysate, 10 μg per well, was incubated either in the presence or absence of the irreversible pan-caspase inhibitor, carbobenzoxy-val-ala-asp-[O-methyl]-fluoromethylketone (z-VAD-fmk, 50μM final concentration), for 30 minutes at 4°C with rotation. The caspase inhibited (+ z-VAD-fmk) and non-inhibited (- z-VAD-fmk) samples were then incubated with fluorogenic peptide caspase substrates (50 μM final concentration) in 1X activity buffer with 20 mM dithiothreitol (DTT). Hydrolysis of the fluorogenic peptide substrates for caspase 3/7 (acetyl-Asp-Glu-Val-Asp-7-trifluoromethylcoumarin: ac-DEVD-AFC), caspase 6 (ac-VEID-AFC), caspase 8 (ac-IETD-AFC), caspase 9 (ac-LEHD-AFC), and caspase 1 (ac-WEHD-AFC) were tested in triplicate for each sample (with and without z-VAD-fmk) for each time point. A mixture of lysis buffer and activity buffer containing each separate fluorogenic substrate served as the negative controls. The rate of substrate cleavage was determined (excitation, 390 nm; emission, 490 nm) over an 18 hr period with measurements taken at 1 hr intervals using a BMG FLUOstar plate reader (Ortenberg, Germany).

Reactive Oxygen Species (ROS) Detection

Two milliliters of culture was gravity filtered onto a black 5 μm polycarbonate filter (Poretics, K50BP02500). Cells were washed with 1 ml of seawater 3 times. Cells were stained with H_2-DFFDA (Invitrogen, C13293) at a final concentration of 10 μM for 10 minutes at room temperature in the dark. The filter was mounted onto a microscope slide with Slowfade Gold

Antifade reagent (Invitrogen, S36936). Cells were visualized on an Olympus BX51 epifluorescence microscope with an excitiation wavelength of 450-490 nm and an emission of 523 nm. For each treatment (logarithmic phase, stationary phase, and 80mM H2O2-treated), three individual biological replicates were prepared and examined.

DNA Fragmentation: Terminal Deoxynucleotidyl Transferase-Mediated dUTP Nick End Labeling Assay (TUNEL)

DNA fragmentation was assessed using the APO-Brd-U TUNEL Assay Kit (Invitrogen) with a modified protocol. The APO-Brd-U TUNEL assay exploits the fact that DNA breaks expose a large number of 3'-hydroxyl ends that are used as starting points for terminal deoxynucleotidyl transferase (TdT). Addition of deoxythymidine analog 5-bromo-2'-deoxyuridine 5'-triphosphate (BrdUTP) by TdT to the break sites was detected by an anti-BrdU antibody labeled with Alexa Fluor 488 dye that was visualized with a fluorescein filter. Following treatment with 80 μM H_2O_2 to induce cell death, 25 mls of *K. brevis* culture was fixed with 1% paraformaldehyde in seawater (final concentration) for 10 minutes at room temperature. Fixed cells were pelleted (1000xg for 5 minutes) and subsequently washed and pelleted in seawater. Cells were permeabilized in methanol for 10 minutes at -20°, and subsequently washed once in seawater as above. Cells were labeled following manufacturer's protocol. Samples were resuspended in PBS and green fluorescence was observed with an Olympus BX51 epifluorescence microscope with an excitation wavelength of 450 – 490 nm and emission of 523 nm. A positive control consisting of control culture treated with DNase I (Sigma) for 15 minutes prior to labeling, demonstrated staining (97% of cells were stained positive). Data reported is the average percent of positive

cells derived from four biological replicates for each treatment group, in which three slides were counted per replicate with a minimum of 200 cells counted per slide.

Western Blotting Analysis

Samples for immunochemical analysis were extracted using a cell lysis buffer (Anaspec) as described above for the caspase activity assay preparation and protein concentration determined by the Bradford assay (Pierce), loaded on an equal basis (10µg/lane), and separated on a 4-12% Bis-Tris gradient protein gel using MES buffer (Invitrogen) (200V, 1 hr). After SDS-PAGE, total protein was transferred to a PVDF membrane at 20 volts for 8 minutes (iBlot, Invitrogen). Blots were probed with either the polyclonal antibody against the active form of human caspase 3 (Sigma, C8487) at 1:1000, KbMC1 custom peptide antibody (ProSci; 1:2000), and MnSOD (StressGen; 1:2000) in tris buffered saline with 1% Tween 20 (TBST) overnight at 4°C, then probed with a polyclonal donkey anti-rabbit IgG horseradish peroxidase (Sigma Aldrich) 1:2000 in TBST, 1 hr at room temperature), detected using the West Pico HRP Chemiluminescent detection kit (Pierce), and developed using standard film methods.

Screening of K. brevis EST libraries for Putative Caspase Enzymes

A *K. brevis* EST library (version 3; http://www.marinegenomics.org/node/27110/assembly) was annotated and Gene Ontology (GO) categories were assigned for the 65,292 ESTs using BLAST2GO version 2.3.6 using both standard and GO SLIM analyses (Conesa et al. 2005). Top BLAST hit descriptions and GO terms were queried for sequences with BLASTx E-values < 10^{-4} containing metacaspase, caspase, subtilisin, and vacuolar processing enzyme annotations. Annotations were confirmed by performing BLASTx searches on the *K. brevis* EST library with previously characterized sequences from other organisms (Uren et al. 2000; Madeo et al. 2002;

Hatsugai et al. 2004; Vercammen et al. 2004; Hatsugai et al. 2009; Chichkova et al. 2010; Jiang et al. 2010). BLASTp searches were performed to determine the presence and position of conserved domains (http://www.ncbi.nlm.nih.gov/). Multiple sequence alignments were constructed using ClustalW (BioEdit) to verify conserved domain positions and identify the catalytic sequence positions and catalytic pocket amino acid contexts when available.

Caspase Substrate Identification

The *K. brevis* EST library (version 3; http://www.marinegenomics.org/node/27110/assembly) was translated using OrfPredictor (Min et al. 2005) and queried for caspase cleavage sites using the Random Forest trained classifier (RF-12-12) by Pripper (Piippo et al. 2010) for the canonical caspase substrate motifs DEVD, IETD, VEID, LEHD, and WEHD independently. Identified proteins were confirmed through CasCleave (Song et al. 2010) and functionally characterized using the phylogenetic classification scheme of Clusters of Orthologous Groups of proteins for eukaryotic organisms (KOGs) using Kognitor (http://www.ncbi.nlm.nih.gov/COG). P8 – P8' cleavage context around the P1 aspartic acid canonical site was characterized only for proteins positively identified by both Pripper and CasCleave predictions.

Matrix-Assisted Laser Desorption/Ionization (MALDI) Mass Spectrometry (MS) Analysis of K. brevis S-adensosylmethionine Synthetase (KbAdoMet) DEVD Cleavage

Whole cell extracts from vehicle control and 80 μM H_2O_2/10 minutes treatments were obtained as stated in the Western blotting methods. The KbAdoMetS peptide (20 nmol) was incubated with either the control *K. brevis* lysates (10 μg protein/reaction, n = 3), the H_2O_2 treated *K. brevis* lysates (10 μg protein/reaction, n = 3), or with 10 units of recombinant human caspase 3 enzyme (PHZ0014, Invitrogen) in 25mM HEPES, pH 7.4 for 4 hours at room

temperature (n = 3). Buffer only, peptide only, inhibitor only, control and experimental cell lysate only, and enzyme only controls were run in parallel to assess background noise and nonspecific degradation of the peptide over time (n = 3/treatment). Following the 4 hour incubation, which was based on optimization data to maximize the cleavage signal deduced from the biochemical caspase 3 cleavage assay prior to MS analysis, peptides were purified by C18 Zip tip columns (Millipore, Billerica, MA). Briefly, Zip-tips were equilibrated in 100% acetonitrile (ACN), washed with 0.1% trifluoroacetic acid (TFA), and loaded with 20 ml of 0.1% TFA acidified reaction material. Columns were then washed twice with 0.1% TFA, and eluted with a low pH MALDI matrix compound (10 g/L α cyano-4 hydroxycinnamic acid in 1:1 with 50% ACN and 0.1% TFA.) Eluted matrix (1.5 µl) was applied to the MALDI plate in triplicate per treatment. Spectra were collected on a Waters LR MALDI-TOF, with 20 spectra collected and combined for each sample. Raw MALDI-TOF spectra were processed using Progenesis MALDI software package (Nonlinear USA Inc., Durham NC). Spectra were preprocessed by subtracting background, setting the noise filter to 5, and a top hat filler size of 200. The spectra were then aligned using a search area of 5 with 20 iterative cycles. Peaks with a weighted average of 1500 cps were automatically selected. In addition, manual inspection of the proposed products (1148 and 1130 m/z) was performed as peaks were present, but low intensity in some samples. Normalized peak height for full length KbAdoMetS peptide (2430 m/z) and the proposed products (1148 and 1300 m/z) were compared between treatments. Due to the fact that the cleavage products demonstrated such low intensities in the *K. brevis* samples, statistical tests were not employed and only non-quantitative conclusions were drawn.

RESULTS

Physiological Changes Associated with Chronological Aging

To investigate the role caspase-like activities may play in the chronological aging process of *K. brevis*, 21 1-liter cultures were seeded at approximately 1000 cells/ml on day 0. Independent triplicate liters were harvested every other day from day 6 – 18 to assess the physiological response of *K. brevis* over natural aging. The cultures reached a maximum specific growth rate (K') of 0.30 ± 0.12 d^{-1} on day 6, which marked mid-logarithmic phase growth (Fig. 1A). Subsequently, the transition into stationary phase occurred on day 10 and was defined by a decrease in growth rate at the maximum cell concentration of 1.4×10^4 cells/mL. Stationary phase was sustained for the duration of the sampling regime, and a death phase was not observed, as the cell counts remained at approximately 1×10^4 cells/mL until termination of the experiment on day 18 (Fig. 1A). Photosynthetic efficiency (F_V/F_M) was measured across time as an indicator of cellular stress. Mid-logarithmic phase cultures demonstrated high F_V/F_M values (0.62 ± 0.10), indicative of a healthy physiological state. F_V/F_M declined by 58% at the transition into stationary phase, and oscillated between $0.34 - 0.48$ until the end of the sampling regime (Fig. 1B). The decrease in the specific growth rate was correlated with the decrease in the physiological health status ($\rho = .4584$, $p = 0.037$). The SYTOX green viability data indicated that cell viability remained above 97.5% throughout the entire experiment, further demonstrating that a massive cell lysis event did not occur (Fig. 1C).

Caspase-like Activity During Chronological Aging

To determine the presence and magnitude of caspase-like activity during chronological aging in *K. brevis*, the rate of hydrolysis of fluorogenic canonical caspase substrates was measured. Caspase-like activity specific to the initiator caspases 1 (WEHD), 8 (IETD), 9 (LEHD) as

well as the executioner caspases 3/7 (DEVD) and caspase 6 (VEID) were assessed (Figure 2A – E), with the rate of hydrolysis of the fluorescent AFC molecule (caspase activity) for each substrate expressed as pmol AFC cleaved · μg^{-1} protein · h^{-1}. Enzymatic activity corresponding to executioner caspases demonstrated elevated activity at the transition into stationary phase and peaked during mid-stationary phase (day 12) (Fig. 2A – C). Activity for initiator caspase 1 (WEHD) demonstrated a similar pattern, with peak activity on day 14; however, activity levels were much lower compared to caspases 3/7, 6, and 9 activities (Fig. 2D). Although caspase 8-like activity was detected and demonstrated elevated levels during stationary phase, it was more variable than for the other substrates and did not appear to follow the same pattern (Fig. 2E). Across all substrates, one of the cultures on day 12 demonstrated noticeably higher activity than any other culture throughout the experiment. There is no indication that this phenomenon was driven by assay error, and appears to be biologically driven. The distribution of caspase activity over time was tested using the Kruskal Wallis test, as the data was not normally distributed, and was found to be significantly changing for caspase 3 (DEVD), caspase 9 (LEHD), caspase 6 (VEID), and caspase 1 (WEHD) activities. These results were not influenced by the extreme caspase activities observed on day 12 as the statistical test remained robust when this data point was excluded from the analysis. Although the distribution of caspase 8-like activity was not significantly changing over time due to the high biological variability for this substrate, elevated levels in stationary phase did provide evidence that caspase-like activities for all substrates tested in *K. brevis* are induced upon transition into the non-dividing phase of growth. Activity for all substrates was found to be significantly, negatively correlated with specific growth rate (Fig. 2F).

H₂O₂-induced PCD-like Cell Death in *K. brevis*

Experimental rationale and H₂O₂-dose/time response experiment

Although caspase-like activities were found to be elevated in stationary phase, connecting this to PCD morphologies proved to be difficult in aging cultures as complete decline happened at variable rates and over several days. In order to follow death in real time, a treatment regime was needed that would induce cell death through a caspase-dependent mechanism, in a timeframe suitable for the investigation of morphological changes associated with PCD. Since ROS has previously been shown to induce PCD in other phytoplankton species, we tested the ability of H_2O_2 treatment to induce ROS and subsequent cell death in *K. brevis*. A dose/time response range finding experiment (60, 80, 100 µM H_2O_2 at 5, 10, 30, 60, and 120 minutes) was designed to evaluate which parameters would result in over 50% of the cells as caspase 3/7-positive (CellEvent *in situ* Caspase 3/7 Marker), but contain < 10% propidium iodide positive cells (data not shown). ROS staining in cells 80 µM H_2O_2 treatment for 10 minutes demonstrated that the cells bear a heavy ROS load, with uniform and bright staining in >95% of cells. ROS staining in stationary phase demonstrated that the majority of cells (>65%) were positively stained and ROS staining precedes death. Control cells from logarithmic phase stained negative for ROS. Minimal staining was observed in a small population of control cells (<5%) of logarithmic phase cells (Figure 3).

Caspase 3/7-like activity following H₂O₂-treatment

To determine whether *K. brevis* exhibits DEVDase activity during ROS-induced cell death, two independent methods were utilized. To directly compare the magnitude of DEVD activity to that observed in chronological aging, *K. brevis* was assayed using the same biochemical cleavage assay. H_2O_2 treated cells demonstrated a significant induction in DEVDase activity (9.5 pmole

AFC cleaved/mg protein/hour) when compared to untreated control cells (0.5 pmol AFC cleaved/mg protein/hr) (Fig. 4A). H_2O_2 treated *K. brevis* exhibited comparable levels of DEVDase activity as found in stationary phase cultures in the chronological aging experiment (Fig. 1A). Pre-incubation of the cell extracts with the irreversible pan-caspase inhibitor, zVAD-FMK (50 µM, final concentration) for 30 minutes prior to the substrate addition inhibited > 80% of fluorescence in all samples, suggesting that only a minor portion of the activity was from general proteases, confirming that the cleavage assay results report fluorescence specific to caspase-like enzymes in *K. brevis.*

The CellEvent Caspase 3/7 Detection Marker was used in conjunction with the biochemical cleavage assay to provide a secondary measure of caspase-like activity, but also as a means to assessing the morphological changes that accompany caspase activity in *K. brevis* (Figure 4B). The CellEvent marker was optimized for *K. brevis* (10 minute incubation/10 µM final concentration), as longer incubation time (>30 minutes in the manufacturer's protocol) produced false positive results, as determined by PI positive staining. Only PI negative cells were counted for the CellEvent quantification analysis (Figure 4B). As with the biochemical cleavage assay, the CellEvent marker results demonstrated that *K. brevis* caspase 3/7-like enzyme activity is significantly increased during H_2O_2 treatment (Figure 4C). In addition, optimization of the CellEvent marker for live cell imaging allowed for inspection of the morphological changes associated with caspase activation. Following H_2O_2 treatment, K. brevis cells underwent one of two distinct sets of morphological changes prior to cell death. Approximately 70% of cells exhibited nuclear migration from the lower quadrant to the middle of the cell, followed by nuclear swelling; however, cell shape and size remained the same. The contents of the cells undergoing this type of death were maintained inside the cell and were observed to eventually slowly leak over the following two hours that they were observed. A

subset of these cells did show signs of chloroplast swelling and rupture, but only after the nuclear migration. In contrast, roughly 30% of cells exhibited extensive cytoplasmic blebbing and cellular swelling, but did not undergo nuclear migration. Nuclear size and shape remained similar to pre-treatment control cells, although chloroplasts appeared to swell and rupture in the majority of the cells. Time to death was greatly extended in this population compared to the first morphotype, sometimes lasting up to 2 hours before becoming PI positive once the cell ruptured and its contents spewn into the medium. Interestingly, caspase activity was only present in cells that exhibited nuclear migration and swelling (~ 60%), rather than cells undergoing cytoplasmic blebbing (~40%) (Figure 5).

DNA fragmentation following H₂O₂-treatment

The presence of DNA degradation was assessed in *K. brevis* following 80 μM H_2O_2 treatment and in control samples using the TUNEL assay. Since dinoflagellates lack nucleosomes, DNA laddering analysis by gel electrophoresis would not yield interpretable data; therefore, utilizing the anti-BrdU TUNEL system results in a more accurate reflection of DNA damage in a dinoflagellate, and was thus employed in this study. Following H_2O_2 treatment, TUNEL fluorescent label (Figure 6) was identified in both in the nucleus, as well as in the chloroplasts. Microscope counts were conducted on the nuclear staining to quantify the percentage of cells demonstrating positive TUNEL staining. Approximately 60% of 80 μM H_2O_2 treated cells were positive for DNA damage, while only 5% of control cells were TUNEL positive (Figure 6A − TUNEL⁻ panel). Negative control samples, lacking the terminal transferase, were run in parallel for both the control and experimental samples, and showed no staining in either treatment.

Given the significant induction of DEVDase activity, Western blot analysis was performed on *K. brevis* whole cell extracts from mid-logarithmic phase, the transition into stationary, and stationary phase with a polyclonal antibody raised to the active form of human caspase 3 (Fig. 7, lanes 3 – 5). Immunohybridization was observed to distinct bands ranging from 22kDa to 66kDa, with the most intense immunohybridization occurring at 42kDa and 52kDa (lane 4 and 6), which corresponded, to the transition to stationary phase timepoint. Immunoreactivity was inhibited more than 50%, based on densiometry analyses, when the caspase 3 antibody was pre-incubated in the presence of recombinant active caspase 3 enzyme to block specific binding (lane 7). The 66kDa protein band appeared to only be present in late stationary phase cultures (lane 5). Blocking of this band was not determined due to limited material, but it was present in two of the three independent cultures, which corresponded to crashing cultures. The immunoreactivity appears to be distinct from KbMC1, as pre-incubation of KbMC1 antibody with recombinant caspase 3 had no effect on immunohybridization (lanes 8 and 9).

To determine the extent to which caspase 3-like proteins are involved in the induction of H_2O_2-induced cell death, extracts from control and 80μM H_2O_2 treated cells were immunohybridized with the anti-caspase 3 antibody. Following H_2O_2-treatment, the human caspase 3 antibody cross-reacted with the three distinct bands (66, 52, and 42 kDa bands) previously seen in the chronological aging experiment. Immunoreactivity for all three bands significantly increased following the H_2O_2-treatment (Figure 8).

Candidate Proteins in *K. brevis* with Caspase Function.

Since bona fide caspases are not present in other phytoplankton and have not been found in the K. brevis EST library, we next sought to identify potential proteins responsible for this activity.

Metacaspases

Seven metacaspase sequences were identified in a translated *K. brevis* EST library (version 3; http://www.marinegenomics.org/ node/27110/assembly) with BLASTx Expect (e) values ranging from $7e^{-11}$ to $2e^{-80}$ (Table 1A). Five EST sequences contained the well-conserved peptidase_C14 (pfam00656) caspase conserved domain, with four of the sequences containing the conserved catalytic histidine and cysteine dyad. Further analysis of the sequence context around the catalytic HC dyad, however, identified that the histidine residue is replaced in one case by Y (MGID2080273), but overall they contain a (H/Q)(F/Y)SG(H/Y)G context demonstrating that *K. brevis* metacaspases utilize an adjacent glycine for cleavage stabilization as seen in caspases and metacaspases (Earnshaw et al. 1999). Similar to other characterized metacaspases, the catalytic cysteine context of **D**(C/S)CHSG suggests that *K. brevis* metacaspases contain an acidic catalytic pocket due to the aspartic acid residue (bolded), and thus appears to coordinate cleavage of arginine and lysine residues in the P1 site, rather than aspartic acid. Given the biochemical specificity of *K. brevis* metacaspases towards Arg/Lys deduced from sequence context, alternative candidates for the observed caspase activity were explored.

_Peptidase_C14 caspase catalytic p20 subunit containing proteins_

Eleven proteins annotated as peptidase C14 catalytic p20 subunit containing proteins were identified from the translated _K. brevis_ EST library with E-values ranging from $9E^{-5}$ to $4E^{-30}$ (Table 1B). Ten of the eleven proteins demonstrated high similarity with a metacaspase in _Trichodesmium erythraeum_, a filamenteous cyanobacterial species. _T. erythraeum_ contains 10 metacaspases that, in addition to containing a caspase domain (pfam00656), possess 62 additional protein domains such as EZ-Heat, WD40, DUF323, and Chase2. The conserved p20 domain and H/C sites were not identified in any of the eleven peptidase_C14 caspase catalytic p20 containing proteins identified in _K. brevis_; however, like _Trichodesmium_, these ESTs contained a number of domains including TPR repeats, EZ-Heat repeats, armadillo domains, a chromatin condensation complex (condensing) subunit, and a 26S proteasomal regulatory domain subunit that likely drove their homology to the _T. erythraeum_ metacaspase. The absence of conserved p20 domain and H/C sites from these proteins disqualified them as candidates for caspase-like activity in _K. brevis_.

Subtilisin and Vacuolar Processing Enzyme

Given the Arg/Lys cleavage context in other metacaspases, and the absence of the conserved p20 domain and catalytic dyad in the proteins annotated as peptidase_C14 caspase catalytic p20 containing proteins, other proteases known to exhibit caspase activities were analyzed in _K. brevis_ (Table 1C). Vacuolar processing enzyme (VPE) (Hatsugai et al. 2004), proteosome subunit PBI (Hatsugai et al. 2009), and subtilisins (Chichkova et al. 2010) are candidates that have demonstrated caspase substrate cleavage specificity in _Arabidopsis_. Using tBLASTx searches, two sequences (MGID2026497: $4E^{-71}$ and MDID1977692: $2E^{-22}$) annotated as peptidase_S8 subtilisins were identified, both containing the conserved subtilisin domain

(pfam00082) (Table 1). While all active site residues were identified for MGID2026497, only two of the three active site residues were identified in MGID1977692 due to incomplete sequence information. Further sequence analysis using COG classification identified both sequences as containing strong homology to KOG1153, subtilisin-related protease/vacuolar protease β. No homologous proteins to the *Arabidopsis* proteasomal subunit PB1 were identified in *K. brevis*. Thus, given our current *K. brevis* genomic resources, two sequences with homology to subtilisin-related protease/vacuolar protease β present the most viable candidates for the observed caspase 3-like activity in *K. brevis*.

Candidate Caspase Substrates Identified in *K. brevis*

Three classes of caspases have been previously identified in mammalian systems based on their preference for different amino acid residue chemistry in the P1 – P4 positions, with all containing strict preference for aspartic acid at P1 (Talanian et al. 1997). The cytokine processor/ICE-like caspase family, represented in this study by caspase 1 activity, prefers bulky hydrophobic residues in the P4 position (WEHD). The initiator caspases, with preference for branched aliphatic amino acids in P4, were assayed in this study with VEID, IETD, and LEHD for caspases 6, 8, and 9, respectively. The last biochemical class of caspases, the executioner CPP32-like subfamily, prefers aspartic acid in the P4 position, with a DXXD general consensus site and assayed in this study with DEVD.

To identify the potential caspase targets for the assayed caspase activity, the translated *K. brevis* EST library was queried using two independent algorithms for caspase substrate cleavage specificity, Pripper and Cascleave. Pripper utilizes a Random Forest classifier (RF-12-12) that takes into consideration not just the P1 aspartic acid cut site but also the 12 residues upstream (P2 – 12) and downstream (P1′ – P12′) (Piippo et al. 2010). As the RF-12-12 considers

neighboring residues, caspase candidates were scored by Pripper based not only on the presence of the specific cleavage P1 – P4, but on the broader biochemical context surrounding the motif which has been previously shown to increase the predictive power in reliably identifying caspase substrate targets (Wee et al. 2006; Wee et al. 2007; Wee et al. 2009; Piippo et al. 2010). A total of 86 proteins (40 DEVD, 12 LEHD, 23 VEID, 2 WEHD, 9 IETD) were identified by Pripper to be caspase substrates, of which 44 (21 DEVD, 7 LEHD, 11 VEID, 1 WEHD, 4 IETD) were annotated with BLASTx E-values less than 10^{-4} (Table 2).

The 44 target substrates identified by the Pripper analysis, with known functions, were next screened using CasCleave (Song et al. 2010), an independent predictive tool for caspase target substrate identification. CasCleave utilizes an extended support vector machine (SVM) model, whereby a support vector regression (SVR) was utilized to not only provide two-state predictions, such as in Pripper, but also an estimated probability for each candidate site. While this model also takes into account the residue context around the P1-P4 motifs, it also considers predicted secondary structure, solvent accessibility, and natively disordered regions for positions P8 – P8' (Song et al. 2010). Using this approach, of the 44 candidates identified in Pripper, a predictive caspase cleavage performance probability score of 0.5 or greater was confirmed for 31 substrates (Table 2, bolded).

Statistical distribution of substrate cleavage sites

The statistical distribution of amino acids in the P8 – P8' positions around the identified substrate cleavage sites were next evaluated for the 31 candidate proteins identified by both Pripper and CasCleave. The percentage occurrence for each amino acid class was calculated and displayed in a two-dimensional heat map to identify patterns of context specificity for *K. brevis* substrates (Figure 9). Similar patterns of specificity were found relative to those identified

through the combined prediction by CasCleave (Song et al. 2010), of the CASBAH (Fischer et al. 2003), MEROPS (Rawlings et al. 2008), CASVM webserver (Wee et al. 2006; Wee et al. 2007), and Uniprot databases (Bairoch and Apweiler 2000), whereby small amino acids were present in 70% of P1' in caspase 6 (VEID) substrates. Substrates with LEHD, WEHD, or IETD sites were not evaluated for statistical distribution patterns due to their smaller sample sizes. When evaluated by individual amino acid residue, a modest preference was observed for the small amino acids, alanine (30%) in caspase 3/7 substrates (DEVD) and glycine (57%) in caspase 6 substrates (VEID), in the P1' position (Figure 10). Upstream of VEID, site preference was also identified for E, K, R, or L (combined 28%) at P8 – P5. Preference for D and E (each 20%) was apparent at positions P6 and P5, respectively, in caspase 3/7 substrates (DEVD). Interestingly, substrates with a VEID site motif demonstrated a preference for nucleophilic residues (57%) at P5'.

Biological functions of caspase target substrate

Annotated proteins with caspase substrate motifs represented 0.14% of the known *K. brevis* proteome (31 identified substrates/22,078 total proteins screened). Annotation and functional classifications for the caspase substrates was carried out in Blast2GO and Koginator (Tatusov et al. 2000) in order to gain insight into the biological connections of caspase activity in *K. brevis* (Table 2). KOG analysis indicated that a diverse group of functions are encoded by proteins with caspase cleavage sites. Five of the identified proteins encoded known caspase target substrates (Luthi and Martin 2007), three of which were categorized as involved in posttranslational processes, protein turnover, and chaperones. The constituents of this group included a ubiquitin carboxyl terminal hydrolase (Mahrus et al. 2008), a 26S proteasome regulatory ATPase ATP1 subunit (Adrain et al. 2004; Sun et al. 2004), and a polyadenylation factor complex protein (Dix et al. 2008). Two proteins involved in signal transduction processes

included a Ca2+/calmodulin dependent protein kinase EF-hand superfamily protein (Mcginnis et al. 1998), and a conserved protein containing a JmjC domain, which is a cupin metalloenzyme superfamily member (Dix et al. 2008). The remaining 26 caspase substrates predicted in *K. brevis* have not been previously identified as caspase substrates in other organisms; however, many are connected with pertinent processes related to coenzyme metabolism, lipid metabolism, cell cycle checkpoint regulation, and death processes (Table 2).

Cleavage of the Predicted Substrate, *K. brevis* S-adensosylmethionine Synthetase (KbAdoMet), is Confirmed by MALDI-TOF as a Caspase Substrate Analysis of *K. brevis*

The bioinformatics screen predicted numerous proteins in the K. brevis library not previously identified as caspase substrates in other organisms. To evaluate the validity of the bioinformatics screen, we selected one novel predicted substrate, KbAdoMetS (498 aa), to test if it is a bona fide caspase 3 substrate using an in vitro cleavage assay. A 22 amino acid peptide was designed around the predicted DEVD cleavage site (D484) starting at K474 to K495 resulting in a 2430 m/z peptide (Figure 11A). The KbAdoMetS peptide was incubated with the active form of recombinant human caspase 3 and analyzed by MALDI-TOF MS. Incubation of the AdoMet peptide with active human caspase 3 resulted in cleavage of the peptide at the predicted site, resulting in a significant increase of the predicted fragmentation products, which were not present in the peptide alone or caspase 3 alone treatments (Figure 11B, C). The observed increase in both of the predicted peaks was inhibited by the addition of the caspase inhibitor, demonstrating that the cleavage was caspase 3 specific and not general nonspecific degradation of the peptide during the four hour incubation. This was also evidenced by comparable amounts of the 2430 m/z peaks in the peptide alone versus the peptide/caspase 3 enzyme/inhibitor reaction (Figure 11B, C). Overall, these results confirm that the novel

predicted *K. brevis* caspase substrate, KbAdoMetS, was correctly predicted to be cleaved by an active caspase 3 enzyme, and lends support to the overall bioinformatics approach taken to gain insight into *K. brevis* caspase-dependent processes.

DISCUSSION

Understanding the processes regulating the aging and demise of *K. brevis* red tides is of both ecological and management interest. This study identified a role for caspase-like activity in both the transition from log phase to stationary phase of growth and in ROS induced cell death. The enzymes responsible for caspase-like activity were investigated and the putative substrates for this activity in *K. brevis* were identified.

A broad range of functional studies utilizing caspase activity assays, caspase inhibitors, and western blotting with human caspase antibodies have defined a role for caspase-like enzymes in modulating cell death in a number of phytoplankton species. In turn a diverse array of cell death processes, such as PCD, necrosis, and parapoptosis has been identified. However, the biological and evolutionary context for these pathways is not well defined and the concept of altruistic suicide in unicellular lineages is still considered a matter of "ongoing debate" (Deponte 2008; Nedelcu et al. 2011). Numerous studies, however, dispel the assumption that because all unicellular cell death eventually leads to complete loss of the individual, there is no benefit to the population. Studies in the yeast, *S. cerevicae* demonstrate a direct benefit of cell death via a PCD-like pathway to the fitness of the surviving population (Fabrizio et al. 2004; Herker et al. 2004). This phenomenon has also been observed in the marine dinoflagellate *Peridinium* gatunense, whereby an excreted thiol protease from older cultures sensitizes younger cells to oxidative stress, and thus prohibits damaged cell populations from forming reproductive cysts and propagating unstable future populations (Vardi et al. 2007). For the

unicellular green alga, *Clamydomonas reinharditti,* PCD appears to positively modulate the fitness of other cells, whereas death via nonprogrammed events results in the release of substances that negatively impact the population (Durand et al. 2011). Based on these observations, it has been proposed that alternative death modes may have played a role in the origin and maintenance of PCD, as well as the transition to multicellular life (Rao et al. 2006).

A distinct set of biochemical and morphological characteristics that can be uniformly assigned to phytoplankton PCD have not been identified, although many instances have been documented where typical PCD characteristics have been observed. In addition to caspase activation, these include the inversion of phosphotidylserine in the outer leaflet of the plasma membrane and DNA fragmentation (Taylor et al. 2008). Studies to date on the aging process of the diatom *Thalassiosira* pseudonana, and the cyanobacterium, *Trichodesmium erythraeum,* also demonstrate a robust correlation between caspase activation and mortality (Berman-Frank et al. 2004; Bidle and Bender 2008). While caspase activities have been shown to be involved in phytoplankton death, their involvement in modulating the aging and death process in dinoflagellates has not received as much attention. In this light, the current study sought to evaluate *K. brevis* caspase activities during the chronological aging process as well as during culture demise.

Caspase-like Activity is Induced During Chronological Aging in *K. brevis*

In the study of chronological aging in *K. brevis*, we found that caspase activity against all five caspase substrates tested (caspase 1, 3/7, 6, 8, and 9) was induced at during stationary. Caspase activity has been previously documented in *K. brevis* (Bouchard and Purdie 2011); however in that study caspase activity spiked during an incubator failure in which the *K. brevis* cultures were subjected to 7°C drop over the course of one night, suggesting a stress and not an

aging associated activity . Although age associated caspase activity data was inconclusive, that study did demonstrate that *K. brevis* exhibited DNA fragmentation suggestive of PCD in late stage culture decline (Bouchard and Purdie 2011). In the current study, cell viability did not significantly change at any timepoint, so it is clear that the observed induction of caspase activity did not coincide with culture decline; rather, the peak in caspase activity coincided with a decline in photosynthetic efficiency as cells entered stationary phase. This suggests a role for stress acclimation during chronological aging, and therefore a possible role in the survival of cells during that phase. This observation is consistent with genomic and biochemical findings in the diatom *T. pseudonana*, in which caspase activity has been associated with stress acclimation processes (Thamatrakoln et al. 2011). However, in contrast to the *T. pseudonana* study, where only 76 upregulated transcripts (0.67% of the arrayed transcriptome) coincided with caspase activity, *K. brevis* caspase activity occurs when 30% of the arrayed transcriptome is being restructured (described in Chapter 2). Processes including energy acquisition, calcium signaling, stress response dynamics, and gene expression regulation were altered during the chronological aging process, while no significant changes in cell death transcripts were observed, further supporting the involvement of caspase-like enzymes in non-death roles during chronological aging in *K. brevis*.

Caspase-like Activity Appears to Modulate ROS-induced PCD in *K. brevis*

Characterizing cell death associated with chronological aging proved to be difficult in *K. brevis,* as the diversity in size, shape, and organellar structure was too great to conclude that *K. brevis* has a distinct set of morphological changes associated with PCD during natural culture. The cell size and shape do appear to be skewed towards smaller, rounder cells, which were observed in the late stationary phase cultures in the Bouchard 2011 study of *K. brevis*. However,

like *Amphidinium cartarae*, in our study aging *K. brevis* cells did not stain positively for DNA fragmentation the TUNEL assay (Franklin and Berges 2004). It should be mentioned that extensive optimization of an Annexin V staining procedure to detect the externalization of phosphatidylserine was performed; however, the assay did not provide interpretable data. Thus, this mechanism remains unresolved, and requires careful consideration, as *K. brevis* is an unarmored dinoflagellate with fragile membranes whose compromised integrity during cell manipulation, which may interfere with proper Annexin V staining interpretations.

After various methods were exhausted to reliably sample at the "point of no return" prior to culture demise during chronological aging, it became obvious that characterizing the involvement of caspase-like activities in cell death required a model that provided a shorter time interval to accurately describe the temporal changes directly downstream of caspase activation. Because accumulation of ROS is a natural stressor in phytoplankton aging, we selected H_2O_2 to induce cell death in a timeframe that would allow for live cell imaging techniques. In this model, caspase activity was demonstrated following the 80 μM H_2O_2 exposure by both the hydrolysis of DEVD-AFC and the CellEvent Caspase 3/7 detection marker. Live cell imaging with the CellEvent marker proved to be an invaluable tool in classifying the subsequent morphological events as microscopic observations concluded that two distinct morphotypes were present. Morphological changes associated with cell death in the dinoflagellate *Amphidinium cartarae* spanned a broad range of phenotypes demonstrating that strict classification of cells in the metazoan PCD classification scheme does not appear to always accurately describe dinoflagellate morphology (Vardi et al. 1999; Franklin and Berges 2004). In the current study, *K. brevis* cells that were caspase and TUNEL positive demonstrated nuclear migration and swelling. In contrast, the other morphotype was caspase negative and underwent extensive cytoplasmic blebbing. The two morphotypes appeared to be mutually exclusive as cells that demonstrated

nuclear perturbations did not undergo cytoplasmic swelling and vice versa; however, both

populations were ROS positive. Previous observations in *Amphidinium* described nonspecific

organellar dissolution with negative TUNEL staining, cell shrinkage and extensive vacuolization

during senescence and light deprivation (Franklin et al. 2006). As previously discussed, *K. brevis*

did exhibit smaller cell sizes during aging, but in the ROS-induced death, where cells either

remained the pre-treatment size or increased due to the cytoplasmic swelling. *K. brevis* and *K.*

mikimotoi have previously been reported to stain TUNEL positive (Bouchard and Purdie 2011),

but in that study it was unclear if this was a hallmark of death or temporary cyst formation, as

the death process was not monitored as it was in the present study. In terms of the aging cells

in our study, DNA fragmentation was not associated with the small cells that resembled the

morphotype described in Bouchard et al, therefore it is difficult to say with certainty that aging

K. brevis was undergoing the same physiological and biochemical events as previously described.

Metazoan necrosis is characterized by cellular swelling, therefore is likely that the second

morphotype described in this study is necrosis-like, as it was TUNEL and caspase negative.

However, the swelling in a subset of this morphotype did appear to bleb off apoptotic-like

bodies, leaving the remaining cell to survive for a significantly longer length of time than those

that died with the first, caspase positive, morphological characteristics.

Increased immunoreactivity to human caspase antibodies during aging and dark

treatment in *D. virdis*, raised the question of whether *K. brevis* DEVDase activity is correlated

with caspase 3-like protein abundance (ref). To test this, a human caspase 3 antibody was used

to probe *K. brevis* whole cell lysates during ROS-induced PCD. Three immunoreactive bands

were detected, all of which were significantly induced after the 10 minute treatment with 80

μM H_2O_2. BLAST analysis of the active caspase 3-antibody epitope against the *K. brevis* proteome

did not yield any matches and sequence alignment of the caspase 3 antibody epitope with the

four *K. brevis* metacaspases further demonstrated that the immunoreactive bands are not indicative of metacaspase expression. Blocking experiments with the recombinant caspase 3 enzyme did indicate that the *K. brevis* immunoreactive bands are specific to the caspase epitope suggesting that *K. brevis* may contain caspase 3-like proteins that are not represented in the sequence library. Although the identity of the bands remains unknown, the induction of caspase 3-like bands strongly correlates with the induction of DEVDase activity.

The antioxidant systems in phytoplankton appear to be conserved and are used to combat cellular ROS in similar ways to higher metazoans. Superoxide dismutase (SOD) in particular is among the primary line of defense, and is often used as an indicator of cellular ROS levels. The SODs make up a diverse family of metalloproteases and are classified by the metals present in their active sites. MnSOD protein abundance has been previously been investigated in the marine diatom, *T. pseudonana* during iron starvation, and demonstrated a significant increase in immunoreactivity which is diagnostic of a subcellular response to ROS (Bidle and Bender 2008). This induction was concomitant with an induction in metacaspase protein abundance and a drop in photosynthetic efficiency. *K. brevis* MnSOD protein abundance has previously been queried during various stress response regimes, and shown to be induced during 60 μM H_2O_2 treatment after 1 h (Miller-Morey and Van Dolah 2004). We did not see a similar induction of MnSOD during H_2O_2 stress in the current model. Unlike the caspase family that is controlled on a post-translational level, changes in MnSOD are result from increased translation that we would not expect to observe in the short 10 minute exposure used here. Distinct staining of ROS positive cells after H_2O_2 treatment, using the *in situ* H_2-DCFDA ROS stain (Invitrogen), however, clearly demonstrated that *K. brevis* did respond to elevated ROS in this experimental design. This along with the dramatic decrease in photosynthetic efficiency from

0.562 to 0.230 suggests that similar physiological events and subsequent PCD pathway execution occurred compared to other studies (Vardi et al. 1999; Segovia and Berges 2009).

Together these results indicate that *K. brevis* exhibits morphological and biochemical evidence that a PCD-like pathway is induced during ROS-driven cell death. This study, to our knowledge, represents the first report characterizing the direct connection between caspase-like activity and subsequent PCD-like morphological changes in a dinoflagellate.

What Enzymes are Responsible for Caspase-like Activity in *K. brevis?*

To further understand the processes of aging and death, we next sought to identify what enzymes are responsible for caspase-like activity observed. Metacaspases have received much attention over the last decade as the putative enzymes responsible for the caspase-like activities demonstrated across these groups of organisms. Striking correlative evidence in various unicellular organisms, including a number of phytoplankton species, has shown the induction of metacaspases at the transcript and/or protein level concomitant with caspase activity, leading to the long standing supposition that metacaspases may cleave caspase substrates (reviewed inTsiatsiani et al. 2011). However, in the past few years *in vitro* biochemical analyses of metacaspases have demonstrated that their catalytic pocket specificity coordinates cleavage after arginine and lysine residues, rather than aspartic acid. Using *in silico* EST searches and sequence alignments, we have identified that *K. brevis* does in fact contain seven putative metacaspases of which five contain the peptidase_C14 catalytic domain. Sequence alignments with other known metacaspases defined that the *K. brevis* metacaspase catalytic pocket contains the stabilizing aspartic acid residue that has previously been shown to coordinate cleavage of basic residues. This provides strong evidence that metacaspases are not capable of being responsible for the assayed caspase activity in *K. brevis*. Similarly, several

sequences annotated by top blast hits as peptidase_C14 caspase catalytic p20 subunit containing proteins, with high homology to *T. erythraeum* metacaspases were initially promising; however, COG analysis and CDD search (NCBI) identified that a conserved caspase domain was not present in any of the *K. brevis* sequences with catalytic pocket chemistry able to coordinate cleavage after aspartic acid residues.

Once plant metacaspases were biochemically demonstrated to contain Arg/Lys specificities, studies aimed at identifying the enzymes responsible caspase activity associated with PCD yielded three major candidates, now known to contain caspase specific activities: vacuolar processing enzyme, proteasome subunit PB1, and subtilisins (Sanmartín et al. 2005; Watanabe and Lam 2005; Bonneau et al. 2008). Vacuolar processing enzymes (VPE), which are cysteine proteinases involved in the maturation of vacuolar proteins, have been shown to contain caspase-1-like activity (YVAD) and mediate PCD in plants. VPEs are present in the legumain family and are members of the clan CD cysteine proteases with YVADase activity (Kuroyanagi et al. 2002). In the current study, YVADase activity demonstrated a similar pattern of induction in *K. brevis* to that of the other substrates, with peak activity occurring on day 14 (data not shown), making this protein class a candidate for caspase –like activity. Subtilisins, serine proteases with caspase-like cleavage, have also been identified in plants and have been termed saspases. Saspase involvement in caspase activities was first described in a study in which RUBISCO proteolysis was indirectly inhibited during victorin-induced PCD by caspase inhibitors (Coffeen and Wolpert 2004). Further biochemical analysis of this enzyme determined its specificity for VKMD, VEHD, and VNLD activity, although it lacked catalytic potential against other known caspase 6 substrates including VEID (Coffeen and Wolpert 2004). In the current study, two subtilisins from the peptidase_S8 protein domain family were identified with the conserved Asp/His/Ser catalytic position making them good candidates for caspase-like activity

in *K. brevis*. Additional subtilisin-like sequences were identified in the cDNA library through annotation descriptions; however, they were not included in this analysis since the conserved domain or catalytic sites were not present due to incomplete sequences. Lastly, proteasome subunit PB1 has been shown to exhibit DEVDase activity during vacuolar/membrane fusion events during the hypersensitive response against infection in plants (Hatsugai et al. 2004). No homologs of proteasome subunit PB1 in *K. brevis*, although other constituents of the proteasome pathway has been identified, suggesting that either *K. brevis* does not contain a highly homologous member or that is it not present in the current EST library. Given its enormous genome size, deeper sequencing of *K. brevis* may be helpful in identifying PBI homologs.

The identification of subtilisin/VPE-like enzymes in the transcriptome provides a foundation from which to structurally and functionally define the enzymes responsible for caspase activity in *K. brevis*. Furthermore, identification of immunoreactive bands towards the caspase 3 antibody and verification of the protein's involvement in carrying out the assayed DEVDase activity is of utmost concern. Until now, discussions focusing on the putative involvement of metacaspases in phytoplankton caspase-like activity have minimized the understanding of the breadth of enzymes that may be driving this activity. While functional studies are limited in dinoflagellates, given that a gene knockdown system has not yet been established, structural and biochemical analyses may define these alternative candidate enzymes as capable of cleaving the assayed substrates.

Identification of Caspase Substrates in *K. brevis* Connects Caspase Activities with Aging and Death Processes

In addition to a lack of understanding of what enzymes are responsible for caspase activation in phytoplankton, few studies have defined the targets of this activity. The combinatorial approach taken in the current study defined a core set of target sequences with DEVD, LEHD, VEID, WEHD, and IETD sequence motifs, and used predicted structural data to confirm the caspase substrate predictions. While previous studies have defined putative target substrates by sequence context (P4 – P1), the results from this study highlight the potential false positive rate if sequence context (P8 – P8') and secondary structure are not considered. It is important to note that the approach taken in this study limited the identification of caspase substrates to those activities assayed, therefore suggesting that the number of putative caspase substrates, including other known canonical as well as non-canonical specifities, in the *K. brevis* proteome is projected to be greater than described here.

Computational prediction of caspase substrates in the *K. brevis* transcriptome, using a combination of Pripper and CasCleave programs, yielded a total of 31 target sequences with BLASTx E-values $< 10^{-4}$, of which approximately 65% contained the DEVD motif. Comparisons of the identified list of substrates with the CASBAH database demonstrated that five of the *K. brevis* substrates have been previously shown to be caspase substrates in metazoans, suggesting a similar downstream functional response in dinoflagellates. Included in this list were members of the ubiquitin/proteasome degradation pathway as well as a polyadenylation factor complex subunit, suggesting that caspase activity in *K. brevis* may be involved in the disruption of proteasomal degradation of ubiquitinated proteins and mRNA maturation. An EF-handed Ca^{2+} calmodulin-dependent protein kinase was also identified in *K. brevis* with DEVD sequence context. This family of proteins has been previously shown to regulate plant early defense

signal transduction (Blumwald et al. 1998). ScDSP, a death specific protein with a Ca^{2+} EF hand domain in the diatom *Skeletonema costatum*, has been implicated in regulating death, and thus is an interesting protein to direct future studies in defining the connection of this family of proteins with death in dinoflagellates (Chung et al. 2005; Chung et al. 2008). Furthermore, Ca^{2+} DSP's have been identified to be targeted to the chloroplast and facilitate cyclic electron flow around photosystem I, and appear to regulate the levels of important photosystem proteins in *T. pseudonana* (Thamatrakoln et al. in review PLoS Biology). Transcripts for calcium binding, transport, and signaling are statistically enriched among those changing in expression at the transition to and maintenance of stationary phase in *K. brevis* (Johnson et al. 2012). Together, the role of calcium homeostasis appears to be important to the aging process in *K. brevis*, and is an area that deserves further attention. While this bioinformatic analysis demonstrated that *K. brevis* contains previously known caspase target substrates, it also identified novel substrates previously undefined in any system to date. Interestingly, an autophagy-like protein with caspase 8 cleavage specificity was identified, lending new insights into the connection between death programs in a dinoflagellate. Autophagy, the death process involving the lysosomal degradation of cellular components, has not been previously linked with phytoplankton bloom demise; however, further work characterizing the connection between caspase activity and autophagic-like death processes appears to be a worthwhile area to investigate in relation to aging and cell death in dinoflagellates. Overall, our analysis identified transcripts from a diverse group of processes, many of which revealed previously unknown connections to caspase activities. Since signaling proteases can act by releasing positive regulators or by degrading negative regulators, the exact role of these substrates in the aging process needs to be examined; however, this systematic computational screening analysis has provided insight into the substrate specificities for dinoflagellate caspase activities and has allowed us to further

characterize one of the identified substrates *in* vitro to determine if it is capable of being cleaved at the proper DEVD recognition motif by human caspase 3.

MALDI-TOF Mass Spectrometry Analysis of Cleavage of *K. brevis* S-adenosylmethionine Synthetase (KbAdoMetS) at the DEVD Recognition Motif

One of the most intriguing findings from the bioinformatic caspase substrate screen was the identification of an S-adenosylmethionine synthetase (AdoMetS), as it has been shown to have a central role in transmethylation and polyamine biosynthesis in dinoflagellates. AdoMetS is a highly conserved enzyme that specifically catalyzes the formation of S-adenosylmethionine (SAM) from L-methionine and ATP, which is an important biochemical intermediate that serves as the precursor to a large number of bioactive compounds across all kingdoms. AdoMet's involvement in such a diverse set of biological processes in founded in its ability to transfer a methyl group to a diverse set of biological substrates through the aid of a broad family of methyl transferases. Since AdoMet is the primary methyl donor, AdoMet is thus the primary cofactor for methylation of DNA, RNA, proteins, phospholipids, as well as other small molecules such as steroids. In addition to this, a nucleophilic attack at the 3-amine-3-carboxy propyl portion, rather than at the sulfur bond of ribose, leads to the precursor for polyamine biosynthesis. Polyamine precursors, formed from the decarboxylated AdoMet precursor, are used in the biosynthesis of ubiquitously important molecules such as spermidine and spermine. Spermidine, a polyamine involved in cellular metabolism has been shown to affect the aging process in higher metazoans through the induction of autophagy (Eisenberg et al. 2009), while its metabolite spermine also has a key role in DNA synthesis and gene expression. Polyamines play a major role in cell migration, proliferation, and differentiation, and may play a key role in the rapid growth and development of algal blooms (Chan et al. 2002). Ethylene, another

classical metabolite of AdoMet in plants, plays a role in ripening, senescence, and response to

stress. The pathways that AdoMet fuels are extraordinarily diverse. In the toxic dinoflagellate,

Alexandrium spp., AdoMet serves as a precursor to saxitoxin biosynthesis (Gupta et al. 1989;

Shimizu 1996). Brevetoxin biosynthesis and that of similar polyether ladder toxins, also relies on

methyl donor activity for the pendant methyl groups from both S-adensylmethionine and

acetate methyl (Kellmann et al. 2010). Dinoflagellates encode an unusual S-adenosylmethionine

synthetase gene that produces a fully functional AdoMetS that contains several extra loops

located closely to the methionine binding site (Ho et al. 2007). The AdoMetS identified in the *K.*

brevis bioinformatics screen contained the AdoMetS domain (KOG: S-adenosylmethionine

synthetase, e-value – 1 e-^{111}) contains the same additional dinoflagellate loops, as well as the

conserved methionine binding site (GHPDK), the active signature hexapeptide (GAGDQG) for

ATP binding, and the nonapeptide (GGGAFSGKD) which forms the P loop for phosphate binding

(Ho et al. 2007). The *K. brevis* AdoMetS ranked in the top 25% range for the CasCleave

probability score, suggesting its strong likeliness as a true caspase 3 substrate. The DEVD motif

was identified in the extreme C-terminal end of KbAdoMetS, and at first glance this may suggest

that it could be classified as a bystander substrate (Crawford and Wells 2011); however, studies

characterizing rat AdoMetS localization concludes that the C-terminal end is important in its

nuclear/cytoplasmic localization, and thus cleavage of this are may affect compartment specific

activities (Reytor et al. 2009). To evaluate the ability of KbAdoMetS to be cleaved at the

identified DEVD cleavage site, a 22 amino acid peptide was designed around the cleavage site,

resulting in a 2431 m/z peptide with proposed cleavage product masses at 1300 and 1148 m/z.

The KbAdoMetS peptide was incubated with recombinant caspase 3, and cleavage of the

peptide produced the proposed cleavage products. In addition to this, the signal was drastically

dampened when the pan caspase inhibitor zVAD-fmk, further demonstrating that KbAdoMetS is

capable of being cleaved at the proposed DEVD caspase 3 cleavage motif by caspase 3. Further

evaluation of the ability of *K. brevis* cell lysates extracted after 10 minutes of 80 μM H_2O_2

treatment to cleave the KbAdoMetS peptide was attempted in the same manner as the

recombinant caspase 3 experiment. Mass spectrometry analysis of the cleavage of KbAdoMetS

by *K. brevis* undergoing ROS-induced PCD did not result in a significant increase in the proposed

cleavage products compared to control samples. However, the results were unclear as samples

did contain high enough concentrations of caspase-like enzymes to result in enough cleavage

product for detection. Efforts to concentrate the caspase-like enzymes in the *K. brevis* lysates by

immunoprecipitation were carried out, although they did not recover enough protein to

effectively boost the signal to the recombinant signal level. Future efforts to capture caspase-

like enzymes using a zVAD-biotinyalated approach may be used to effectively boost signal for

analysis (Bidle, personal communication). In summary, the bioinformatic screen identified a

number of putative substrates for the caspase-like activity observed in *K. brevis*, some of which

are known caspase substrates, and some of which are novel. This study confirmed that

KbAdoMetS caspase cleavage site is biochemically appropriate for caspase catalytic pocket

recognition and cleavage, suggesting that cleavage of KbAdoMetS may be an important protein

to direct future studies to understand the biological consequence of its cleavage during PCD.

CONCLUSIONS

While caspase activity has mostly been correlated with cell death processes in

phytoplankton, it appears that *K. brevis* may utilize this specific enzyme capacity to modulate

the aging process during stationary phase growth as well as during ROS-induced cell death. The

K. brevis transcriptome does not appear to include any bona fide caspases; however, *K. brevis*

does show immunoreactivity with a human caspase 3 antibody at three distinct bands, all of

which are dramatically induced during ROS treatment. Based on the bioinformatic findings, the only candidates for this activity are the subtilisin-like enzymes, which have been observed to have caspase-like activity in plants. The metacaspases, long proposed to be responsible for this activity, in phytoplankton do not appear to be. Concomitant with caspase activity during ROS treatment, DNA fragmentation by TUNEL assay was identified, suggesting that *K. brevis* executes a PCD-like process. This study further explored the *K. brevis* proteome for caspase substrates, revealing both previously known as well as novel substrates. To test the accuracy of this bioinformatic screen, one novel predicted substrate, KbAdoMetS, was confirmed to be a caspase 3 substrate by mass spectrometry analysis; however, further studies are needed to confirm the activity in *K. brevis.* Future studies directed towards understanding the role of caspase activity in the aging process and the persistence of *K. brevis* in the coastal environment during bloom events as well as during bloom termination may provide key clues to understanding bloom dynamics in field populations.

REFERENCES

Adrain C, Creagh EM, Cullen SP, Martin SJ (2004) Caspase-dependent inactivation of proteasome function during programmed cell death in *Drosophila* and Man. J Biol Chem **279**: 36923-36930

Bairoch A, Apweiler R (2000) The SWISS-PROT protein sequence database and its supplement TrEMBL in 2000. Nucleic Acids Res **28**: 45-48

Berman-Frank I, Bidle K, Haramaty L, Falkowski P (2004) The demise of the marine cyanobacterium, *Trichodesmium* spp., via an autocatalyzed cell death pathway. ASLO **49**: 9

Bidle KA, Haramaty L, Baggett N, Nannen J, Bidle KD (2010) Tantalizing evidence for caspase-like protein expression and activity in the cellular stress response of Archaea. Environmental Microbiology **12**: 1161-1172

Bidle KD, Bender SJ (2008) Iron starvation and culture age activate metacaspases and programmed cell death in the marine diatom *Thalassiosira pseudonana*. Eukaryotic Cell **7**: 223-236

Bidle KD, Haramaty L, Barcelos e Ramos J, Falkowski P (2007) Viral activation and recruitment of metacaspases in the unicellular coccolithophore, *Emiliania huxleyi*. P Natl Acad Sci USA **104**: 6049-6054

Blumwald E, Aharon GS, B CHL (1998) Early signal transduction pathways in plant-pathogen interactions. Trends Plant Sci **3**: 342-346

Bonneau L, Ge Y, Drury GE, Gallois P (2008) What happened to plant caspases? J Exp Bot **59**: 491-499

Bouchard JN, Purdie DA (2011) Temporal variation of caspase 3-like protein activity in cultures of the harmful dinoflagellates *Karenia brevis* and *Karenia mikimotoi*. Journal of Plankton Research **33**: 961-972

Chan KL, New D, Ghandhi S, Wong F, Lam CMC, Wong JTY (2002) Transcript Levels of the Eukaryotic Translation Initiation Factor 5A Gene Peak at Early G1 Phase of the Cell Cycle in the Dinoflagellate *Crypthecodinium cohnii*. Appl Environ Microb **68**: 2278-2284

Chichkova NV, Shaw J, Galiullina RA, Drury GE, Tuzhikov AI, Kim SH, Kalkum M, Hong TB, Gorshkova EN, Torrance L, Vartapetian AB, Taliansky M (2010) Phytaspase, a relocalisable cell death promoting plant protease with caspase specificity. Embo J **29**: 1149-1161

Chung CC, Hwang SL, Chang J (2005) Cooccurrence of ScDSP gene expression, cell death, and DNA fragmentation in a marine diatom, *Skeletonema costatum*. Appl Environ Microbiol **71**: 8744–8751

Chung CC, Hwang SL, Chang J (2008) Nitric oxide as a signaling factor to upregulate the death-specific protein in a marine diatom, *Skeletonema costatum*, during blockage of electron flow in photosynthesis Appl Environ Microbiol **74**: 6521–6527

Coffeen WC, Wolpert TJ (2004) Purification and characterization of serine proteases that exhibit caspase-like activity and are associated with programmed cell death in *Avena sativa*. The Plant Cell Online **16**: 857-873

Conesa A, Götz S, García-Gómez JM, Terol J, Talón M, Robles M (2005) Blast2GO: a universal tool for annotation, visualization and analysis in functional genomics research. Bioinformatics **21**: 3674-3676

Crawford ED, Wells JA (2011) Caspase substrates and cellular remodeling. Annu Rev Biochem **80**: 1055-1087

Degterev A, Yuan J (2008) Expansion and evolution of cell death programmes. Nat Rev Mol Cell Biol **9**: 378-390

Deponte M (2008) Programmed cell death in protists. Biochim Biophys Acta **1783**: 1396 - 1405

Dix MM, Simon GM, Cravatt BF (2008) Global mapping of the topography and magnitude of proteolytic events in apoptosis. Cell **134**: 679-691

Durand PM, Rashidi A, Michod RE (2011) How an organism dies affects the fitness of its neighbors. The American naturalist **177**: 224-232

Earnshaw WC, Martins LM, Kaufmann SH (1999) Mammalian caspases: structure, activation, substrates, and functions during apoptosis. Annu Rev Biochem **68**: 383-424

Eisenberg T, Knauer H, Schauer A, Buttner S, Ruckenstuhl C, Carmona-Gutierrez D, Ring J, Schroeder S, Magnes C, Antonacci L, Fussi H, Deszcz L, Hartl R, Schraml E, Criollo A, Megalou E, Weiskopf D, Laun P, Heeren G, Breitenbach M, Grubeck-Loebenstein B, Herker E, Fahrenkrog B, Frohlich KU, Sinner F, Tavernarakis N, Minois N, Kroemer G, Madeo F (2009) Induction of autophagy by spermidine promotes longevity. Nat Cell Biol **11**: 1305-1314

Fabrizio P, Battistella L, Vardavas R, Gattazzo C, Liou LL, Diaspro A, Dossen JW, Gralla EB, Longo VD (2004) Superoxide is a mediator of an altruistic aging program in *Saccharomyces cerevisiae*. J Cell Biol **166**: 1055-1067

Fischer U, Janicke RU, Schulze-Osthoff K (2003) Many cuts to ruin: a comprehensive update of caspase substrates. Cell Death Differ **10**: 76-100

Franklin DJ, Berges JA (2004) Mortality in cultures of the dinoflagellate *Amphidinium carterae* during culture senescence and darkness. Proc Biol Sci **271**: 2099-2107

Franklin DJ, Brussaard CPD, Berges JA (2006) What is the role and nature of programmed cell death in phytoplankton ecology? Eur J Phycol **41**: 1-14

Gupta S, Norte M, Shimizu Y (1989) Biosynthesis of saxitoxin analogues: the origin and introduction mechanism of the side-chain carbon. Journal of the Chemical Society, Chemical Communications: 1421-1424

Hatsugai N, Iwasaki S, Tamura K, Kondo M, Fuji K, Ogasawara K, Nishimura M, Hara-Nishimura I (2009) A novel membrane fusion-mediated plant immunity against bacterial pathogens. Genes Dev **23**: 2496-2506

Hatsugai N, Kuroyanagi M, Yamada K, Meshi T, Tsuda S, Kondo M, Nishimura M, Hara-Nishimura I (2004) A plant vacuolar protease, VPE, mediates virus-induced hypersensitive cell death. Science **305**: 855-858

Herker E, Jungwirth H, Lehmann KA, Maldener C, Frohlich KU, Wissing S, Buttner S, Fehr M, Sigrist S, Madeo F (2004) Chronological aging leads to apoptosis in yeast. J Cell Biol **164**: 501-507

Ho P, Kong KF, Chan YH, Tsang JS, Wong JT (2007) An unusual S-adenosylmethionine synthetase gene from dinoflagellate is methylated. BMC Mol Biol **8**: 87

Jiang Q, Qin S, Wu QY (2010) Genome-wide comparative analysis of metacaspases in unicellular and filamentous cyanobacteria. BMC Genomics **11**: 198

Johnson JG, Morey JS, Neely MG, Ryan JC, Van Dolah FM (2012) Transcriptome remodeling associated with chronological aging in the dinoflagellate *Karenia brevis*. Marine Genomics: 10.1016/j.margen.2011.1008.1005

Kellmann R, Stuken A, Orr RJ, Svendsen HM, Jakobsen KS (2010) Biosynthesis and molecular genetics of polyketides in marine dinoflagellates. Marine drugs **8**: 1011-1048

Kuroyanagi M, Nishimura M, Hara-Nishimura I (2002) Activation of *Arabidopsis* vacuolar processing enzyme by self-catalytic removal of an auto-inhibitory domain of the C-terminal propeptide. Plant and Cell Physiology **43**: 143-151

Levasseur M, Thompson PA, Harrison PJ (1993) Physiological acclimation of marine phytoplankton to different nitrogen sources. J Phycol **29**: 587-595

Luthi AU, Martin SJ (2007) The CASBAH: a searchable database of caspase substrates. Cell Death Differ **14**: 641-650

Madeo F, Herker E, Maldener C, Wissing S, Lachelt S, Herlan M, Fehr M, Lauber K, Sigrist SJ, Wesselborg S, Frohlich KU (2002) A caspase-related protease regulates apoptosis in yeast. Mol Cell **9**: 911-917

Mahrus S, Trinidad JC, Barkan DT, Sali A, Burlingame AL, Wells JA (2008) Global sequencing of proteolytic cleavage sites in apoptosis by specific labeling of protein N termini. Cell **134**: 866-876

McGinnis KM, Whitton MM, Gnegy ME, Wang KKW (1998) Calcium/calmodulin-dependent protein kinase IV is cleaved by caspase-3 and calpain in SH-SY5Y human neuroblastoma cells undergoing apoptosis. J Biol Chem **273**: 19993-20000

Miller-Morey JS, Van Dolah FM (2004) Differential responses of stress proteins, antioxidant enzymes, and photosynthetic efficiency to physiological stresses in the Florida red tide dinoflagellate, *Karenia brevis*. Comp Biochem Phys C **138**: 493-505

Min XJ, Butler G, Storms R, Tsang A (2005) OrfPredictor: predicting protein-coding regions in EST-derived sequences. Nucleic Acids Res **33**: W677-W680

Nedelcu AM, Driscoll WW, Durand PM, Herron MD, Rashidi A (2011) On the paradigm of altruistic suicide in the unicellular world. Evolution; international journal of organic evolution **65**: 3-20

Piippo M, Lietzen N, Nevalainen OS, Salmi J, Nyman TA (2010) Pripper: prediction of caspase cleavage sites from whole proteomes. BMC Bioinformatics **11**: 320

Rao BJ, Moharikar S, D'Souza JS, Kulkarni AB (2006) Apoptotic-like cell death pathway is induced in unicellular chlorophyte *Chlamydomonas reinhardtii* (Chlorophyceae) cells following UV irradiation: Detection and functional analyses. J Phycol **42**: 423-433

Rawlings ND, Morton FR, Kok CY, Kong J, Barrett AJ (2008) MEROPS: the peptidase database. Nucleic Acids Res **36**: 320-325

Reytor E, Perez-Miguelsanz J, Alvarez L, Perez-Sala D, Pajares MA (2009) Conformational signals in the C-terminal domain of methionine adenosyltransferase I/III determine its nucleocytoplasmic distribution. FASEB J **23**: 3347-3360

Sanmartín M, Jaroszewski L, Raikhel NV, Rojo E (2005) Caspases. Regulating Death Since the Origin of Life. Plant Physiol **137**: 841-847

Segovia M, Berges JA (2005) Effect of inhibitors of protein synthesis and DNA replication on the induction of proteolytic activities, caspase-like activities and cell death in the unicellular chlorophyte *Dunaliella tertiolecta*. Eur J Phycol **40**: 21-30

Segovia M, Berges JA (2009) Inhibition of caspase-like activities prevents the appearance of reactive oxygen species and dark-induced apoptosis in the unicellular chlorophyte *Dunaliella tertiolecta*. J Phycol **45**: 1116-1126

Segovia M, Haramaty L, Berges JA, Falkowski PG (2003) Cell death in the unicellular chlorophyte *Dunaliella tertiolecta*. A hypothesis on the evolution of apoptosis in higher plants and metazoans. Plant Physiol **132**: 99-105

Shimizu Y (1996) Microalgal metabolites: a new perspective. Annu Rev Microbiol **50**: 431-465

Song J, Tan H, Shen H, Mahmood K, Boyd SE, Webb GI, Akutsu T, Whisstock JC (2010) Cascleave: towards more accurate prediction of caspase substrate cleavage sites. Bioinformatics **26**: 752-760

Sun X-M, Butterworth M, MacFarlane M, Dubiel W, Ciechanover A, Cohen GM (2004) Caspase activation inhibits proteasome function during apoptosis. Molecular Cell **14**: 81-93

Talanian RV, Quinlan C, Trautz S, Hackett MC, Mankovich JA, Banach D, Ghayur T, Brady KD, Wong WW (1997) Substrate specificities of caspase family proteases. J Biol Chem **272**: 9677-9682

Tatusov RL, Galperin MY, Natale DA, Koonin EV (2000) The COG database: a tool for genome-scale analysis of protein functions and evolution. Nucleic Acids Research **28**: 33-36

Taylor RC, Cullen SP, Martin SJ (2008) Apoptosis: controlled demolition at the cellular level. Nat Rev Mol Cell Biol **9**: 231-241

Thamatrakoln K, Korenovska O, Niheu AK, Bidle KD (2011) Whole-genome expression analysis reveals a role for death-related genes in stress acclimation of the diatom Thalassiosira pseudonana. Environmental Microbiology: no-no

Tsiatsiani L, Van Breusegem F, Gallois P, Zavialov A, Lam E, Bozhkov PV (2011) Metacaspases. Cell Death Differ **18**: 1279-1288

Uren AG, O'Rourke K, Aravind L, Pisabarro MT, Seshagiri S, Koonin EV, Dixit VM (2000) Identification of paracaspases and metacaspases: Two ancient families of caspase-like proteins, one of which plays a key role in MALT lymphoma. Molecular Cell **6**: 961-967

Vardi A, Berman-Frank I, Rozenberg T, Hadas O, Kaplan A, Levine A (1999) Programmed cell death of the dinoflagellate *Peridinium gatunense* is mediated by CO_2 limitation and oxidative stress. Curr Biol **9**: 1061-1064

Vardi A, Eisenstadt D, Murik O, Berman-Frank I, Zohary T, Levine A, Kaplan A (2007) Synchronization of cell death in a dinoflagellate population is mediated by an excreted thiol protease. Environ Microbiol **9**: 360-369

Vercammen D, van de Cotte B, De Jaeger G, Eeckhout D, Casteels P, Vandepoele K, Vandenberghe I, Van Beeumen J, Inzé D, Van Breusegem F (2004) Type II metacaspases Atmc4 and Atmc9 of *Arabidopsis thaliana* cleave substrates after arginine and lysine. J Biol Chem **279**: 45329-45336

Vincent WF, Neale PJ, Richerson PJ (1984) Photoinhibition: algal responses to bright light during diel stratification and mixing in a tropical alpine lake. J Phycol **20**: 201-211

Watanabe N, Lam E (2005) Two *Arabidopsis* metacaspases AtMCP1b and AtMCP2b are arginine/lysine-specific cysteine proteases and activate apoptosis-like cell death in yeast. J Biol Chem **280**: 14691-14699

Wee LJ, Tan TW, Ranganathan S (2006) SVM-based prediction of caspase substrate cleavage sites. BMC Bioinformatics **7 Suppl 5**: S14

Wee LJ, Tan TW, Ranganathan S (2007) CASVM: web server for SVM-based prediction of caspase substrates cleavage sites. Bioinformatics **23**: 3241-3243

Wee LJ, Tong JC, Tan TW, Ranganathan S (2009) A multi-factor model for caspase degradome prediction. BMC Genomics **10** 6

Table 1. K. brevis EST sequences potentially responsible for caspase activity during chronological aging.

Protein ID	Top BLAST Hit Description[a]	BLASTx E value	BLAST Accession	Conserved Domain	Pfam E value	Domain Position	H95 (F/YSGHG)[b]	C147 (DC/SCHSG)[c]
MGID2041795	metacaspase CasA [Aspergillus fumigatus]	9.00E-48	B0XPP3.2	Pfam00656 Peptidase_C14	5.41E-23	162-423	YSGHG	DCCHSG
MGID2055388	metacaspase 1 precursor [Toxoplasma gondii ME49]	2.00E-80	XP_002367830.1	Pfam00656 Peptidase_C14	1.11E-40	105-351	FSGHG	DSCHSG
MGID2080978	metacaspase CasA [Metarhizium anisopliae ARSEF 23]	3.00E-38	EFY99590.1	Pfam00656 Peptidase_C14	7.62E-25	121-247	FSGHG	DSCHSG
MGID2080273	metacaspase [Chlorobium chlorochromatii CaD3]	1.00E-08	YP_379199.1	Pfam00656 Peptidase_C14	4.75E-06	1-267	FTGYG	DCCHST
MGID2027748	metacaspase-1 [Schizosaccharomyces japonicus yFS275]	7.00E-17	XP_002171430.1	Pfam00656 Peptidase_C14	1.87E-10	308-392		
MGID2063352	metacaspase 1 precursor [Toxoplasma gondii ME49]	8.00E-11	XP_002367830.1					
MGID2073387	metacaspase [Ectocarpus siliculosus]	7.00E-11	CBN76943.1	Pfam00168, C2 Domain	6.20E-06			

Protein ID	Top BLAST Hit Description[d]	BLASTx E value	BLAST Accession	Conserved Domain (E value)
MGID2024084	peptidase C14, caspase catalytic subunit p20 [Methylobacterium nodulans ORS 2060]	4.00E-30	YP_002497753.1	cd00189, TPR Motif (5.02E-14)
MGID0107031	peptidase C14, caspase catalytic subunit p20 [Trichodesmium erythraeum IMS101]	6.00E-17	YP_721570.1	COG1413, FOG: HEAT Repeat (3.21E-04)
MGID0107600	peptidase C14, caspase catalytic subunit p20 [Trichodesmium erythraeum IMS101]	9.00E-05	YP_721570.1	COG1413, FOG: HEAT Repeat (4.24E-03)
MGID1967466	peptidase C14, caspase catalytic subunit p20 [Trichodesmium erythraeum IMS101]	1.00E-19	YP_721570.1	
MGID2022866	peptidase C14, caspase catalytic subunit p20 [Trichodesmium erythraeum IMS101]	3.00E-16	YP_721570.1	COG1413, FOG: HEAT Repeat (1.09E-10), COG5116, 26S Proteosomal Regulatory Domain (9.06E-06)
MGID2046356	peptidase C14, caspase catalytic subunit p20 [Trichodesmium erythraeum IMS101]	1.00E-18	YP_721570.1	COG1413, FOG: HEAT Repeat (2.24E-06)
MGID2049920	peptidase C14, caspase catalytic subunit p20 [Trichodesmium erythraeum IMS101]	5.00E-08	YP_721570.1	COG1413, FOG: HEAT Repeat (6.3E-04), COG5218, YCG1 (4.1E-06)
MGID2052384	peptidase C14, caspase catalytic subunit p20 [Trichodesmium erythraeum IMS101]	3.00E-13	YP_721570.1	pfam01602, Adaptin Domain (9.72E-03), COG1413, FOG: HEAT Repeat (2.12E-07)
MGID2073823	peptidase C14, caspase catalytic subunit p20 [Trichodesmium erythraeum IMS101]	5.00E-27	YP_721570.1	
MGID2074455	peptidase C14, caspase catalytic subunit p20 [Trichodesmium erythraeum IMS101]	4.00E-24	YP_721570.1	cd00020, ARM (7.28E-04), COG1413, FOG: Heat Repeat, (3.03E-07), PRK09687, putative lyase (3.56E-05)
MGID2078979	peptidase C14, caspase catalytic subunit p20 [Trichodesmium erythraeum IMS101]	1.00E-19	YP_721570.1	COG1413, FOG: HEAT Repeat (4.59E-06)

Protein ID	Top BLAST Hit Description[e]	BLASTx E value	BLAST Accession	Conserved Domain	Pfam E value	Domain Position	Asp/His/Ser Catalytic Position[f]
MGID2028549	peptidase S8 subtilisin [Shewanella denitrificans OS217]	4.00E-71	YP_563870.1	Pfam00082 Peptidase_S8	8.95E-55	191-431	217/259/414
MGID1977692	peptidase, S8A (subtilisin) subfamily [Streptomyces griseoflavus Tu4000]	2.00E-22	ZP_07313175.1	Pfam00082 Peptidase_S8	4.65E-11	173-251	199/241/x

[a] Metacaspase sequences.

[b] Catalytic histidine (underlined) sequence context for metacaspases.

[c] Catalytic cysteine (underlined) sequence context for metacaspases, demonstrating alternative pocket chemistry (aspartic acid residue - bolded).

[d] Peptidase C14, caspase catalytic subunit p20 containing sequences.

[e] Subitilisin/vacuolar peptidase enzyme sequences.

[f] Sequence positions of the three subtilisin catalytic residues (x constitutes residue number unknown).

Table 2. *K. brevis* proteins containing DEVD, IETD, VEID, LEHD, and WEHD caspase cleavage sites annotated with BLASTx e values < 10^{-4}.

P4,P3,P2,P1 Substrate Specificity	Protein ID*	Sequence Description	NCBI Accession	BLASTx E value	P1 Location	CasCleave Prob. Score	KOG Cat./#		KOG E value	KOG Description
DEVD	MGID0102898	sperm-specific sodium proton exchanger [*Strongylocentrotus purpuratus*]	NP_001091927	4.06E-09	157	0.949	S			
DEVD	MGID1946126	light polypeptide [*Xenopus laevis*]	NP_001086688	1.83E-08	77	1.231	S			
DEVD	MGID1957111	ubiquitin domain-containing protein [*Dictyostelium discoideum* AX4]	XP_643687	9.16E-09	80	1.218	O	1863	1 e-08	Ubiquitin carboxyl-terminal hydrolase
DEVD	MGID1981494	f-box and leucine-rich repeat protein 2 [*Mus musculus*]	BAC32036	1.10E-39	50	1.034	R	4341	3 e-40	F-box protein containing LRR
DEVD	MGID1983083	abc transporter related [*Lentisphaera araneosa* HTCC2155]	ZP_01874597	7.33E-37	151	1.324	S			
DEVD	MGID1990736	amp-binding enzyme family expressed [*Ricinus communis*]	ABC02882	1.16E-11	80	1.096	I	1256	1 e-12	Long-chain acyl-CoA synthetases (AMP-forming)
DEVD	MGID1992462	kif1 binding protein [*Xenopus* (Silurana) *tropicalis*]	NP_001072796	1.99E-17	62	1.069	S			
DEVD	MGID1992863	dna (cytosine-5-)-methyltransferase 8 [*Physcomitrella patens* subsp. *patens*]	XP_001761999	2.35E-20	39	1.333	S			
DEVD	MGID1993397	choline-sulfatase [*Karenia brevis*]	ABV49389	3.18E-117	49	1.047	S			
DEVD	MGID2034299	26s proteasome regulatory atpase subunit [*Phaeodactylum tricornutum* CCAP 1055/1]	XP_002185707	0	278	1.255	O	0729	0	26S proteasome regulatory complex, ATPase RPT1
DEVD	MGID2039477	cysteine protease 1 [*Noctiluca scintillans*]	ABV22332	9.49E-117	369	1.364	O	0284	3 e-76	Polyadenylation factor I complex, subunit PFS2
DEVD	MGID2047523	cobalamin synthesis protein p47k [*Micromonas* sp. RCC299]	ACO60866	1.17E-33	129	1.000	H	2743	1 e-20	Cobalamin synthesis protein
DEVD	MGID2050489	calcium-dependent protein [*Toxoplasma gondii* GT1]	EEE19066	1.96E-73	501	1.125	T	0032	3 e-57	Ca2+/calmodulin-dependent protein kinase, EF-Hand protein superfamily
DEVD	MGID2053052	protein [*Ostreococcus lucimarinus* CCE9901]	XP_001417798	7.31E-15	127	0.916	S			
DEVD	MGID2053669	glutamic acid reigh protein [*Micromonas* sp. RCC299]	ACO61940	1.02E-06	459	1.358	S			
DEVD	MGID2060076	loc733353 protein [*Ostreococcus tauri*]	CAL57510	4.90E-16	204	1.050	BT	2132	5 e-13	Uncharacterized conserved protein, contains JmjC domain
DEVD	MGID2064552	methionine s-adenosyl transferase [*Asterionella glacialis*]	BAH30216	3.48E-175	483	1.112	H	1506	1 e-111	S-adenosylmethionine synthetase
DEVD	MGID2073449	inosine-5 -monophosphate [*Toxoplasma gondii* GT1]	EEE26779	1.20E-131	459	0.136	F	2550	1 e-119	IMP dehydrogenase/GMP reductase
DEVD	MGID2077931	preprotein translocase subunit [*Amoebophilus asiaticus* 5a2]	YP_001958210	1.27E-06	183	1.187	S			
DEVD	MGID2079096	zinc-binding dehydrogenase family [*Bacillus coahuilensis* m4-4]	ZP_03225209	1.49E-55	40	1.238	R	1196	7 e-53	Predicted NAD-dependent oxidoreductase
DEVD	MGID2080113	ylr387 2x c2h2 like zinc fingers globular domain [*Cryptosporidium hominis* TU502]	XP_665524	3.07E-16	92	1.190	S			
LEHD	MGID1981750	predicted protein [*Nematostella vectensis*]	XP_001639387	9.04E-07	221	0.596	S			
LEHD	MGID1985572	trna-splicing endonuclease positive effector [*Ostreococcus tauri*]	CAL56344	2.01E-43	44	0.179	A	1802	5 e-36	RNA helicase nonsense mRNA reducing factor (pNORF1)
LEHD	MGID1987917	family methyltransferase [*Solibacter usitatus* 6076]	YP_821940	7.94E-12	70	0.028	S			
LEHD	MGID2027111	ac026758_4 proline oxidase [*Physcomitrella patens* subsp. *patens*]	XP_001757226	5.67E-05	230	0.191	S			
LEHD	MGID2031015	ankyrin unc44 [*Aspergillus oryzae* RIB40]	XP_001824279	1.37E-23	104	0.483	S			
LEHD	MGID2033333	RUBISCO large subunit n- chloroplast precursor [*Ostreococcus lucimarinus* CCE9901]	XP_001421544	1.09E-05	403	0.057	R	1337	2 e-03	N-methyltransferase
LEHD	MGID2037550	PREDICTED: hypothetical protein [*Mus musculus*]	XP_001478231	1.84E-16	227	0.915	S			
VEID	MGID1943724	upf0326 protein fam152a [*Caligus rogercresseyi*]	ACO11290	1.67E-09	20	1.030	S	0324	2 e-10	Uncharacterized conserved protein
VEID	MGID1967828	glycoprotein 96-92 [*Leishmania infantum*]	XP_001470263	3.52E-04	214	0.215	S			
VEID	MGID1981598	c-5 cytosine-specific dna methylase [*Micromonas* sp. RCC299]	ACO61513	6.55E-19	152	0.764	S			
VEID	MGID1984244	protein [*Trypanosoma brucei* TREU927]	XP_823237	2.20E-22	53	0.479	R	4197	7 e-19	FOG: PPR repeat
VEID	MGID2033906	chromosome 14 open reading frame 166b [*Monodelphis domestica*]	XP_001374437	2.51E-04	184	0.997	S			
VEID	MGID2034128	protein [*Micromonas* sp. RCC299]	ACO62381	8.32E-28	362	0.893	S			
VEID	MGID2039273	keratin associated protein 4-like [*Mus musculus*]	NP_001119792	7.06E-04	149	1.195	S			
VEID	MGID2040705	cog3781: membrane protein [*Ostreococcus tauri*]	CAL52384	1.30E-17	166	0.207	S			
VEID	MGID2041310	hypothetical protein BF1421 [*Bacteroides fragilis* YCH46]	YP_098706	9.79E-37	159	0.772	S			
VEID	MGID2042374	intraflagellar transport particle protein ift140 [*Chlamydomonas reinhardtii*]	XP_001696098	2.87E-32	16	0.297	R	3617	2 e-29	Lysosomal-associated membrane protein
VEID	MGID2043655	predicted protein [*Coprinopsis cinerea okayama* 7#130]	XP_001839218	2.19E-04	39	0.911	S			
IETD	MGID1981394	elegans protein partially confirmed by transcript evidence [*Ustilago maydis* 521]	XP_761160	1.21E-07	139	0.575	D	2277	1 e-07	S-M checkpoint control protein CID1 and related nucleotidyltransferases
IETD	MGID1992002	sperm-associated cation channel 2 isoform 2 [*Macaca mulatta*]	XP_001108392	7.92E-13	79	0.299	PT	2301	3 e-13	Voltage-gated Ca2+ channels, alpha1 subunits
IETD	MGID2047667	autophagy 5-like [*Vitis vinifera*]	XP_002276604	1.70E-20	20	0.641	O	2976	2 e-18	Protein involved in autophagy and nutrient starvation
IETD	MGID2053397	isoamyl acetate-hydrolyzing esterase [*Vitis vinifera*]	XP_002282452	1.76E-17	59	0.265	I	3035	8 e-12	Isoamyl acetate-hydrolyzing esterase
WEHD	MGID2062880	hypothetical protein SACE_5139 [*Saccharopolyspora erythraea* NRRL 2338]	YP_001107309	2.27E-06	63	0.227	S			

*Bolded protein ID numbers indicates the protein was identified as containing caspase cleavage sites by both Pripper and CasCleave analyses.

Figure 1. Growth, photosynthetic efficiency, and viability during chronological aging.

(A) Cell abundance for each biological replicate (■) and average growth rate (x) at each timepoint. Error bars represent the standard deviation of the biological replicates (n=3); x-axis, time (days); left y-axis, cell concentration (cells mL^{-1}); right y-axis, growth rate (d^{-1}). **(B)** Photosynthetic efficiency of photosystem II for each biological replicate plotted represents the average of three technical replicates, and error bars reflects the standard deviation of the replicates (n=3). **(C)** Mean cell viability (% Sytox-negative) measured across time (error bars represent the standard deviation of the biological replicates, n=3).

A.

B.

C.

SYTOX-positive   SYTOX-negative
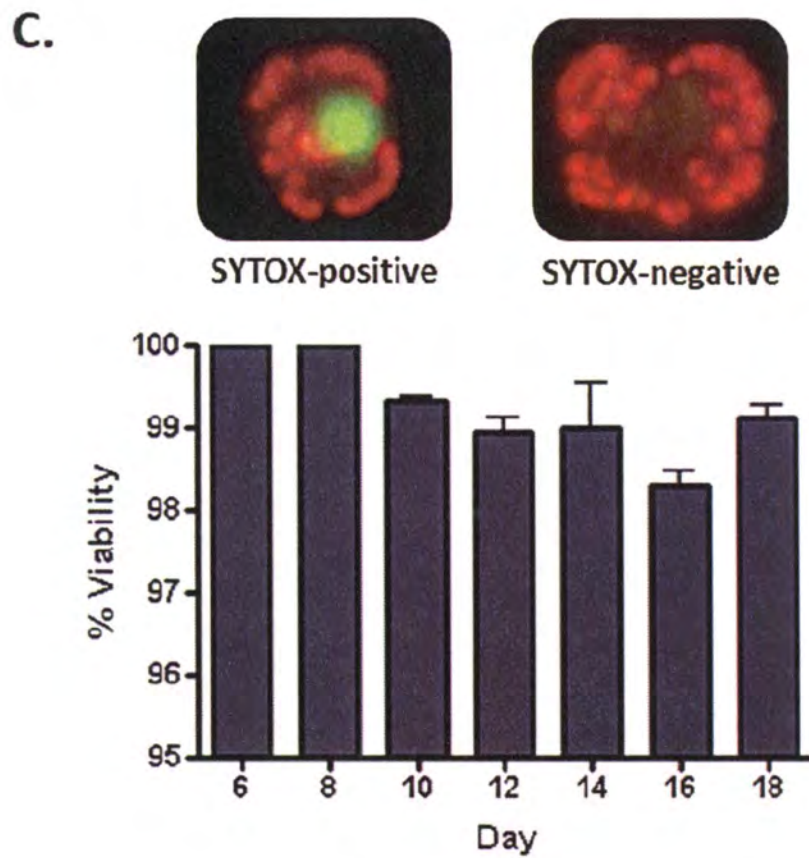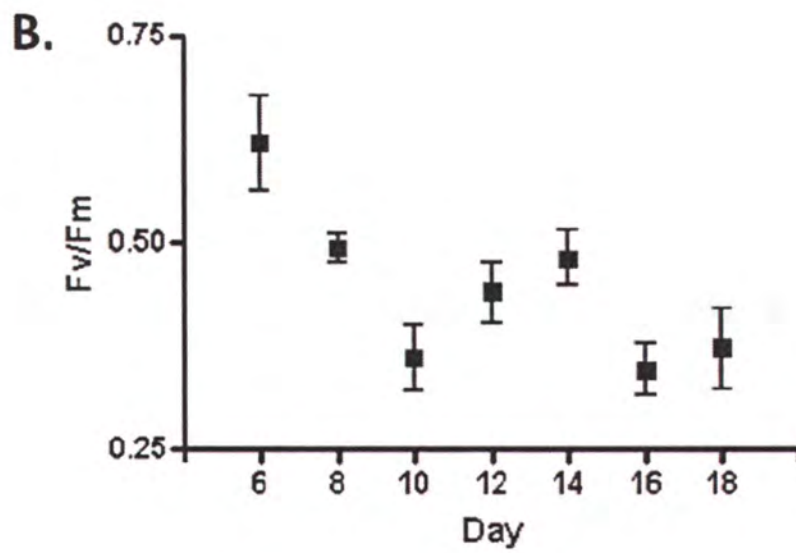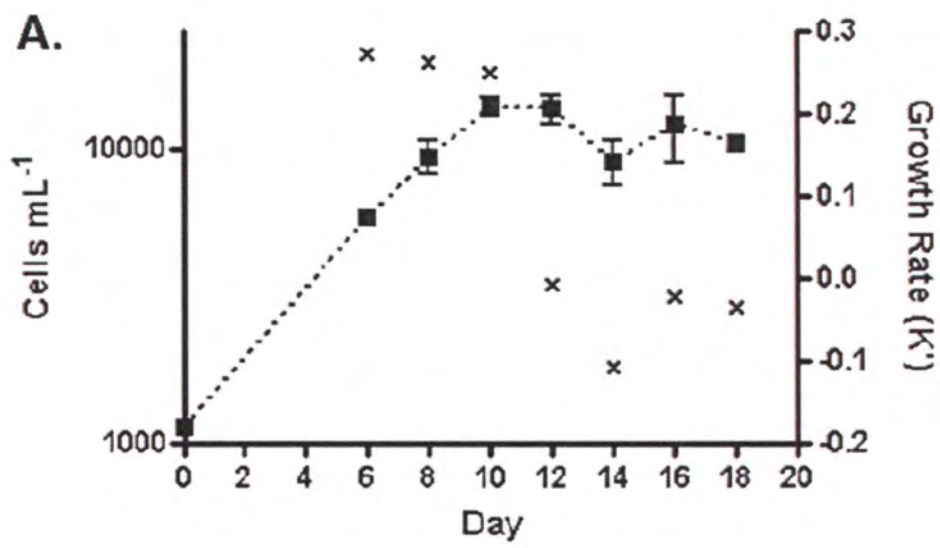
Figure 2. Caspase activity during chronological aging.

(A-E) Caspase specific activity, expressed as pcmol AFC cleaved/mg protein/hr, over a growth

curve. Individual biological replicates plotted represent an average of three technical assay

replicates (technical error bars are smaller than symbols). The distribution in caspase activity

was tested over time, and demonstrated a significant change over the growth curve ($p < 0.05$).

(A) Ac-DEVD activity (Kruskal Wallis, $p = 0.0065$), **(B)** Ac-LEHD activity (Kruskal Wallis, $p =$

0.0104), **(C)** Ac-VEID activity (Kruskal Wallis, $p = 0.0127$), **(D)** Ac-WEHD activity (Kruskal Wallis, p

$= 0.0165$), **(E)** Ac-IETD activity (Kruskal Wallis, $p = 0.1404$). **(F)** Spearman's Rho Correlation of

growth rate and caspase activities (all substrates) ($\rho = 0.7618$, $p < 0.0001$).

131
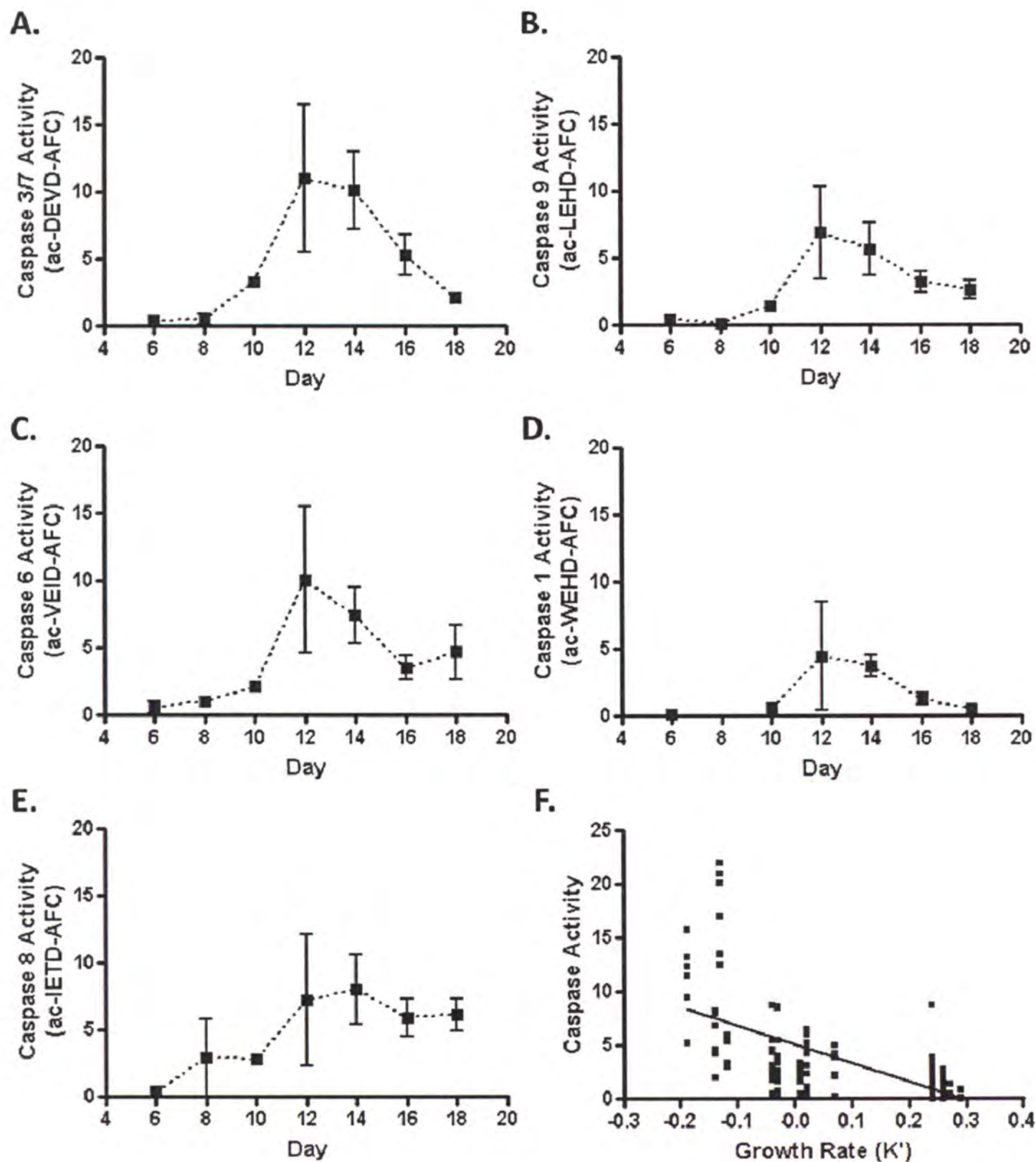
Figure 3. Oxidative Stress in Stationary Phase Cells and 80 mM H_2O_2 Treatment.

Control cells from logarithmic phase stained negative for ROS (panels A and B). Minimal staining was observed in a small population of control cells (<5%) of logarithmic phase cells (inset A.2, yellow spots are naturally occurring non-specific fluorescence of unknown origin). ROS staining in cells 80 μM H_2O_2 treatment for 10 minutes demonstrated that the cells bear a heavy ROS load, with uniform and bright staining in >95% of cells (panels C and D). ROS staining in stationary phase demonstrated that the majority of cells (>65%) were positively stained (panels E and F) and ROS staining precedes death (inset E.2.)
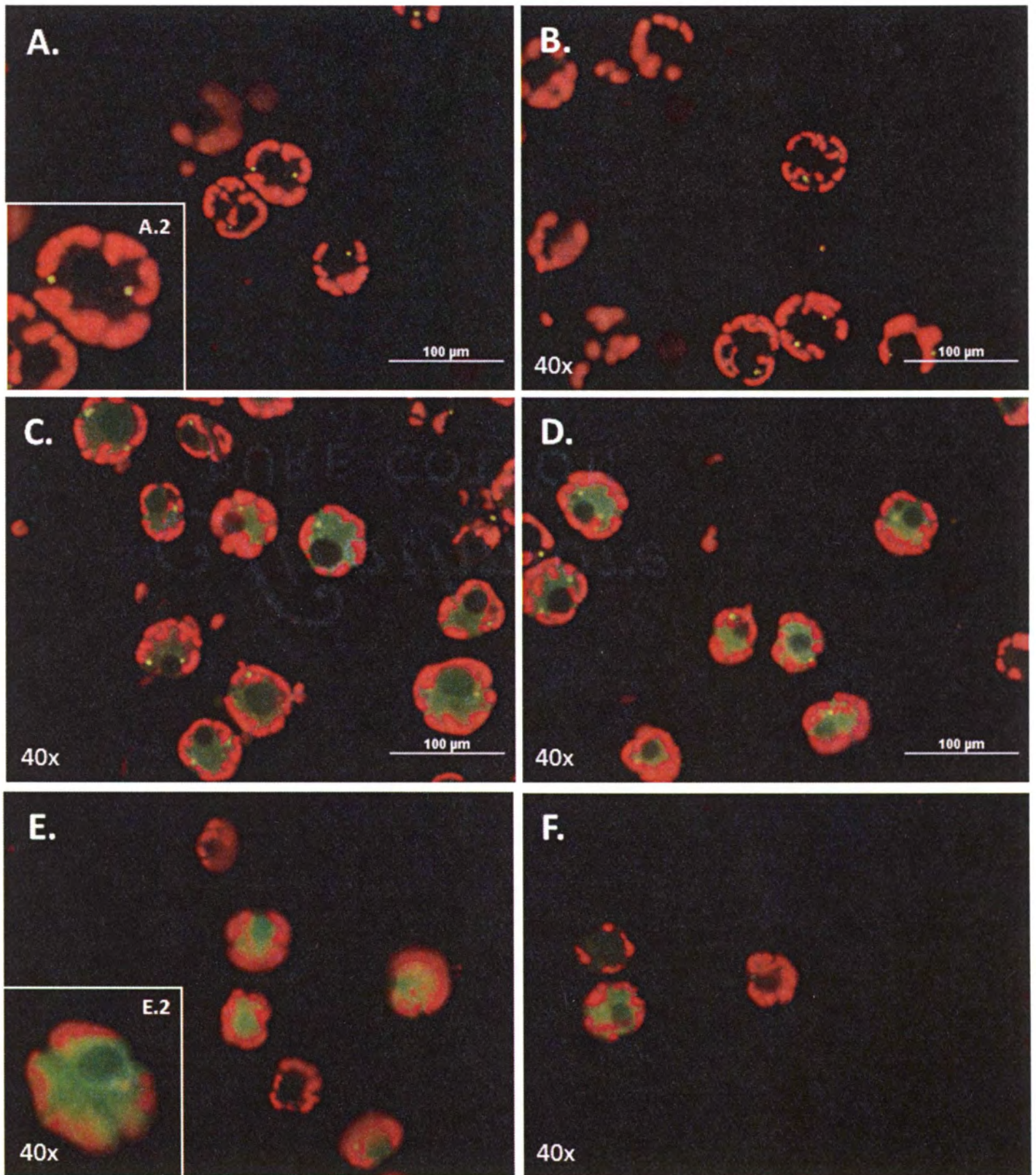
Figure 4. Caspase 3/7-like activity during ROS-induced cell death.

(A) Caspase 3/7 biochemical cleavage assay (DEVD activity). Caspase activity, expressed as pcmol of AFC cleaved/mg protein/hr, in control and 80 μM H_2O_2 treated cells. Individual replicates (n=3) represent an average of three technical replicates. The mean caspase activity values were compared using the Student's t-test as both treatment values demonstrated a normal distribution and equal variances, and were found to be significantly different from each other (P < 0.0001), with a 9.5-fold induction of caspase activity in treated cells. **(B)** *In situ* visualization of caspase 3/7-like activity during ROS-induced cell death. *K. brevis* cells (1 x 10^6) were incubated with the CellEvent Caspase 3/7 Green Detection reagent (final concentration, 5μM) and propidium iodide (final concentration, 1μg/mL) after treatment with 80 μM H_2O_2 (right) or vehicle control (left). Caspase positive cells were visualized with a FITC filter, and fluoresced bright green, while caspase positive cells only demonstrated chloroplast autoflourescence (red). PI positive cells (dead cells) were not included in any analyses. Magnification: 60X. **(C)** Quantification of *in situ* CellEvent Caspase 3/7 positive *K. brevis* cells during ROS-induced cell death. The percentage of caspase positive cells were quantified (error bars represent the average of three biological replicates, in which an average of three slides per replicate, with a minimum of 200 cells were counted per slide), and demonstrated a significant increase in caspase 3/7 activity in the 80 μM H_2O_2 treated cells compared to control (Welch's t-test, p < 0.0001).

A.
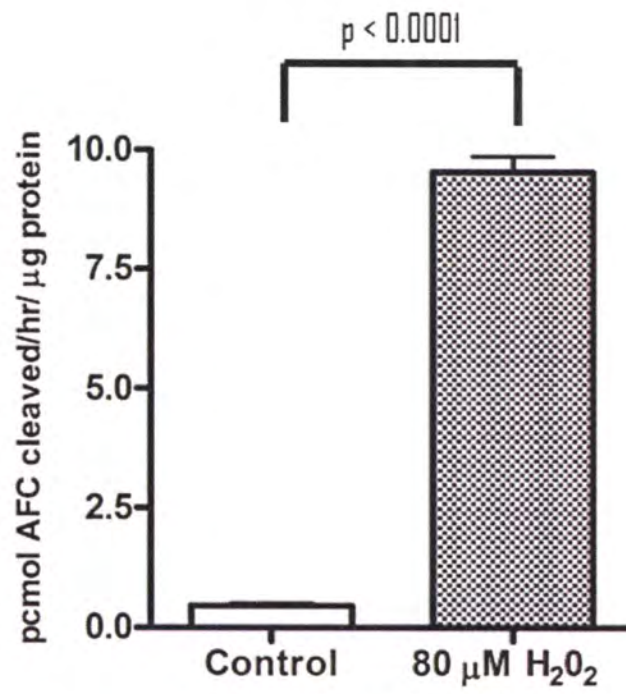
B.

Caspase-neg.
K. brevis cell
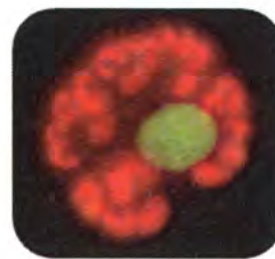
Caspase 3/7-pos.
K. brevis cell

C.
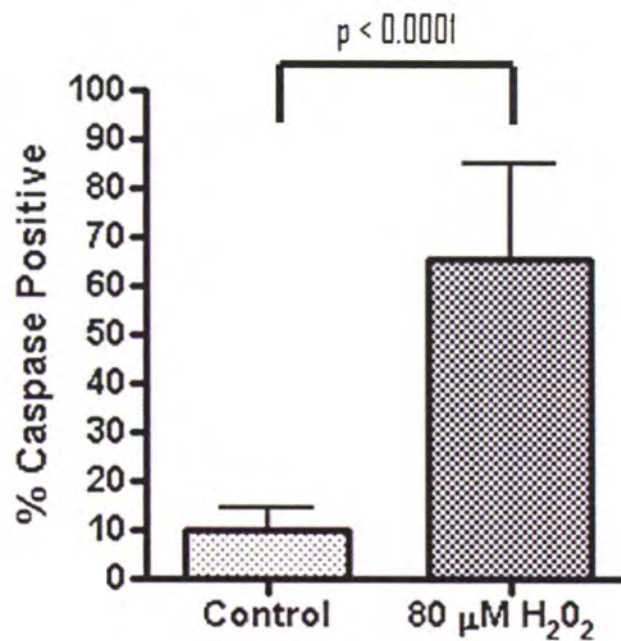
Figure 5. *K. brevis* **appears to die with two distinct sets of morphological changes during ROS-induced cell death.**

(A) *K. brevis* cells appear to either maintain cell shape and size, with nuclear migration and swelling (left representative cell), or undergoes dramatic blebbing (right representative cell). **(B)** Caspase activity only appears to be present in the former mode of death, whereas blebbing cells did not demonstrate caspase activation. Both cells were PI negative, magnification: 40X.

A.

Cytoplasmic bleb

Nuclear migration and swelling

100 µm
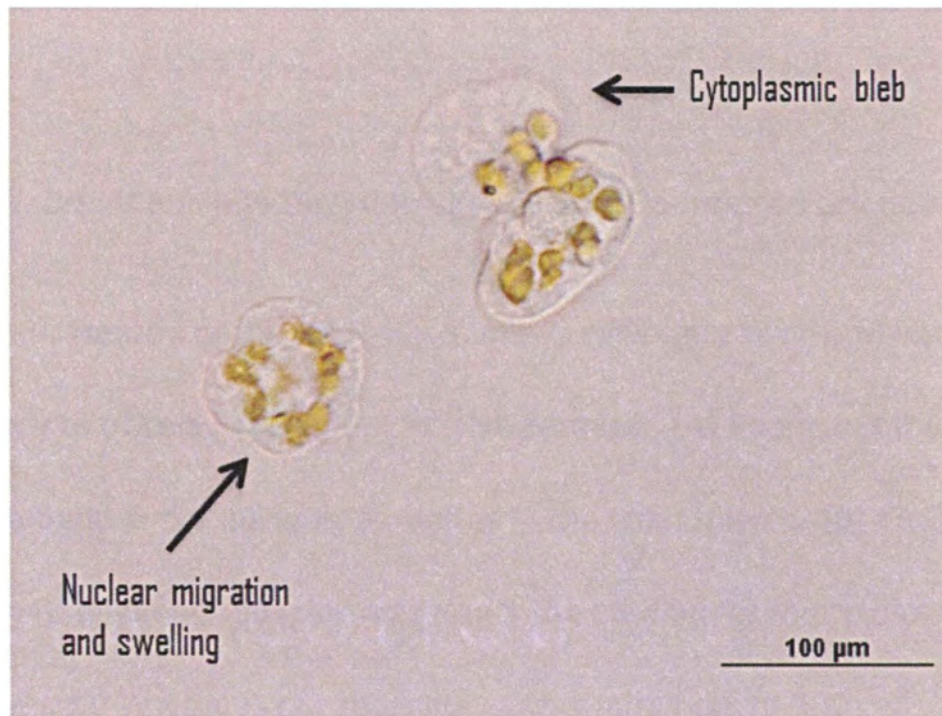
B.

Figure 6. *K. brevis* exhibits DNA damage during ROS-induced cell death.

Following treatment (untreated or 80 μM H_2O_2), *K. brevis* cells were fixed and immunostained with anti-BrdU antibody to observe the extent of DNA damage. **(A)** Representative positive cell demonstrating DNA damage in the nucleus, as well as in the chloroplasts. **(B)** The percentage of TUNEL positive cells were qualified (boxplot represents the median for four biological replicates, in which an average of three slides per replicate, with a minimum of 200 cells/slide were counted) and when compared between treatments (Student's t-test, $p < 0.0001$) demonstrated a significant increase in DNA damage in H_2O_2-treated cells.

A.
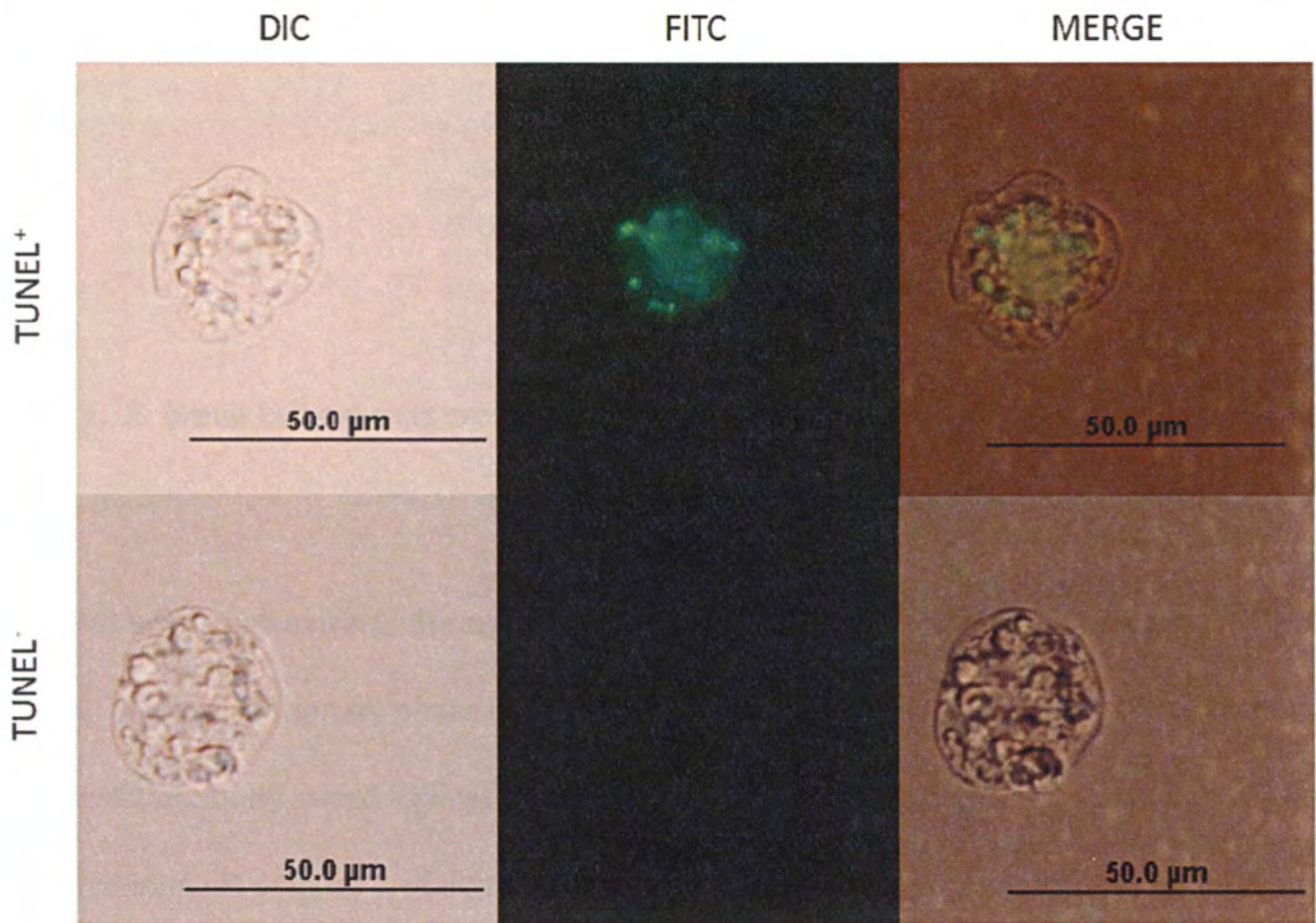
B.
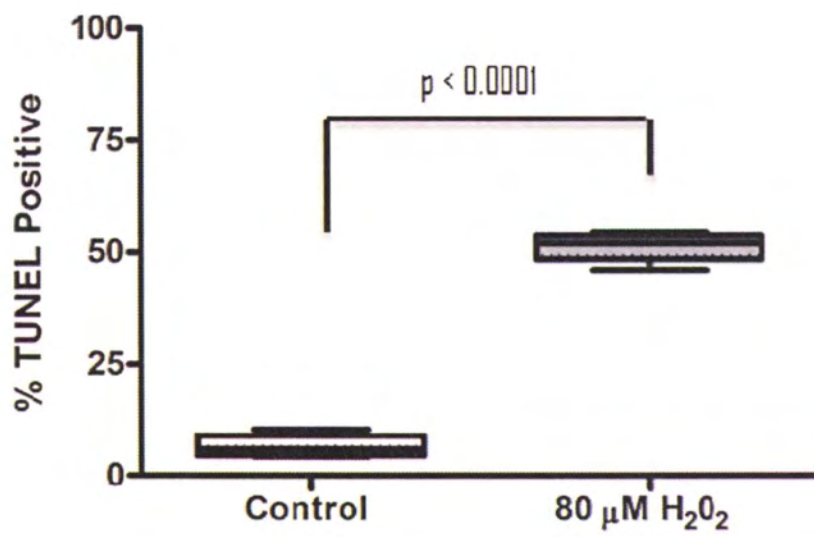
Figure 7. *K. brevis* **cell extracts cross-react with a polyclonal antibody raised against the active**

form of human caspase 3.

K. brevis whole cell extracts during mid-logarithmic (lane 3), the transition to stationary phase

(lane 4), and late stationary phase (lane 5) reveals immunohybridization of distinct proteins to a

polyclonal antibody raised against the recombinant active human caspase 3. 5X peptide block

with recombinant caspase 3 of extracts from the transition to stationary phase resulted in >50%

loss of signal when probed with the caspase 3 antibody (lane 6 – unblocked, lane 7 – blocked),

but immunoreactivity of *K. brevis* extracts to KbMC1 antibody (lane 8) was not affected by

caspase 3 peptide incubation (lane 9). Recombinant active caspase 3 protein probed with the

caspase 3 antibody served as a positive control (lane 2).
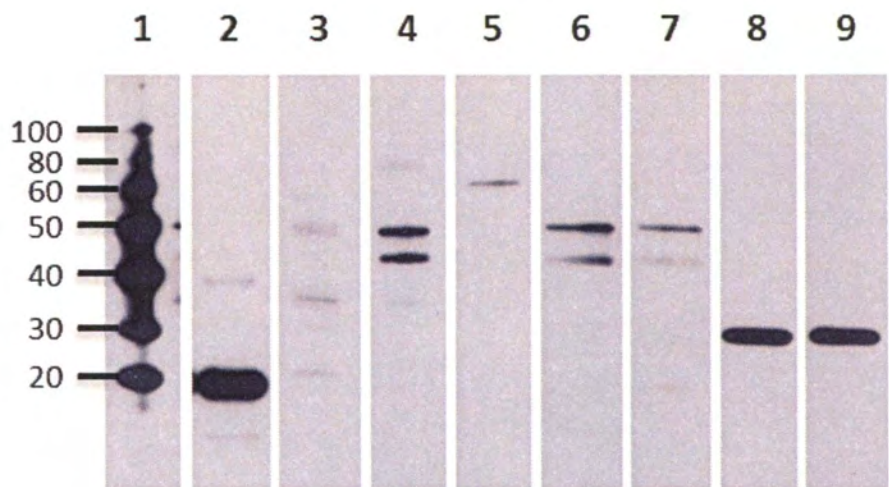
	1	2	3	4	5	6	7	8	9
Magic Marker (Invitrogen)	X								
Recombinant Caspase 3		X							
K. brevis: Mid-logarithmic			X						
K. brevis: Trans. to Stat. Phase				X		X	X	X	X
K. brevis: Stationary Phase					X				
Human Caspase 3 Ab		X	X	X	X	X	X		
KbMC1 Ab								X	X
Blocked w/ Casp. 3 Peptide							X		X

Figure 8. Caspase 3-like proteins in *K. brevis* are elevated, while KbMC1 decreases, during

H_2O_2-treatment

Western blot analysis of *K. brevis* extracts during control and H_2O_2-treatment for KbMC1 **(A)**, Mn

Superoxide Dismutase (MnSOD) **(B)**, and human caspase 3 **(C-E)** antibodies. Boxplots represent

densitometry values (n=4).

A. MnSOD Reactivity

B. Caspase 3 (66 kDa band) Reactivity

C. Caspase 3 (52 kDa band) Reactivity

D. Caspase 3 (42 kDa band) Reactivity
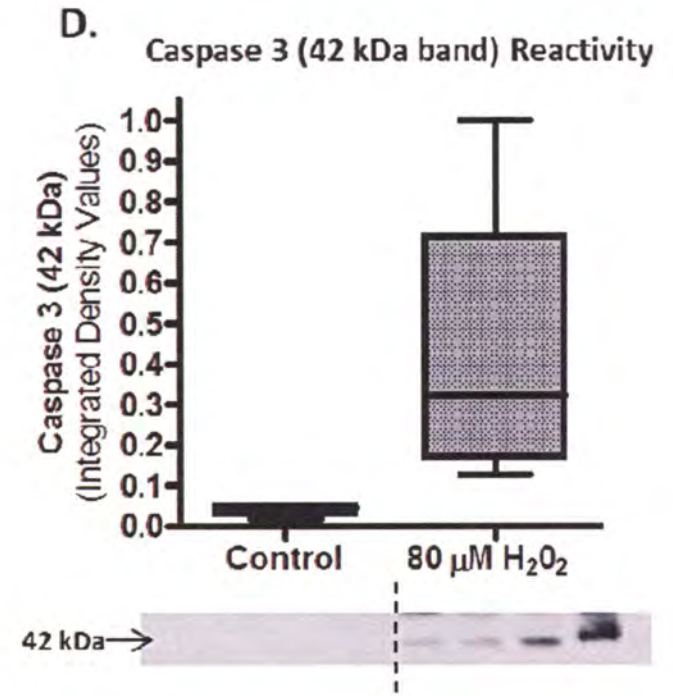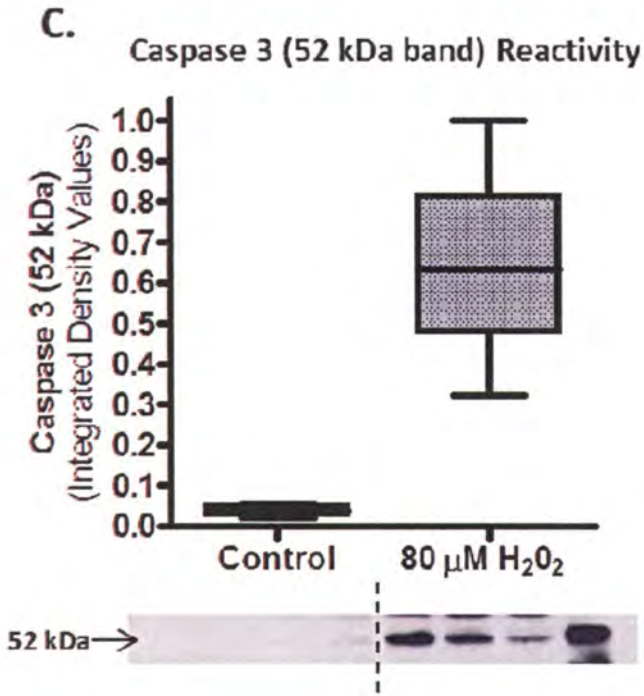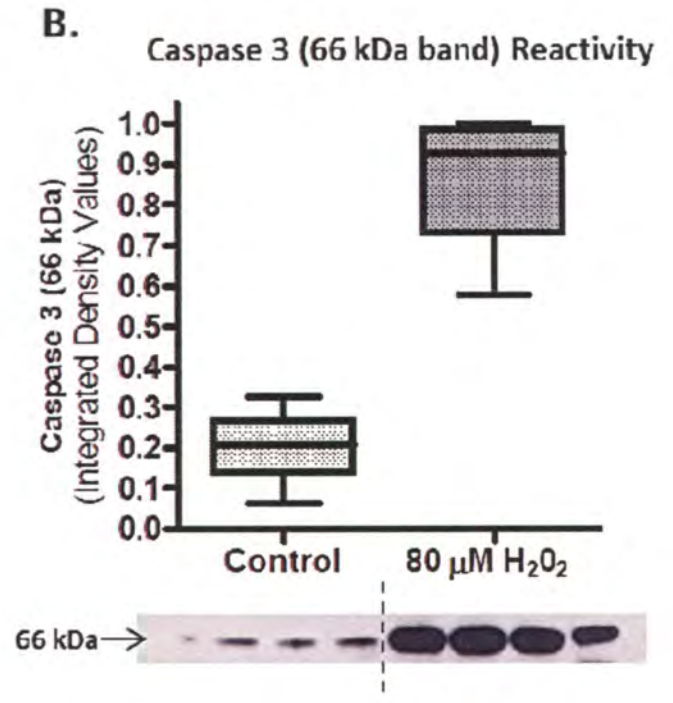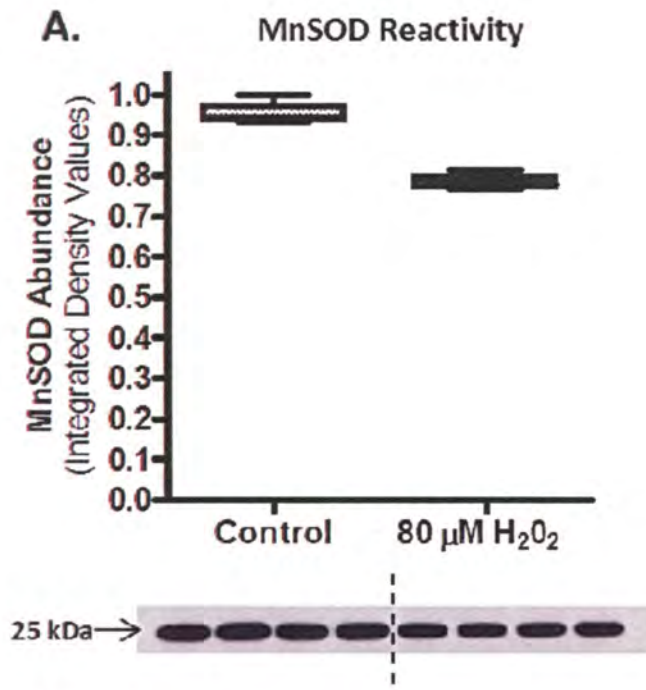
Figure 9. Substrate cleavage sites for the P8-P8' position by amino acid class.

The average amino acid class occurrences in the P8-P8' positions were calculated for (A) all

substrates combined (n = 31 substrates total), (B) DEVD only (n = 20 substrates), (C) VEID only

(n = 7 substrates).
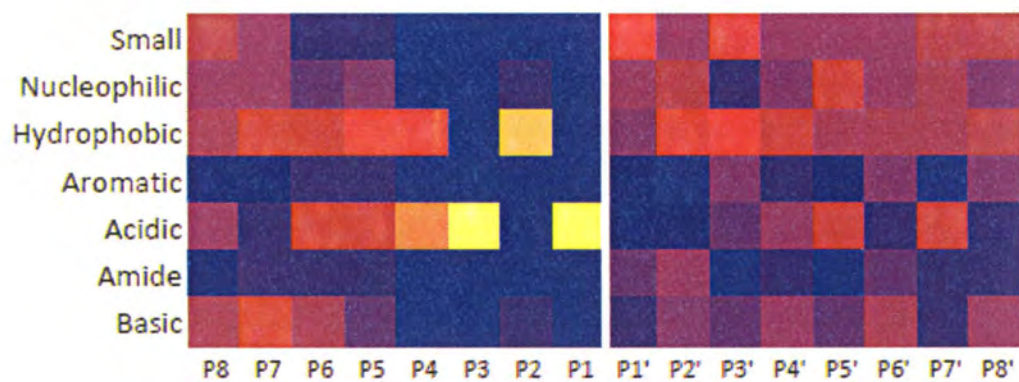
A. All Substrates
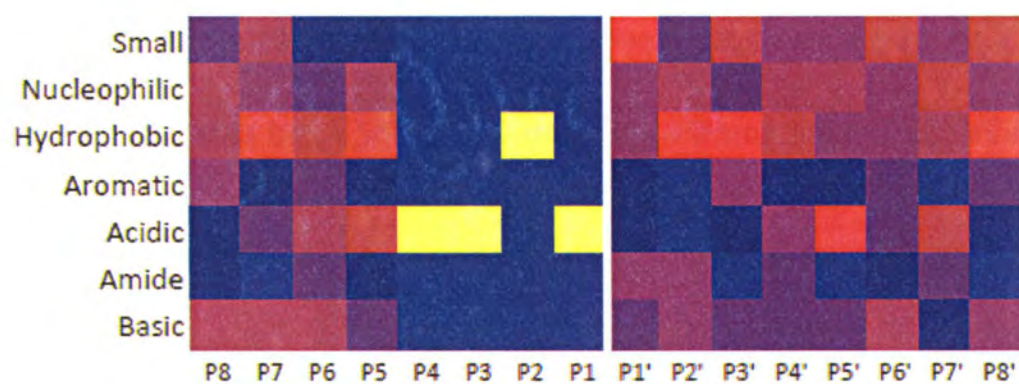
B. DEVD Substrate

C. VEID Substrate
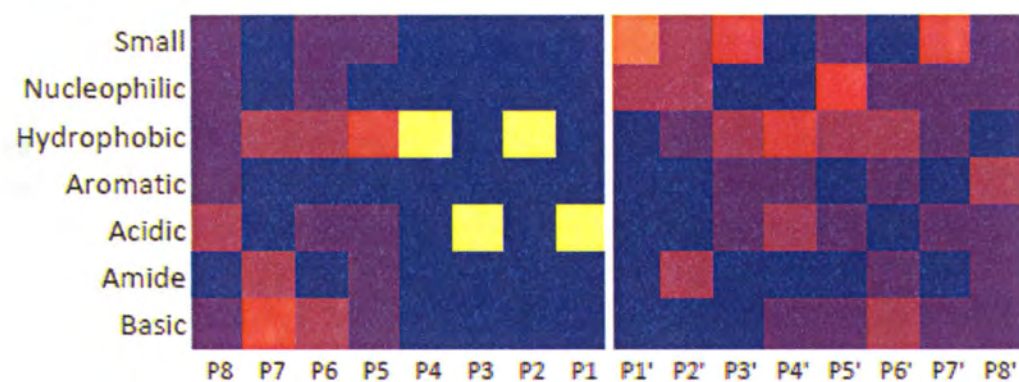
Residue Occurrence (%)

Figure 10. Substrate cleavage sites for the P8-P8′ position by individual amino acid. The

average amino acid occurrences in the P8-P8′ positions were calculated for (A) all substrates

combined (n = 31 substrates total), (B) DEVD only (n = 20 substrates), (C) VEID only (n = 7

substrates).

A. All Substrates

B. DEVD Substrate

C. VEID Substrate

Residue Occurrence (%)

147
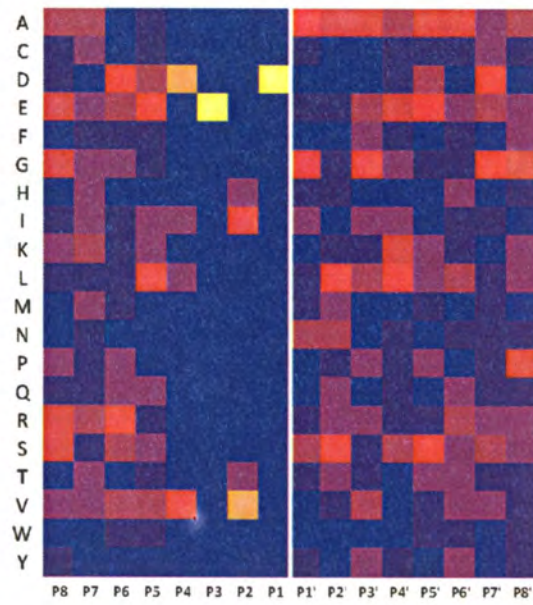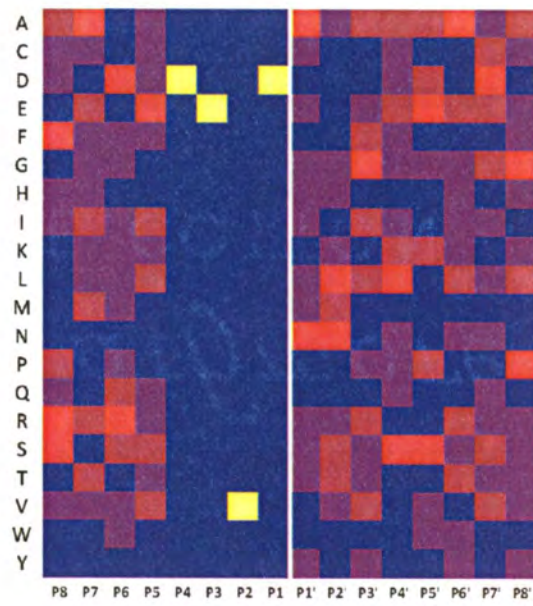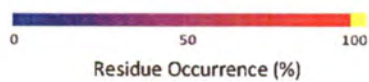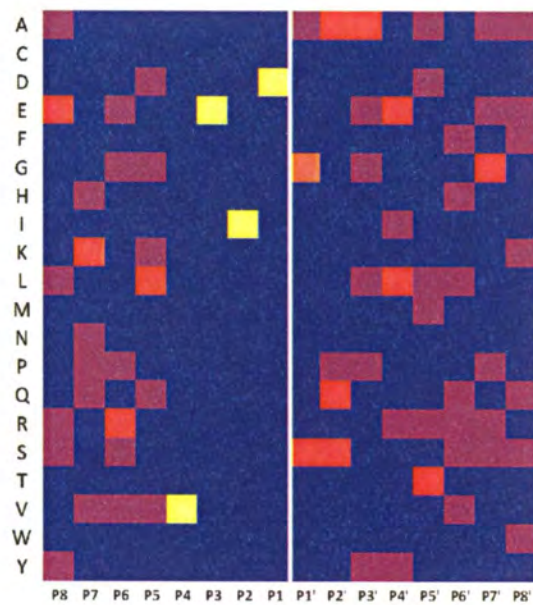
Figure 11. Cleavage of KbAdoMetS by Recombinant Human Caspase 3

KbAdoMetS peptide (22 amino acids) contains an acetylated N-terminus and an amidated C-terminus for prevention of peptide degradation by exopeptidases. Cleavage of KbAdoMetS at the indicated DEVD cleavage site should result in a 1300 m/z N-terminal fragment and an 1148 m/z C-terminal fragment (A). Spectra for the full length (red – 2430 m/z), N-terminus fragment (green – 1300 m/z), and C-terminus (orange – 1148 m/z) products are shown for caspase 3 enzyme alone, caspase 3 + peptide, and caspase 3 + peptide + inhibitor, peptide alone, and inhibitor alone (B). Percent of total signal for the full-length product, N-terminal fragment, and C-terminal fragment for caspase 3 + peptide and caspase 3 + peptide + inhibitor experiments (C).
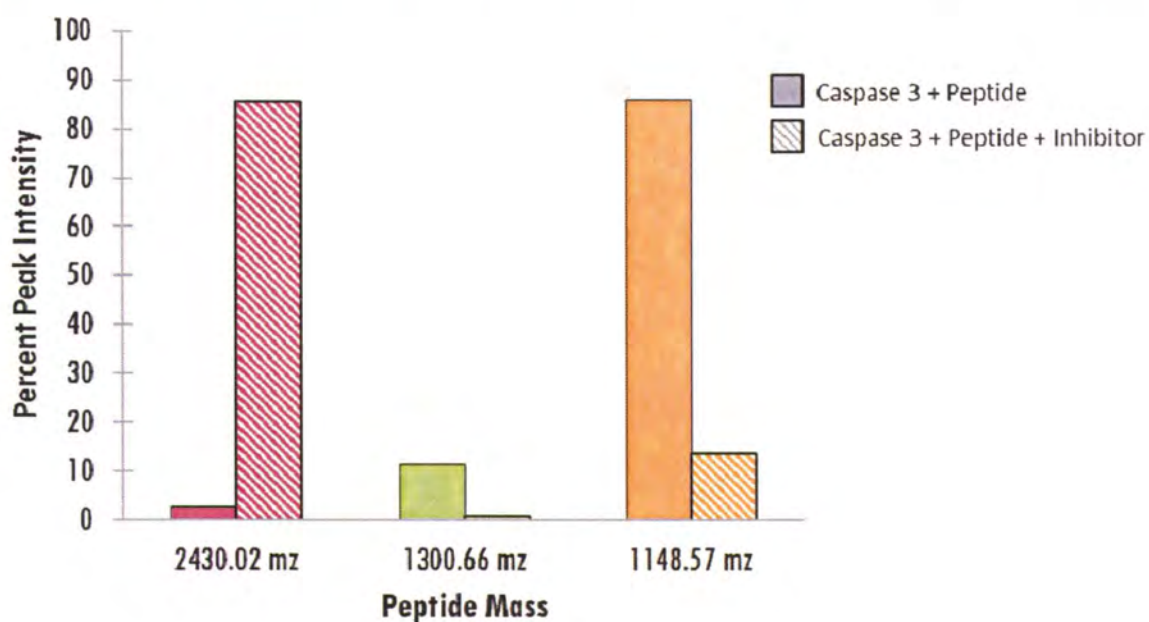
A.

Ac-KYKGMSSDEVDAALKASNYLAK-amide

1300 m/z	1148 m/z

2430 m/z

B.
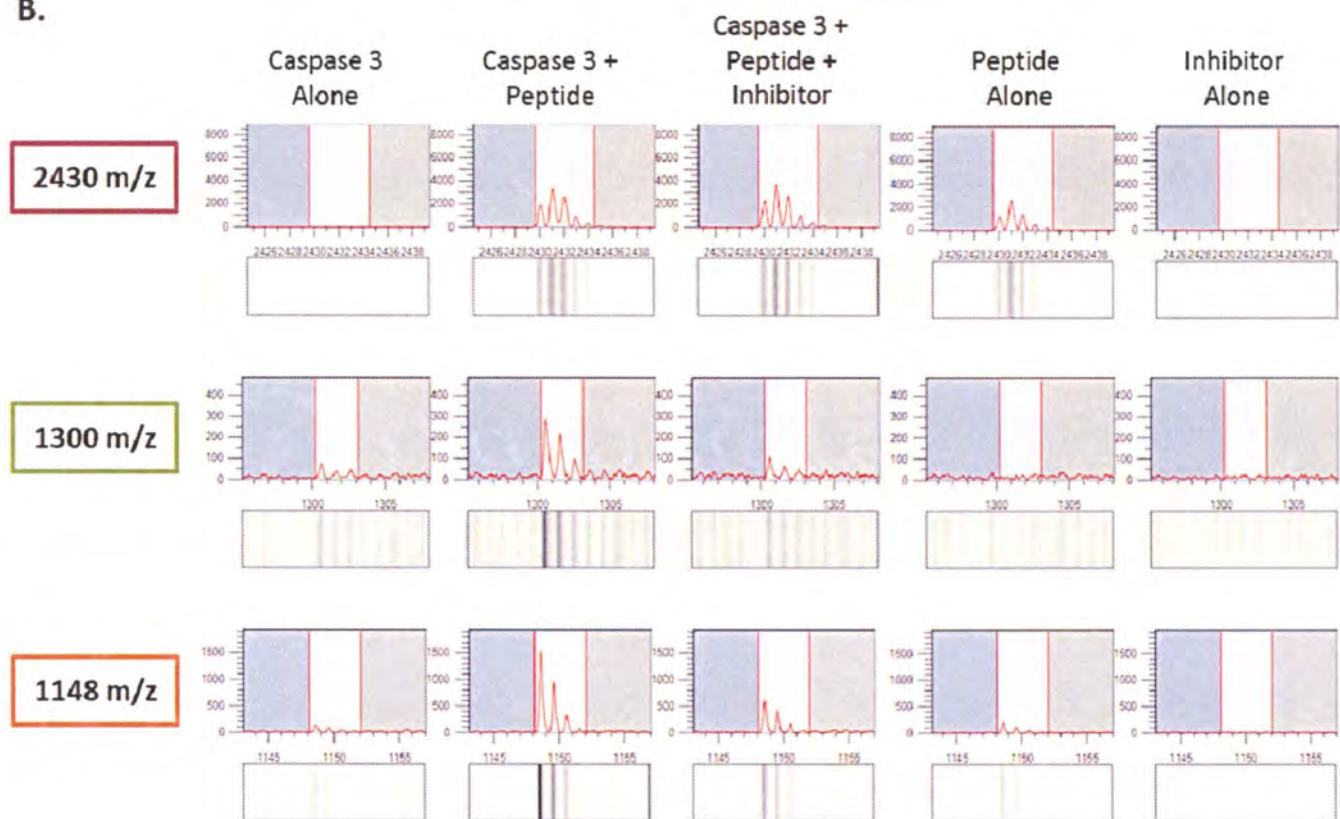
C.

CHAPTER 4

IDENTIFICATION AND CHARACTERIZATION OF *K. BREVIS* METACASPASE 1 (KbMC1) DURING

CHRONOLOGICAL AGING AND PROGRAMMED CELL DEATH

INTRODUCTION

The caspase enzyme family, most notably known for their role in executing programmed cell death (PCD), is a highly regulated set of enzymes that coordinate cleavage of their protein substrates in an extremely specific manner. Although they are most especially known for their role in mediating apoptosis, their involvement in other processes such as differentiation and inflammation has become more evident (Degterev et al. 2003; Chowdhury et al. 2008). Apoptosis, defined in the metazoan context, is an irreversible rearrangement of cellular content that gives rise to apoptotic bodies that can be phagocytosed. The caspase family plays an integral role in the execution of this process, and it is the specific enzyme chemistry of the caspase catalytic pocket that allows for strict regulation and execution. Aberrant execution of such a pathway has detrimental effects at the cellular, tissue, and organismal levels, and therefore it is in the regulated activation and coordinated cleavage of the downstream substrates that has received much attention in this field (Taylor et al. 2008).

Caspases are members of the C14 peptidase clan CD, and are grouped according to their sequence similarity, and are further divided based on their physiological function between inflammatory, initiator, and executioner (Degterev et al. 2003; Chowdhury et al. 2008). Caspases are synthesized as inactive zymogens and require proteolytic cleavage into their active form to function. In general, a caspase enzyme consists of an N-terminal prodomain, a large subunit (p20), and a small subunit (p10). Given that the context of this dissertation lies in the programmed cell death process, the inflammatory caspases (caspase 1, 4, and 5) are not discussed, but it should be mentioned that their catalytic pocket chemistry is in accordance with

151

the other caspases. In the apoptotic pathway, initiator caspases (caspase 2, 8, 9, 10) are

recruited to scaffolding complexes that acquire and potentiate the death signal. Once activated

upon complexing, they go on to cleave the downstream effector caspases (caspase 3, 6, and 7).

These two functionally distinct groups of caspases are classified based on their unique structural

characteristics in that the initiator caspases bear a long prodomain that consists of a caspase-

recruitment domain (CARD) or death effector domain (DED) that aids in the binding and

organization to the scaffolding complex, whereas the effector caspases contain a short

prodomain. In all types, activation is required, and is carried out by separation of the large and

small subunits, removal of the prodomain, and dimerization between two small subunits and

two large subunits (Boatright and Salvesen 2003). Each caspase active site consists of a very

well conserved histidine-cysteine catalytic dyad as well as a large pocket that allows for the P4-

P1 residues of its substrate to bind in an extended conformation. It is this unique pocket

chemistry that allows for the specific cleavage of substrates after aspartic acid residues, but it is

also the surrounding amino acid context that determines its specificity (Grütter 2000). The

caspase S1 catalytic pocket consists of three conserved residues (R179, R341, and Q283)

creating a deep basic pocket that is perfectly shaped to accommodate an aspartate side chain,

and thus the functional basis for its strict specificity. The S2 – S4 pocket (or S5 in the case of

caspase 2) chemistry is also important for substrate differentiation, whereby the S2 pocket

allows small aliphatic residues and the S3 coordinates a glutamic acid residue in the P3 position

largely through the S1 pocket player, R341. The S4 pocket is the most discerning for classifying

the different subclasses in that inflammatory caspases coordinate large aromatic side chains,

initiator caspase S4 pockets mainly coordinate small hydrophobic residues, while the

executioners coordinate acidic residues such as aspartic acid. The S1' pocket is less restrictive,

but structural data does support the higher propensity of small residues (namely G, A, and S) in

the P1' position for all subclasses. Together, the pocket chemistry of caspases, utilizing the conserved catalytic cysteine as the nucleophile, coordinates cleavage of the substrate after a P1 aspartic acid at the N-terminal side of the scissile bond. The biochemical properties of the strictly regulated activation of the caspase enzymes and the downstream substrate specificity allow this family of enzymes to function only when appropriate, and to efficiently catalyze irreversible proteolytic reactions on a very specific set of substrates (Fuentes-Prior and Salvesen 2004). This most striking attribute of caspase enzymes is embedded in their pocket chemistry, and allows them to recognize and cleave hundreds to thousands of different substrates, while still maintaining fidelity for its targets but not causing widespread digestion (Crawford and Wells 2011).

Just over a decade ago, PSI-BLAST searches uncovered two distinct sets of distant caspase relatives termed paracaspases and metacasapses, both containing the well-conserved catalytic histidine-cysteine dyad and structural predictions indicated the presence of a caspase/hemoglobinase fold (Uren et al. 2000). The paracaspases, found mainly in bacteria and metazoans, the metacaspases, found in plants, fungi, protists, and chromista, and the caspases are evolutionarily equally distant from each other and thus make up separate classes within the clan CD peptidases along with the legumains, separases, bacterial clostripains and gingipains (Vercammen et al. 2007). Because of the evolutionary distance between these groups, it has been hypothesized that metacaspases arose from a horizontal gene transfer event between the mitochondrial endosymbionts with the early eukaryotes (Koonin and Aravind 2002). Metacaspases have been delineated into Type I or Type II depending on whether the enzyme contains a prodomain (Type I) or an extended linker region between the p20 and p10 domains (Type II). Type I metacaspases have been found in plants, fungi, and protists, while type II metacasapses have only been found in plants. Based on this, alternative hypotheses have been

suggested regarding the notion that caspases, paracaspases, and type I metacaspases arose from a common ancestor through HGT between mitochondrial endosymbionts and eukaryotic host cells, while the type II metacaspases arose from a second HGT event during the endosymbiotic event leading to the establishment of plastids (Vercammen et al. 2007).

Over the last decade, controversial reports in the literature bearing provocative titles such as, *Are metacaspases caspases?* (Vercammen et al. 2007), *Metacaspases are caspases. Doubt no more.* (Carmona-Gutierrez et al. 2010), and *Metacaspases are not caspases – always doubt.* (Enoksson and Salvesen 2010), highlight the ongoing debate concerning metacaspase cleavage pocket chemistry and their biological function as mediators of PCD. Due to the fact that the metacaspases contain the C14 caspase domain, initial studies focused on making connections between the induction of caspase-like activity, measured by cleavage of a particular canonical caspase tetrapeptide motif labeled with a fluorogenic moiety, and the increased expression of metacaspase encoding genes or subsequent protein levels. This led to confusing connections between the activity measured and the actual culprits carrying out this activity. Unlike the basic caspase cleavage pocket, the metacaspase S1 pocket contains a leucine at the R179 site, an aspartic acid residue is replaced by Q283, and R341 is replaced by either an aspartic acid or glutamic acid residue, together forming a highly acidic pocket better suited to accept basic P1 residues such as arginine or lysine. Biochemical studies using recombinant metacaspases or cell extracts from gain or loss of function mutants in yeast have demonstrated that the inferred PI specificity for Arg and Lys from sequence information is accurate (Tsiatsiani et al. 2011). The elucidation of the metacaspase pocket chemistry has led to the identification of a natural substrate of a metacaspase, Tudor staphylococcal nuclease (TSN). TSN is involved in gene regulation, transcription, mRNA splicing, and RNA silencing, remains the only identified substrate to be cleaved by a metacaspase *in vivo* (Sundstrom et al. 2009). However, a better

154

understanding of the pocket chemistry has substantially increased the tools available for *in silico* prediction of the metacaspase degradome. Cleavage of TSN by metacaspase 2 in Norway spruce embryos during both development and oxidative stress induced cell death demonstrates the breadth of biological functions metacaspases may play. Furthermore, TSN contains a caspase specific cleavage site along with four metacaspase cleavage sites, suggesting evolutionary conservation among PCD pathways. The cleavage of TSN represents the most substantial biochemical evidence of the functional diversity metacaspases may possess. However, there is an extensive body of literature further supporting metacaspase involvement not only in cell death, but also protein aggregation and ER stress (Richie et al. 2007; Lee et al. 2010), cell proliferation (Lee et al. 2008), and immune system evasion (Jimenez et al. 2008; Wanderley and Barcinski 2010; Coll et al. 2011) in plants, yeast, and protists. Thus it is clear that the identification of more metacaspase substrates is essential to understanding the biology of metacaspases.

Seminal work in the bloom forming dinoflagellate, *Peridinium gatunense*, brought attention to the possibility that cysteine proteases may also be involved with death processes in phytoplankton (Vardi et al. 1999). This work, along with other foundational studies (Berges and Falkowski 1998; Veldhuis et al. 2001) sparked the development of a new field that sought to answer questions about the role PCD may play in the ecology of phytoplankton. Interest in phytoplankton PCD, particularly in its potential role in coupling primary productivity to the microbial food web, led to convincing morphological, biochemical, and molecular evidence of metacaspase-mediated PCD in response to nutrient limitation and cell age in the marine diatom, *Thalassiosira pseudonana* (Bidle and Bender 2008) and during viral lysis in the coccilithophore, *Emiliania huxleyi* (Bidle et al. 2007). These reports utilized an *E. huxlyei* specific metacaspase antibody, which was used to demonstrate the induction of metacaspases in the aforementioned

studies. This work has led to a profound shift in understanding the biological processes that are affected by the interaction between phytoplankton and viruses, and how this interaction is at the crux of large-scale open ocean biogeochemistry (Bidle and Vardi 2011). This work, along with many other examples of PCD in phytoplankton outlined in Chapter 1, has provided a greater context for understanding the possible functions metacaspases may have in the regulation of phytoplankton bloom dynamics.

Although over the last decade, an extensive body of literature on PCD in phytoplankton has formed, the role of metacaspases in dinoflagellates has remained largely uninvestigated since the initial study linking general cysteine protease activity with the induction of ROS-driven PCD in *Peridinium gatunense* (Vardi et al. 1999). Dinoflagellates present many challenges to answering mechanistic questions regarding cell signaling pathways and biochemistry due to their unique genome structures and the lack of success to date in the development of effective transformation or knock out systems. Dinoflagellates do, however, represent an important group of phytoplankton for many reasons, but most notably they represent the largest number of toxin forming phytoplankton species (Anderson et al. 2012). Owing to the fact that dinoflagellates are involved in the overwhelming majority of toxin related issues arising from harmful algal blooms, they are an important group to direct questions regarding PCD and the role of metacaspases in bloom dynamics. These questions have provided the foundation for this dissertation work.

We have previously shown in Chapter 3 that *K. brevis* induces caspase-like activities during chronological aging and ROS-induced death. In addition, morphological changes indicative of PCD were observed, which indicate a role for caspase-like activity in mediating this process. Bioinformatic analysis of potential substrates for this activity revealed that *K. brevis*

contains previously known as well as novel caspase-like substrates. Evaluation of the *K. brevis* proteome for enzymes responsible for the caspase-like activities indicated that *K. brevis* subtilisins should be considered the family of enzymes most likely responsible for this activity, rather than the metacaspases based on catalytic pocket chemistry. In this light, it remains unclear whether *K. brevis* metacaspases are involved in the PCD process.   In this study, we sought to characterize the presence of metacaspases in *K. brevis* and their activity during natural cell aging and death in culture. Through 3' RACE and spliced leader/gene specific sequencing, the full-length transcript was obtained for the *K. brevis* metacaspase 1 (KbMC). Characterization of the metacaspase sequence led to the development of a custom peptide antibody to the *K. brevis* metacaspase 1 protein (KbMC1). Using this tool, biochemical studies were was carried out to characterize its proteolytic fragments, its localization by immunocytochemistry, subcellular fractionation, and western blotting, as well as its expression by following the mRNA transcript level and protein abundance over the natural chronological aging as well as during ROS-induced PCD.   Results from this study indicate that KbMC1 may be involved in the execution of PCD through its chloroplastic localization through possible degradation of the photosynthetic machinery.

METHODS

Identification and Characterization of *K. brevis* Metacaspases

The *K. brevis* EST library (version 3; http://www.marinegenomics.org/node/27110/assembly) was annotated and Gene Ontology (GO) categories were assigned for the 65,292 expressed sequence tags (EST) using BLAST2GO version 2.3.6 with both standard and GO SLIM analyses (Conesa et al. 2005). Top BLAST hit descriptions and GO terms were queried for sequences with BLASTx E-values < 10^{-4} containing metacaspase. Annotations were confirmed by performing BLASTx searches on the *K. brevis* EST library (Lidie, 2005) with previously characterized metacaspase sequences from other organisms (Uren et al. 2000; Madeo et al. 2002; Hatsugai et al. 2004; Vercammen et al. 2004; Hatsugai et al. 2009; Chichkova et al. 2010; Jiang et al. 2010).

Additional 3' sequence was obtained through 3' rapid amplification of cDNA ends (RACE) using the Marathon Race kit (Clontech laboratories, Mountain View, CA). First and second strand cDNA synthesis was performed from poly(A$^+$) *K. brevis* RNA template. The marathon cDNA adaptor was ligated to double-stranded cDNA creating a library of adaptor – ligated double-stranded cDNAs. Using the adaptor-ligated double-stranded cDNAs as the template, RACE PCR was carried out in 50µl reactions containing sequence specific primers designed per manufacturer's suggestion (23-28nt, 50-70% GC, $T_m \geq 65°C$) (Table 1), adaptor primer, 10X cDNA PCR buffer, dNTP mix, advantage2 polymerase mix, and nuclease-free water. The cycling parameters were as follows: 94°C for 1 min. and 30 cycles of 94°C for 30s and 68°C for 4 min. Amplicons were analyzed on an Agilent Bioanalyzer 2100 for size and purity. To obtain the 5' sequence information of KbMC1, spliced leader (SL) and gene specific (GS) primers (Table 1) were used. SL/GS PCR reactions were carried out in 50µl reactions with nuclease-free water, 10X PCR buffer, dNTP mix, gene-specific primer, SL primer, and *Taq* polymerase (Invitrogen).

Reactions were performed under the following cycling parameters: 94°C for 40s, 35 cycles of 94°C for 20s, 68°C for 2 min., and a final extension of 72°C for 10 min. Amplicons were analyzed using an Agilent Bioanlayzer 2100.

All PCR products were cloned using the TOPO TA cloning kit for sequencing (Invitrogen) and sequenced by SeqWright Inc. (Houston, TX) using M13F and M13R primers. RACE sequences were aligned with KbMC1 contigs in BioEdit to construct full-length transcript contigs. Nucleotide sequences were translated using NCBI's open reading frame finder (ORF Find) and sequence characterization was performed in BioEdit.

Western Blot Analysis

A peptide antibody was developed to a 15 amino acid peptide within the p20 domain containing the catalytic H187 (HGAQQPDPHGYEQD). This peptide antigen was chosen based on structural criteria including predicted number of turns, hydrophilicity, and antigenicity as well as sequence criteria including conjugation method constraints, amino acid composition, and the presence of potential post-translational modifications (ProSci, Inc.). This peptide was also compared to the KbMC2, 3, and 4 sequences to determine specificity for KbMC1, and identified that KbMC1-4 share only six conserved residues in the identified peptide, therefore providing supporting criteria for developing the peptide antibody. Western blot was performed on whole cell lysates to evaluate the immunohybridization of the peptide antibody to KbMC1. Peptide blocking of the antibody with 100 fold excess of peptide (HGAQQPDPHGYEQD, 0.105 mg/mL final concentration) was performed to determine antibody specificity.   Western blot analysis on whole cell lysates or subcellular fractions (described below in the KbMC1 localization methods) was performed. For whole cell lysates, *K. brevis* cells were pelleted by centrifugation at 600 x *g*

for 10 minutes at room temperature. Cell pellets were lysed in 1X lysis buffer (Anaspec, Fremont, CA) for 30 minutes at 4°C with rotation. Cell extracts were centrifuged at 10,000 x *g* for 10 minutes at 4°C. The protein concentration of the supernatant was determined by the Bradford Assay (Pierce). 10μg of total protein/sample was heat denatured at 70°C for 10 minutes in SDS-PAGE sample buffer (Invitrogen) and separated by size on a 4-12% Bis-Tris gradient protein gel using MES buffer (Invitrogen) (200V, 1 hr). After SDS-PAGE, total protein was transferred to a PVDF membrane at 20 volts for 8 minutes (iBlot, Invitrogen). The membrane was developed in a S.N.A.P. Id detection system (Millipore), which uses a vacuum system rather than rocking method for blocking, washing, and antibody incubations. The membrane was blocked in 1% alkali casein in Tris Buffered Saline (TBS), and KbMC1 protein was detected by western blot experiments using the anti-KbMC1 antibody (ProSci) diluted 1:2000 in block solution, incubated for 10 minutes, and washed three times with TBS-T (TBS with 1% Tween 20). A polyclonal donkey anti-rabbit IgG horseradish peroxidase (Sigma) diluted 1:2000 in block solution was incubated for 10 minutes then washed three times with TBS-T. Immunoreactive bands were detected using the West Pico HRP Chemiluminescent detection kit (Pierce), and developed using standard film methods. Densitometry analysis was performed using AlphaEase Innotech Software.

KbMC1 Localization

The subcellular location of KbMC1 was characterized using an immunolocalization and a western blot approach. *K. brevis* cells from a stationary phase culture were fixed overnight in 2% paraformaldehyde. Cells were harvested by centrifugation for 10 minutes at 250 x*g*, washed with phosphate buffered saline (PBS), resuspended in 2ml of -20°C methanol, and incubated at

4°C for 10 minutes. Cells were washed and centrifuged onto poly-L-lysine coated glass slides (1500 xg for 10 minutes at 24 °C). Staining and wash steps were performed in PBS with 0.1% Tween 20. Slides were incubated with normal goat serum at 4°C for 1h and then incubated overnight at 4°C in primary rabbit-anti-KbMC1 peptide antibody (1:100). Cells were incubated with primary antibody blocked with 100-fold excess of peptide to test specificity. The cells were then incubated for 1h at 4°C with FITC-labeled goat anti- rabbit secondary antibody (1:2000). A secondary only control was performed to determine nonspecific binding. Images were obtained on a Zeiss 510 Meta Confocal Microscope.

To verify localization, western blot analysis on whole cell extracts, chloroplast extracts, and cytoplasm fractions were performed. Chloroplasts were isolated by a modification of the method of Laatsch et al (2004). Cell pellets were resuspended in chloroplast isolation buffer (CIB) consisting of 50 mM Tris, pH 7.5, 1 mM $MgCl_2$, 10 mM EDTA, 0.25% PVP, and 0.4 M mannitol and homogenized in a Dounce homogenizer on ice until chloroplasts free of nuclei were apparent by epifluorescent microscopic inspection of a DAPI (0.1 µg/ml; 4',6-diaminido-2-phenylindole, Molecular Probes, Carlsbad, CA) stained sample. The homogenate was then layered onto a gradient of 4 mL 2.2 M sucrose and 12 mL 1.6 M sucrose, then centrifuged at 14,000 x g (28,000 rpm) for 30 min. The plastid band, visible by its dark pigmentation was removed using transfer pipets and an aliquot stained with DAPI (0.1 µg/ml) and inspected by epifluorescence microscopy to ensure the plastid band was free of nuclei or unbroken cells. The chloroplast containing fractions were diluted 1:6 in CIB, then harvested by centrifugation at 12,000 x g for 10 min at 4°C. The chloroplast pellets were either frozen at -80°C or extracted immediately for protein as described above in cell lysis buffer (Anaspec). To obtain the cytoplasmic protein fractions, cell pellets were resuspended in CIB and homogenized in a Dounce homogenizer on ice. The homogenate was centrifuged at 2000 x g for 10 minutes to

remove chloroplasts and nuclei, then centrifuged at 20,000 x *g* to remove mitochondria,

followed by a 100,000 x *g* for 1 hour centrifugation in an ultracentrifuge (Sorvall, M120SE

Ultracentrifuge). The protein concentration on the supernantant cytosol fraction was

determined by Bradford Protein Assay (Pierce). Whole cell lysates were obtained in Anaspec cell

lysis buffer as previously stated, as well as with Trizol according to the manufacturer's protocol

(Invitrogen). 10 µg protein/sample was separated by size on a Bis-Tris gradient protein gel,

transferred to a PVDF membrane, and probed with the anti-KbMC1 peptide antibody as

previously described.

Putative Metacaspase Substrate Identification

The *K. brevis* EST library (v3; (http://www.marinegenomics.org/node /27110/assembly)

was translated using OrfPredictor (Min et al. 2005) and queried for metacaspase cleavage sites

using the Random Forest trained classifier (RF-12-12) by Pripper (Piippo et al. 2010) for the

following metacaspase substrate motifs previously shown to be recognized and cleaved by

metacaspases: AFK, EGR, FESR, GGR, GKR, IISK, VKKR, VRPR (Vercammen, 2004; Watanabe,

2011; Moss, 2007; Watanabe, 2005; Vercammen, 2006; He, 2008; Sundstrom, 2009). The

predicted substrates were functionally characterized using the phylogenetic classification

scheme of Clusters of Orthologous Groups of proteins for eukaryotic organisms (KOGs) using

Kognitor (http://www.ncbi.nlm.nih.gov/COG).

RESULTS

K. brevis Metacaspase 1 (KbMC1) Identification and Characterization

We identified seven metacaspase sequences in *K. brevis* EST library; however, further

analysis revealed that only four sequences were true metacaspases (Chapter 3). Partial

sequence information for the four metacaspases demonstrated the presence of catalytic

histidine and cysteine residues characteristic of caspase-like proteins (Figure 1). In addition all

four KbMCs contain the well-conserved peptidase_C14 caspase domain (pfam00656) (E values

of $3e^{-6}$ to $7e^{-41}$). Although four metacaspases were identified in this study, the focus, rather than

superficially characterizing all four KbMCs (KbMC1-4), was to characterize KbMC1

(MGID2055388) more deeply, as it is the most homologous to known metacaspases. Rapid

amplification of cDNA ends (RACE) was performed to obtain the 3' portion of the KbMC1 gene

sequence and the 5' end was obtained and the presence of the spliced leader sequence was

confirmed by using spliced leader and KbMC1 specific primers. Sequencing analysis (n = 100

sequences) revealed that the KbMC1 transcript is 1275 bp in length and included the spliced

leader to the stop codon. Single nucleotide polymorphisms (SNPs) were found at 103 nucleotide

positions throughout the transcript (Figure 2), suggesting that this sequence represents a family

of proteins as is common in dinoflagellates. The 5' UTR was shown to be 76 bp in length

including the SL sequence (data not shown). The KbMC1 transcript encodes a 424 amino acid

protein with 21 amino acid positions containing alternative amino acid composition from the

SNPs identified in the transcript; however, amino acid substitution did not occur at any of the

necessary autocatalytic cleavage sites or catalytic pocket constituents (Figure 3). KbMC1

contains a prodomain which has a CxxC-type Zn finger motif typical of many type I plant

metacaspases, a p20 domain (pfam00656, $7e^{-41}$), and p10 domains (Figure 3 and 4A). Like type 1

metacaspases, KbMC1 contains a short linker region (27 amino acids) between the p20 and p10. The sequence context around the catalytic histidine in KbMC1 is similar to other known metacaspases (Vercammen et al. 2004), HFSGHG, with the adjacent glycine previously identified to play a stabilizing role in caspases (Earnshaw et al. 1999). KbMC1's catalytic cysteine has a DCCHSG context, suggesting that unlike caspases, which coordinate cleavage of aspartic acids in the P1 site by a glutamine residue, KbMC1, like other metacaspases, uses an aspartate (Figure 1, position 40) (Vercammen et al. 2004). Together, the amino acid composition forms an acidic S1 catalytic pocket. Based on sequence information, the predicted size of the full-length KbMC1 protein is approximately 46 kDa (Figure 4A).

A peptide antibody was developed to a 15 amino acid peptide within the p20 domain containing the catalytic histidine (Figure 4A). Western blot analysis with the anti-KbMC1 peptide antibody in *K. brevis* whole cell lysates identified a strong band at approximately 29 kDa (Figure 4B, lane 1). Based on previous data in *Arabidopsis*, this suggests that KbMC1 is activated in a similar manner through cleavage of the p10 domain, and not by cleavage of the prodomain as in mammalian caspases (Watanabe and Lam 2005). Western blot analysis using this antibody also identified a faint band at approximately 48 kDa suggestive of the full-length form (Figure 4B, lane 3), although this band is enigmatic and has no consistent pattern of expression. Antibody specificity has been tested by blocking with the peptide antigen prior to western blot analysis. This resulted in the complete disappearance of the 29 kDa and the transient 48 kDa band (Figure 4B, lane 2).

KbMC1 is Localized to the Chloroplast

In order to gain insight into the function of KbMC1 during the aging process, subcellular localization of KbMC1 using confocal microscopy, subcellular fractionation with subsequent Western blot analysis was performed. Confocal microscopy using the anti-KbMC1 antibody detected by incubation with FITC-conjugated secondary antibody showed that KbMC1 protein signal (Figure 5A) overlapped with chloroplast autofluorescence (Figure 5B), demonstrating that KbMC1 is diffusely localized within the chloroplast. KbMC1 signal was also detected between chloroplast structures, indicating that KbMC1 may also be located in the cytosol. Confirmation of the microscopy results by Western blotting with the anti-KbMC1 peptide antibody identified the previously demonstrated 29 kDa band is present in stationary phase whole cell lysate extracts (Figure 5B, lanes 1 and 2). However, immunohybridization to a dominant 24 kDa band was identified in chloroplasts (Figure 5B, lane 3) along with a faint 29 kDa band, while the only the 29 kDa band was present in the isolated cytosol fraction (Figure 5B, lane 4). Both the 24 kDa and 29 kDa bands were blocked when probed with antibody pre-incubated with 100-fold excess of peptide.

The immunolocalization and subcellular fractionation results demonstrating that KbMC1 is localized to both the cytoplasm, as well as the chloroplast, prompted further sequence analysis to identify if KbMC1 bears a signal peptide and transit peptide on its N-terminus to further support its chloroplastic localization. To identify if KbMC1 contains a signal peptide, programs designed to predict signal peptides (SignalP-NN, SignalP-HMM, and iPSORT) and N-terminal targeting signals (TargetP, ChloroP, iPSORT, and WolfPSort) were utilized. Our analysis yielded unexpected results, in that no signal peptide was identified, and only 3 out of the 4 targeting programs identified a chloroplast transit peptide; however, all three program

predictions to the chloroplast contained very weak scores. Signal peptides are hydrophobic in nature, and upon further inspection of the N-terminal end of KbMC1 with hydrophobicity profiling, it was confirmed that KbMC1's N-terminal sequence does not appear to contain any sequence resembling a signal peptide. iPSORT and ChloroP did predict a transit peptide cleavage site following residue A20.

The alternative banding pattern of KbMC1 in the isolated chloroplasts also prompted further sequence analysis to define whether KbMC1 has the potential for multiple cleavage products. Recently, crystal structures for the yeast metacaspase 1 (YCA1) (Wong et al. 2012) and the *Trypanosome brucei* metacaspase 2 (TbMC2) (Zalila et al. 2011) were solved, providing templates for protein modeling. KbMC1 was modeled against both templates, which yielded the same structural results; therefore, only models against the TbMC2 crystal are presented for brevity (Figure 6). TbMC2 undergoes autcatalytic processing at K55 in the N-terminal region and at K268 in the C-terminal region; however, cleavage does not generate separate subunits. Given that KbMC1 has alternative banding patterns based on localization, cleavage at the homologous sites, K100 and R257 were assessed and would yield a 16.98 kDa active fragment. Cleavage at R329 also appears to be possible based on sequence specificity and would result in a 21.40 kDa fragment if proteolytically cleaved at K100 – R329. The existence of post-translational modifications is currently experimentally unknown for KbMC1; however, prediction software suggested that KbMC1 might be myristoylated at G2 (MYR Predictor, 0.96/1.00 confidence score) and S-nitrosylated at the catalytic dyad cysteine, C300 (PPS, 3.554 confidence score), which may explain the discrepancy in Western band size versus alternative fragment prediction sizes. Evaluation of KbMC1 modeled against the TbMC2 crystal structure in its full-length form (Figure 6A) demonstrates that the N-terminus, like TbMC2 hides the active site, and once in its active form (Figure 6B), the catalytic site is structurally primed for substrate recognition. KbMC1

also contains the homologous residues for calcium binding, further suggesting that the KbMC1 prodomain may act as a gatekeeper for substrate binding until the enzyme is activated by calcium in the presence of the substrate. Not all metacaspases require calcium for activation, and may therefore explain alternative functions or activation processes amongst different metacaspases (Watanabe and Lam 2011).

KbMC1 is not Induced During Aging

Due to the extensive transcriptomic remodeling associated with chronological aging in *K. brevis* (Johnson et al. 2012) Chapter 2), the extent to which KbMC1 expression changes was evaluated by measuring the KbMC1 transcript and protein abundance over the growth phases. KbMC1 is not represented on the 11K microarray, therefore the transcript abundance was not evaluated in the previous study (Chapter 2). qPCR was run on the three biological replicates from Days 4, 6, 10, 14, and 18 to provide a "snap shot" of the KbMC1 transcript levels at early logarithmic, logarithmic, the transition to stationary phase, and late stationary phase respectively (Figure 7A. Log_2 ratios were calculated for each day with Day 6 acting as the control sample (Figure 7B). KbMC1 transcript levels were significantly reduced in the stationary phase timepoints, and followed the same pattern as the general microarray results in that the greatest decrease was seen in the Day 14 samples.

KbMC1 protein abundance was measured over the growth curve by western blot and densitometry analysis to define whether KbMC1 is induced in the aging process. In a similar, but independent study (Figure 8), KbMC1 protein abundance evaluated by western blot demonstrated that the 29 kDa band is present in all growth phases, is slightly increased overtime, but is drastically decreased in two of three cultures at the late stationary phase

timepoint that may represent imminent culture demise (Figure 8B). The 24 kDa band was not detected in any of the growth curve samples, but three of the samples did contain a faint full length band; however, there was no discernible pattern of full-length band expression (data not shown). Since immunohybridization only identified the 29 kDa KbMC1 band, this suggests that the main active form remained the cytoplasmic form throughout the aging process.

Since KbMC1 protein abundance did not change over the growth curve, dark treatment was utilized to cause a more abrupt and synchronized death phase to evaluate KbMC1 abundance changes (Figure 9B and 9C – dark treatment). Cultures were kept in 24h dark starting on Day 8, and whole cell lysates were evaluated for changes in KbMC1 expression each subsequent day. Immunohybrization to the KbMC1 antibody significantly increased on day 9, although growth curve data suggests that culture demise did not start until days later, and at that time KbMC1 abundance again began to decrease, although not as precipitously as in the two day 12 cultures above.

Chloroplastic KbMC1 is Induced during ROS-driven PCD in *K. brevis*

Previous studies presented in Chapter 3 demonstrated that *K. brevis* exhibits PCD-like morphologies during ROS-induced death. To determine the extent to which KbMC1 is involved in the induction of H_2O_2-induced cell death, extracts from control and 80μM H_2O_2 treated cells were immunohybridized with the anti-KbMC1 antibody (Figure 9). Upon H_2O_2-treatment, the active form of KbMC1 (29kDa) was significantly decreased; however the 24 kDa chloroplast band was induced, suggesting that the chloroplast localized KbMC1 may be involved in the induction of PCD.

Putative Metacaspase Substrates Encode a Wide Variety of Biological Functions

To evaluate the extent to which the *K. brevis* proteome may be influenced by metacaspase enzyme activity, the proteome was scanned for metacaspase cleavage sites using the Pripper program (Piippo et al. 2010) for previously published metacaspase cleavage motifs (Vercammen et al. 2004; Watanabe and Lam 2005; Vercammen et al. 2006; Moss et al. 2007; He et al. 2008; Sundstrom et al. 2009; Watanabe and Lam 2011) (Table 2). Metacaspase substrate motifs were found in 1.2% of the known *K. brevis* proteome (268 identified substrates/22,078 total proteins screened). Annotation and functional classifications for the metacaspase substrates was carried out in Blast2GO (Conesa et al. 2005) and Koginator (Tatusov et al. 2000) in order to gain insight into the biological connections of metacaspase activity in *K. brevis* (Table 2). All KOG classes contained at least one representative, except for nucleotide metabolism and transport (F), cell motility (N), and nuclear structure (Y). Post-translational modification, protein turnover, and chaperone function (O) category contained the largest number of substrates (25), including HSP70, E3 ubiquitin ligase, DnaJ proteins, cyclophilin, and BiP. Glutathione s-transferase, the major detoxification enzyme, was also included in this group. The second largest number of potential substrates were in the signal transduction (T) category, which most interestingly contained calmodulins and EF-hand proteins, both identified as significantly changing in the microarray experiment and involved with calcium regulation. Cytoskeleton (Z) and extracellular structural molecules (W) were also identified as potential metacaspase substrates. All steps of the information storage and processing scheme from chromatin remodeling (B) to proteins involved in translation (J) were identified as metacaspase substrates. Most interestingly in these categories, major mediators of replication (DNA topoisomerase), transcription of small RNAs (RNA polymerase III), and translational elongation (elongation factors 4G and 5) were identified. Many general metabolic processes were identified as

potential targets of metacaspase activity, but most noticeably, members of the putative

brevetoxin biosynthetic pathway were identified (3-oxoacyl-(acyl-carrier-protein) synthase (I

and II), as well as polyamine biosynthetic pathway members (spermine/spermidine synthase).

DISCUSSION

The identification of a PCD-like pathway in *K. brevis* regulated by capsase-like activities

in response to ROS is in accordance with findings in other bloom forming dinoflagellates (Vardi

et al. 1999; Franklin and Berges 2004) and has led to questions regarding the role metacaspases

play in this process. Although it is now understood that metacaspases are not responsible for

the caspase-like activities, this does not preclude them from being involved in the signaling

cascade. In fact, there is a body of evidence demonstrating that metacaspases are involved in

the PCD process in phytoplankton (Bidle and Bender 2008), which together with the findings in

Chapter 3 formed the basis for investigating KbMC1 in the aging and death process of *K. brevis.*

Data mining of the current *K. brevis* transcriptome has uncovered four metacaspase

sequences, all of which contain the well-conserved His/Cys catalytic dyad with S1 pocket

specificity for cleaving after Arg/Lys residues. The number of sequences and specificity is in

accordance with other characterized metacaspases in phytoplankton; however, to our

knowledge this is the first in depth analysis of metacaspases in dinoflagellates. Although it is

important to distinguish the role of all the identified KbMCs in aging and death, further analyses

focused on KbMC1, as is the most homologous MC to yeast, trypanosomes, and type I plants,

therefore suggesting it might function similarly in dinoflagellates. Like the type I *Arabidopsis*

MC1 (AtMC1), KbMC1 contains a short linker region between the p20 and p10 domains, as well

as a CxxC LSD1-like Zn finger in the N-terminus. Lesion stimulating disease 1 (LSD1) was first

identified in plants to promote chlorosis and necrosis through an O_2^- - dependent mechanism after exposure to elongated photoperiods or avirulent infection (Dietrich et al. 1994). This mechanism has been further characterized, and more recent studies have demonstrated that LSD1 interacts with AtMC1 through the CxxC Zn finger motif on AtMC1. LSD1 acts as a negative regulator of AtMC1 by binding and sequestering AtMC1 to the cytoplasm. Upon infection, this interaction is broken, and AtMC1 is localized to the chloroplast (Coll et al. 2010; Coll et al. 2011), although it remains unclear what substrates AtMC1 is acting upon once in the chloroplast. When LSD1 is absent in this model, AtMC1-dependent cell death depends on other unknown signals and is developmentally regulated, thus demonstrating that the activation of AtMC1 is context specific. LOL1, 2, and 6 (LSD one-like proteins) also contain a zinc finger domain, and through yeast-two-hybrid screens have been shown to interact with AtMC1. LOL1 has been validated through genetic approaches, and is classified as a positive regulator of plant hypersensitive response (HR)/PCD. It is now hypothesized that LSD1 acts as a scaffolding protein for positive regulators, namely LOL1, AtMC1, and AtbZIP10, where interaction with these proteins prevents cell death (Coll et al. 2010). BLAST searches with the *Arabidopsis* Zn-finger domain proteins (LSD1, LOL1, 2, and 6) were performed against the *K. brevis* transcriptome, but did not yield any homologous matches. This may be due to the fact that the library construction was through 3' sequencing, and these domains are found in the N-terminus, thus not finding these sequences may be due to incomplete sequencing information, or they may not exist. Deeper sequencing of the transcriptome will shed light on this question, and provide a better understanding of the possible interactions KbMC1 may have *in vivo.*

Like AtMC1, KbMC1 appears to contain dual localization in the cytoplasm as well as in the chloroplast. Immunocytochemistry and subcellular fractionation followed by western blot analysis utilizing the custom peptide KbMC1 antibody demonstrated that KbMC1 contains two

171

cleavage products, with the 29 kDa representing the major cytoplasmic form and the 24 kDa represented in the chloroplast. The dinoflagellate plastid evolutionary history is complex, and deciphering the mechanisms by which proteins are imported into the chloroplast remains elusive and controversial. *K. brevis* is a dinoflagellate that evolutionarily underwent a tertiary endosymbiotic event with a subsequent plastid replacement from a peridinin plastid to a plastid with haptophyte origin (Yoon et al. 2002). The peridinin plastids contain unique, highly reduced genome composition consisting of approximately 15 genes arranged on a series of mini circles, and most of the photosynthetic machinery is encoded in the nuclear genome, thus nuclear-encoded proteins trafficked to the plastid is necessary for the organism. *K. brevis* replaced the peridinin plastid with a haptophyte origin, thus containing the fucoxanthin pigments, and through endosymbiotic gene transfer (EGT) and horizontal gene transfer (HGT some transfer of plastid encoded genes to the nucleus has occurred; however, their chloroplast genome is more typical of a haptophyte chloroplast and contains >60 genes (Van Dolah, unpubl.) The *K. brevis* plastid appears to have a chimeric proteome with a complex history containing both red and green algal lineages (Nosenko et al. 2006). Dinoflagellates contain three classes of N-terminal targeting signals: Class I is distinguished by a signal peptide, followed by a chloroplast transit peptide, and then a hydrophobic domain that functions as a stop transfer sequence, Class II only contain a signal peptide and a transit peptide, and Class III contain a signal peptide, a transit peptide, and a thylakoid targeting sequence (Patron et al. 2005). The resulting chloroplast ultrastructure from the endosymbiotic events gave rise to a plastid surrounded by three membranes, thus hypothesized homologous machinery for the Tic/Toc complexes are not available to cytoplasmic proteins for direct import, as this machinery is embedded in the second membrane. Thus, the targeting pathways for dinoflagellates have an added layer of complexity. The functional classification of chloroplast targeting is a parallel scheme to the above sequence

172

classes, in that Class I plastid proteins are co-translationally translocated into the ER, where the

signal peptide is cleaved off and the protein is anchored in the membrane by the stop transfer

domain. The protein is then trafficked to the Golgi where it is sorted into vesicles that then fuse

with the outer membrane of the chloroplast where a proposed Tic/Toc complex recognizes and

imports the protein past the last two membranes. This is however greatly oversimplified, and

much of this is still unknown in dinoflagellates, especially how Class II and III proteins lacking a

stop transfer domain are trafficked from the ER, given the whole protein would presumably fully

enter the ER lumen during translation. In addition to these complexities, dinoflagellates appear

to contain unique transit peptide sequences, possibly because of the loss of the fourth

membrane, and thus further complicates studying such mechanisms (Keeling 2010). These

alternative transit peptide sequences have been identified to namely contain an FVAP

recognition motif at the N-terminus of the transit peptide; however, not all plastid-localized

proteins in dinoflagellates contain such sequences, and prediction software programs are

unable to discernibly predict dinoflagellate plastid targeted proteins because of these

complications (Armbrust et al. 2004; Kilian and Kroth 2005; Nosenko et al. 2006) KbMC1 is no

exception to this enigmatic targeting scheme. Characterization of the KbMC1 protein sequence

by a number of signal peptide and transit peptide software programs resulted in conflicting

results regarding its target location. KbMC1 does not contain a signal peptide, as there are no

discernible hydrophobic regions that would suggest otherwise. The protein does however

appear to have a chloroplast transit peptide sequence, albeit weakly supported

bioinformatically, and does not appear to contain a stop transfer domain. KbMC1 is not the

exception in *K. brevis* chloroplast targeted proteins; many known nuclear-encoded chloroplast

targeted proteins do not contain a signal peptide, or are erroneously predicted to other

compartments using conventional prediction tools (Nosenko et al. 2006; Van Dolah,

unpublished). KbMC1 does not contain a FVAP target peptide motif at its N-terminus, but iPSORT and ChloroP predicted cleavage of the transit peptide after residue A20. The mechanism utilized in trafficking KbMC1 is unclear; however it can be hypothesized that KbMC1 acts similarly to AtMC1 in that it is synthesized as a full-length protein, and is in its active, but bound form in the cytsol (29 kDa). Upon release from a Zn-finger binding partner, KbMC1 can translocate to the chloroplast via a currently unrecognized mechanism involving the possible recruitment of SNARE-like proteins (Patron et al. 2005). Based on the current *Leishmania* model for metacaspase activation, chloroplast-localized KbMC1 may undergo further processing where it forms its fully active form resulting in autocatalytic cleavage of the N-terminus at K100 or R105. Based on alignments, the chloroplast-localized sequence of KbMC1 may reflect an active cleavage product from K100/R105 to R329, resulting in a 21.40 kDa fragment (Zalila et al. 2011). This size prediction is smaller than the observed fragment by western blotting; however, possible post-translational modifications to KbMC1 may account for the larger size observed by western blotting. S-nitrosylation of the catalytic cysteine in AtMC9 prevents autocatalytic processing and proteolytic activity (Belenghi et al. 2007). Therefore, future studies designed to test the validity of S-nitrosylation predictions could be informative in discerning the mechanism of activation for KbMC1. Taken together, the biochemistry, cell biology, and bioinformatic approach to characterizing KbMC1 demonstrates that it may be functioning similarly to AtMC1 in the chloroplast. This is most interesting given that KbMC1 and AtMC1 have diverged from such distinct lineages, being that plants diverged from the green plastid lineage, and dinoflagellates from the red plastid lineage, thus suggesting that these metacaspases may have evolved from a common ancestor prior to the divergence of these lines.

The transcriptomic response to chronological aging in Chapter 2 demonstrated that *K. brevis* undergoes a drastic shift in stationary phase. Based on previous reports in other

phytoplankton species demonstrating an induction of metacaspases during aging (Bidle and Bender 2008), as well as metacaspase involvement in the aging process in plants and yeast (Herker et al. 2004; Fabrizio and Longo 2008), the expression profile of KbMC1 over a complete growth curve was performed. Firstly, the 29 kDa band was the prominent band in all samples, although the enigmatic full-length form was observed, suggesting that the KbMC1 inactive zymogen is quickly activated once made, and that the main pool of KbMC1 does not remain in the inactive form. Unlike *T. pseudonana*, the cytosolic KbMC1 active form is present in early logarithmic phase, suggesting that it functions more like a housekeeping enzyme in the cytosol rather than an executioner of death. The 24 kDa band was not detected in any of the samples, suggesting that the cytoplasmic form remained the dominant form; however, immunolocalization data demonstrated that KbMC1 is located in both the cytoplasm and chloroplast in both logarithmic and late stationary phase cultures. The abundance of the 29 kDa band did not significantly change over the growth curve, and decreased prior to culture demise. This suggests that KbMC1 may not be a positive regulator of cell death; however, the chloroplast cleavage product was not detected, therefore suggesting that cell death may be occurring via a KbMC1/chloroplast-independent mechanism. The culture demise lasted over several days, therefore in order to assess whether KbMC1 is ever involved in cell death, cultures were placed in the dark on day 8 to invoke a quicker and more synchronized death. Following dark treatment, KbMC1 expression (29 kDa) appeared to increase; however, over the next three days decreased as the cells began to die. Again, this suggested that KbMC1 is not executing the cell death that *K. brevis* is undergoing following natural aging. From these studies, it can be concluded that the cytosolic form of KbMC1 is present at all growth phases and does not significantly change, suggesting that it may not play a role in executing cell death following natural aging.

Given that *K. brevis* exhibited PCD-like morphologies in response to oxidative stress in Chapter 3, the KbMC1 expression pattern was determined following 80 μM H_2O_2 treatment. Similar to the observed decrease in KbMC1 during chronological aging, activated KbMC1 (29 kDa) expression during H_2O_2 treatment also decreased; however, the induction of the 23 kDa band suggests a positive involvement of KbMC1 in mediating PCD through its chloroplastic localization.

Prior to this study, AtMC1 was the only metacaspase experimentally localized to the chloroplast. Chloroplasts represent the powerhouse of photosynthetic organisms and tight regulation of organellar homeostasis is important for cell survival. Understanding the role metacaspases have in the chloroplast is important for understanding cell death programs in photosynthetic organisms. In order to gain insight into the metacaspase degradome, a bioinformatic approach was taken to identify the possible downstream targets of metacaspases in *K. brevis*. By understanding the cleavage pocket chemistry of metacaspases, and how they differ from the caspases, it was possible to accurately search the *K. brevis* proteome for MC substrates. The metacaspase screen identified substrates involved in a wide range of biological processes, supporting the hypothesis that downstream substrates may act contain both positive and negative regulators of the pathway. Although general hypotheses regarding the potential involvement of the identified substrates can be made, focus was put on the chloroplast localized proteins given KbMC1's unique localization and induction of its chloroplastic form during PCD. Of the 268 substrates, 8 were identified as being localized to the chloroplast by sequence information. Of these, 5 encode members of the photosynthetic machinery, which include protein fucoxanthin chlorophyll a c proteins, chloroplast light harvesting proteins, and the photosystem II 12 kDa subunit. Other chloroplast localized metacaspase substrates include a chloroplast specific molecular chaperone as well as an ion channel. Together, it appears that

176

inference of KbMC1 cleavage specificity does predict its interaction with the photosynthetic machinery. Future studies aimed at understanding whether KbMC1 mediates death via degradation of the photosynthetic pathway, or whether it has general housekeeping functions in the chloroplast such as directing pigment recycling processes may shed light on the enigmatic role metacaspases have in dinoflagellate physiology.

CONCLUSION

To our knowledge, this is the first study characterizing a dinoflagellate metacaspase. A directed analysis of the *K. brevis* metacaspase 1 protein through sequence analysis, immunocytochemistry, and western blotting demonstrated that KbMC1 is localized to the both the cytoplasm and chloroplast. It appears that KbMC1 does not have a direct role in the execution of cell death during the natural aging process, but may be involved in chloroplast homeostasis. However, the expression of a chloroplast specific 24 kDa form of metacaspase under ROS stress and the identification of photosynthesis specific KbMC1 substrates suggest that KbMC1 may be interacting with the photosynthetic machinery.

REFERENCES

Anderson DM, Cembella AD, Hallegraeff GM (2012) Progress in understanding harmful algal blooms: paradigm shifts and new technologies for research, monitoring, and management. Annual review of marine science **4**: 143-176

Armbrust EV, Berges JA, Bowler C, Green BR, Martinez D, Putnam NH, Zhou S, Allen AE, Apt KE, Bechner M, Brzezinski MA, Chaal BK, Chiovitti A, Davis AK, Demarest MS, Detter JC, Glavina T, Goodstein D, Hadi MZ, Hellsten U, Hildebrand M, Jenkins BD, Jurka J, Kapitonov VV, Kroger N, Lau WW, Lane TW, Larimer FW, Lippmeier JC, Lucas S, Medina M, Montsant A, Obornik M, Parker MS, Palenik B, Pazour GJ, Richardson PM, Rynearson TA, Saito MA, Schwartz DC, Thamatrakoln K, Valentin K, Vardi A, Wilkerson FP, Rokhsar DS (2004) The genome of the diatom *Thalassiosira pseudonana*: ecology, evolution, and metabolism. Science **306**: 79-86

Belenghi B, Romero-Puertas MC, Vercammen D, Brackenier A, Inzé D, Delledonne M, Van Breusegem F (2007) Metacaspase Activity of Arabidopsis thaliana Is Regulated by S-Nitrosylation of a Critical Cysteine Residue. J Biol Chem **282**: 1352-1358

Berges JA, Falkowski PG (1998) Physiological stress and cell death in marine phytoplankton: Induction of proteases in response to nitrogen or light limitation. Limnol Oceanogr **43**: 129-135

Bidle KD, Bender SJ (2008) Iron starvation and culture age activate metacaspases and programmed cell death in the marine diatom *Thalassiosira pseudonana*. Eukaryotic Cell **7**: 223-236

Bidle KD, Haramaty L, Barcelos ERJ, Falkowski P (2007) Viral activation and recruitment of metacaspases in the unicellular coccolithophore, *Emiliania huxleyi*. Proc Natl Acad Sci U S A **104**: 6049-6054

Bidle KD, Vardi A (2011) A chemical arms race at sea mediates algal host-virus interactions. Curr Opin Microbiol **14**: 449-457

Boatright KM, Salvesen GS (2003) Mechanisms of caspase activation. Current Opinion in Cell Biology **15**: 725-731

Carmona-Gutierrez D, Frohlich KU, Kroemer G, Madeo F (2010) Metacaspases are caspases. Doubt no more. Cell Death Differ **17**: 377-378

Chichkova NV, Shaw J, Galiullina RA, Drury GE, Tuzhikov AI, Kim SH, Kalkum M, Hong TB, Gorshkova EN, Torrance L, Vartapetian AB, Taliansky M (2010) Phytaspase, a relocalisable cell death promoting plant protease with caspase specificity. Embo J **29**: 1149-1161

Chowdhury I, Tharakan B, Bhat GK (2008) Caspases — An update. Comp. Biochem. Physiol. Part B Biochem. Mol. Biol. **151**: 10-27

Coll NS, Epple P, Dangl JL (2011) Programmed cell death in the plant immune system. Cell Death Differ **18**: 1247-1256

Coll NS, Vercammen D, Smidler A, Clover C, Van Breusegem F, Dangl JL, Epple P (2010) *Arabidopsis* Type I Metacaspases Control Cell Death. Science **330**: 1393-1397

Conesa A, Gotz S, Garcia-Gomez JM, Terol J, Talon M, Robles M (2005) Blast2GO: a universal tool for annotation, visualization and analysis in functional genomics research. Bioinformatics **21**: 3674-3676

Crawford ED, Wells JA (2011) Caspase substrates and cellular remodeling. Annu Rev Biochem **80**: 1055-1087

Degterev A, Boyce M, Yuan J (2003) A decade of caspases. Oncogene **22**: 8543 - 8567

Dietrich RA, Delaney TP, Uknes SJ, Ward ER, Ryals JA, Dangl JL (1994) *Arabidopsis* mutants simulating disease resistance response. Cell **77**: 565-577

Earnshaw WC, Martins LM, Kaufmann SH (1999) Mammalian caspases: structure, activation, substrates, and functions during apoptosis. Annu Rev Biochem **68**: 383-424

Enoksson M, Salvesen GS (2010) Metacaspases are not caspases - always doubt. Cell Death Differ **17**: 1221-1221

Fabrizio P, Longo VD (2008) Chronological aging-induced apoptosis in yeast. Biochim Biophys Acta **1783**: 1280-1285

Franklin DJ, Berges JA (2004) Mortality in cultures of the dinoflagellate *Amphidinium carterae* during culture senescence and darkness. Proc Biol Sci **271**: 2099-2107

Fuentes-Prior P, Salvesen GS (2004) The protein structures that shape caspase activity, specificity, activation and inhibition. Biochem J **384**: 201-232

Grütter MG (2000) Caspases: key players in programmed cell death. Current Opinion in Structural Biology **10**: 649-655

Hatsugai N, Iwasaki S, Tamura K, Kondo M, Fuji K, Ogasawara K, Nishimura M, Hara-Nishimura I (2009) A novel membrane fusion-mediated plant immunity against bacterial pathogens. Genes Dev **23**: 2496-2506

Hatsugai N, Kuroyanagi M, Yamada K, Meshi T, Tsuda S, Kondo M, Nishimura M, Hara-Nishimura I (2004) A plant vacuolar protease, VPE, mediates virus-induced hypersensitive cell death. Science **305**: 855-858

He R, Drury G, Rotari V, Gordon A, Willer M, Farzaneh T, Woltering E, Gallois P (2008) Metacaspase-8 modulates programmed cell death induced by ultraviolet light and H2O2 in *Arabidopsis*. J Biol Chem **283**: 774 - 783

Herker E, Jungwirth H, Lehmann KA, Maldener C, Frohlich KU, Wissing S, Buttner S, Fehr M, Sigrist S, Madeo F (2004) Chronological aging leads to apoptosis in yeast. J Cell Biol **164**: 501-507

Jiang Q, Qin S, Wu QY (2010) Genome-wide comparative analysis of metacaspases in unicellular and filamentous cyanobacteria. BMC Genomics **11**: 198

Jimenez V, Paredes R, Sosa MA, Galanti N (2008) Natural programmed cell death in *T. cruzi* epimastigotes maintained in axenic cultures. Journal of Cellular Biochemistry **105**: 688-698

Johnson JG, Morey JS, Neely MG, Ryan JC, Van Dolah FM (2012) Transcriptome remodeling associated with chronological aging in the dinoflagellate *Karenia brevis*. Marine Genomics: 10.1016/j.margen.2011.1008.1005

Keeling PJ (2010) The endosymbiotic origin, diversification and fate of plastids. Philosophical Transactions of the Royal Society B: Biological Sciences **365**: 729-748

Kilian O, Kroth PG (2005) Identification and characterization of a new conserved motif within the presequence of proteins targeted into complex diatom plastids. Plant J **41**: 175-183

Koonin E, Aravind L (2002) Origin and evolution of eukaryotic apoptosis: the bacterial connection. Cell Death Differ **9**: 394 - 404

Laatsch T, Zauner S, Stoebe-Maier B, Kowallik KV, Maier UG (2004) Plastid-derived single gene minicircles of the dinoflagellate *Ceratium horridum* are localized in the nucleus. Mol. Biol. Evol. **21**: 1318-1322

Lee RE, Puente LG, Kaern M, Megeney LA (2008) A non-death role of the yeast metacaspase: Yca1p alters cell cycle dynamics. PLoS One **3**: e2956

Lee REC, Brunette S, Puente LG, Megeney LA (2010) Metacaspase Yca1 is required for clearance of insoluble protein aggregates. P Natl Acad Sci USA

Madeo F, Herker E, Maldener C, Wissing S, Lachelt S, Herlan M, Fehr M, Lauber K, Sigrist SJ, Wesselborg S, Frohlich KU (2002) A caspase-related protease regulates apoptosis in yeast. Mol Cell **9**: 911-917

Min XJ, Butler G, Storms R, Tsang A (2005) OrfPredictor: predicting protein-coding regions in EST-derived sequences. Nucleic Acids Res **33**: W677-W680

Moss CX, Westrop GD, Juliano L, Coombs GH, Mottram JC (2007) Metacaspase 2 of *Trypanosoma brucei* is a calcium-dependent cysteine peptidase active without processing. FEBS Lett **581**: 5635-5639

Nosenko T, Lidie KL, Van Dolah FM, Lindquist E, Cheng J-F, Institute UDoEJG, Bhattacharya D (2006) Chimeric Plastid Proteome in the Florida "Red Tide" Dinoflagellate *Karenia brevis*. Molecular Biology and Evolution **23**: 2026-2038

Patron N, Waller R, Archibald J, Keeling P (2005) Complex protein targeting to dinoflagellate plastids. Journal of Molecular Biology **348**: 1015

Piippo M, Lietzen N, Nevalainen OS, Salmi J, Nyman TA (2010) Pripper: prediction of caspase cleavage sites from whole proteomes. BMC Bioinformatics **11**: 320

Richie DL, Miley MD, Bhabhra R, Robson GD, Rhodes JC, Askew DS (2007) The *Aspergillus fumigatus* metacaspases CasA and CasB facilitate growth under conditions of endoplasmic reticulum stress. Mol Microbiol **63**: 591-604

Sundstrom J, Vaculova A, Smertenko A, Savenkov E, Golovko A, Minina E, Tiwari B, Rodriguez-Nieto S, Zamyatnin A, Valineva T (2009) Tudor staphylococcal nuclease is an evolutionarily conserved component of the programmed cell death degradome. Nat Cell Biol **11**: 1347 - 1354

Tatusov RL, Galperin MY, Natale DA, Koonin EV (2000) The COG database: a tool for genome-scale analysis of protein functions and evolution. Nucleic Acids Research **28**: 33-36

Taylor RC, Cullen SP, Martin SJ (2008) Apoptosis: controlled demolition at the cellular level. Nat Rev Mol Cell Biol **9**: 231-241

Tsiatsiani L, Van Breusegem F, Gallois P, Zavialov A, Lam E, Bozhkov PV (2011) Metacaspases. Cell Death Differ **18**: 1279-1288

Uren AG, O'Rourke K, Aravind L, Pisabarro MT, Seshagiri S, Koonin EV, Dixit VM (2000) Identification of paracaspases and metacaspases: Two ancient families of caspase-like proteins, one of which plays a key role in MALT lymphoma. Molecular Cell **6**: 961-967

Vardi A, Berman-Frank I, Rozenberg T, Hadas O, Kaplan A, Levine A (1999) Programmed cell death of the dinoflagellate *Peridinium gatunense* is mediated by CO_2 limitation and oxidative stress. Curr Biol **9**: 1061-1064

Veldhuis MJW, Kraay GW, Timmermans KR (2001) Cell death in phytoplankton: correlation between changes in membrane permeability, photosynthetic activity, pigmentation and growth. Eur J Phycol **36**: 167-177

Vercammen D, Belenghi B, Cotte B, Beunens T, Gavigan J, De Rycke R, Brackenier A, Inze D, Harris J, Van Breusegem F (2006) Serpin1 of *Arabidopsis thaliana* is a suicide inhibitor for metacaspase 9. J Mol Biol **364**: 625 - 636

Vercammen D, Declercq W, Vandenabeele P, Van Breusegem F (2007) Are metacaspases caspases? J Cell Biol **179**: 375 - 380

Vercammen D, van de Cotte B, De Jaeger G, Eeckhout D, Casteels P, Vandepoele K, Vandenberghe I, Van Beeumen J, Inzé D, Van Breusegem F (2004) Type II metacaspases Atmc4 and Atmc9 of *Arabidopsis thaliana* cleave substrates after arginine and lysine. J Biol Chem **279**: 45329-45336

Wanderley J, Barcinski M (2010) Apoptosis and apoptotic mimicry: the *Leishmania* connection. Cellular and Molecular Life Sciences **67**: 1653-1659

Watanabe N, Lam E (2005) Two *Arabidopsis* metacaspases AtMCP1b and AtMCP2b are arginine/lysine-specific cysteine proteases and activate apoptosis-like cell death in yeast. J Biol Chem **280**: 14691 - 14699

Watanabe N, Lam E (2011) Calcium-dependent activation and autolysis of *Arabidopsis* metacaspase 2d. J Biol Chem **286**: 10027-10040

Wong AH, Yan C, Shi Y (2012) Crystal structure of the yeast metacaspase yca1. J Biol Chem **287**: 29251-29259

Yoon HS, Hackett JD, Bhattacharya D (2002) A single origin of the peridinin- and fucoxanthin-containing plastids in dinoflagellates through tertiary endosymbiosis. P Natl Acad Sci USA **99**: 11724-11729

Zalila H, Gonzalez IJ, El-Fadili AK, Delgado MB, Desponds C, Schaff C, Fasel N (2011) Processing of metacaspase into a cytoplasmic catalytic domain mediating cell death in *Leishmania major*. Mol Microbiol **79**: 222-239

Table 1. *K. brevis* metacaspase sequences.

Protein ID	Top BLAST Hit Description	BLASTx E value	BLAST Accession	Conserved Domain	Pfam E value	Domain Position	H95 (F/YSGHG)	C147 (DC/SCHSG)
MGID2041795	metacaspase CasA [*Aspergillus fumigatus*]	9.00E-48	B0XPP3.2	Pfam00656 Peptidase_C14	5.41E-23	162-423	YSGHG	DCCHSG
MGID2055388	metacaspase 1 precursor [*Toxoplasma gondii*	2.00E-80	XP_002367830.1	Pfam00656 Peptidase_C14	1.11E-40	105-351	FSGHG	DSCHSG
MGID2080978	metacaspase CasA [*Metarhizium anisopliae*	3.00E-38	EFY99590.1	Pfam00656 Peptidase_C14	7.62E-25	121-247	FSGHG	DSCHSG
MGID2080273	metacaspase [*Chlorobium chlorochromatii* CaD3]	1.00E-08	YP_379199.1	Pfam00656 Peptidase_C14	4.75E-06	1-267	FTGYG	DCCHST
MGID2027748	metacaspase-1 [*Schizosaccharomyces japonicus*	7.00E-17	XP_002171430.1	Pfam00656 Peptidase_C14	1.87E-10	308-392		
MGID2063352	metacaspase 1 precursor [*Toxoplasma gondii*	8.00E-11	XP_002367830.1					
MGID2073387	metacaspase [*Ectocarpus siliculosus*]	7.00E-11	CBN76943.1	Pfam00168, C2 Domain	6.20E-06			

Table 2. Putative *K. brevis* Metacaspase Substrates

	MGID#	KOG	KOG Description	KOG#	eValue	GO Description	eValue
AFK	MGID2037117	A	Nucleolar protein NOP52/RRP1	KOG3911	1.00E-26	ribosomal rna processing 1 homolog	5.21E-24
AFK	MGID2076841	A	Protein involved in mRNA turnover and stability	KOG1609	6.00E-06	kinesin light chain	1.47E-10
AFK	MGID2079451	A	RNA splicing factor - Slu7p	KOG2560	4.00E-56	step ii splicing factor	1.24E-60
AFK	MGID2052976	BK	Class IV sirtuins (SIR2 family)	KOG1905	4.00E-71	transcription regulator sir2-like protein	2.28E-60
AFK	MGID2073043	BK	Hismacro and SEC14 domain-containing proteins	KOG2633	2.00E-15	appr-1-p processing domain protein	3.49E-17
AFK	MGID1967616	DK	Putative protein methyltransferase involved in meiosis and transcriptional silencing (Dot1)	KOG3924	1.00E-07	ribosomal protein l11	4.20E-10
AFK	MGID2048701	G	Uncharacterized enzymes related to aldose 1-epimerase	KOG1594	3.00E-54	protein	5.32E-59
AFK	MGID1986114	H	Cobalamin synthesis protein	KOG2743	4.00E-22	cobalamin synthesis protein	3.05E-21
AFK	MGID2021427	I	Oxidosqualene-lanosterol cyclase and related proteins	KOG0497	e-101	cycloartenol synthase - -epoxysqualene m	1.01E-115
AFK	MGID1976293	O	Tubulin-tyrosine ligase-related protein	KOG2158	2.00E-16	tubulin tyrosine ligase-like member 7	6.25E-22
AFK	MGID1975292	R	Carboxylesterase and related proteins	KOG1516	1.00E-44	carboxylesterase type b	7.73E-45
AFK	MGID2080587	R	TPR repeat-containing protein	KOG0553	5.00E-08	unc-45 homolog a	3.23E-10
AFK	MGID108716	S				snf2 family	1.05E-29
AFK	MGID2030603	S				isocitrate nadp-dependent	0
AFK	MGID2075815	S				mitochondrial rna ligase 2	4.42E-10
AFK	MGID2076773	S				hypothetical protein P9211_15361 [Proch	1.28E-33
AFK	MGID106533	S				adenylyl cyclase, putative [Toxoplasma gor	2.74E-13
AFK	MGID1959457	S				isocitrate nadp-dependent	8.51E-79
AFK	MGID2024222	S				nad(+) adp-ribosyltransferase-3-like prote	4.20E-18
AFK	MGID2026164	S				proteophosphoglycan ppg4	1.10E-04
AFK	MGID2050260	S				isocitrate nadp-dependent	1.50E-127
AFK	MGID2073028	S				atpase of the abc class-like protein	1.11E-84
AFK	MGID2076066	S	Predicted membrane protein, contains two CBS domains	KOG2118	1.00E-29	protein	4.42E-42
AFK	MGID1977578	S				cdpk2_plafk ame: full=calcium-dependent	7.91E-04
AFK	MGID1985111	S				calcium-dependent protein kinase	3.69E-16
AFK	MGID2033488	S				kelch-like 5	1.39E-07
AFK	MGID2079067	S				cyclopropane-fatty-acyl-phospholipid synt	9.60E-75
AFK	MGID2053132	T	Ca2+/calmodulin-dependent protein kinase, EF-Hand protein superfamily	KOG0032	8.00E-65	calcium-dependent protein	3.70E-56
AFK	MGID2078065	T	Calmodulin and related proteins (EF-Hand superfamily)	KOG0027	9.00E-10	calcium-binding protein 2	2.65E-07
AFK	MGID2051906	T	Calmodulin and related proteins (EF-Hand superfamily)	KOG0027	9.00E-69	calmodulin	7.48E-53

Table 2 (cont). Putative *K. brevis* Metacaspase Substrates

	MGID#	KOG	KOG Description	KOG#	eValue	GO Description	eValue
AFK	MGID2061063	T	Calmodulin and related proteins (EF-Hand superfamily)	KOG0027	8.00E-09	protein kinase domain containing protein	1.20E-16
AFK	MGID2074787	T	Calmodulin and related proteins (EF-Hand superfamily)	KOG0027	3.00E-09	calmodulin-like protein	2.42E-08
AFK	MGID2073056	U	Vesicle coat complex COPII, subunit SEC23	KOG1986	1.00E-42	protein transport protein sec23	7.03E-46
EGR	MGID2022303	B	Predicted histone tail methylase containing SET domain	KOG2084	6.00E-10	mynd finger family expressed	1.38E-12
EGR	MGID2035392	BT	Uncharacterized conserved protein, contains JmjC domain	KOG2132	1.00E-39	jumonji domain containing 5	1.34E-37
EGR	MGID2076857	C	Succinate dehydrogenase, flavoprotein subunit	KOG2403	0	succinate dehydrogenase flavoprotein alp	0
EGR	MGID2080235	C	Isocitrate lyase	KOG1260	2.00E-56	carboxyvinyl-carboxyphosphonate phospl	1.66E-82
EGR	MGID1946385	G	Ribokinase	KOG2855	3.00E-09	#NAME?	1.11E-08
EGR	MGID109400	G	Predicted sugar kinase	KOG3974	0.016	hypothetical protein HRM2_12830 [Desul	5.25E-32
EGR	MGID1986772	G	UDP-galactose transporter related protein	KOG1581	4.00E-07	solute carrier family 35	1.10E-31
EGR	MGID2075437	GOT	O-linked N-acetylglucosamine transferase OGT	KOG4626	8.00E-04	tpr repeat-containing protein	2.42E-07
EGR	MGID2048084	I	2-enoyl-CoA hydratase/3-hydroxyacyl-CoA dehydrogenase/Peroxisomal 3-ketoacyl-CoA-thiol	KOG4170	2.00E-10	isoform cra_b	2.63E-08
EGR	MGID2032869	J	Translation initiation factor 5 (eIF-5)	KOG2767	5.00E-48	eukaryotic translation initiation factor 5	6.77E-45
EGR	MGID2066856	K	RNA polymerase III, second largest subunit	KOG0215	1.00E-97	dna-directed rna polymerase iii	6.82E-98
EGR	MGID2080904	K	Glucose-repressible alcohol dehydrogenase transcriptional effector CCR4 and related protei	KOG0620	8.00E-04	predicted protein [Chlamydomonas reinhː	6.23E-06
EGR	MGID1993093	KL	RNA polymerase II transcription initiation/nucleotide excision repair factor TFIIH, 3'-5' helica	KOG1123	3.00E-19	at5g41370 myc6_8	4.64E-16
EGR	MGID2023997	L	TatD-related DNase	KOG3020	5.00E-83	deoxyribonuclease tatd	2.59E-76
EGR	MGID106781	L	Apurinic/apyrimidinic endonuclease and related enzymes	KOG1294	1.00E-22	apurinic endonuclease-redox protein	8.81E-21
EGR	MGID2055147	L	DNA topoisomerase III alpha	KOG1956	6.00E-04	signal transduction protein containing nac	3.22E-08
EGR	MGID2028835	O	Molecular chaperones GRP78/BiP/KAR2, HSP70 superfamily	KOG0100	0	heat shock protein	0
EGR	MGID103360	O	FOG: Predicted E3 ubiquitin ligase	KOG0800	3.00E-05	sel1 domain protein repeat-containing prc	9.89E-06
EGR	MGID2056243	O	FKBP-type peptidyl-prolyl cis-trans isomerase	KOG0543	4.00E-40	rof1 (rotamase fkbp 1) fk506 binding calm	2.15E-35
EGR	MGID2078095	O	Aspartyl beta-hydroxylase	KOG3696	6.00E-11	aspartyl asparaginyl beta-hydroxylase	3.33E-12
EGR	MGID2080865	O	Ubiquitin protein ligase RSP5/NEDD4	KOG0940	1.00E-07	ww domain containing protein	5.87E-06
EGR	MGID2023677	O	Molecular chaperone (DnaJ superfamily)	KOG0715	8.00E-56	dnaj protein	1.09E-80
EGR	MGID2051780	OR	Ubiquitin and ubiquitin-like proteins	KOG0001	7.00E-11	ubiquitin isoform cra_a	4.65E-13
EGR	MGID2061726	OT	Myosin phosphatase, regulatory subunit	KOG0505	5.00E-14	ankyrin repeat protein e4_2	1.69E-11
EGR	MGID1939079	R	Junctional membrane complex protein Junctophilin and related MORN repeat proteins	KOG0231	9.00E-09	morn motif precursor	1.97E-07
EGR	MGID1971143	R	FOG: Ankyrin repeat	KOG0504	3.00E-12	ankyrin unc44	6.18E-14
EGR	MGID2024638	R	Reductases with broad range of substrate specificities	KOG0725	2.00E-06	short-chain dehydrogenase reductase sdr	5.76E-17

Table 2 (cont). Putative _K. brevis_ Metacaspase Substrates

	MGID#	KOG	KOG Description	KOG#	eValue	GO Description	eValue
EGR	MGID2058320	S				hypothetical protein ROSEINA2194_0280:	9.70E-04
EGR	MGID2073415	S				large ala glu-rich protein	5.07E-10
EGR	MGID2073900	S				predicted protein [Phaeodactylum tricorn	4.21E-05
EGR	MGID2079457	S				autoinducer-2 (ai-2) modifying protein	9.77E-14
EGR	MGID1981219	T	Natriuretic peptide receptor, guanylate cyclase	KOG1023	8.00E-12	guanylate cyclase	8.66E-11
EGR	MGID1990712	T	EGL-Nine (EGLN) protein	KOG3710	6.00E-05	protein	4.06E-17
EGR	MGID2063936	T	Serine/threonine protein phosphatase	KOG0698	3.00E-08	protein phosphatase	7.75E-15
EGR	MGID103385	TR	Proteins containing BTB/POZ and Kelch domains, involved in regulatory/signal transduction	KOG4441	2.00E-16	isoform a	2.92E-17
EGR	MGID2075965	TU	Reticulocalbin, calumenin, DNA supercoiling factor, and related Ca2+-binding proteins of the	KOG4223	7.00E-09	cg31650- isoform c	2.74E-12
EGR	MGID2034941	ZD	Ca2+-binding protein (centrin/caltractin), EF-Hand superfamily protein	KOG0028	1.00E-09	centrin 2 variant 2	2.23E-09
GGR	MGID2023652	A	RNA-binding protein musashi/mRNA cleavage and polyadenylation factor I complex, subunit	KOG4205	3.00E-10	heterogeneous nuclear ribonucleoprotein	2.12E-11
GGR	MGID2060151	A	Nonsense-mediated mRNA decay 2 protein	KOG2051	9.00E-25	initiation factor eif-4 middle up-frameshift	1.57E-26
GGR	MGID1966402	B	Predicted histone tail methylase containing SET domain	KOG2084	2.00E-04	protein	3.10E-04
GGR	MGID2035990	C	Predicted mitochondrial carrier protein	KOG0769	4.00E-16	peroxisomal carrier	1.56E-19
GGR	MGID2042509	C	Dihydrolipoamide dehydrogenase	KOG1335	5.00E-48	mercuric reductase	2.95E-110
GGR	MGID2030231	C	Succinyl-CoA synthetase, beta subunit	KOG2799	e-134	succinyl- ligase beta-chain	2.13E-114
GGR	MGID2029056	E	Phospholipase/carboxyhydrolase	KOG2551	0.003	cog3129-like protein	1.95E-119
GGR	MGID2029094	K	Glucose-repressible alcohol dehydrogenase transcriptional effector CCR4 and related protein	KOG0620	1.00E-10	protein	1.01E-21
GGR	MGID2026854	L	Single-stranded DNA-binding replication protein A (RPA), large (70 kD) subunit and related s:	KOG0851	8.00E-55	replication protein 70kda	2.80E-48
GGR	MGID2054360	L	DNA replication licensing factor, MCM6 component	KOG0480	e-114	elegans protein confirmed by transcript ev	7.94E-97
GGR	MGID2074515	MOT	Extracellular protein SEL-1 and related proteins	KOG1550	0.012	enhanced entry protein	6.02E-10
GGR	MGID2021476	O	Protein disulfide isomerase (prolyl 4-hydroxylase beta subunit)	KOG0190	3.00E-34	protein	2.35E-43
GGR	MGID2072819	O	Oligosaccharyltransferase, STT3 subunit	KOG2292	2.00E-38	oligosaccharyl transferase	6.40E-83
GGR	MGID2074510	O	Molecular chaperone (DnaJ superfamily)	KOG0714	9.00E-08	dnaj subfamily c member 7	7.52E-11
GGR	MGID108918	O	Predicted pilin-like transcription factor	KOG0856	5.00E-14	methionine-r-sulfoxide reductase	8.38E-27
GGR	MGID1963346	O	Molecular chaperone (DnaJ superfamily)	KOG0712	3.00E-44	dnaj subfamily c member 7	3.03E-47
GGR	MGID2027673	O	Cyclophilin type peptidyl-prolyl cis-trans isomerase	KOG0865	5.00E-78	peptidyl-prolyl cis-trans isomerase - cyclo|	6.99E-66
GGR	MGID2076148	O	Cyclophilin type peptidyl-prolyl cis-trans isomerase	KOG0881	3.00E-24	peptidyl-prolyl cis-trans isomerase	1.17E-65
GGR	MGID2059795	P	K+/Cl- cotransporter KCC1 and related transporters	KOG2082	3.00E-32	solute carrier family 12 (potassium chloric	1.80E-30
GGR	MGID2032157	Q	Pyridine nucleotide-disulphide oxidoreductase	KOG0405	2.00E-49	glutathione reductase	2.19E-48

Table 2 (cont). Putative *K. brevis* Metacaspase Substrates

MGID#		KOG	KOG Description	KOG#	eValue	GO Description	eValue
GGR	MGID108817	R	Predicted NAD-dependent oxidoreductase	KOG1196	1.00E-32	nadp-dependent oxidoreductase	2.56E-38
GGR	MGID2039744	R	Putative Zn-finger protein	KOG1777	1.00E-54	f-box only protein	6.40E-75
GGR	MGID1963302	S				peptidase u34 dipeptidase	1.96E-49
GGR	MGID1985310	S				type iii effector ripb protein	1.82E-52
GGR	MGID1993688	S				protein	1.28E-23
GGR	MGID2019162	S				cysteine repeat modular	1.05E-04
GGR	MGID2031545	S				hypothetical protein STIAU_8355 [Stigmat	5.35E-04
GGR	MGID2041773	S				protein fucoxanthin chlorophyll a c protei	4.02E-31
GGR	MGID2042020	S				arylamine n-acetyltransferase	5.72E-30
GGR	MGID2045460	S				dna ligase	6.88E-61
GGR	MGID2058816	S				protein	2.16E-18
GGR	MGID2073067	S				secreted hydrolase	1.87E-17
GGR	MGID2077275	S				protein	1.80E-72
GGR	MGID1985599	S				nicotinic acetylcholine receptor epsilon su	8.35E-07
GGR	MGID2020190	S				protein	1.06E-72
GGR	MGID2023423	S				scavenger receptor protein	1.36E-20
GGR	MGID2032103	S				yth domain containing 2	5.17E-11
GGR	MGID2036863	S				carbohydrate binding family 6	1.27E-06
GGR	MGID2058425	S				2og-fe oxygenase family oxidoreductase	8.79E-21
GGR	MGID2058568	S				protein	2.94E-72
GGR	MGID2060644	S				PREDICTED: hypothetical protein [Mus mu	7.28E-04
GGR	MGID2067651	S				OnnF [symbiont bacterium of Theonella s	1.13E-20
GGR	MGID2073387	S				C2 domain containing protein	1.49E-07
GGR	MGID2073884	S				lipase	7.33E-54
GGR	MGID2079492	S				rho guanine nucleotide exchange factor	1.89E-08
GGR	MGID2080172	S				ankyrin partial	6.52E-06
GGR	MGID2081099	S				transcriptional regulator	5.08E-10
GGR	MGID102942	S				opioid growth factor receptor	2.43E-33
GGR	MGID107341	S				5FI8BORFP (ISS) [Ostreococcus tauri]	2.68E-09
GGR	MGID1942823	S				OnnF [symbiont bacterium of Theonella s	2.47E-18

Table 2 (cont). Putative *K. brevis* Metacaspase Substrates

	MGID#	KOG	KOG Description	KOG#	eValue	GO Description	eValue
GGR	MGID1951889	S				protein	1.04E-08
GGR	MGID1969933	S				predicted protein [Micromonas sp. RCC29	9.07E-36
GGR	MGID1970374	S				protein	5.26E-12
GGR	MGID1971979	S				monooxygenase fad-binding	2.46E-61
GGR	MGID1983431	S				tubulin-tyrosine ligase family protein	9.18E-25
GGR	MGID2022152	S				kelch-like protein 5	1.13E-22
GGR	MGID2040976	S				phosphatidylinositol 4-phosphate 5-kinase	8.02E-27
GGR	MGID2052799	S				protein	2.31E-72
GGR	MGID2057482	S				protein fucoxanthin chlorophyll a c protein	8.98E-17
GGR	MGID2070243	S				type i polyketide synthase-like protein kbε	6.51E-17
GGR	MGID2073512	S				protein	1.37E-72
GGR	MGID2075174	S				protein	8.17E-11
GGR	MGID2076045	S				tubulin binding protein	4.33E-44
GGR	MGID2068259	TR	Proteins containing BTB/POZ and Kelch domains, involved in regulatory/signal transduction	KOG4441	4.00E-45	klh12_xenla ame: full=kelch-like protein 1	6.12E-40
GGR	MGID105535	Z	Kinesin (KAR3 subfamily)	KOG0239	7.00E-45	kinesin-like calmodulin-binding protein	3.98E-40
GGR	MGID1961870	Z	Beta tubulin	KOG1375	e-167	beta tubulin	3.12E-143
GGR	MGID2031634	Z	Kinesin light chain	KOG1840	1.00E-08	tpr repeat-containing protein	2.50E-22
GGR	MGID2032016	Z	Beta tubulin	KOG1375	0	beta-tubulin	0
GKR	MGID2025504	B	SNF2 family DNA-dependent ATPase	KOG0389	2.00E-74	helicase smarcad1	2.66E-71
GKR	MGID2028246	IQ	3-oxoacyl-(acyl-carrier-protein) synthase (I and II)	KOG1394	6.00E-06	polyketide synthase	0
GKR	MGID2080904	K	Glucose-repressible alcohol dehydrogenase transcriptional effector CCR4 and related protein	KOG0620	8.00E-04	predicted protein [Chlamydomonas reinha	6.23E-06
GKR	MGID2022838	O	Molecular chaperone (DnaJ superfamily)	KOG0714	4.00E-07	chaperone protein	9.12E-07
GKR	MGID2020208	O	Glutathione S-transferase	KOG0867	5.00E-32	elongation factor-1 gamma	1.38E-42
GKR	MGID2030055	O	Cyclophilin-related peptidyl-prolyl cis-trans isomerase	KOG0882	6.00E-50	protein	1.35E-50
GKR	MGID2032849	R	Junctional membrane complex protein Junctophilin and related MORN repeat proteins	KOG0231	3.00E-39	hypothetical protein TTHERM_00535430		1.28E-75
GKR	MGID2073463	R	Cdc4 and related F-box and WD-40 proteins	KOG0274	5.00E-39	wd-40 repeat protein	8.42E-51
GKR	MGID2072748	R	Peroxisomal membrane protein MPV17 and related proteins	KOG1944	4.00E-15	mvp17 pmp22 family	4.82E-11
GKR	MGID2024352	S				protein serine threonine kinase	1.23E-21
GKR	MGID2028024	S				protein	1.72E-75
GKR	MGID2040295	S				af204951_52 -1-52	1.01E-13

188

Table 2 (cont). Putative *K. brevis* Metacaspase Substrates

	MGID#	KOG	KOG Description	KOG#	eValue	GO Description	eValue
GKR	MGID107587	S				cell surface protein	2.77E-07
GKR	MGID1939115	S				chloroplast photosystem ii 12 kda extrinsic	1.88E-28
GKR	MGID1939192	S				predicted protein [Micromonas sp. RCC29	4.80E-56
GKR	MGID1982332	S				glycosyltransferase 8 domain containing 2	4.83E-06
GKR	MGID1986509	S				capsular polysaccharide	6.84E-16
GKR	MGID2034837	S				fad dependent oxidoreductase precursor	8.72E-31
GKR	MGID2076066	S	Predicted membrane protein, contains two CBS domains	KOG2118	1.00E-29	protein	4.42E-42
GKR	MGID2080817	S				serine threonine-protein phosphatase 5 (p	4.07E-05
GKR	MGID103107	S				protein	2.72E-12
GKR	MGID2020746	S				lmbr1-like conserved region family protein	4.49E-65
GKR	MGID2030089	S				protein of clr family	3.41E-06
GKR	MGID2078684	S				elegans protein partially confirmed by trai	2.77E-05
GKR	MGID2079869	U	Peroxisomal biogenesis protein (peroxin 16)	KOG4546	6.00E-10	peroxisomal biogenesis factor 16	1.11E-09
GKR	MGID1951143	W	Collagens (type IV and type XIII), and related proteins	KOG3544	9.00E-05	collagen type i alpha 1	6.30E-04
GKR	MGID2065806	W	Collagens (type IV and type XIII), and related proteins	KOG3544	0.002	collagen-like protein with amino-end fibrc	3.39E-04
GRR	MGID2044548	A	Spliceosomal protein FBP21	KOG0150	1.00E-13	ww domain binding protein 4	2.11E-24
GRR	MGID2081112	A	FtsJ-like RNA methyltransferase	KOG3673	1.00E-20	ensangp00000010174-like protein	6.63E-38
GRR	MGID1974870	A	RNA-binding protein CUGBP1/BRUNO (RRM superfamily)	KOG0144	4.00E-06	fca protein	2.78E-05
GRR	MGID1981849	A	ATP-dependent RNA helicase	KOG0331	3.00E-61	dead-box rna helicase	6.63E-51
GRR	MGID2028092	A	RNA helicase nonsense mRNA reducing factor (pNORF1)	KOG1802	2.00E-04	hemolysin-type calcium-binding region	6.03E-12
GRR	MGID2073035	BD	Nucleosome assembly protein NAP-1	KOG1507	3.00E-14	nucleosome assembly protein 1	2.65E-15
GRR	MGID107607	C	Vacuolar H+-ATPase V1 sector, subunit B	KOG1351	e-132	vacuolar atp synthase subunit	4.79E-114
GRR	MGID2080194	C	Vacuolar H+-ATPase V1 sector, subunit B	KOG1351	0	vacuolar atp synthase subunit	0
GRR	MGID103446	E	Cysteine synthase	KOG1481	2.00E-57	cysteine synthase	4.66E-55
GRR	MGID2025171	E	Prolyl 4-hydroxylase alpha subunit	KOG1591	3.00E-15	prolyl 4-hydroxylase alpha	2.93E-14
GRR	MGID2065777	E	Kynurenine aminotransferase, glutamine transaminase K	KOG0257	1.00E-04	glutamine--scyllo-inositol transaminase	0
GRR	MGID1952935	E	Predicted spermine/spermidine synthase	KOG2352	0.023	hypothetical protein OsI_15593 [Oryza sat	6.11E-04
GRR	MGID1988163	E	Amino acid transporter protein	KOG1305	5.00E-15	solute carrier family member 10	4.68E-13
GRR	MGID1958488	G	Galactosyltransferases	KOG2246	2.00E-15	isoform c	6.34E-16
GRR	MGID2034112	H	Cobalamin synthesis protein	KOG2743	7.00E-16	cobalamin synthesis p47k	3.62E-21

Table 2 (cont). Putative *K. brevis* Metacaspase Substrates

	MGID#	KOG	KOG Description	KOG#	eValue	GO Description	eValue
GRR	MGID1983599	J	Predicted RNA-binding protein containing PIN domain and invovled in translation or RNA pr(	KOG3070	2.00E-07	cold shock protein	7.29E-09
GRR	MGID2027707	J	Translation initiation factor 4F, ribosome/mRNA-bridging subunit (eIF-4G)	KOG0401	0.001	asparagine-rich protein	3.98E-05
GRR	MGID2074989	L	Helicase of the DEAD superfamily	KOG1132	0.001	dead_2 domain-containing protein	1.06E-04
GRR	MGID2055147	L	DNA topoisomerase III alpha	KOG1956	6.00E-04	signal transduction protein containing nac	3.22E-08
GRR	MGID2074510	O	Molecular chaperone (DnaJ superfamily)	KOG0714	9.00E-08	dnaj subfamily c member 7	7.52E-11
GRR	MGID1982766	O	FOG: Predicted E3 ubiquitin ligase	KOG0800	5.00E-06	ring-h2 finger protein atl5a	1.05E-05
GRR	MGID2036677	O	FOG: Predicted E3 ubiquitin ligase	KOG0800	1.00E-33	ring finger protein 32	6.40E-34
GRR	MGID2041804	O	Predicted E3 ubiquitin ligase	KOG2164	4.00E-09	ring finger 10 kiaa0262 rie2 alternatively s	1.96E-14
GRR	MGID2021402	R	Sulfatase	KOG3867	5.00E-15	choline-sulfatase	1.80E-139
GRR	MGID2045008	R	Ca2+-dependent lipid-binding protein CLB1/vesicle protein vp115/Granuphilin A, contains C	KOG1012	5.00E-05	c2 domain containing protein	9.35E-06
GRR	MGID1955215	R	Junctional membrane complex protein Junctophilin and related MORN repeat proteins	KOG0231	1.00E-25	morn repeat	9.81E-39
GRR	MGID103532	S				helicase-associated [Arthrobacter chlorop	5.44E-08
GRR	MGID104910	S				predicted protein [Thalassiosira pseudona	1.94E-05
GRR	MGID105462	S				monooxygenase, FAD-binding [Octadecab	1.22E-15
GRR	MGID107311	S				protein	1.93E-29
GRR	MGID1943450	S				hypothetical protein Mflv_4120 [Mycobac	4.25E-05
GRR	MGID1969766	S				truncated qxw lectin repeat-containing pr	2.64E-04
GRR	MGID2023238	S				hypothetical protein BRAFLDRAFT_91328	4.47E-06
GRR	MGID2040424	S				predicted protein [Phaeodactylum tricorn	1.97E-09
GRR	MGID2041106	S				nod3 protein	2.92E-13
GRR	MGID2041563	S				hydratase decarboxylase family protein	8.14E-10
GRR	MGID2046356	S				pbs lyase heat domain protein repeat-con	3.15E-21
GRR	MGID2052649	S				methyltransferase type 11	2.58E-22
GRR	MGID2058702	S				glyceraldehyde-3-phosphate dehydrogena	7.87E-04
GRR	MGID2063496	S				aldehyde dehydrogenase	1.15E-38
GRR	MGID2064432	S				hypothetical protein PGUG_04173 [Pichia	6.71E-04
GRR	MGID2074362	S				transposon unclassified	4.11E-06
GRR	MGID2074394	S				glycosyl transferase family 28	1.26E-08
GRR	MGID2079429	S				cysteinyl-trna synthetase	2.35E-12
GRR	MGID106013	S				predicted protein [Phaeodactylum tricorn	3.72E-05

Table 2 (cont). Putative *K. brevis* Metacaspase Substrates

|	MGID#	KOG	KOG Description	KOG#	eValue	GO Description	eValue
GRR	MGID1955391	S				major basic nuclear protein	1.23E-20
GRR	MGID1985773	S				p80 protein	5.83E-11
GRR	MGID2021083	S				calcium-dependent protein	1.10E-17
GRR	MGID2036004	S				glutamine--scyllo-inositol transaminase	0
GRR	MGID104384	S				purple acid	5.24E-29
GRR	MGID105419	S				glyoxalase bleomycin resistance protein di	2.90E-11
GRR	MGID106246	S				flagellar calcium-binding protein	1.66E-27
GRR	MGID108468	S				predicted protein [Thalassiosira pseudona	8.99E-04
GRR	MGID1974285	S				mucin epithelial isoform cra_a	2.03E-04
GRR	MGID1982264	S				purple acid	6.69E-35
GRR	MGID1984606	S				riken cdna 2610003j06	9.24E-09
GRR	MGID2031882	S				t-complex-associated testis expressed 1	7.09E-12
GRR	MGID2053674	S				cytochrome c5530 family protein	3.25E-46
GRR	MGID2055844	S				uncharacterized iron-regulated protein	6.13E-33
GRR	MGID2080859	T	Mitogen-activated protein kinase	KOG0660	1.00E-14	mitogen-activated protein	1.13E-26
GRR	MGID1969209	TR	Proteins containing BTB/POZ and Kelch domains, involved in regulatory/signal transduction	KOG4441	4.00E-22	kelch-like 18	4.71E-21
GRR	MGID2052384	U	Vesicle coat complex AP-1/AP-2/AP-4, beta subunit	KOG1061	3.00E-04	pbs lyase heat-like repeat domain protein	2.32E-15
GRR	MGID1985943	Z	Dyneins, heavy chain	KOG3595	9.00E-27	dynein heavy chain	1.73E-33
GRR	MGID1959130	Z	Kinesin light chain	KOG1840	5.00E-06	tetratricopeptide repeat family	1.79E-12
GRR	MGID2021242	Z	Kinesin-like protein	KOG4280	2.00E-16	kinesin family protein	2.00E-15
VKKR	MGID2075769	S				outer membrane protein precursor gna20	8.37E-08
VRPR	MGID1983277	B	Chromatin remodeling protein HARP/SMARCAL1, DEAD-box superfamily	KOG1000	8.00E-19	zinc ran-binding domain containing 3	2.13E-16
VRPR	MGID1949929	B	Chromatin remodeling protein HARP/SMARCAL1, DEAD-box superfamily	KOG1000	4.00E-27	zinc ran-binding domain containing 3	4.52E-28
VRPR	MGID104889	S				PREDICTED: hypothetical protein [Mus mu	8.28E-05
VRPR	MGID1971307	S				hypothetical protein MC7420_2255 [Micr	3.05E-08
VRPR	MGID1985111	S				calcium-dependent protein kinase	3.69E-16
VRPR	MGID2043583	Z	Dyneins, heavy chain	KOG3595	6.00E-04	cytoplasmic dynein heavy chain	1.01E-04

Figure 1. Partial multiple sequence alignment of the p20 domain of KbMC1-4.

Sequences were aligned using ClustalW (BioEdit) and displayed as a sequence logo

(WebLogo.berkeley.org). Sequence conservation at each position is indicated by overall height

of the stack with the height of symbols within a stack representing relative frequency of each

amino acid at a given position. Conservation of the catalytic dyad histidine (pos. 8) and cysteine

(pos. 64) along with the coordinating aspartic acid (pos. 62) are shared among all four *K. brevis*

metacaspases.
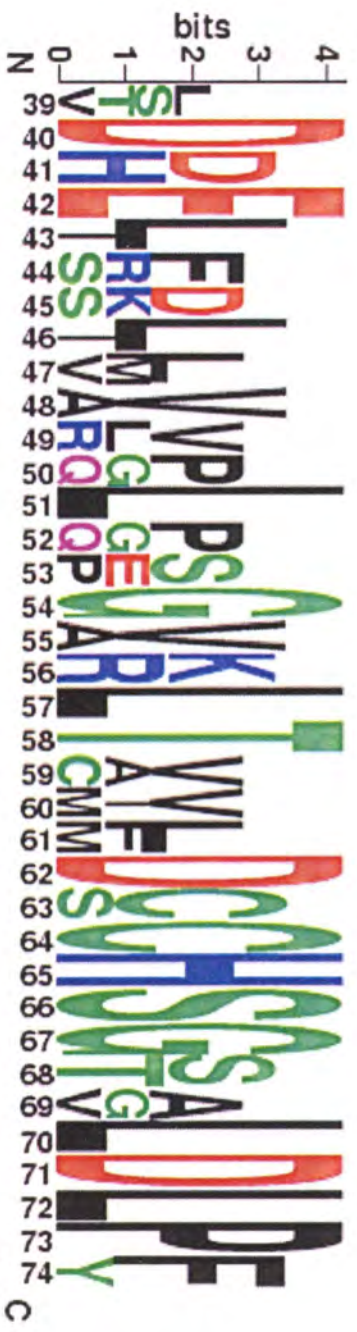
Figure 2. KbMC1 transcript contains single nucleotide polymorphisms (SNPs).

Sequences (n = 100) were aligned using ClustalW (BioEdit) and displayed as a sequence logo

(WebLogo.berkeley.org). Sequence conservation at each position is indicated by overall height

of the stack with the height of symbols within a stack representing relative frequency of each

nucleotide at a given position. ATG start site (pos. 1) to stop codon is presented (1275 bp ORF).

Figure 3. KbMC1 protein sequence

Translated KbMC1 sequences (n = 100) were aligned using ClustalW (BioEdit) and displayed as

sequence logo (WebLogo.berkeley.org). Sequence conservation at each position is indicated by

overall height of the stack with the height of symbols within a stack representing relative

frequency of each amino acid at a given position. The following domains are underlined:

prodomain (yellow), p20 domain (green), linker region (dark blue), p10 domain (light blue), and

KbMC1 antibody epitope (ink). Red stars indicate putative autocatalytic processing sites and

yellow arrows indicate the conserved histidine/cysteine catalytic sites.

Figure 4. Immunoreactivity of *K. brevis* whole cell lysates with KbMC1 antibody.

A peptide antibody was developed to a 15 amino acid portion of the p20 domain (ProSci Inc). The peptide sequence (pink) includes the catalytic diad histidine (**A**). Western blot analysis of mid-logarithmic phase cell lysate identifies a discrete protein band of approximately 29 kDa in size corresponding to the proposed activated form of KbMC1 (**B**, lane 1). 100X peptide incubation with the antibody prior to Western blotting blocked 100% of the identified protein band (lane 2). KbMC1 antibody crossreacts with the proposed full-length form (48 kDa, lane 3).

A.
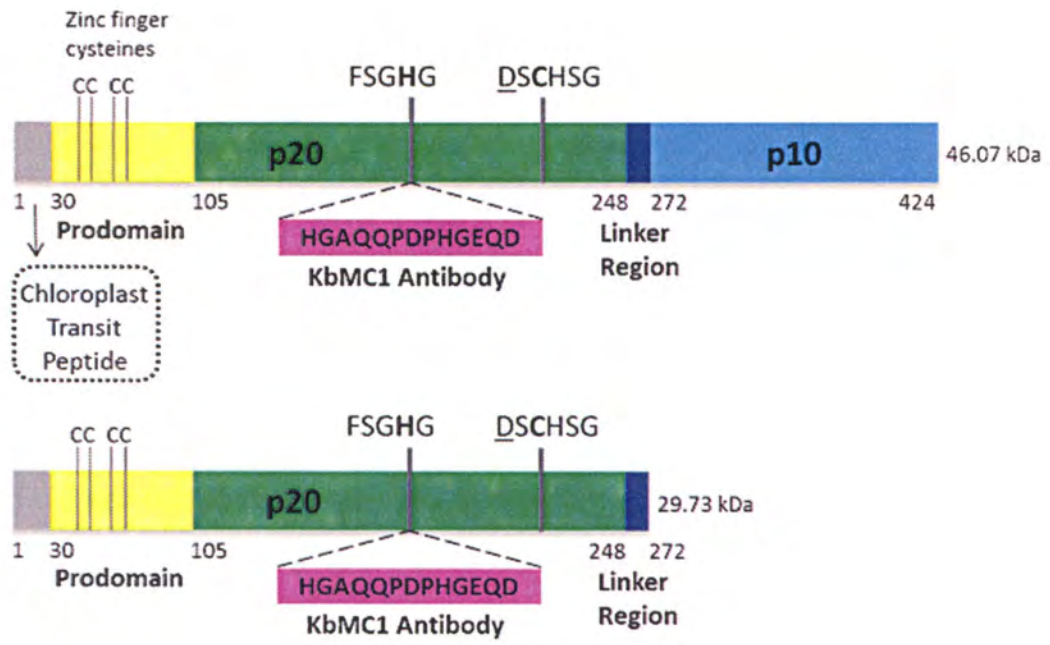
B.
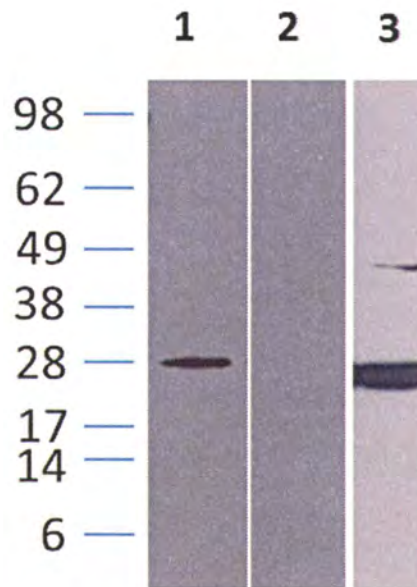
Figure 5. Subcellular localization of KbMC1 during culture demise.

(**A**) Subcellular localization was determined using the anti-KbMC1 peptide antibody, detected by incubation with FITC-conjugated secondary antibody, and visualized with confocal microscopy (Zeiss 510 Meta Confocal Microscope) (a). Chloroplast autofluorescence (b), Differential interference contrast (DIC) (c), and FITC, autoflourescence, and DIC channels merged (d). (**B**) Western blot analysis with anti-KbMC1 peptide antibody cross reacts with a 29 kDa band in Trizol extracted whole cell lysate (lane 1), Anaspec lysis buffer extracted whole cell lysate (lane 2), and 100,000g cytosol prep (lane 4). Chloroplast isolations crossreact with the 29 kDa band; however, the prominent band of interest is at approximately 24 kDa (M, marker).

A.
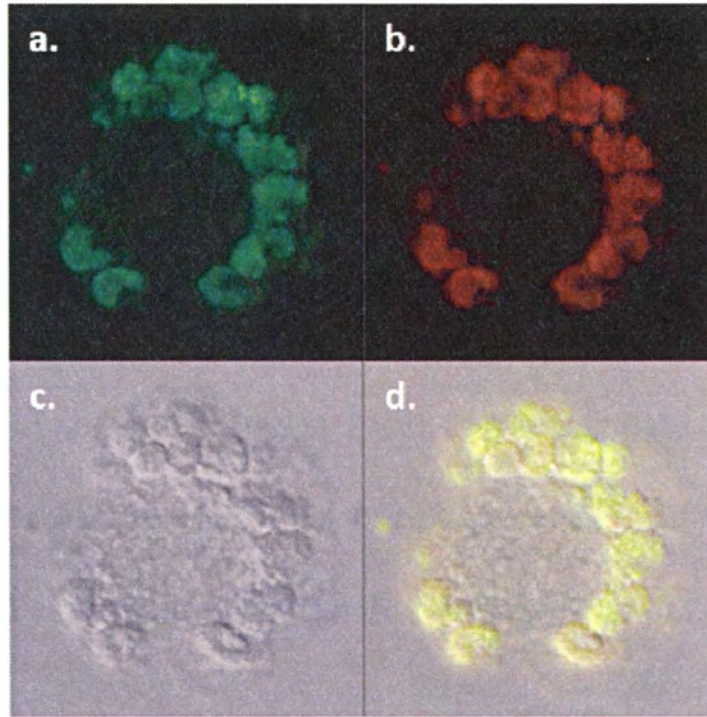
B.
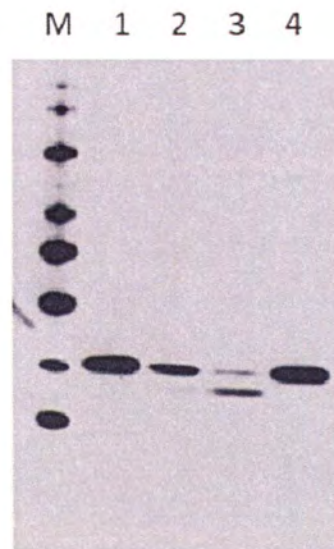
Figure 6. Assumed biological model of KbMC1 protein.

The secondary structure of KbMC1 inferred by EMBL-EBI Protein Data Bank (PDB) (A). The

Trypanosome brucei metacaspase 2 (TbMC2) crystal structure was utilized to project the

biological modelof KbMC1 in its full-length form (B) and active form (C, amino acids (K100 –

R329) using Swiss PDB Viewer (http://www.expasy.org/spdbv/). The domain coloring is in

accordance with the scheme outlined in Figures 3 and 4A. Red arrow indicates active KbMC1

catalytic pocket accessibility.

A.
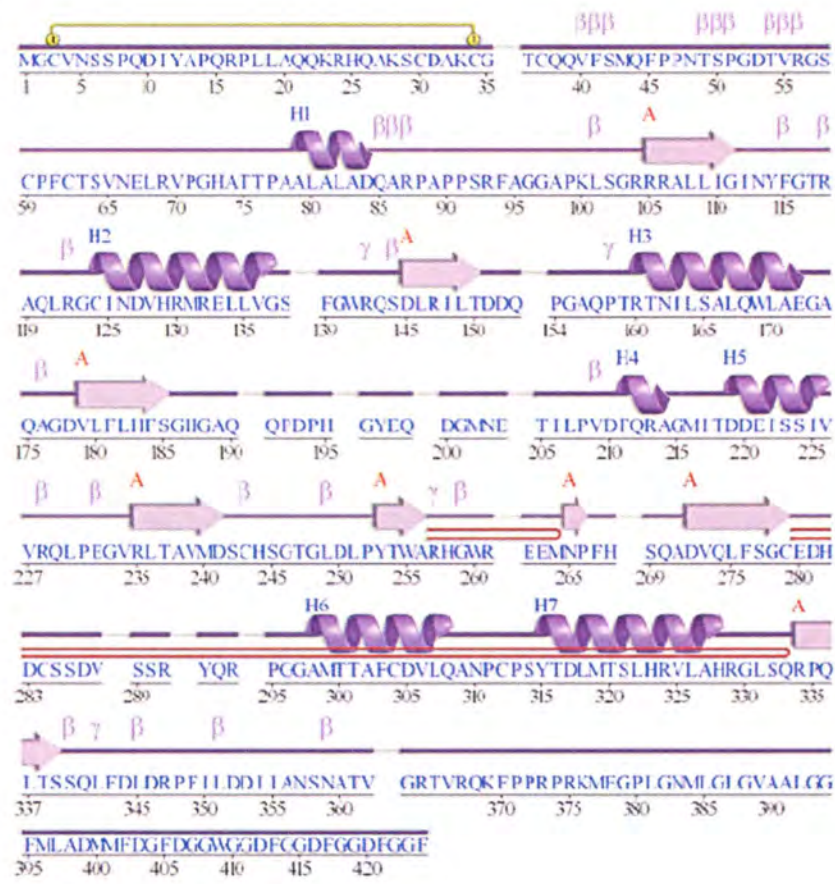
B.
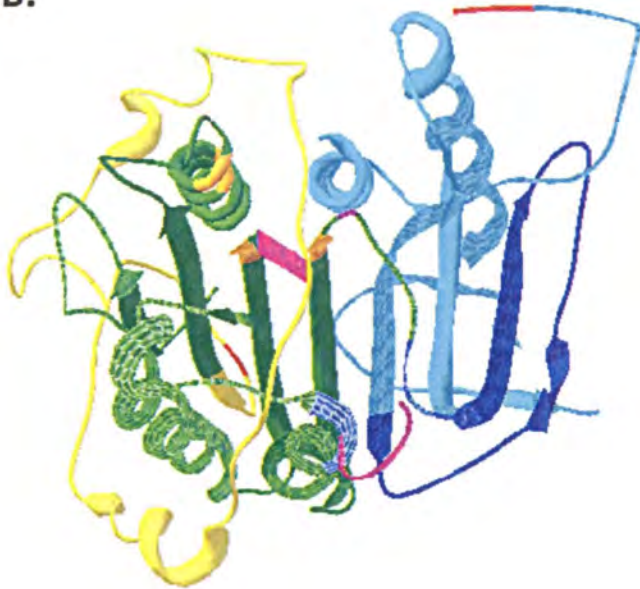
C.
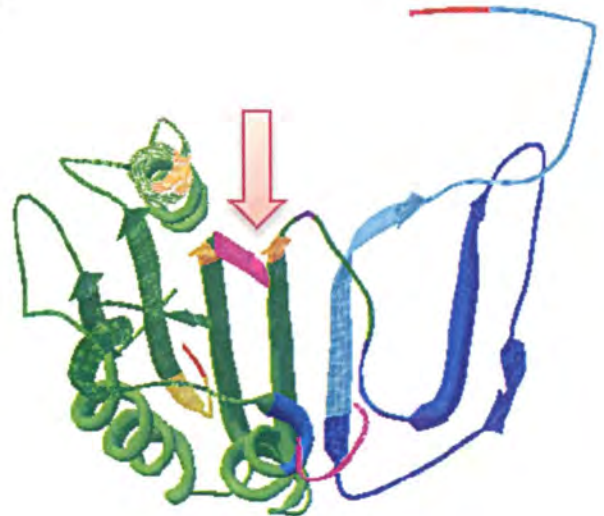
Figure 7. KbMC1 transcript levels decrease during chronological aging

Independent biological triplicate cultures were sampled for cell abundance (■) and average

division•day^{-1} ± standard deviation were calculated for each time point (□) (**A**). KbMC1

transcript abundance presented as Log$_2$ ratio for days 4, 10, 14, and 18 compared to day 6. Bars

indicate an average of three technical replicates from biological sample A (Ch. 2).

A.
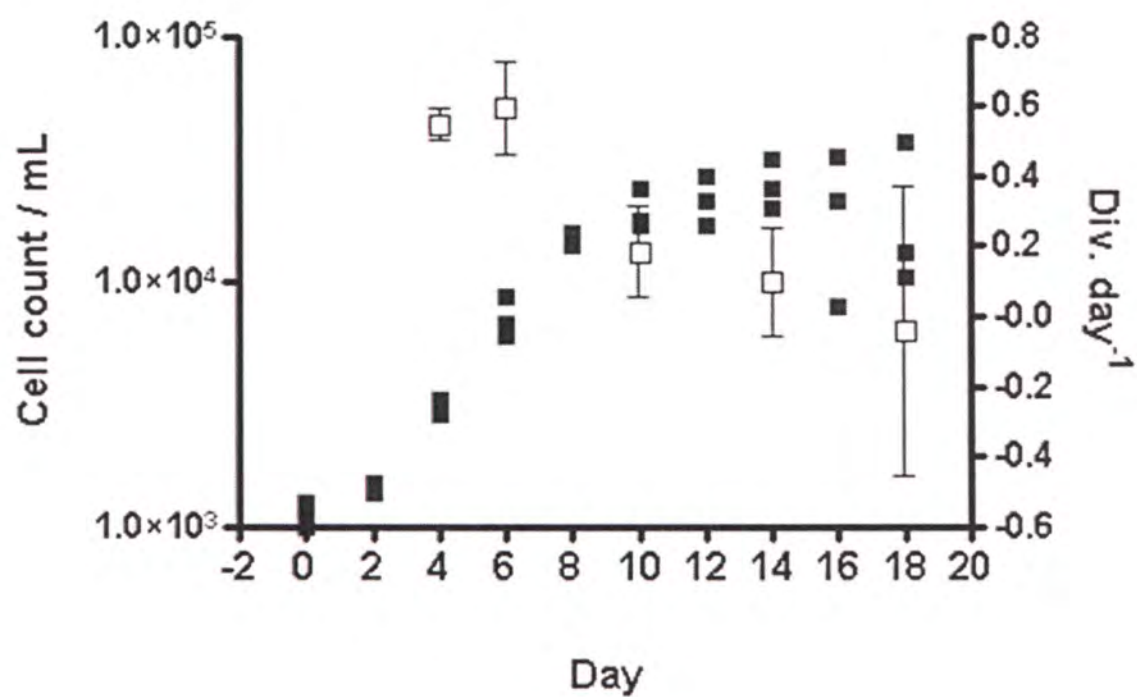
B.
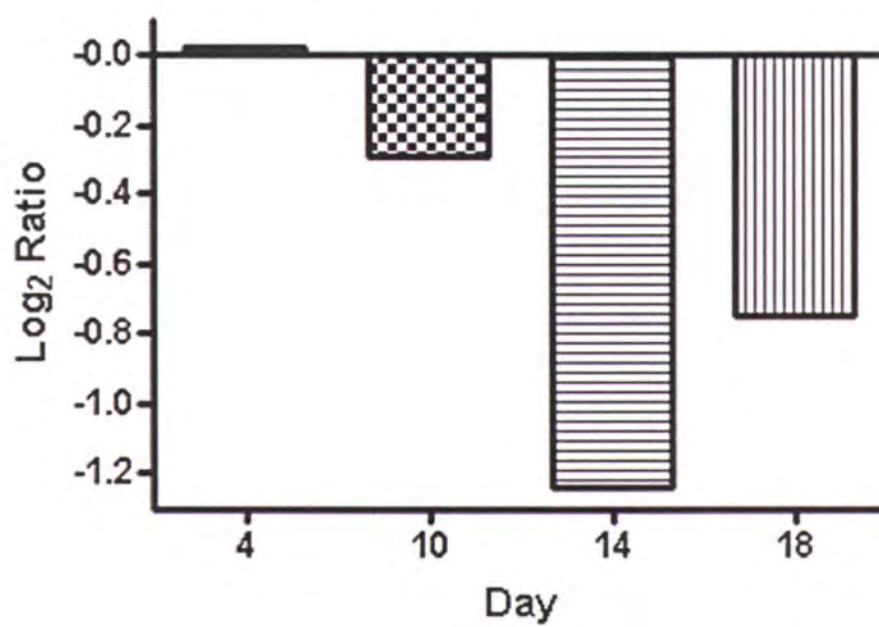
Figure 8. KbMC1 protein abundance during chronological aging and dark treatment

K. brevis cell abundance (n = 3/timepoint) over a growth curve (**A** – control) and after dark

treatment (**A** – dark treatment, arrow indicates day 8 start to 24h dark treatment). Boxplots for

densitometry values (**B**) for control (**C**, days 4 - 12) and dark treatment (**D**, days 9 - 11) samples

(n = 3/timepoint for each treatment). Abbreviations: M, marker; LC, loading control.
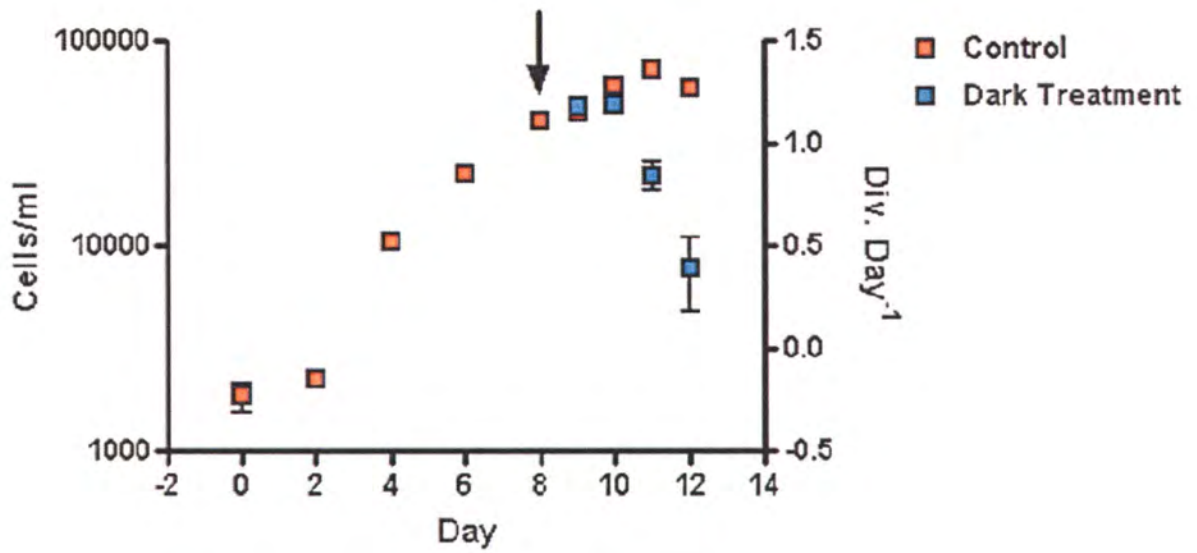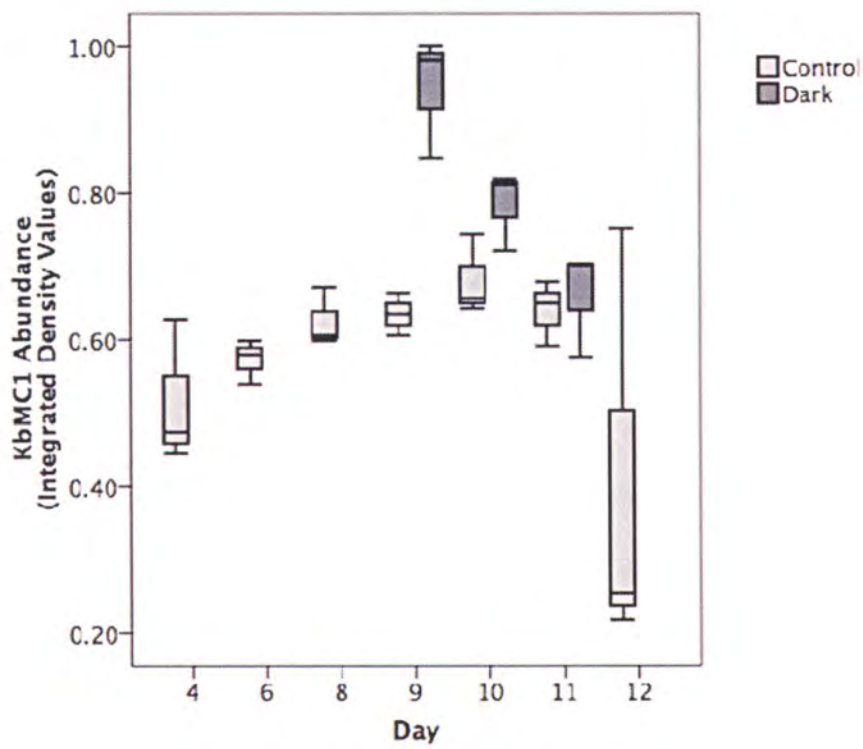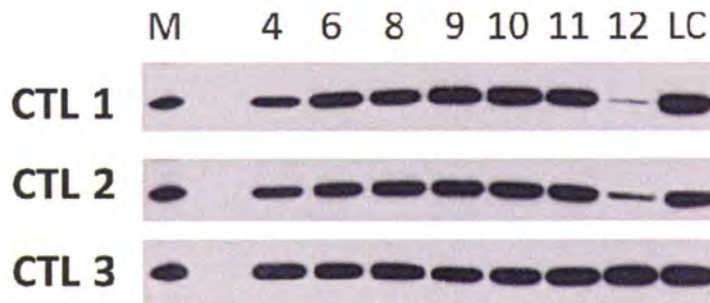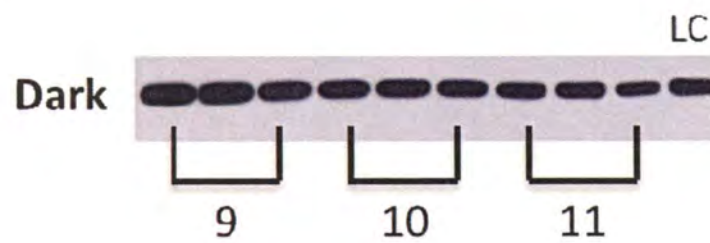
Figure 9. KbMC1 chloroplast form (24 kDa) is induced during ROS-driven death.

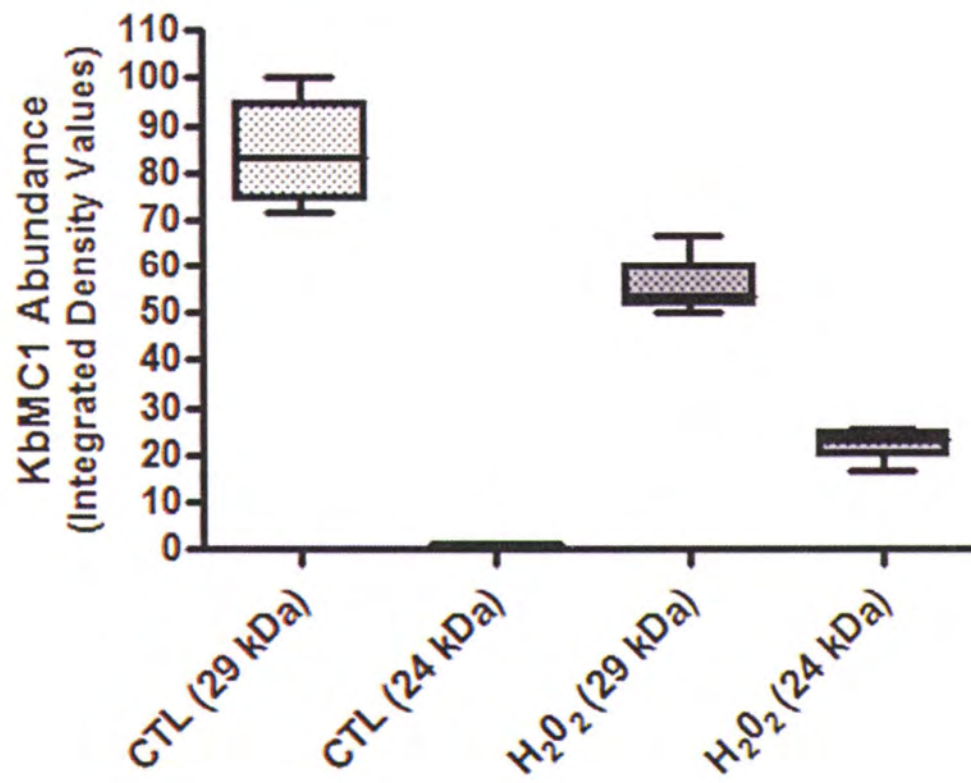(**A**) Immunoreactivity of control (CTL) and 80 μM H_2O_2 (H_2O_2) to KbMC1 antibody. (**B**) Densitometry analysis reveals the induction of the chloroplast form of KbMC1 (24 kDa) concomitant with a decrease in the cytoplasmic form (29 kDa). Abbreviations: M, marker.
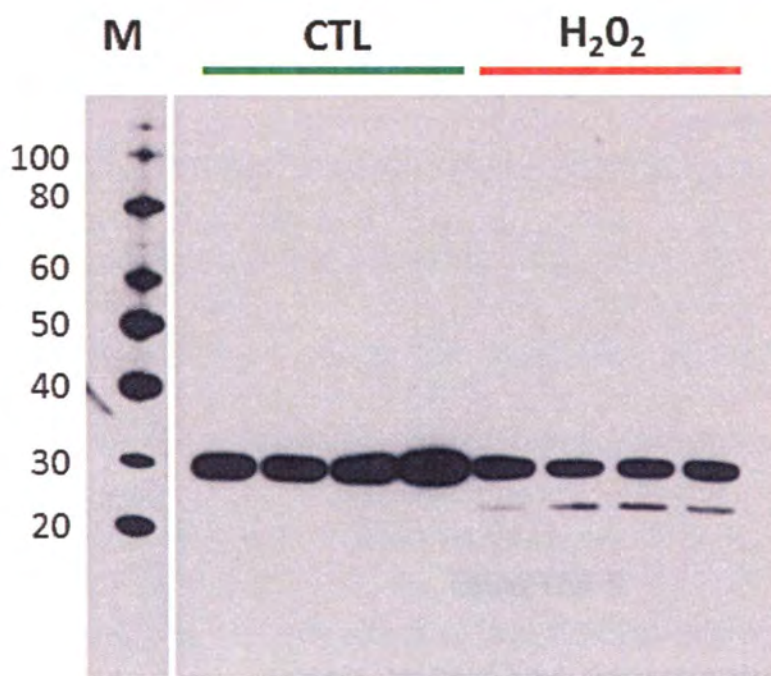
CHAPTER 5

CONCLUSIONS AND PERSPECTIVES

Over the last decade, significant advances in understanding the molecular biology of

growth and toxicity in the dinoflagellate, *Karenia brevis*, have provided a foundation for

developing tools for answering questions regarding the molecular processes underlying bloom

progression in this economically and ecologically important organism. *K. brevis* is responsible

for the near annual harmful algal bloom events in the Gulf of Mexico. Through the production

of a suite of potent neurotoxins, the brevetoxins, blooms of *K. brevis* cause marine animal

mortalities, human illness, and economic loss in the fisheries and tourism sectors (Larkin and

Adams 2007). Given that the frequency, severity, and global distribution of harmful algal

blooms have substantially increased over the last 50 years (Hallegraeff 1993; Hoagland and

Scatasta 2006), understanding the molecular mechanisms regulating the physiology behind this

organism's ability to persist for long periods at bloom concentrations, and the often rapid

termination, has become critical. The molecular mechanisms that underlie these processes

have remained unexplored in the past because of the complexities of *K. brevis* molecular

biology, but with the recent advances in defining the mechanisms regulating *K. brevis* gene

expression, directing studies towards understanding these processes have become possible. In

this dissertation, we investigated the chronological aging process using a transcriptomic

approach in order to define signatures of bloom progression and determine the genetic context

K. brevis encompasses when primed for bloom termination. From here, biochemical and

morphological hallmarks of programmed cell death were explored to determine whether *K.

brevis* contains the machinery to induce cell suicide. Finally, a directed approach was taken to

understanding the involvement of a metacaspase protein in the PCD process. These studies

provide the first comprehensive investigation into the involvement of a metacaspase in aging and the execution of death in a dinoflagellate.

The involvement of PCD in the maintenance of unicellular life represents an intriguing and, until recently, controversial field of study. Programmed cell death is best understood in the context of multicellular life, where it is a driver of development and homeostasis through its ability to regulate the removal of damaged or mutated cells (Danial and Korsmeyer 2004). Through this process, altruistic death at the level of the individual cell benefits the fitness of the whole organism. Hallmarks of programmed cell death have now been identified in prokaryotes including archaea, gram-positive and gram-negative bacteria, as well as in the eukaryotic lineage with members of the *Chromalveolata, Excavata, Plantae,* and *Unikonts* represented (reviewed in Nedelcu et al. 2011). PCD in multicellular organisms is initiated in response to a wide range of stress factors ranging from cellular senescence to oxidative stress (Petit et al. 1996; Zhivotovsky and Kroemer 2004), and relies on the strict coordination of the caspase family of cysteine proteases for cellular execution (Earnshaw et al. 1999). Although cell death with morphological changes diagnostic of PCD has been identified in unicellular taxa, the molecular machinery appears to differ greatly. For instance, canonical caspases are only found in metazoans genomes (Boyce et al. 2004; Degterev and Yuan 2008). In addition, differences in PCD machinery across unicellular taxa have been documented, such as the existence of the apoptosis-inducing factor (AIF) in Apicomplexans, but not in the Typanpsomatids (Cande et al. 2002; Wissing et al. 2004; Kaczanowski et al. 2011). In this light, characterizing the PCD pathway and the molecular machinery involved in its execution is important for the elucidation of this pathway's evolutionary history. The characterization of this pathway in dinoflagellates is vital to our understanding of unicellular PCD, as their position in the tree of life is an important juncture (Hackett et al. 2004). Dinoflagellates have a complex evolutionary history: they acquired

photosynthesis through secondary, and in some instances (such as in *K. brevis)*, teriary

endosymbiotic events, giving rise to their possession of nuclear, mitochondrial, and chloroplastic

genomes (Keeling 2009). The existence of PCD in unicellular organisms has greatly shifted the

understanding of its evolution, and several hypotheses regarding the selective pressures on its

existence and divergence have been proposed (Nedelcu et al. 2010). The consideration that

PCD has evolved from the resolution of conflicting genomes (Ameisen 1996; Ameisen 2002)

places dinoflagellates in an interesting position, as they have reconciled many instances of

genomic conflict and subsequent resolution in their unique evolutionary history (Hackett et al.

2004; Lukeš et al. 2009).

Historically, the study of PCD, or any other pathway, in dinoflagellates has been

complicated by their unusual molecular biology. In addition to their complex evolutionary

history, dinoflagellates contain many molecular features that complicate the central dogma

regarding the movement of genetic material from DNA to protein, and confound attempts to

manipulate them genetically. Dinoflagellates contain an enormous amount of DNA (5×10^{10} bp

in *K. brevis*) that is packaged into permanently condensed chromosomes with transcription

thought to occur on peripheral loops (Sigee 1983). *K. brevis*, like other dinoflagellates, contains

tandemly repeated copies of the same gene, that often display single nucleotide

polymorphisms, raising the question of isoform preference and outcomes (Bachvaroff and Place

2008). Unlike most other eukaryotes, the *K. brevis* genome is transcribed into polycistronic

messages that are resolved into monocystronic messages through *trans*-splicing (Lidie and Van

Dolah 2007; Zhang et al. 2007; Zhang et al. 2009). Spliced leader (SL) *trans*-splicing is also found

in the Trypanosomatids, although is missing from their nearest evolutionary neighbors, the

apicomplexans and ciliates (Campbell et al. 2000). Interestingly, recent studies have provided

strong evidence that the SL *trans*-splicing mechanism has connections with ER-stress induced

PCD in these parasitic protozoa (Goldshmidt et al. 2010). Since PCD is defined as a genetically controlled cell death process, and its activation is extremely well regulated at many levels, the unique evolutionary history and molecular characteristics possessed by dinoflagellates make them an important group in the elucidation of this process.

Due to the extensive repertoire of now available molecular biology tools (Lidie et al. 2005), *K. brevis* represents an ideal species in which to address PCD in dinoflagellates. The construction of an extensive EST library and subsequent microarray for *K. brevis* has been previously used to investigate the coordination of a stress response pathway in *K. brevis* (Lidie 2007; Monroe 2008). Microarray analysis following acute exposure to heat, peroxide, sodium nitrite, and lead resulted in an absence of stress-specific transcripts, although across all treatments, a global reduction in transcript abundance suggested a transient shutdown of transcription. These findings, along with the discovery of the SL *trans*-splicing mechanism, suggested that *K. brevis* does not modulate gene expression at the transcriptional level. However, these studies only queried the acute stress response in logarithmic phase cultures, and did not discriminate whether the transcriptome of *K. brevis* is affected by longer term stress resulting from natural aging. To address this distinction, the first objective of this project presented in Chapter 2 was to determine if *K. brevis* contained transcriptomic signatures of bloom maintenance, in order to identify discrete pathways involved in the natural aging process. This study observed an unprecedented number of significantly changing genes, with nearly 30% of the microarray differentially expressed. This reorganization of the transcriptome over the growth curve demonstrates that it is in fact responsive, although it suggests that differential gene expression occurs on a much longer temporal scale, further adding to the body of evidence suggesting that *K. brevis* regulates its transcriptome at the post-transcriptional level. Since the inception of this project, a study on the relative rates of mRNA stability in *K. brevis*

suggested that transcripts remain stable over a range of several hours to three days (Morey, in prep). The significantly up- and down-regulated transcripts identified in the chronological aging microarray were queried for mRNA stability estimates, and both possessed an average half-life of approximately 1.5 days. Furthermore, the individual biological processes that were found to be enriched demonstrated similar half-life estimates. Together, these observations suggest that coordinated differential expression may be regulated by mRNA stability, but since half-lives associated with both directions of transcript abundance change were not different from each other, the aging microarray results accurately reflect the poised transcriptomic environment in this context. Studying the mechanisms by which transcripts are differentially stabilized may provide better resolution of their function over the aging process (Rossini et al. 2003), and the current work has identified a substantial list of biological processes to direct such studies. Overall, this is the first study in *K. brevis* demonstrating that drastic transcriptomic reorganization is possible, and reflects the physiological changes associated with the transition to a nondividing state during the chronological aging process.

Although the microarray yielded an extensive list of biological processes altered over the aging process, putative genes involved in the induction of programmed cell death were not identified. To better understand the connection between the transcriptomic context identified in the first aim and presence of a PCD-like pathway in *K. brevis*, hallmark morphological and biochemical changes associated with PCD were examined in Chapter 3. In this work, we identified that *K. brevis* exhibits caspase-like activity, whose induction coincided with the transition into stationary phase. During the course of this project, a similar study was reported in *K. brevis* and *K. mikimotoi* demonstrating the induction of caspase-like activity over a long timescale, further supporting the finding that *K. brevis* contains caspase-like activities during the aging process (Bouchard and Purdie 2011). The morphological changes indicative of a PCD

pathway over the growth curve were difficult however to resolve, but it was apparent that *K. brevis* cells were experiencing oxidative stress. Oxidative stress has previously been implicated in the chronological aging program and the induction of PCD in yeast and other unicellular eukaryotes (Madeo et al. 1999; Jeon et al. 2002; Fabrizio et al. 2004; Herker et al. 2004; Carmona-Gutierrez et al. 2010). Furthermore, a seminal study in the dinoflagellate *Peridinium gatunense* by Vardi et al. (1999) experimentally linked ROS with the induction of PCD phenotypic changes that were dependent on cysteine protease activity. Based on the precedence in the literature and the apparent increase in ROS levels during stationary phase, we chose to use a discrete hydrogen peroxide treatment to induce caspase-dependent cell death, and to better elicit the morphological changes indicative of PCD. In addition to the examination of caspase activity through the cleavage of fluorogenic substrates (Gurtu et al. 1997), the induction of caspase-like activity was evaluated with an *it situ* marker and demonstrated that caspase activity is induced in a context specific manner. The observation that *K. brevis* caspase-like activity is induced in cells undergoing nuclear migration and swelling, as opposed to massive cytoplasmic blebbing, suggests that the caspase activity is specific to a PCD-like morphotype during oxidative stress, lending new insight into the connection between capase activity and PCD morphology in a dinoflagellate (Vardi et al. 1999; Franklin and Berges 2004). In addition, the observation that DNA fragmentation appeared to occur in the caspase positive cells further exemplifies that *K. brevis* contains hallmark changes in accordance with a PCD pathway (Bouchard and Purdie 2011). DNA fragmentation has been identified in a number of other studies in phytoplankton (Vardi et al. 1999; Bouchard and Purdie 2011); however, the mechanisms of DNase activity in dinoflagellates are not fully understood. The TUNEL assay reflects the presence of DNA nicks through the staining of free 3-OH ends of DNA, and does not evaluate the typical DNA laddering pattern associated with PCD-driven endonuclease activity; given that dinoflagellates lacks

216

nucleosomes, the exact mechanism of DNA damage in during PCD is unknown (Herzog and

Soyer 1981; Rizzo 2003). In summary, this work has demonstrated for the first time in a

dinoflagellate the direct connection between caspase activity and the induction of PCD

morphologies (Vardi et al. 1999; Franklin and Berges 2004; Bouchard and Purdie 2011).

One of the most novel findings in this dissertation was the identification of canonical

caspase substrates in the *K. brevis* proteome and the subsequent characterization of the

cleavage potential of S-adneosylmethionine synthetase (KbAdoMetS) by caspase 3.

Bioinformatic investigation of the caspase degradome has become increasingly more accurate

as prediction algorithms have begun to account for secondary structure and solvent exposure

dramatically decreasing the false positives rate (Wee et al. 2009). The combined approach with

Pripper and CasCleave predicted previously described caspase substrates as well as novel

targets. The cleavage analysis by MALDI-TOF of the KbAdoMetS caspase cleavage motif went

beyond the currently used approaches to understanding the PCD process in phytoplankton, and

provided a novel analysis of the connection between caspase-like enzymes and the biological

consequences of their activity. The determination of KbAdoMetS as a caspase substrate of

DEVDase activity in *K. brevis* bears exciting implications, as AdoMetS is a biological hub for many

processes (Pajares and Markham 2011). Dinoflagellates contain unique S-adenosylmethionine

synthetases that have been shown to regulate cell proliferation (Ho et al. 2007). Cleavage of

KbAdoMetS by recombinant caspase 3 represents the first step in understanding the connection

between the assayed caspase activity and the dinoflagellate degradome. Further clarification of

this process *in vivo* is needed to identify the biological consequences of *K. brevis* AdoMetS

cleavage, and represents an exciting avenue for further research in the context of PCD.

AdoMetS also represents a major hub in the biosynthetic pathway of the ecologically important

compound, dimethylsulfoniopropionate (DMSP), produced by various phytoplankton species

(Kiene et al. 2000). Over the last few decades, regulation of DMSP in the environment has become an important topic as perturbations in the DMSP biogeochemical cycle have major implications for climate change (Lyon et al. 2011). The connection between the dinoflagellate caspase degradome and global climate regulation represents an interesting line of future work.

The identification of caspase 3-like enzyme activity and increased protein abundance during ROS-driven death with diagnostic morphological changes indicative of a PCD pathway in *K. brevis* supports previous work in dinoflatellates demonstrating the existence of a PCD pathway. This work makes clear the connection between caspase activity and PCD, although like other groups, we suggest that *K. brevis* does not contain bona fide caspases, and the subtilisin family is the most likely culprit for coordinating this activity in *K. brevis* (Coffeen and Wolpert 2004; Chichkova et al. 2010; Thamatrakoln et al. 2011; Vartapetian et al. 2011). This finding has been inferred from sequence analysis, and thus future work empirically demonstrating caspase activity by *K. brevis* subtilisins is essential for deciphering the PCD machinery. Although the sequence analysis presented in this work, along with other studies, clearly excludes the metacaspases as coordinating the observed caspase activities, there is precedence for a potentially separate role for metacaspases in the PCD pathway (Bidle et al. 2007; Bidle and Bender 2008). To this end, the final aim of this study sought to test whether the *K. brevis* metacaspase 1 protein (KbMC1) was involved in PCD pathway.

In Chapter 4, the characterization of KbMC1 led to the intriguing finding that it possesses dual localization in the cytosol and chloroplast. Based on its sequence homology with AtMC1, we have hypothesized similar interactions of KbMC1 with other Zn-finger domain-containing proteins as a mechanism for KbMC1 regulation (Watanabe and Lam 2005). Given that the KbMC1 DNA sequence contained SNPs indicative of a tandemly repeated genetic

arrangment, questions regarding whether KbMC1 contains different isoforms resulting in the opposing locations or whether KbMC1 contains alternative autocatalytically active forms remain unresolved. The resolution of KbMC1's protein expression pattern during ROS-driven PCD identified for the first time a connection between chloroplastic metacaspase expression and the onset of PCD in a phytoplankton species. Moreover, the modified bioinformatic approach from Chapter 3 to investigate the metacaspase degradome in *K. brevis* represents the first study to identify metacaspase substrates in a phytoplankton species. This approach contained obvious drawbacks since substrate recognition motif searches for the fluorogenic substrates previously cleaved by other metacaspases are quite common in the proteome. We therefore suggest that the false positive rate in this analysis is most likely very high and targeted biochemical and mass spectrometry analyses like those presented in Chapter 3 may resolve this question. However, the observed induction of the chloroplastic form of KbMC1 coincided with the induction of PCD, and connections between the putative chloroplast-specific metacaspase substrates and the resolution of PCD in this organism are intriguing. The selective degradation of mitochondria during mitophagy has received considerable attention in its connection to metazoan death programs including PCD, autophagy, and necrosis (Youle and Narendra 2011), while the involvement of chloroplast degradation (chlorophagy) remains largely uninvestigated in photosynthetic organisms (Hayward et al. 2009; Seay et al. 2009). The data in this study clearly raises questions regarding the function of KbMC1 in chloroplast physiology; therefore, future work could be directed toward identifying the potential role of chlorophagy in PCD, and whether KbMC1 mediates these processes in *K. brevis*. The crosstalk between caspase and metacaspase activity has been identified in the shared cleavage of Tudor Staphylococcal Nuclease (TNS) in the Norway spruce (Sundstrom et al. 2009), and raised questions regarding the connection between the *K. brevis* caspase and metacaspase degradomes. The current study identified a shared

substrate (MGID2075952) containing both DEVD and FESR cleavage motif sites, annotated as an ankryin domain containing protein. Interestingly, the protein targeting software, WolfPSort, found this protein to contain a weak chloroplast transit peptide. Ankryin repeat proteins have connections to chloroplast differentiation, protein import, as well as the direct connection to PCD, thus the characterization of this substrate in future studies is of interest (Zhang et al. 1992; Chan et al. 1999; Schünemann 2004; Li et al. 2006). The coordinated expression of photosynthesis related genes was also found to be enriched during the aging process. Together, the work described in this dissertation highlights the need for a better understanding of the role of chloroplasts in the death processes of dinoflagellates.

Dinoflagellates represent an important group of organisms for our understanding of the programmed cell death pathway, and acquiring more knowledge of this pathway in *K. brevis* is important for directing mitigation and control strategies. As outlined in the 2005 – 2015 Harmful Algal Research and Response National Environmental Science Strategy (HARRNESS), management and control strategies are needed to reduce impacts on coastal resources, local economies, and threats to public health (Ramsdell 2005). The plan outlines the need to develop indicators of bloom progression as well as effective and environmentally sound techniques to reduce and control HABs. Currently, *K. brevis* HAB forecasting relies on satellite-derived images of chlorophyll concentrations, in combination with wind and current models (Stumpf et al. 2008). The work outlined in Chapter 2 has provided the means to develop the global aging signature into a portable method for forecasting bloom progression. The microarray work clearly demonstrates that *K. brevis* contains drastically different transcriptomic signatures in logarithmic (growth) and stationary (maintenance) phases. Antibody-based approaches for HAB toxin detection are currently employed on the Environmental Sample Processor (ESP) (Doucette et al. 2009), and have the potential to include additional chemistries to create new assays. In

addition, many of the morphological and biochemical changes associated with PCD (defined in Chapter 3) may be used as indicators of bloom termination. This work may be optimized to integrate into the FlowCAM system, which provides semi-automated recognition and enumeration of *K. brevis* cells. The work from this dissertation provides a framework to direct the possible integration of morphological data into this system (Buskey and Hyatt 2006). The extent to which *K. brevis* exhibits these morphological changes in bloom populations is currently unknown, although current discussions with collaborators are already underway to carry out such studies (Paul Zimba, personal communication).

The work presented in this dissertation has greatly advanced our understanding of PCD in a toxic dinoflagellate, provided insights into the physiological changes associated with chronological aging, and provoked new questions to be explored. This work established that *K. brevis* exhibits PCD under oxidative stress, and has provided a framework to answer questions regarding the exact role KbMC1 plays in this system. The data presented here suggest KbMC1 could be acting similarly to AtMC1; thus, understanding the mechanism of activation and localization is critical. Since it appears that the chloroplastic for of KbMC1 is important in PCD, the verification of its substrates in the chloroplast would provide insight into whether this protein does in fact degrade the photosynthetic machinery, as hypothesized. Verification of proposed caspase and metacaspase substrates by MALDI-TOF would aid in discriminating false substrate predictions, and elaborating the biological consequences of enzyme activity. The role of KbMC1 in the chloroplast is of utmost concern given its induction during PCD. Co-immunoprecipitation of KbMC1 and its interacting proteins would provide further clues into its function in the chloroplast. Together, this study has resulted in novel findings and important tools for the continuation of this work into the future. Continued expansion of our knowledge

of aging and death in *K. brevis* will greatly contribute to biological strategies for HAB mitigation

and control, as well as elucidate the evolutionary history of these fascinating processes.

REFERNCES

Ameisen JC (1996) The origin of programmed cell death. Science **272**: 1278-1279

Ameisen JC (2002) On the origin, evolution, and nature of programmed cell death: a timeline of four billion years. Cell Death Differ **9**: 367-393

Bachvaroff T, Place A (2008) From stop to start: tandem gene arrangement, copy number and trans-splicing sites in the dinoflagellate *Amphidinium carterae*. PLoS One **13**: e2929

Bidle KD, Bender SJ (2008) Iron starvation and culture age activate metacaspases and programmed cell death in the marine diatom *Thalassiosira pseudonana*. Eukaryotic Cell **7**: 223-236

Bidle KD, Haramaty L, Barcelos ERJ, Falkowski P (2007) Viral activation and recruitment of metacaspases in the unicellular coccolithophore, *Emiliania huxleyi.* Proc Natl Acad Sci U S A **104**: 6049-6054

Bouchard JN, Purdie DA (2011) Temporal variation of caspase 3-like protein activity in cultures of the harmful dinoflagellates *Karenia brevis* and *Karenia mikimotoi*. Journal of Plankton Research **33**: 961-972

Boyce M, Degterev A, Yuan J (2004) Caspases: an ancient cellular sword of Damocles. Cell Death Differ **11**: 29 - 37

Buskey EJ, Hyatt CJ (2006) Use of the FlowCAM for semi-automated recognition and enumeration of red tide cells (*Karenia brevis*) in natural plankton samples. Harmful Algae **5**: 685-692

Campbell DA, Sturm NR, Yu MC (2000) Transcription of the Kinetoplastid Spliced Leader RNA Gene. Parasitology Today **16**: 78-82

Cande C, Cecconi F, Dessen P, Kroemer G (2002) Apoptosis-inducing factor (AIF): key to the conserved caspase-independent pathways of cell death? J Cell Sci **115**: 4727 - 4734

Carmona-Gutierrez D, Eisenberg T, Buttner S, Meisinger C, Kroemer G, Madeo F (2010) Apoptosis in yeast: triggers, pathways, subroutines. Cell Death Differ **17**: 763-773

Chan S-L, Tan K-O, Zhang L, Yee KSY, Ronca F, Chan M-Y, Yu VC (1999) F1Aα, a Death Receptor-binding Protein Homologous to theCaenorhabditis elegans Sex-determining Protein, FEM-1, Is a Caspase Substrate That Mediates Apoptosis. J Biol Chem **274**: 32461-32468

Chichkova NV, Shaw J, Galiullina RA, Drury GE, Tuzhikov AI, Kim SH, Kalkum M, Hong TB, Gorshkova EN, Torrance L, Vartapetian AB, Taliansky M (2010) Phytaspase, a relocalisable cell death promoting plant protease with caspase specificity. Embo J **29**: 1149-1161

Coffeen WC, Wolpert TJ (2004) Purification and characterization of serine proteases that exhibit caspase-like activity and are associated with programmed cell death in *Avena sativa*. The Plant Cell Online **16**: 857-873

Danial NN, Korsmeyer SJ (2004) Cell Death: Critical Control Points. Cell **116**: 205-219

Degterev A, Yuan J (2008) Expansion and evolution of cell death programmes. Nat Rev Mol Cell Biol **9**: 378-390

Doucette GJ, Mikulski CM, Jones KL, King KL, Greenfield DI, Marin Iii R, Jensen S, Roman B, Elliott CT, Scholin CA (2009) Remote, subsurface detection of the algal toxin domoic acid onboard the Environmental Sample Processor: Assay development and field trials. Harmful Algae **8**: 880-888

Earnshaw WC, Martins LM, Kaufmann SH (1999) Mammalian caspases: structure, activation, substrates, and functions during apoptosis. Annu Rev Biochem **68**: 383-424

Fabrizio P, Battistella L, Vardavas R, Gattazzo C, Liou LL, Diaspro A, Dossen JW, Gralla EB, Longo VD (2004) Superoxide is a mediator of an altruistic aging program in *Saccharomyces cerevisiae*. J Cell Biol **166**: 1055-1067

Franklin DJ, Berges JA (2004) Mortality in cultures of the dinoflagellate *Amphidinium carterae* during culture senescence and darkness. Proc Biol Sci **271**: 2099-2107

Goldshmidt H, Matas D, Kabi A, Carmi S, Hope R, Michaeli S (2010) Persistent ER stress induces the spliced leader RNA silencing pathway (SLS), leading to programmed cell death in *Trypanosoma brucei*. PLoS Pathog **6**: e1000731

Gurtu V, Kain SR, Zhang G (1997) Fluorometric and Colorimetric Detection of Caspase Activity Associated with Apoptosis. Anal Biochem **251**: 98-102

Hackett JD, Anderson DM, Erdner DL, Bhattacharya D (2004) Dinoflagellates: a remarkable evolutionary experiment. American Journal of Botany **91**: 1523-1534

Hallegraeff GM (1993) A review of harmful algal blooms and their apparent global increase. Phycologia **32**: 79-99

Hayward AP, Tsao J, Dinesh-Kumar SP (2009) Autophagy and plant innate immunity: Defense through degradation. Semin Cell Dev Biol **20**: 1041-1047

Herker E, Jungwirth H, Lehmann KA, Maldener C, Frohlich KU, Wissing S, Buttner S, Fehr M, Sigrist S, Madeo F (2004) Chronological aging leads to apoptosis in yeast. J Cell Biol **164**: 501-507

Herzog M, Soyer MO (1981) Distinctive features of dinoflagellate chromatin. Absence of nucleosomes in a primitive species *Prorocentrum micans* E. Eur J Cell Biol **23**: 295-302

Ho P, Kong KF, Chan YH, Tsang J, Wong J (2007) An unusual S-adenosylmethionine synthetase gene from dinoflagellate is methylated. BMC Molecular Biology **8**: 1-15

Hoagland P, Scatasta S (2006). Ecological Studies 189: Ecology of Harmful Algae. E. Graneli and J. T. Turner. Springer-Verlag, Berlin: 391-402.

Jeon BW, Kim KT, Chang SI, Kim HY (2002) Phosphoinositide 3-OH kinase/protein kinase B inhibits apoptotic cell death induced by reactive oxygen species in *Saccharomyces cerevisiae*. Journal of biochemistry **131**: 693-699

Kaczanowski S, Sajid M, Reece S (2011) Evolution of apoptosis-like programmed cell death in unicellular protozoan parasites. Parasites & Vectors **4**: 44

Keeling PJ (2009) Chromalveolates and the evolution of plastids by secondary endosymbiosis. J Eukaryot Microbiol **56**: 1-8

Kiene RP, Linn LJ, Bruton JA (2000) New and important roles for DMSP in marine microbial communities. Journal of Sea Research **43**: 209-224

Larkin SL, Adams CM (2007) Harmful algal blooms and coastal business: Economic consequences in Florida. Society & Natural Resources **20**: 849-859

Li J, Mahajan A, Tsai M-D (2006) Ankyrin Repeat: A Unique Motif Mediating Protein–Protein Interactions†. Biochemistry-Us **45**: 15168-15178

Lidie K (2007) Characterization and regulation of gene expression networks in response to acute environmental stress in the Florida red tide dinoflagellate, *Karenia brevis*. PhD thesis

Lidie K, Ryan J, Barbier M, Van Dolah F (2005) Gene expression in Florida red tide dinoflagellate *Karenia brevis* : Analysis of an expressed sequence tag library and development of DNA microarray. Mar Biotechnol **7**: 481 - 493

Lidie K, Van Dolah F (2007) Spliced leader RNA-mediated trans-splicing in a dinoflagellate, *Karenia brevis*. Journal of Eukaryotic Microbiology **54**: 427 - 435

Lukeš J, Leander BS, Keeling PJ (2009) Cascades of convergent evolution: The corresponding evolutionary histories of euglenozoans and dinoflagellates. P Natl Acad Sci USA **106**: 9963-9970

Lyon BR, Lee PA, Bennett JM, DiTullio GR, Janech MG (2011) Proteomic analysis of a sea-ice diatom: salinity acclimation provides new insight into the dimethylsulfoniopropionate production pathway. Plant Physiol **157**: 1926-1941

Madeo F, Frohlich E, Ligr M, Grey M, Sigrist SJ, Wolf DH, Frohlich KU (1999) Oxygen stress: a regulator of apoptosis in yeast. J Cell Biol **145**: 757-767

Monroe EA (2008). Characterization of polyketide synthases in the Florida red tide dinoflagellate *Karenia brevis.* Molecular Cellular Biology and Pathobiology. Charleston, Medical University of South Carolina. **PhD:** 193.

Nedelcu AM, Driscoll WW, Durand PM, Herron MD, Rashidi A (2011) On the paradigm of altruistic suicide in the unicellular world. Evolution; international journal of organic evolution **65**: 3-20

Pajares MA, Markham GD (2011). Methionine Adenosyltransferase (S-Adenosylmethionine Synthetase). Advances in Enzymology, John Wiley & Sons, Inc.: 449-521.

Petit PX, Susin SA, Zamzami N, Mignotte B, Kroemer G (1996) Mitochondria and programmed cell death: back to the future. FEBS Lett **396**: 7-13

Ramsdell JS, Anderson, D.M., Glibert, P.M. (2005). Harmful Algal Research and Response: A National Environmental Science Strategy 2005 - 2015. Washington DC.

Rizzo PJ (2003) Those amazing dinoflagellate chromosomes. Cell research **13**: 215-217

Rossini C, Taylor W, Fagan T, Hastings JW (2003) Lifetimes of mRNAs for clock-regulated proteins in a dinoflagellate. Chronobiol Int **20**: 963-976

Schünemann D (2004) Structure and function of the chloroplast signal recognition particle. Current Genetics **44**: 295-304

Seay M, Hayward AP, Tsao J, Dinesh-Kumar SP (2009) Something old, something new: plant innate immunity and autophagy. Current topics in microbiology and immunology **335**: 287-306

Sigee DC (1983) Structural DNA and genetically active DNA in dinoflagellate chromosomes. Biosystems **16**: 203-210

Stumpf RP, Litaker RW, Lanerolle L, Tester PA (2008) Hydrodynamic accumulation of *Karenia* off the west coast of Florida. Cont Shelf Res **28**: 189-213

Sundstrom J, Vaculova A, Smertenko A, Savenkov E, Golovko A, Minina E, Tiwari B, Rodriguez-Nieto S, Zamyatnin A, Valineva T (2009) Tudor staphylococcal nuclease is an evolutionarily conserved component of the programmed cell death degradome. Nat Cell Biol **11**: 1347 - 1354

Thamatrakoln K, Korenovska O, Niheu AK, Bidle KD (2011) Whole-genome expression analysis reveals a role for death-related genes in stress acclimation of the diatom *Thalassiosira pseudonana*. Environmental Microbiology: no-no

Vardi A, Berman-Frank I, Rozenberg T, Hadas O, Kaplan A, Levine A (1999) Programmed cell death of the dinoflagellate *Peridinium gatunense* is mediated by CO_2 limitation and oxidative stress. Curr Biol **9**: 1061-1064

Vartapetian AB, Tuzhikov AI, Chichkova NV, Taliansky M, Wolpert TJ (2011) A plant alternative to animal caspases: subtilisin-like proteases. Cell Death Differ

Watanabe N, Lam E (2005) Two Arabidopsis metacaspases AtMCP1b and AtMCP2b are arginine/lysine-specific cysteine proteases and activate apoptosis-like cell death in yeast. J Biol Chem **280**: 14691 - 14699

Wee L, Tong J, Tan T, Ranganathan S (2009) A multi-factor model for caspase degradome prediction. BMC Genomics **10**: 1-12

Wissing S, Ludovico P, Herker E, Buttner S, Engelhardt S, Decker T, Link A, Proksch A, Rodrigues F, Corte-Real M (2004) An AIF orthologue regulates apoptosis in yeast. J Cell Biol **166**: 969 - 974

Youle RJ, Narendra DP (2011) Mechanisms of mitophagy. Nat Rev Mol Cell Biol **12**: 9-14

Zhang H, Campbell DA, Sturm NR, Lin S (2009) Dinoflagellate spliced leader RNA genes display a variety of sequences and genomic arrangements. Mol Biol Evol **26**: 1757-1771

Zhang H, Hou Y, Miranda L, Campbell D, Sturm N, Gaasterland T, Lin S (2007) Spliced leader RNA *trans*-splicing in dinoflagellates. P Natl Acad Sci USA **104**: 4618 - 4623

Zhang H, Scheirer DC, Fowle WH, Goodman HM (1992) Expression of antisense or sense RNA of an ankyrin repeat-containing gene blocks chloroplast differentiation in *Arabidopsis*. The Plant Cell Online **4**: 1575-1588

Zhivotovsky B, Kroemer G (2004) Apoptosis and genomic instability. Nat Rev Mol Cell Biol **5**: 752-762